I. Rhenium and Iridium in Natural Waters

II. Methyl Bromide: Ocean Sources, Ocean Sinks, and Climate Sensitivity

III. CO_2 Stability and Heterogeneous Chemistry in the Atmosphere of Mars

Thesis by

Ariel David Anbar

In Partial Fulfillment of the Requirements

for the Degree of

Doctor of Philosophy

California Institute of Technology

Pasadena, California

1996

(Submitted January 5, 1996)

To Marni,
who understands

"...you are somewhat narrow in your training and outlook..."

In a memo from the author's qualifying exam committee
12 October 1990

"Früher die Helden, heute die Spezialisten"

(There used to be heroes, now there are specialists)

Graffiti on a monument to Gutenberg in Mainz

Acknowledgments

So many have contributed to the success of this work... First and foremost, Profs. G. J. Wasserburg and Y. L. Yung provided the logistical and material support which made my years at Caltech possible. More important than this, though, both provided the intellectual guidance which gave these years value far beyond any material measure. Words on a page cannot properly express the magnitude of this contribution, or the depth of my gratitude.

Interactions with many other faculty have made these years memorable. Most notably, Prof. G. R. Rossman spent countless hours patiently listening to my frustrations and offering advice. The warmth of Prof. S. Epstein has touched me since I first visited the campus, and helped make N. Mudd feel like home. Prof. H. D. Holland at Harvard University first steered me to Caltech, and has encouraged me from afar. I also feel fortunate to have interacted with Profs. G. A. Blake, D. S. Burnett, K. Farley, M. R. Hoffmann, J. J. Morgan, C. C. Patterson, R. Sharp, L. T. Silver and E. M. Stolper, and with visiting faculty M. Magaritz, M. Tredoux and K. K. Turekian.

I have learned much from Dr. D. A. Papanastassiou about mass spectrometry and analytical chemistry. He has also taught me to face experimental setbacks with calm resolve. My efforts in the Lunatic Asylum would not have gone far without his help. Similarly, Dr. M. Allen was a patient teacher during my bug-infested early days with the KINETICS code.

I owe a great debt to many senior graduate students and post-docs. Over countless cups of coffee, Don Porcelli helped me to refine my ideas, and to discard those not worth the effort. Interactions with Rob Creaser and Yigal Erel were critical in my first few years as a trace element geochemist. From

Rob I gained a practical knowledge of analytical chemistry, and an appreciation for innovation and ingenuity in the laboratory. Yigal taught me much about surface chemistry and aquatic chemistry. Rose Capo and Brian Stewart provided object lessons in grit and determination. Their uncompromising passion for science and a complete life is deeply inspiring. I have also learned much from Per Andersson, Noreen Evans, Peter Green, Candace Martin, David Peate, Matthieu Roy-Barman, and Mukul Sharma.

I am fortunate to have been here at the same time as John Holt, Laurie Leshin, Elaine Marzluff, Elizabeth Moyer, Hari Nair, Eve Shaffer, Jim Spotilla, Kim Tryka, Liz Warner, and Laura Wasylenki, fellow students who helped make the difficult times here more bearable, and who were there to share the good times. Also, Kathie Venturelli, Priscilla Piano and Mary Eleanor Johnson were always there to lend a hand, or a sympathetic ear.

Finally, my deepest gratitude goes to my family. My love of science, learning and life flows directly from my parents, Michael and Ada, and my brother, Ran. Marni, my wife, has provided vital emotional support throughout my time here. This thesis is as much her triumph as it is mine.

Abstract

Part I: Rhenium and iridium were measured in natural waters by isotope dilution and negative thermal ionization mass spectrometry, following clean chemical separation from 200 mL (Re) and 4 L (Ir) samples. In the Pacific Ocean, Re is well-mixed in the water column, confirming predictions of conservative behavior. The Re concentration is 7.42 ± 0.04 ng kg^{-1}. The concentration of Ir in the oceans is fairly uniform with depth and location, ranging from 2.9 to 5.7 x 10^8 atoms kg^{-1}. Pristine river water contains ≈ 20 x 10^8 atoms kg^{-1} while polluted rivers have 50 - 100 x 10^8 atoms kg^{-1}. Concentrations in the Baltic Sea are much lower than expected from conservative estuarine mixing, indicating rapid removal of ≈75% of riverine Ir. Under oxidizing conditions, Ir is scavenged by Fe-Mn oxyhydroxides. Ir is enriched in anoxic waters relative to overlying oxic waters, indicating that anoxic sediments are not a major Ir sink. The residence time of dissolved Ir in the oceans is 10^3 - 10^4 years, based on these and other observations. The amount of Ir in K/T boundary sediments is ≈ 10^3 times the total quantity in the oceans.

Part II: The biogeochemistry of methyl bromide (CH_3Br) in the oceans was studied using a steady-state mass-balance model. CH_3Br concentrations are sensitive to temperature and the rate of CH_3Br production. Model production rates correlate strongly with chlorophyll concentrations, indicating CH_3Br biogenesis. This correlation explains discrepancies between two observational studies, and supports suggestions that the ocean is a net sink for atmospheric CH_3Br. The Southern Ocean may be a CH_3Br source.

Part III: High resolution, temperature-dependent CO_2 cross sections were incorporated into a 1-D photochemical model of the Martian atmosphere. The calculated CO_2 photodissociation rate decreased by as much as 33% at some altitudes, and the photodissociation rates of H_2O and O_2 increased by as much as 950% and 80%, respectively. These results minimize or even reverse the sense of the CO_2 chemical stability problem due to increased production of HO_x species which catalyze CO oxidation. The effect of heterogeneous chemistry on the abundance and distribution of HO_x was assessed using observations of dust and ice aerosols and laboratory adsorption data. Adsorption of HO_2 can deplete OH in the lower atmosphere enough to significantly reduce the CO/CO_2 ratio.

Table of Contents

Preface

The unifying theme of my research, and of this thesis, is the exploration of the evolution of the Earth's surface environment. This research addresses environmental change, and the processes which drive it, from the earliest Precambrian abiotic Earth to the modern, tightly-coupled web of biogeochemical cycles.

I am particularly interested in the interactions between biological processes and the "inorganic" world. These interactions are complex and poorly understood; biological processes have a profound impact on the environment, while, at the same time, environmental conditions shape the course of biological evolution. Understanding this interplay is of great importance. From a practical perspective, as we develop our knowledge of the biogeochemical processes which regulate conditions at the Earth's surface, we gain perspective on the anthropogenic modification of present and future environments, obtain insights which help solve pressing environmental problems, and begin to understand the vulnerability of life on this planet. More fundamentally, as we come to understand the interactions between life and the inorganic world, we approach the answer to one of *the* first-order questions of human existence: How did we get here?

Obviously, such issues can not be thoroughly addressed in a single thesis! Additionally, my interest in these issues has evolved during my years of graduate research; only in retrospect is it apparent that a unifying thread led me to explore three separate problems, each of which is relevant to a general understanding of biosphere/geosphere interactions. These projects all reflect my training in low temperature, inorganic geochemistry. However, I have deliberately maintained a wide focus, since progress in interdisciplinary

science requires a foundation in more than one subspecialty. In each case, I have made substantial, original contributions. Several of the chapters have already been published or have been accepted for publication. They are included here in their published forms, with only minor reformatting to provide the thesis a uniform style.

Part I, *Rhenium and Iridium in Natural Waters,* grew out of two areas of interest. First, I have long been interested in finding new ways to constrain the abundance of oxygen in the atmosphere and ocean through time, since these quantities are closely coupled to biological activity in many ways. Since Re is removed slowly from seawater primarily through burial in anoxic sediments, a study of the Re geochemical budget may yield new insights into the extent of deep sea anoxia. This quantity is important in understanding climate change, since models of the carbon cycle (which seek to explain variations in atmospheric CO_2 in response to glacial cycles) predict varying degrees of deep-sea anoxia. In Chapters 2 and 3, high-precision measurements of Re in seawater are used to demonstrate the extremely non-reactive nature of Re in the water column, and a simple model of Re in seawater through time is developed to place limits on the area of the seafloor overlain by anoxic waters during glacial periods.

Second, I find the mass extinction at the Cretaceous/Tertiary boundary one of the most compelling events in Earth history. The impact/extinction model, based in large part on the observation of anomalous Ir abundances in boundary sediments, is one of the more clear-cut and spectacular examples of a completely abiotic process having a profound impact on environmental conditions and life. It therefore demands close scrutiny. Through the development and application of novel analytical methods, the chemistry of Ir

in natural waters is examined for the first time (Chapters 4 and 5). The extremely low content of Ir observed in the oceans eliminates seawater as the primary source of Ir in boundary sediments, which strengthens the impact model. The rapid removal of Ir from natural waters, apparently by particulate scavenging, indicates that detailed study of platinum group element abundances in sediments deposited soon after the impact could be used to reconstruct the details of environmental change at that time.

Part II, *Methyl Bromide: Ocean sources, Ocean Sinks, and Climate Sensitivity*, quantifies the importance of the marine biosphere in the production of methyl bromide. This is accomplished by modeling the production rate of methyl bromide in the oceans, using a steady-state approach and previously published observations of marine methyl bromide. The model production rate is found to correlate strongly with observed primary production, indicating a close connection to biological activity. Methyl bromide has been implicated in stratospheric ozone depletion. In contrast to Part I, then, Part II is an exploration of a biological process which influences the environment. Although other biological processes have more profound environmental impact, this particular problem has attracted much recent interest due to its immediate economic importance; a ban on the anthropogenic production and use of methyl bromide, an important agricultural fumigant, is under consideration.

Finally, Part III, *CO_2 Stability and Heterogeneous Chemistry in the Atmosphere of Mars*, is an exploration of the chemistry of a clearly abiotic atmosphere. To a large degree, the bulk Martian atmosphere is a chemical analog of the Earth's stratosphere, but subject to different boundary conditions, and devoid of the complications introduced by biogenic

contributions (which are difficult to model *a priori,* and which introduce poorly-understood feedbacks). A satisfactory explanation for the CO_2:CO ratio in the Martian atmosphere has long been elusive (the "CO_2 stability problem"). In Chapter 1, the incorporation of high resolution, temperature-dependent CO_2 photoabsorption cross sections in computational models changes this problem from an underabundance to an overabundance of CO_2. A solution based on heterogeneous chemistry is explored in Chapter 2. Our ability to explain this atmosphere's composition in terms of chemical kinetics and thermodynamics is an important test of our understanding of inorganic chemistry in planetary atmospheres. Such understanding is a prerequisite for determining the influence of biological processes on the Terrestrial atmosphere.

Part I.

Rhenium and Iridium in Natural Waters

**"Nothing is yet known
about dissolved platinum metals
in sea water."**

V. M. Goldschmidt, 1954

**"This value for iridium
may be the lowest reported concentration
for a stable element in seawater"**

*Hodge et al., 1986, after determining
iridium concentrations tenfold
higher than in the present study*

Chapter 1.

Not So Noble: An Introduction to the Low-Temperature Geochemistry of Rhenium and Iridium

1.1. Overview

There has been intense interest in the geologic occurrence of iridium and the other Platinum Group Elements (the PGE: Ru, Rh, Pd, Os, Ir and Pt) since the discovery of an enrichment of Ir in the sediments at the Cretaceous/Tertiary (K/T) boundary (Alvarez *et al.*, 1980; Ganapathy, 1980; Kyte *et al.*, 1980; Orth *et al.*, 1981; Smit and Hertogen, 1980). The PGE are extremely scarce at the Earth's surface, and relatively enriched in meteorites (*e.g.,* the Ir content of average continental crust is ≈ 0.05 ppb, *vs.* 481 ppb in chondritic meteorites, Anders and Grevesse, 1989; Esser and Turekian, 1993; Fenner and Presley, 1984). Therefore, a connection between an asteroid impact and the mass extinction 65 million years ago was deduced from this geochemical anomaly. This theory has generated interdisciplinary excitement, stimulating inquiry in a number of areas. Foremost among these are investigations into the causes of mass extinction, and of the frequency of impact events in the geologic record (*e.g.,* Rampino and Caldeira, 1993; Raup and Sepkoski, 1984; Sepkoski, 1986). The intellectual stakes of this research are rather high. The possibility that the trajectory of biological evolution is modified by catastrophic impacts of asteroids and/or comets with the Earth's surface is unsettling to the classical Darwinian model of gradual, progressive evolution, and to the Uniformitarian principles underlying much of the Geological Sciences. The practical stakes may also be high. The collision of the Earth with even a modest object could cause regional devastation and

human misery, if not global mass extinction. Chapman and Morrison (1994) have estimated that there is a 1-in-10,000 chance of a 2 km diameter object colliding with the Earth in the next century. In the wake of the collision of comet Shoemaker-Levy 9 with Jupiter in 1994, this possibility has attracted public attention (*e.g.,* Reston, 1994). The United States government has shown interest in quantifying the risk of such an event, and in developing a means of diverting or destroying earthbound objects (Chapman and Morrison, 1994; Matthews, 1992; Reichhardt, 1994).

Advocates of the impact/extinction model have apparently located the K/T boundary impact site at Chicxulub (Hildebrand *et al.*, 1991), and linked features in the boundary sediments other than the Ir abundance to an impact event (*e.g.,* Alvarez *et al.*, 1995; Bohor *et al.*, 1987a; Bohor *et al.*, 1987b; Izett, 1991). There has also been a search for Ir enrichments at other stratigraphic boundaries marked by paleontological upheaval (*e.g.,* Alvarez *et al.*, 1982; Orth *et al.*, 1988a; Orth *et al.*, 1988b; Playford *et al.*, 1984). Opponents have tried to connect the unique characteristics of the K/T boundary sediments to endogenous mechanisms (*e.g.,* volcanism), and argued that small Ir enrichments elsewhere in the record are the result of diagenetic processes. Additionally, it has been claimed that the K/T extinctions were gradual, and that they began prior to the Ir anomaly (Keller *et al.*, 1993; Keller *et al.*, 1994; Macleod and Keller, 1994). At the present time, the dating of the Chicxulub structure proves that a massive impact event occurred 65 million years ago (Swisher *et al.*, 1992). However, the link between the impact and extinctions is hotly debated, with contemporaneous volcanism (*i.e.,* the Deccan Traps flood basalts) still a viable agent of evolutionary forcing. At other stratigraphic boundaries, matters are even less settled.

Ir remains the prime tracer of extraterrestrial input to the Earth's surface, especially where large impact events are concerned. While the isotopic composition of He in marine sediments is also sensitive to exogenous sources (Farley, 1995; Farley and Patterson, 1995), it is not clear how far back in time the $^{3}He/^{4}He$ record can be pushed. Additionally, the sedimentary $^{3}He/^{4}H$ signal may be unsuitable for detecting the accretion of large objects, since He can be lost to the atmosphere upon vaporization of the impactor.

Thus, questions about the geochemistry of Ir and the other PGE permeate the debate over impacts and extinctions. What is the abundance of the PGE in terrestrial source materials? Can the PGE be remobilized from some sedimentary environments, and concentrated into others? Can the PGE be fractionated from one another by terrestrial mechanisms? These questions were anticipated in D. Raup's review of the 1980 manuscript by Alvarez *et al.* in which he wrote:

> "... We are presented with the fact that the boundary clays are much higher in iridium than the overlying and underlying limestones but we are given little or no perspective on iridium distribution in other clays, recent sediments, organisms, sea water, and so on..."
>
> - Raup, 1987

Almost two decades later, the database is somewhat improved. However, a quantitative understanding of PGE geochemistry at the Earth's surface remains elusive.

A critical entry point to these issues is the chemistry of the PGE in natural waters. Natural water chemistry determines the concentrations of these elements in the oceans, affects their primary abundances in different

types of sediments, and modifies their distribution in the geologic record during diagenesis. However, PGE natural water chemistry is poorly understood. This is not for lack of interest. Since most of the classical K/T boundary sediments are submarine, the importance of determining Ir in seawater was recognized early-on (Alvarez *et al.*, 1980; Kyte *et al.*, 1985). A small but crucial body of evidence suggests that scavenging of dissolved PGE modifies their sedimentary abundances (Crocket and Kuo, 1979; Goldberg *et al.*, 1986; Koide *et al.*, 1991), and that inter-element variations exist in PGE post-depositional mobility (Colodner *et al.*, 1992).

The primary obstacles to a better understanding of the PGE in natural waters have been analytical. The same crustal scarcity which makes these elements useful tracers of extraterrestrial material makes their analysis in typical crustal materials one of the most difficult challenges in analytical geochemistry (Fig. 1.1). A range of techniques have been applied to this problem; these are discussed in Chapter 4. The high sensitivity of neutron activation analysis (NAA) for the detection of Ir (*e.g.,* Crocket and Cabri, 1981) has made this the dominant technique, by far, and has made Ir something of a surrogate for the PGE as a group.

Although NAA is more sensitive than most analytical methods toward Ir, the detection limits are not low enough for routine analysis of Ir in most crustal materials, or in natural waters. This has had an important biasing effect on research in this field. Most PGE geochemical studies have focused on ore bodies, meteorites and mantle rocks, because of the higher abundances in these samples. These materials are also favored because they require little sample preparation before neutron activation. The PGE distributions in these materials are dominated by high-temperature processes (*i.e.,*

temperatures > 500°C). As a result, most of the geochemical community considers the PGE "noble metals" since, under these conditions, the elements are frequently in their metallic, chemically resistant forms. Geochemical investigations have concentrated mainly on the genesis of PGE ores, and on questions relating to the abundance of the PGE in the Earth's mantle. Relatively little research has addressed questions in PGE low-temperature geochemistry, where low abundances and solution chemistry predominate.

Recent developments in negative thermal ionization mass spectrometry (NTIMS) open the way for rapid, precise analysis of all the PGE with extremely high sensitivity (Creaser *et al.*, 1991; Völkening *et al.*, 1991; Zeininger, 1984). The purpose of the present study is to use this technique to begin a thorough, systematic examination of the low-temperature geochemistry of the PGE, in order to improve our understanding of the distribution of these elements in the sedimentary record. This understanding is especially important for future applications of Os isotope geochemistry to processes of global change, where critical unknowns include the behavior of Os during weathering, riverine transport and residence in seawater (Esser and Turekian, 1993; Pegram *et al.*, 1994; Pegram *et al.*, 1992; Peucker-Ehrenbrink *et al.*, 1995; Ravizza and McMurtry, 1993; Ravizza *et al.*, 1991). The first stage of this research is to characterize the distribution of the PGE in seawater and river waters, in order to achieve a basic understanding of their geochemical cycles.

Two elements were chosen for this initial work. The first is Re. While not strictly a PGE, Re is a closely allied element, with some similar chemical properties. Additionally, the decay of ^{187}Re to ^{187}Os produces the $^{187}Os/^{186}Os$ isotopic variations which give Os isotope geochemistry its utility. The

extreme sensitivity of Re solution chemistry to redox conditions makes it a geochemically interesting element in its own right (Colodner, 1991; Goldberg *et al.*, 1988). Re also happens to be more abundant in crustal rocks than the PGE, and is more abundant in seawater, making it a good target for a first test of the NTIMS technique. Analytical methods and results for the determination of Re in the Pacific Ocean are presented in Chapter 2. In Chapter 3, some implications of these results are explored.

The second element chosen is Ir. The geochemical interest in this element is clear from the preceding discussion. The measurement of Ir in natural waters is a far greater analytical challenge than is the case for Re, due to its thousand-fold lower abundance and its more complex solution chemistry. However, Ir chemistry is simpler than that of Os. Analytically, then, the characterization of Ir in natural waters is a "stepping stone" to the characterization of Os. In Chapter 4, the analytical methods developed for this purpose are described in detail. In Chapter 5, the Ir distribution in seawater and in the Baltic Sea system are presented and discussed, along with the implications for the interpretation of Ir concentrations in sediments.

The remainder of this introductory chapter consists of an overview of the (geo)chemistry of Ir and of Re. This overview is not intended to be comprehensive, but merely to provide a context for subsequent chapters. Section **1.2** surveys the properties, history and uses of these elements as metals. Section **1.3** gives a brief overview of their solid-Earth geochemistry. Section **1.4** includes a summary of the Ir and Re solution chemistry relevant to natural waters. Excellent, comprehensive reviews of the PGE include the historical survey of McDonald and Hunt (1982), the geochemical review edited by Cabri (1981), and the chemical overviews of Hartley (1991) and

Cotton and Wilkinson (1988). Peacock (1966) has written a thorough monograph on Re. A thorough, recent survey of the literature on the PGE and Re in the solid Earth and meteorites is that of Blum (1990). The information in this chapter is drawn from these sources, and references therein, except where otherwise noted.

1.2. The Noble Metals

1.2.1. *Iridium and the Other PGE*

Some of the chemical properties of these elements are summarized in Table 1.1. At high temperatures and under reducing conditions, the PGE form highly refractory metals. It was in this form that Pt was discovered in alluvial deposits in Columbia, in the 16th century. In these early years, Pt was noted primarily for its tendency to alloy with Au, making it an annoyance for refiners, and of benefit to counterfeiters. In 1741, C. Wood brought the first samples of Pt metal to Europe. These were passed on to W. Brownrigg, who noted the resistance of this new metal to tarnish, comparing it favorably with Au. The insolubility of Pt in mineral acids (aside from aqua regia) and its metallurgical properties were finally recognized in the 1750's by W. Lewis. The discovery that this metal actually consisted of several elements was not recognized until 1803. Ir and Os were discovered in that year by S. Tennant, during his investigations into the residues remaining after dissolution of Pt metal in aqua regia. Given this history, it is not surprising that these elements were declared the "noble metals". By analogy with the noble gases, the PGE were viewed as highly inert elements, due to their resistance to most solvents and their high melting temperatures.

Early applications leveraged the inert chemical character of the metals. Pioneered by W. H. Wollaston, these included Pt crucibles, metal touch-holes on flintlock pistols, and sulfuric acid boilers. By the middle of the 19^{th} century, the inertness of these metals made them useful in the early electrochemical investigations of M. Faraday and his disciples. Also at about this time, the commercial uses of the PGE were aggressively promoted by P. N. Johnson and G. Matthey, founders of the Johnson Matthey corporation.

The more recent uses of the PGE are based on their catalytic properties. As noted by Hartley (1991), the nobility and catalytic abilities of these elements both stem from their large number of *d*-shell electrons. These allow for tight bonding in the metallic form. However, they also provide a range of orbital energies and symmetries for bonding with catalytic substrates. Thus, the PGE have found widespread use as automobile emission catalysts, particularly in Japan and the United States. These catalysts are now made mainly of Pt and Rh, although Pd was used in earlier designs. The catalytic properties of the PGE are also exploited in the chemical industry, where the metals are used to activate hydrogenation and dehydrogenation reactions in the manufacture of many polymers, in the oxidation of ammonia to nitric acid, and in the refining of petroleum. Modern non-catalytic applications include the use of Pt in jewelry, and in the processing of optical glass. Pt is also used in the commercial production of fiberglass, since its noble properties make it an ideal material through which to draw molten glass to produce fibers. The electronics industry has also made extensive use of these metals, due to their ability to withstand corrosion, and their low electrical resistance. One more recent application of Pt is the use of the compound cisplatin ($PtCl_2(NH_3)_2$) as an anti-tumor drug.

Ir is not dramatically superior to the other PGE in these applications, although it is the most corrosion-resistant element and, with Os, one of the two densest metals known. However, it is far less abundant than Pt or Pd. Thus, its use has been rather limited: in 1987, the commercial demand for Ir in the Western World was $\approx 10^6$ gm, compared to nearly $\approx 2 \times 10^8$ gm for the other PGE. Approximately a third of this usage is for purposes similar to the other PGE (*i.e.*, catalysts, crucibles, etc.). Ir has a unique place in the optoelectronics industry, where Yt-Al-garnet crystals are grown in Ir crucibles. It is also a constituent of the standard meter bar of Paris, which is a 90% Pt/10% Ir alloy. The destination of the remaining two thirds of commercial Ir is unknown. Hartley (1990) speculates that the high melting temperature and corrosion resistance of Ir may find specialized applications in the defense and nuclear industries, accounting for this demand.

Economic PGE deposits are found on every continent. The most productive, are the Bushveld Complex in South Africa, and the Noril'sk-Talnakh deposits in Siberia. In 1977, these accounted for > 90% of world production. In the case of the Bushveld complex, chromite and sulfide ore bodies contain 3 to 20 ppm PGE. Both of these deposits were produced by the intrusion of large basaltic magma bodies into continental crust.

1.2.2. *Rhenium*

Re has the distinction of being the last element discovered by conventional chemical methods (Emsley, 1989; Peacock, 1966). W. Noddack, I. Tacke and Berg detected the element from its X-ray spectrum in concentrates of PGE ores and in molybdenites in 1925. By 1928, a gram of this new element had been isolated, and Re became commercially available for

$10,000/gm (Linde, 1990). The chemical properties of Re metal are similar to those of the PGE (Table 1.1). Re is the fourth densest metal, after Ir, Os and Pt, and only W and C have higher melting points. Therefore, Re is widely used as a filament material in mass spectrometers, in ion gauges, and in photoflash lamps (Linde, 1990). Annual demand for Re totals $\approx 4.5 \times 10^6$ gm. Re is produced commercially from flue dusts collected during the processing of molybdenite. It is also enriched in coal (Kuznetsova, 1961), which may lead to anthropogenic introduction of Re into the environment (Colodner *et al.*, 1995).

1.3. The PGE in the Solid Earth

The PGE have a highly siderophile character in the solid Earth; these elements prefer to be alloyed with each other, or with Fe or Ni, than with either O or S. Re has the same tendency. Therefore, during accretion and differentiation of the Earth, the PGE and Re partitioned into the Fe-Ni metal phases which ultimately formed the Earth's core, leaving the crust and mantle strongly depleted in the siderophiles. This was recognized as early as 1922 by V. M. Goldschmidt (Goldschmidt, 1958), and is consistent with the enrichment of the PGE in iron meteorites and in the iron phases of chondritic meteorites (Anders and Grevesse, 1989; Larimer and Wasson, 1988; Taylor, 1988).

The abundances of the PGE in the mantle is not well understood. The PGE contents of the core and bulk Earth are inferred from meteorite observations, while the mantle composition is constrained by analyses of ultramafic rocks (Crocket, 1981). Thermodynamic models of the PGE content of the mantle cannot easily replicate the chondritic relative abundances of

these elements, or their absolute abundances (Jones and Drake, 1986; Newsom, 1990). This is referred to as the "mantle siderophile anomaly." Various models have been used to explain PGE abundances in the mantle, including the impact of a Mars-sized object following core formation. None have met with unequivocal success (a sampling of this literature includes Chyba, 1991; Hillgren *et al.*, 1994; Newsom and Sims, 1991; Rama Murthy, 1991). This remains an outstanding problem in the solid Earth sciences.

Partitioning of the PGE and Re between mantle and crust is better understood, although the mineralogical controls on this behavior are not well known. Ir, Os and Ru are highly compatible in the mantle, and therefore do not readily partition into the melts which form the crust. This produces the extreme PGE depletion of the Earth's surface, which makes Ir so useful as a tracer of exogenous material. Re, however, is somewhat less compatible. This leads to modest Re enrichments, especially in the continental crust. This fractionation of Re from the PGE (and hence, from Os) gives rise to variations in $^{187}Os/^{186}Os$ in different rocks, forming the basis of Os-isotope geochemistry. The literature on this subject was reviewed by Blum (1990).

1.4. The Ignoble Elements: PGE Solution Chemistry

While most of the early interest in the PGE was driven by their metallurgical properties, their rich coordination chemistry was no doubt evident to S. Tennant, who named the element "iridium" for the Greek *iris*, meaning "rainbow". Tennant said that this was on account of "the striking variety of colours which it gives while dissolving in marine acid" (McDonald and Hunt, 1982). He had discovered empirically that the PGE cations will readily form complexes with a variety of ligands once in dissolved form. The

presence of these complexing ligands stabilizes the cations against reduction, allowing them to remain in solution (Westland, 1981). More recent findings suggest that PGE solution chemistry can redistribute these elements in the environment (Bowles, 1986; Fuchs and Rose, 1974; Wallace *et al.*, 1990). These observations are supported by thermodynamic considerations (Mountain and Wood, 1988; Westland, 1981). Aqueous chemical processes may even produce alluvial PGE metal deposits (Cousins and Kinloch, 1976). Since Pt metal was discovered in such deposits, it is ironic that the discovery of the noble metals might have been delayed if not for their solution chemistry! As observed by Cousins and Kinloch (1976), the notion that noble metal character governs PGE distributions in the environment "appears to have been somewhat over-rated". In the realm of low-temperature geochemistry, the PGE are "ignoble".

1.4.1. *Iridium*

In aqueous solution, Ir occurs in either the Ir^{3+} or Ir^{4+} valence state. In the presence of chloride, the octahedral chlorocomplexes predominate (*i.e.*, $IrCl_6^{3-}$ and $IrCl_6^{2-}$). A mobile redox equilibrium exists between these two forms in solution (Peixoto Cabral, 1964; Poulson and Garner, 1962), and can be readily followed visually by the pale green color of $IrCl_6^{3-}$ (d^6) and the intense, red-brown color of $IrCl_6^{2-}$ (d^5). The interconversion of these species occurs spontaneously in solution according to the reaction:

$$2IrCl_6^{2-} + H_2O = 2IrCl_6^{3-} + 1/2O_2 + H_2O$$

$$K = 7 \times 10^{-8}\ atm^{1/2}\ mol^2\ L^{-2}$$

This equilibrium relationship is shown in Fig. 1.2. Conversion between the two species is readily achieved in the laboratory by acid or base titration, and is completely reversible. In natural chloride-bearing waters, the $IrCl_6^{3-}$ complex should predominate. This should be the case in seawater.

The speciation of Ir in low-salinity waters is not as clear, due to the affinity of Ir for hydroxide. The first hydroxide binding constants of a number of cations are plotted in Fig. 1.3. The value for Ir^{3+} is among the highest of the elements. This large hydroxide binding constant has important implications for Ir in natural waters. In general, the aqueous geochemistry of Ir should reflect a balance between the tendency to form chloro and hydroxy complexes (Goldberg *et al.*, 1986). Ir speciation in freshwaters should be dominated by hydroxy complexes. In the estuarine environment, mixed hydroxy-chloro compounds may be important. The affinity of cations for surfaces with O^- donor groups scales with the hydroxide binding constants (*e.g.*, Dzombak and Morel, 1990; Erel and Morgan, 1991). Thus, Ir is likely to be very reactive toward phases commonly found in natural waters, such as Fe-Mn oxyhydroxides and clay mineral surfaces. This reactivity should be most pronounced in fresh waters, where there is little competition from chloride ligands for the Ir^{3+} cation. In the oceans, slow scavenging of Ir by settling particulates or authigenic phases may be an important removal mechanism.

The affinity of the PGE for organic ligands in natural waters has been considered theoretically, and is likely to be important for Pt and Pd (Wood, 1990; Wood *et al.*, 1994). No such analysis has been done for Ir. However, Ir has a rich organometallic chemistry in the laboratory in the Ir^{1+} valence state (Cotton and Wilkinson, 1988). Additionally, Ir is taken up by marine

organisms (Wells *et al.*, 1988) and by some common plants (Dunn *et al.*, 1989). These considerations suggest that organo-Ir complexes could be important in low-temperature systems.

1.4.2. *Rhenium*

The solution chemistry of Re is straightforward. In oxidizing environments, Re is present in the heptavalent oxidation state, which forms strong bonds with oxygen. The dominant dissolved species is therefore the perrhenate anion, ReO_4^- (Brookins, 1986). This oxyanion is extremely unreactive toward other dissolved species, and should show little affinity for most surfaces at typical natural water pH values. Therefore, Re should be conservative in natural waters. The only removal process of consequence should occur in reducing environments, where insoluble Re-sulfide compounds can form.

1.5. References

Alvarez, L. W., W. Alvarez, F. Asaro, and H. V. Michel, Extraterrestrial cause for the Cretaceous-Tertiary extinction: Experimental results and theoretical interpretation, *Science*, *208*, 1095-1108, 1980.

Alvarez, W., F. Asaro, H. V. Michel, and L. W. Alvarez, Iridium anomaly approximately synchronous with terminal Eocene extinctions, *Science*, *216*, 886-888, 1982.

Alvarez, W., P. Claeys, and S. W. Kieffer, Emplacement of Cretaceous-Tertiary boundary shocked quartz from Chicxulub crater, *Science*, *269*, 930-935, 1995.

Anders, E., and N. Grevesse, Abundances of the elements: Meteoritic and solar, *Geochim. Cosmochim. Acta*, *53*, 197-214, 1989.

Blum, J. D., Geochemistry and Resonance Ionization of Platinum-Group Elements, Ph.D. thesis, pp., California Institute of Technology, 1990.

Bohor, B. F., P. J. Modreski, and E. E. Foord, Shocked quartz in the Cretaceous-Tertiary boundary clays: Evidence for a global distribution., *Science*, *236*, 705-709, 1987a.

Bohor, B. F., E. E. Rord, and R. Ganapathy, Magnesioferrite from the Cretaceous/Tertiary boundary, Caravaca, Spain, *Earth Planet. Sci. Lett.*, *81*, 57-66, 1987b.

Bowles, J. F. W., The development of platinum-group minerals in laterites, *Econ. Geol.*, *81*, 1278-1285, 1986.

Brookins, D. G., Rhenium as analog for fissiogenic technetium: Eh-pH diagram (25°C, 1 bar) constraints, *Appl. Geochem.*, *1*, 513-517, 1986.

Cabri, L. J., editor, *Platinum-Group Elements: Mineralogy, Geology, Recovery*, Canadian Institute of Mining and Metallurgy, Montreal, 1981.

Chapman, C. R., and D. Morrison, Impacts on the Earth by asteroids and comets: assessing the hazard, *Nature*, *367*, 33-40, 1994.

Chyba, C. F., Terrestrial mantle siderophiles and the lunar impact record, *Icarus*, *92*, 217-233, 1991.

Colodner, D., J. Edmond, and E. Boyle, Rhenium in the Black Sea: comparison with molybdenum and uranium, *Earth and Planet. Sci. Lett.*, *131*, 1-15, 1995.

Colodner, D. C., The Marine Geochemistry of Rhenium, Iridium and Platinum, Ph.D. Thesis, MIT/WHOI, WHOI-91-30, 1991.

Colodner, D. C., E. A. Boyle, J. M. Edmond, and J. Thomson, Postdepositional mobility of platinum, iridium and rhenium in marine sediments, *Nature*, *358*, 402-404, 1992.

Cotton, F. A., and G. Wilkinson, *Advanced Inorganic Chemistry-5th edition*, J. Wiley & Sons, New York, 1988.

Cousins, C. A., and E. D. Kinloch, Some observations on textures and inclusions in alluvial platinoids, *Econ. Geol.*, *71*, 1377-1398, 1976.

Creaser, R. A., D. A. Papanastassiou, and G. J. Wasserburg, Negative thermal ion mass spectrometry of osmium, rhenium, and iridium, *Geochim. Cosmochim. Acta*, *55*, 397-401, 1991.

Crocket, J. H., Geochemistry of the platinum-group elements, in *Platinum-Group Elements: Mineralogy, Geology, Recovery*, edited by L. J. Cabri, pp. 47-64, Canadian Institute of Mining and Metallurgy, Montreal, 1981.

Crocket, J. H., and L. J. Cabri, Analytical methods for the Platinum-Group Elements, in *Platinum Group Elements: Mineralogy, Geology, Recovery*, edited by L. J. Cabri, Canadian Institute of Mining and Metallurgy, Montreal, 1981.

Crocket, J. H., and H. Y. Kuo, Sources for gold, palladium and iridium in deep-sea sediments, *Geochim. Cosmochim. Acta*, *43*, 831-842, 1979.

Dunn, C. E., G. E. M. Hall, and E. Hoffman, Platinum group metals in common plants of northern forests: Developments in analytical methods, and the application of biogeochemistry to exploration strategies, *J. Geochem. Explor.*, *32*, 211-222, 1989.

Dzombak, D., and F. M. M. Morel, *Surface Complexation Modeling*, John Wiley & Sons, New York, 1-393, 1990.

Emsley, J., *The Elements*, Oxford University Press, Oxford, 1989.

Erel, Y., and J. J. Morgan, The effect of surface reactions on the relative abundances of trace metals in deep-ocean water, *Geochim. Cosmochim. Acta*, *55*, 1991.

Esser, B. K., and K. K. Turekian, The osmium isotopic composition of the continental crust, *Geochim. Cosmochim. Acta*, *57*, 3093-3104, 1993.

Farley, K. A., Cenozoic variations in the flux of interplanetary dust recorded by He-3 in a deep-sea sediment, *Nature*, *376*, 153-156, 1995.

Farley, K. A., and D. B. Patterson, A 100-kyr periodicity in the flux of extraterrestrial He-3 to the sea-floor, *Nature*, *378*, 600-603, 1995.

Fenner, F. D., and B. J. Presley, Iridium in Mississippi River suspended matter and Gulf of Mexico sediment, *Nature*, *312*, 260-262, 1984.

Fuchs, W. A., and A. W. Rose, The geochemical behavior of platinum and palladium in the weathering cycle in the Stillwater Complex, Montana, *Econ. Geol.*, *69*, 332-346, 1974.

Ganapathy, R., A major meteorite impact on the Earth 65 million years ago: Evidence from the Cretaceous-Tertiary boundary clay, *Science*, *209*, 921-923, 1980.

Goldberg, E. D., V. Hodge, P. Kay, M. Stallard, and M. Koide, Some comparative marine chemistries of platinum and iridium, *Appl. Geochem.*, *1*, 227-232, 1986.

Goldberg, E. D., M. Koide, J. S. Yang, and K. K. Bertine, Comparative marine chemistries of platinum group metals and their periodic table neighbors, in *Metal Speciation: Theory, Analysis, and Application*, edited by J. R. Kramer and H. E. Allen, pp. 201-217, Lewis Publishers, Inc., Chelsea, MI, 1988.

Goldschmidt, V. M., Group VIII(2): Platinum metals, in *Geochemistry*, edited by A. Muir, Clarendon Press, Oxford, 1958.

Hartley, F. R., editor, *Chemistry of the Platinum Group Metals: Recent Developments*, Elsevier Scientific Publishers B. V., Amsterdam, 1991.

Hildebrand, A. R., G. T. Penfield, D. A. Kring, M. Pilkington, C. Z. Antonio, S. B. Jacobsen, and W. V. Boynton, Chicxulub Crater: A possible Cretaceous/Tertiary boundary impact crater on the Yucatán Peninsula, Mexico, *Geology*, *19*, 867-871, 1991.

Hillgren, V. J., M. J. Drake, and D. C. Rubie, High-pressure and high-temperature experiments on core-mantle segregation in the accreting Earth, *Science*, *264*, 1442-1445, 1994.

Izett, G. A., Tektites in Cretaceous-Tertiary boundary rocks on Haiti and their bearing of the Alvarez impact extinction hypothesis, *J. Geophys. Res.*, *96*, 20879-20905, 1991.

Jones, J. H., and M. J. Drake, Geochemical constraints on core formation in the Earth, *Nature*, *322*, 221-228, 1986.

Keller, G., E. Barrera, B. Schmitz, and E. Mattson, Gradual mass extinction, species survivorship, and long-term environmental changes across the Cretaceous-Tertiary boundary in high latitudes, *Geol. Soc. Am. Bull.*, *105*, 979-997, 1993.

Keller, G., W. Stinnesbeck, and J. G. Lopezoliva, Age, deposition and biotic effects of the Cretaceous-Tertiary boundary event at Mimbral, NE Mexico, *Palaios*, *9*, 144-157, 1994.

Koide, M., E. D. Goldberg, S. Niemeyer, D. Gerlach, V. Hodge, K. K. Bertine, and A. Padova, Osmium in marine sediments, *Geochim. Cosmochim. Acta*, *55*, 1641-1648, 1991.

Kuznetsova, V. V., Determination of rhenium in coal, *Zhurnal Analiticheskoi Khimii*, *16*, 736-737, 1961.

Kyte, F. T., J. Smit, and J. T. Wasson, Siderophile interelement variations in the Cretaceous-Tertiary boundary sediments from Caravaca, Spain, *Earth Planet. Sci. Lett.*, *73*, 183-195, 1985.

Kyte, F. T., Z. Zhou, and J. T. Wasson, Siderophile-enriched sediments from the Cretaceous-Tertiary boundary, *Nature*, *288*, 651-656, 1980.

Larimer, J. W., and J. T. Wasson, Siderophile-element fractionation, in *Meteorites and the Early Solar System*, *Space Science Series*, edited by J. F. Kerridge and M. S. Matthews, pp. 416-435, The University of Arizona Press, Tucson, 1988.

Linde, D. R., *CRC Handbook of Chemistry and Physics- 71st edition*, CRC Press, Inc., Boca Raton, 1990.

Macleod, N., and G. Keller, Comparative biogeographic analysis of planktonic foraminiferal survivorship across the Cretaceous/Tertiary (K/T) boundary, *Paleobiol.*, *20*, 143-177, 1994.

Matthews, R., A rocky watch for Earthbound asteroids, *Science*, *255*, 1204-1205, 1992.

McDonald, D., and L. B. Hunt, *A History of Platinum and its Allied Metals*, Johnson Matthey, London, 1982.

Mountain, B. W., and S. A. Wood, Chemical controls on the solubility, transport, and deposition of platinum and palladium in hydrothermal solutions: a thermodynamic approach, *Econ. Geol.*, *83*, 492-510, 1988.

Newsom, H. E., in *Origin of the Earth*, edited by H. E. Newsom and J. H. Jones, pp. 273-288, Oxford University Press, New York, 1990.

Newsom, H. E., and K. W. W. Sims, Core formation during early accretion of the Earth, *Science*, *252*, 926-933, 1991.

Orth, C. J., M. Attrep, and X. Y. Mao, Iridium abundance maxima in the upper Cenomanian extinction interval, *Geophys. Res. Lett.*, *15*, 346-349, 1988a.

Orth, C. J., J. S. Gilmore, J. D. Knight, C. L. Pillmore, R. H. Tschudy, and J. E. Fassett, An iridium abundance anomaly at the palynological Cretaceous-Tertiary boundary in northern New Mexico, *Science*, *214*, 1341-1343, 1981.

Orth, C. J., L. R. Quintana, J. S. Gilmore, J. E. Barrick, J. N. Haywa, and S. A. Spesshardt, Pt-group metal anomalies in the Lower Mississippian of southern Oklahoma, *Geology*, *16*, 627-630, 1988b.

Peacock, R. D., *The Chemistry of Rhenium and Technetium*, Elsevier Publishing Company, Amsterdam, 1966.

Pegram, B. J., B. K. Esser, S. Krishnaswami, and K. K. Turekian, The isotopic composition of leachable osmium from river sediments, *Earth Planet. Sci. Lett.*, *128*, 591-599, 1994.

Pegram, W. J., S. Krishnaswami, G. Ravizza, and K. K. Turekian, The record of sea water $^{187}Os/^{186}Os$ variation through the Cenozoic, *Earth Planet. Sci. Lett.*, *113*, 569-576, 1992.

Peixoto Cabral, J. M., Radiochemical processes in iridium complexes, *J. Inorg. Nucl. Chem.*, *26*, 1657-1669, 1964.

Peucker-Ehrenbrink, B., G. Ravizza, and A. W. Hofmann, The marine $^{187}Os/^{186}Os$ record of the past 80 million years, *Earth Planet. Sci. Lett.*, *130*, 155-167, 1995.

Playford, P. E., D. J. McLaren, C. J. Orth, J. S. Gilmore, and W. D. Goodfellow, Iridium anomaly in the Upper Devonian of the Canning Basin, Western Australia, *Science*, *226*, 437-439, 1984.

Poulson, I. A., and C. S. Garner, A thermodynamic and kinetic study of hexachloro and aquopentachloro complexes of iridium(III) in aqueous solutions, *J. Amer. Chem. Soc.*, *84*, 2032, 1962.

Rama Murthy, V., Early differentiation of the Earth and the problem of mantle siderophile elements: A new approach, *Science*, *253*, 303-306, 1991.

Rampino, M. R., and K. Caldeira, Major episodes of geologic change: correlations, time structure and possible causes, *Earth Planet. Sci. Lett.*, *114*, 215-227, 1993.

Raup, D. M., *The Nemesis Affair: A Story of the Death of Dinosaurs and the Ways of Science*, Norton, New York, 1-224, 1987.

Raup, D. M., and J. J. J. Sepkoski, Periodicity of extinctions in the geologic past, *Proc. Natl. Acad. Sci.*, *81*, 801-805, 1984.

Ravizza, G., and G. McMurtry, Osmium isotopic variations in metalliferous sediments from the East Pacific Rise and the Bauer Basin, *Geochim. Cosmochim. Acta*, *57*, 4301-4310, 1993.

Ravizza, G., K. K. Turekian, and B. J. Hay, The geochemistry of rhenium and osmium in recent sediments from the Black Sea, *Geochim. Cosmochim. Acta*, *55*, 3741-3752, 1991.

Reichhardt, T., Congress directs NASA to plan an asteroid hunt, *Nature*, *370*, 407, 1994.

Reston, J. J., Collision course, *Time*, *143*, 54-62, 1994.

Sepkoski, J. J. J., Phanerozoic overview of mass extinction, in *Pattern and Process in the History of Life*, edited by D. M. Raup and D. Jablonski, pp. 277-295, Springer, Berlin, 1986.

Smit, J., and J. Hertogen, An extra-terrestrial event at the Cretaceous-Tertiary boundary, *Nature*, *285*, 198-200, 1980.

Swisher, C. C. I., J. M. Grajales-Nishimura, A. Montanari, S. V. Margolis, P. Claeys, W. Alvarez, P. Renne, E. Cedillo-Pardo, F. J.-M. R. Maurrasse, G. H. Curtis, J. Smit, and M. O. McWilliams, Coeval $^{40}Ar/^{39}Ar$ ages of 65.0

million years ago from Chicxulub crater melt rock and Cretaceous-Tertiary boundary tektites, *Science*, *257*, 1992.

Taylor, S. R., Planetary compositions, in *Meteorites and the Early Solar System*, edited by J. F. Kerridge and M. S. Matthews, pp. 512-534, The University of Arizona Press, Tucson, 1988.

Völkening, J., T. Walczyk, and K. G. Heumann, Osmium isotope ratio determinations by negative thermal ionization mass spectrometry, *Intl. J. Mass Spectrom. Ion Proc.*, *105*, 147-159, 1991.

Wallace, M. W., V. A. Gostin, and R. R. Keays, The Acraman impact ejecta and host shales: Evidence for low-temperature mobilization of iridium and other platinoids, *Geology*, *18*, 132-135, 1990.

Wells, M. C., P. N. Boothe, and B. J. Presley, Iridium in marine organisms, *Geochim. Cosmochim. Acta*, *52*, 1737-1739, 1988.

Westland, A. D., Inorganic chemistry of the platinum-group elements, in *Platinum-Group Elements: Mineralogy, Geology, Recovery*, vol. 23, edited by L. J. Cabri, Canadian Institute of Mining and Metallurgy, Montreal, 1981.

Wood, S. A., The interaction of dissolved platinum with fulvic acid and simple organic acid analogues in aqueous solutions, *Can. Min.*, *28*, 665-673, 1990.

Wood, S. A., C. D. Tait, and D. Vlassopoulos, Solubility and spectroscopic studies of the interaction of palladium with simple carboxylic-acids and fulvic-acid at low-temperature, *Geochim. Cosmochim. Acta*, *58*, 625-637, 1994.

Zeininger, H., Ph.D. Thesis, University of Regensburg, 1984.

Table 1.1. Some Properties of the PGE and Re.

	Os	Ir	Pt	Ru	Rh	Pd	Re
Atomic number:	76	77	78	44	45	46	75
Atomic mass (amu):	190.2	192.2	195.1	101.1	102.9	106.4	186.2
Atomic radius (10^{-12} m):	135.0	135.7	138.0	134.0	134.5	137.6	137.0
Melting point (K):	3327	2683	2045	2583	2239	1825	3453
Boiling point (K):	5300	4403	4100	4173	4000	3413	5900
ΔH_{vap} (kJ mol^{-1}):	738	612	469	567	494	362	704
Density (kg m^{-3}):	22,590	22,420	21,450	12,370	12,410	12,020	21,020
Electrical resistivity (10^{-8} Ω m):	8.12	5.3	10.6	7.6	4.51	10.8	19.3
Thermal conductivity @ 300 K (W m^{-1} K^{-1}):	87.6	147	71.6	117	150	71.8	47.9
ΔE, M -> M^+ (kJ mol^{-1}):	840	880	870	711	720	805	760
ΔE, M -> M^- (kJ mol^{-1}):	106	151	205.3	101	109.7	53.7	14
Electronegativity (Pauling):	2.20	2.20	2.28	2.20	2.28	2.20	1.90

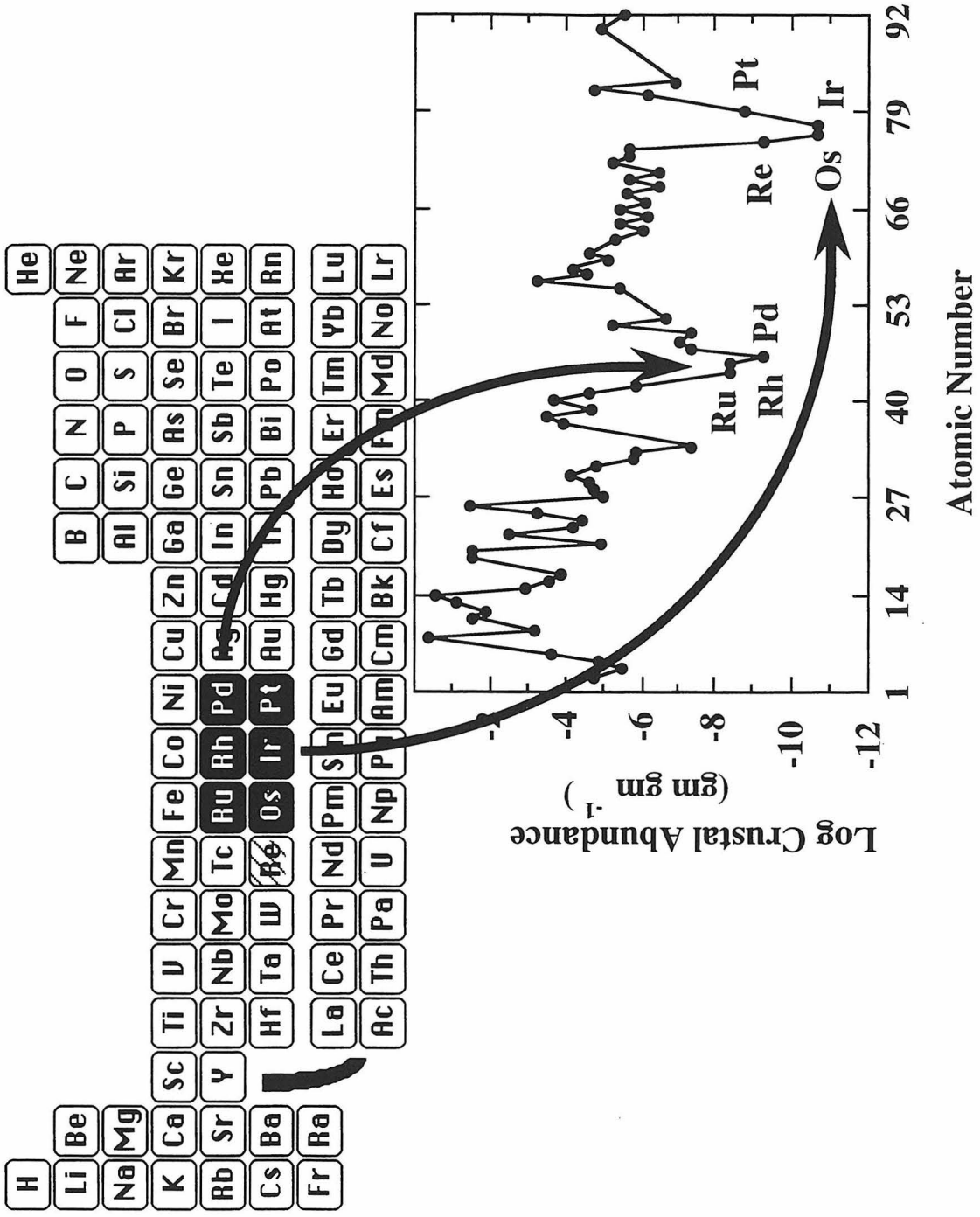

Fig. 1.1. The Platinum Group Elements (PGE) in the Periodic Table, and their abundances in average continental crust.

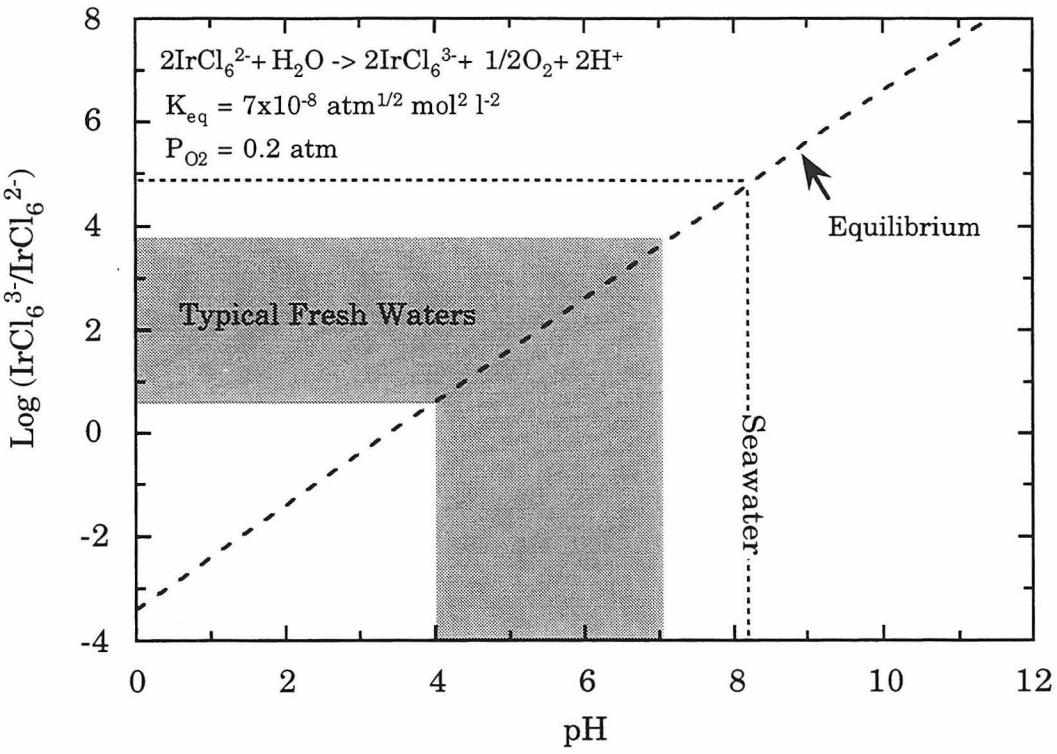

Fig. 1.2. The oxidation state of Ir in the presence of chloride, as a function of pH. The pH of seawater and of typical fresh waters are indicated. K_{eq} is from Cotton and Wilkinson (1988).

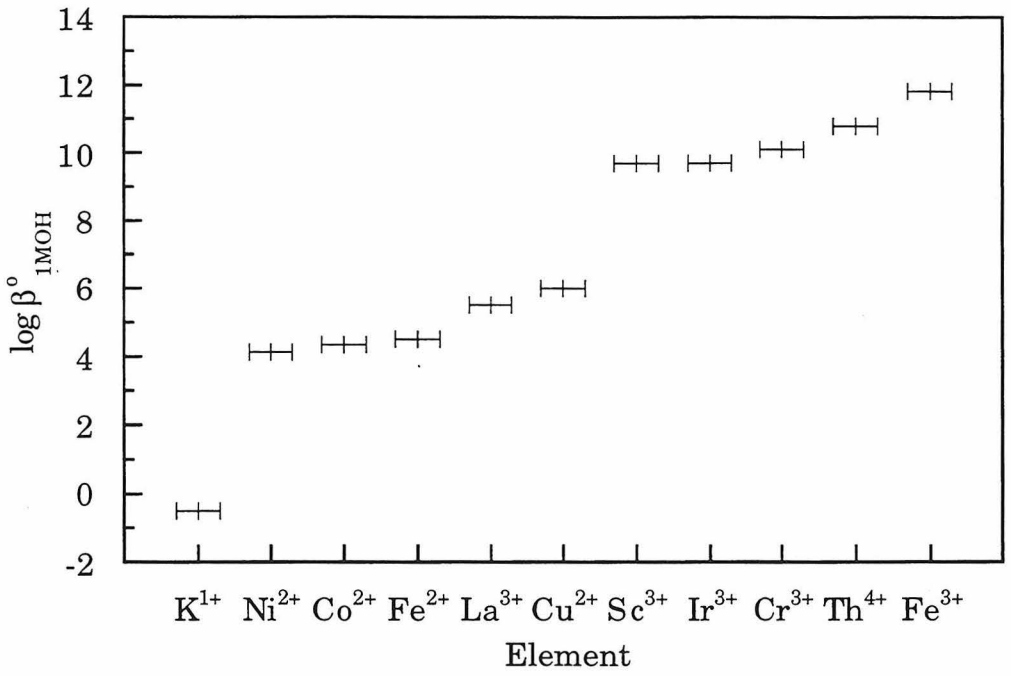

Fig. 1.3. The first hydroxide binding constants, β^{o}_{1MOH}, for an array of cations.

Chapter 2.

Rhenium in Seawater I: Confirmation of Generally Conservative Behavior

The following chapter consists of a published study (Anbar *et al.*, 1992), and an unpublished appendix which discusses analytical details.

2.1. Abstract

A depth profile of the concentration of rhenium was measured in the Pacific Ocean, using a technique we have developed for the clean chemical separation and the precise measurement of Re by isotope dilution and negative thermal ionization mass spectrometry (ID-NTIMS). This technique permits Re concentrations to be determined from 200 mL of seawater with a typical precision of ± 5‰. This is an improvement of at least a factor of 100 over the techniques used in previously published determinations of Re in seawater. We obtain a narrow range for Re from 7.20 ± 0.03 to 7.38 ± 0.03 ng kg^{-1} for depths between 45 m and 4700 m. This demonstrates that Re is relatively well-mixed throughout the water column and confirms the theoretical prediction that the behavior of Re in the oceans is conservative. When examined in detail, both salinity and the concentration of Re increase by approximately 1.5% between 400 and 4700 m, a correlation consistent with conservative behavior. However, Re appears to be depleted relative to salinity by 1.0 - 1.5% at 100 m, and enriched by approximately 4% at the surface. These observations suggest a minor level of Re scavenging in near surface waters, and an aeolian contribution of Re to the ocean surface. This work demonstrates the utility of ID-NTIMS for geochemical investigation of certain trace elements that have not previously been amenable to detailed study.

2.2. Introduction

The geochemistry of the Platinum Group Elements (PGE) and their periodic table neighbors is poorly understood, despite increasing interest in recent years in the use of these elements as isotopic and elemental tracers, and for geochronometry. This problem is particularly acute in the marine environment, where the surface abundances of Os, Ir, Ru and Rh are poorly constrained, and their depth profiles are unknown. Depth profiles have been measured for Pt, Pd and Re (*e.g.,* Pt: Goldberg *et al.*, 1986; Jacinto and van den Berg, 1989; Koide *et al.*, 1987; Pd: Lee, 1983; Re: Matthews and Riley, 1970; Olafsson and Riley, 1972) but these data have raised as many questions as they have answered. For example, the studies of the marine distribution of Pt have each yielded a different trend with depth. The cause of these differences is undetermined.

Uncertainty has also surrounded the marine geochemistry of Re. The concentration of Re in oxygenated seawater is expected to be fairly uniform with depth, as the stable form of Re in these waters should be the perrhenate anion, ReO_4^- (Brookins, 1986; Bruland, 1983). Thus the behavior of Re should be conservative in seawater. This expectation is consistent with the apparent enrichment of Re in seawater relative to its periodic table neighbors (Koide *et al.*, 1987), which suggests that Re has an extremely long residence time in the oceans (Goldberg *et al.*, 1988). However, the published measurements of the concentration of rhenium in seawater indicate a range of approximately 3 to 11 ng kg^{-1} (Koide *et al.*, 1987; Matthews and Riley, 1970; Olafsson and Riley, 1972; Scadden, 1969). These variations probably reveal a lack of precision and sensitivity in the analytical methods used, so

that the content of Re in seawater is determined by these data to no better than a factor of three.

Our understanding of the geochemistry of Re and the PGE is limited largely by their low abundances and, until recently, the lack of analytical techniques which are sensitive, precise and accurate enough to obtain reliable abundance measurements. The application of NTIMS to these elements (Creaser *et al.*, 1991; Delmore, 1987; Heumann, 1988; Völkening *et al.*, 1991; Zeininger, 1984) introduced a highly sensitive new tool for their study. In order to resolve the problem of the Re concentration of seawater and its distribution with depth, we have applied ID-NTIMS to the study of Re in a Pacific Ocean profile.

2.3. Sampling and Analysis

Seawater samples were collected in January 1992, on the HOT-33 cruise (R/V "Wecoma") at Station Aloha, approximately 100 km north of Oahu (22°N; 158°W). Nine samples were collected using PVC Niskin bottles with Teflon-coated internal springs, lowered on a steel cable. One sample (at 45 m) was collected using a Go-Flo bottle on a Kevlar line. Pressure, temperature, conductivity and dissolved oxygen were monitored continuously using a conductivity-temperature-depth probe (CTD) and an oxygen sensor (Karl and Winn, 1991). The depth, salinity and oxygen data reported in this study were derived from the CTD and oxygen sensor data (Table 2.1; D. Karl and R. Lukas, personal communication). After recovery, all samples were filtered within 48 hours through 0.2 μm nitrocellulose filters using a peristaltic pump, then acidified by adding 2 mL of 12 N HCl to each liter of

seawater, and stored in acid-washed high density polyethylene bottles for later analysis.

Accurately weighed 200 mL fractions from all samples, except for the 6 m sample, were spiked with a ^{185}Re-enriched tracer solution approximately 3 months after collection. The 6 m sample was spiked aboard ship, following filtration and acidification. In all spiked solutions, the measured $^{185}Re/^{187}Re$ ratio was close to the optimal value needed to minimize the error propagation factor. After the addition of the tracer, the solutions were periodically shaken and stirred over 24 - 48 hours, which was deemed sufficient time for complete equilibration of the Re isotopes, since Re is presumed to be present as ReO_4^- in both samples and tracer. The Re tracer was prepared by dissolving ^{185}Re-enriched metal (Oak Ridge National Laboratory) in 16 N HNO_3 and diluting to 1 N with ultrapure water. Two dilutions of this stock solution were prepared. Dilution 1 (Dil-1) was used to spike the 6 m sample aboard ship, and a 2800 m fraction in the lab. Dilution 2 (Dil-2) was used for the other samples spiked in the laboratory. The concentration of ^{185}Re in both of these tracer solutions was determined by calibration against a gravimetrically-prepared standard solution of isotopically normal, high purity Re metal (Johnson Matthey). The isotopic composition of the tracer solutions was determined by NTIMS in our laboratory ($^{185}Re/^{187}Re = 37.14 \pm 0.04$), and the isotopic composition of the standard solutions and natural samples is assumed to be $^{185}Re/^{187}Re = 0.5974 \pm 0.0004$ (Gramlich *et al.*, 1973). The isotopic composition of Re standard solutions determined by NTIMS in our laboratory (0.5976 ± 0.0003) is identical to the isotopic abundance ratio determined by Gramlich *et al.* (1973), using carefully controlled procedures.

Rhenium was separated from the seawater samples by anion exchange chromatography using two small Teflon columns (*e.g.,* Huffman *et al.*, 1956). Primary separation utilized 200 μL Bio-Rad AG1-X8, 100-200 mesh resin, onto which ReO_4^- was adsorbed directly from the spiked, acidified seawater. The column was rinsed with 10 mL ultrapure H_2O, followed by 650 μL 4 N HNO_3 to remove Mo and W. These elements are both present as oxyanions in seawater at higher concentrations than Re. Rhenium was then eluted with 2 mL 4 N HNO_3. The resulting solution was evaporated to a small drop at 70 - 80 °C under N_2, and passed through a second column with 5 - 10 μL of resin to purify Re further and to reduce the small amount of organic residue remaining from the first column. This entire separation procedure had a yield of 90%, determined by isotope dilution analysis of a known amount of Re that was passed through the chemistry. The chemical blanks were in the range 2 - 5 pg. For all the data reported below, the quantity 3.5 pg was subtracted from the quantity of sample Re that was determined to be present by isotope dilution analysis. Since approximately 1.5 ng of Re was typically separated from the seawater aliquots, the resulting blank correction was less than 3‰ of the total sample Re present. This is smaller than the total uncertainty of the analytical procedure (see below).

The chemically separated Re was loaded using polyethylene tubing on a microsyringe, onto a high purity Pt filament on which Ba had been loaded as $BaSO_4$ (used to enhance negative ion emission), and analyzed in a Lunatic mass spectrometer configured for negative ions (Creaser *et al.*, 1991; Wasserburg *et al.*, 1969). When prepared as a fine precipitate, $BaSO_4$ forms an even coat on the filament, on which the sample may be easily loaded. The $BaSO_4$ was found to provide a reproducible and efficient method of obtaining

a higher ionization efficiency for both samples and standards than was possible using other Ba salts, such as $Ba((NO)_3)_2$ or $Ba(OH)_2$ (Creaser *et al.*, 1991; Heumann, 1988). The ionization efficiency for Re standards was 20%. The ionization efficiency was lower for separated samples due to the presence of organic material in the final load, and ranged from 1 to 10% for the samples analyzed in this study.

Re was analyzed as ReO_4^- at masses 249 and 251, and the ion intensity at 251 was corrected for the contribution from $^{185}Re^{16}O_3{}^{18}O^-$ using $^{18}O/^{16}O$ = 0.002085 to obtain the ratio $^{185}Re/^{187}Re$. This $^{18}O/^{16}O$ ratio has been measured directly for normal Re, using the $^{187}ReO_4^-$ ion beams (Creaser *et al.*, 1991). The contribution from $^{187}Re^{17}O_2{}^{16}O_2^-$ at mass 251 is negligible. When running seawater samples, ion currents corresponding to 10^7 - 10^8 counts per second (cps; 0.16 - 1.6×10^{-11} A) at masses 249 and 251 were routinely sustained for 30 - 40 minutes on a Faraday collector, at filament temperatures of 840 - 890 °C, as determined by an optical pyrometer.

To determine the level of the ion current due to background contamination, $BaSO_4$ was loaded on a filament without any sample or tracer. Ion currents corresponding to 10^3 - 10^4 cps at mass 251 were measured over the temperature range 840 - 890 °C. This current increased with increasing filament temperature, but was fairly constant over time when the temperature was not varied. The ratio $^{185}Re/^{187}Re$ measured in this experiment was indistinguishable from that of normal Re.

In order to establish the level of the filament blank under controlled conditions, we loaded 36 pg of Re tracer on a Pt filament with $BaSO_4$, and obtained a stable signal at mass 249 equivalent to $\approx 10^6$ cps, at a filament temperature of 850 °C. The initial $^{185}Re/^{187}Re$ measured was 33.4,

corresponding to a blank equivalent to 0.17 pg of normal Re from the filament. The run was continued at constant temperature until approximately 3% of the initially loaded Re tracer had been ionized and detected (determined by integration of the ion beam intensities over time). If a constant, but initially unknown, blank contribution to the measured ion beams is assumed, then the data from this experiment can be used to determine the magnitude of the blank contribution. This contribution corresponds to $\approx 5 \times 10^3$ cps at mass 251.

The Re blank contributions determined from these two experiments are in general agreement. It follows that for our current generation of "clean" Pt filaments, the background current, using $BaSO_4$ as the emitter, corresponds to 10^3 - 10^4 cps at mass 251. This low level of Re blank has broad applicability in Re-Os geochemical studies.

During analyses of seawater samples, the observed drift in the measured ratios led to a typical uncertainty in these ratios of less than ± 1.5‰ amu^{-1}, consistent with mass dependent isotope fractionation associated with sample depletion. No other drift was observed (*e.g.*, as would be obtained from a variable filament blank), even when beam intensities were increased by an order of magnitude under different operating conditions. Replicate analyses of samples at 6 m, 402 m, and 2800 m were in agreement to ± 3‰ (Table 2.1), consistent with this source of uncertainty. The close agreement of the two 2800 m fractions, spiked with different tracer solutions, indicates that the calibrations of the Dil-1 and Dil-2 tracer solutions are well within the analytical uncertainties.

An uncertainty propagation calculation was made for each sample, including the uncertainties in all gravimetric measurements, as well as the

uncertainties in the concentration and isotopic composition of the Re tracer solution, and the uncertainty in the isotopic composition of natural Re. An uncertainty of ± 3‰ was assigned to the measured isotopic ratio of each spiked sample, due to the mass-fractionation uncertainty discussed above. An uncertainty of ± 50% was assigned to the 3 pg chemical blank. The cumulative uncertainties from these sources (at 95% confidence) are reported in Table 2.1, and were typically within ± 5‰. This is consistent with mass fractionation as the primary source of uncertainty for most samples.

2.4. Results and Discussion

The results are shown in Table 2.1. The Re concentrations are presented both as direct determinations, and on a salinity-normalized basis (normalized Re, $Re_N = Re_{sample}$ x 35/sample salinity). A comparison of the depth profile determined in this study with the Pacific Ocean profiles of Koide *et al.* (1987) is shown in Fig. 2.1. In contrast to the previous studies, our data clearly demonstrate that the concentration of Re is essentially constant with depth, and that the chemistry of Re is generally conservative, as was predicted on thermodynamic grounds (Brookins, 1986; Bruland, 1983). This result is consistent with the less precise recent measurements using isotope dilution-inductively coupled plasma mass spectrometry (ICP-MS), which yield marine profiles that are uniform with depth to within ± 4% (Colodner, 1991).

The consistency of our data is a significant improvement over the previous measurements of Re in seawater. Our best estimate of the average Re concentration of seawater is 7.31 ± 0.11 ng kg^{-1}, or 7.42 ± 0.04 ng kg^{-1} on a salinity-normalized basis. These values were obtained by averaging all the

data below 400 m, where the salinity-normalized Re concentrations are most uniform. The uncertainties are ± 2σ of the data used to calculate the averages. The samples from depths shallower than 400 m appear to deviate somewhat from conservative behavior, but it is not clear whether these deviations represent actual variations in the concentration of Re in the water column (see below, and Fig. 2.2). Thus, these measurements are omitted from the best estimate. Table 2.2 compares our best estimate of the concentration of Re in seawater with the corresponding estimates from other studies. Our determination is within the wide range of the analyses of Scadden (1969), Matthews and Riley (1970) and Koide *et al.* (1987), but is substantially higher than the value from the Atlantic Ocean study of Olafsson and Riley (1972). As suggested by Koide *et al.* (1987), we suspect that the uncertainties in these earlier studies are due, in large part, to variability in the yields of the chemical separation of Re from seawater. A systematically low yield could also explain the shift between our average value and that of Olafsson and Riley (1972). Since, in our isotope dilution analyses, the tracer was added prior to chemical separation, yield uncertainties were not a source of error, as long as the sample and tracer isotopes equilibrated. The reproducibility of our data provide support that this was the case.

Our average seawater value is significantly lower than the best estimate by Colodner (1991) of 8.19 ± 0.37 ng kg^{-1}, reported on a salinity normalized basis with 2σ uncertainty. There appears to be a systematic offset between our data and those of Colodner (1991). This discrepancy may in part be due to the fact that the results of this study are based on filtered seawater samples, as compared to the unfiltered samples used by Colodner

(1991). For example, Krishnaswami *et al.* (1981) and Cochran *et al.* (1983, 1990) have shown that a significant fraction of the ^{210}Pb in seawater is bound to particles. This is true for many trace elements (*e.g.,* Bruland, 1983; Whitfield and Turner, 1987). However, if this mechanism alone were to account for the discrepancy between the data sets, it would indicate a much greater reactivity of Re than is implied by the general uniformity of Re concentrations with depth. Further work is needed to determine the source of the discrepancy, and whether differences in acidification or storage procedures are important.*

It should be noted that some of the previous studies included data from several locations (see Table 2.2). Thus, some of their variability could have been due to real geographical variations in the Re content of seawater. We believe such variability is unlikely, however, due to the apparently conservative behavior of Re, as illustrated in Fig. 2.1, and because, for the less precise earlier work, there appears to be as much variability within a depth profile at one location as there is between samples collected at different sites (see especially Koide *et al.*, 1987).

The precision of our data allows detail in the Re profile to be resolved for the first time. The Re concentration decreases from a value of 7.34 ± 0.04 ng kg^{-1} at 4705 m to an average value of 7.22 ± 0.04 at 402 m, and then rises to an average of 7.69 ± 0.07 at 6 m (Fig. 2.2a). The decrease in the Re concentration between 4705 and 402 m is comparable to the percent decrease in salinity over the same depth range (≈ 1.5%), which is consistent with conservative behavior. However, at 100 m, the Re concentration does not

* This discrepancy has since been traced to an error in the calibration of the ^{185}Re spike used for the ICP-MS study (Colodner *et al.*, 1995).

exceed the deep-water value, although there is a pronounced salinity maximum at this depth. A good correlation with salinity should be reflected in a Re concentration of ≈ 7.4 ng kg^{-1} at 100 m (Fig. 2.2b). Although the sampling was not ideally spaced at these depths, this predicted value is nearly 1.0 - 1.5% higher than the average of the measured values at 100 m, and, therefore, should be detectable well within our analytical uncertainty. The salinity-normalized data suggest that the 51 m sample may also be somewhat depleted in Re relative to the deep waters, although this variation is within the uncertainties of the measurements. The surface enrichment is reflected only in the 6 m sample, and persists in the salinity-normalized data. The measured Re concentration at the surface is ≈ 4% higher than the average of the other samples, which is well above the analytical uncertainties.

These observations suggest that while the behavior of Re is essentially conservative, its distribution may be modified by two types of processes. The first process is a slight depletion due to biological or inorganic scavenging near the surface, and subsequent regeneration at depth; this mechanism could account for the apparent depletion at 100 m. The second process is an input of possibly anthropogenic Re to the ocean surface, probably via the atmosphere, which could be reflected in the surface Re enrichment. This mechanism is analogous to that observed for lead (Schaule and Patterson, 1981).

The interpretation of small variations in the Re concentration calls for caution, however, due to potential problems of Re contamination during sample collection, or removal of dissolved Re from solution during sample storage. Although the possibility of contamination cannot be ruled out,

particularly for samples from shallow depths, the fact that the samples from 45 and 51 m are identical within errors, despite being collected using different types of sampling equipment, indicates that there was little or no Re contamination from the sampling procedure itself. As for Re removal during storage, it is possible that a small, but detectable, quantity of Re was lost due to adsorption on the walls of the polyethylene bottles, or reduction of ReO_4^- following addition of HCl to these samples (Cotton and Wilkinson, 1988). This interpretation would demand that a nearly constant amount of Re was lost from most of the samples, to account for the uniformity of the salinity-normalized values below 402 m. Although this seems unlikely, it could account for the apparent enrichment of the 6 m sample, which was spiked aboard ship soon after sample collection, as well as the non-conservative behavior of the 100 m sample. Clearly, further work is needed to ascertain the importance of such sample collection and storage processes before these data are interpreted to the limits of the analytical precision.

These problems notwithstanding, our data confirm that Re is among the more conservative of elements in seawater, as exemplified by its relatively constant concentration with depth. These results also demonstrate that the refined chemical techniques described above, coupled to the ID-NTIMS technique, have the potential to improve substantially our understanding of the geochemistry of trace elements previously studied only with difficulty. We are currently extending this approach to the study of several platinum group elements in seawater.

2.5. Acknowledgments

The authors are grateful to D. Karl, R. Lukas, C. Winn, D. Hebel and the captain and crew of the R/V "Wecoma" for assistance in sample collection and analysis. D. Karl and R. Lukas kindly provided unpublished data from the HOT-33 cruise. We appreciate the helpful comments of K. K. Turekian and a second, anonymous reviewer.

2.6. References

Anbar, A. D., R. A. Creaser, D. A. Papanastassiou, and G. J. Wasserburg, Rhenium in seawater: Confirmation of generally conservative behavior, *Geochim. Cosmochim. Acta*, *56*, 4099-4103, 1992.

Brookins, D. G., Rhenium as analog for fissiogenic technetium: Eh-pH diagram (25°C, 1 bar) constraints, *Appl. Geochem.*, *1*, 513-517, 1986.

Bruland, K. W., Trace elements in sea-water, in *Chemical Oceanography*, vol. 8, edited by J. P. Riley and R. Chester, pp. 157-220, Academic Press, London, 1983.

Colodner, D., J. Edmond, and E. Boyle, Rhenium in the Black Sea: comparison with molybdenum and uranium, *Earth and Planet. Sci. Lett.*, *131*, 1-15, 1995.

Colodner, D. C., The Marine Geochemistry of Rhenium, Iridium and Platinum, Ph.D. Thesis, MIT/WHOI, WHOI-91-30, 1991.

Cotton, F. A., and G. Wilkinson, *Advanced Inorganic Chemistry-5th edition*, J. Wiley & Sons, New York, 1988.

Creaser, R. A., D. A. Papanastassiou, and G. J. Wasserburg, Negative thermal ion mass spectrometry of osmium, rhenium, and iridium, *Geochim. Cosmochim. Acta*, *55*, 397-401, 1991.

Delmore, J. E., Rare-earth catalyzed oxidation of rhenium to ReO_4^- and ReO_3^- as observed by negative surface-ionization mass-spectrometry, *J. Phys. Chem.*, *91*, 2883-2886, 1987.

Goldberg, E. D., V. Hodge, P. Kay, M. Stallard, and M. Koide, Some comparative marine chemistries of platinum and iridium, *Appl. Geochem.*, *1*, 227-232, 1986.

Goldberg, E. D., M. Koide, J. S. Yang, and K. K. Bertine, Comparative marine chemistries of platinum group metals and their periodic table neighbors, in *Metal Speciation: Theory, Analysis, and Application*, edited by J. R. Kramer and H. E. Allen, pp. 201-217, Lewis Publishers, Inc., Chelsea, MI, 1988.

Gramlich, J. W., T. J. Murphy, E. L. Garner, and W. R. Shields, Absolute isotopic abundance ratio and atomic weight of a reference sample of rhenium, *Nat. Bur. Stds. J. Res., 77A*, 691-698, 1973.

Heumann, K. G., Isotope dilution mass spectrometry, in *Inorganic Mass Spectrometry*, edited by F. Adams, R. Gijbels and R. van Grieken, pp. 301-376, J. Wiley & Sons, New York, 1988.

Huffman, E. H., R. L. Oswalt, and L. A. Williams, Anion-exchange separation of molybdenum and technetium and of tungsten and rhenium, *J. Inorg. Nucl. Chem., 3*, 49-53, 1956.

Jacinto, J. S., and C. M. G. van den Berg, Different behavior of platinum in the Indian and Pacific Oceans, *Nature, 338*, 332-334, 1989.

Karl, D. M., and C. D. Winn, A sea of change: Monitoring the oceans' carbon cycle, *Environ. Sci. Tech., 25*, 1977-1981, 1991.

Koide, M., V. Hodge, J. S. Yang, and E. D. Goldberg, Determination of rhenium in marine waters and sediments by graphite furnace atomic absorption spectrometry, *Anal. Chem., 59*, 1802-1805, 1987.

Lee, D. S., Palladium and nickel in north-east Pacific waters, *Nature, 305*, 47-48, 1983.

Matthews, A. D., and J. P. Riley, The determination of rhenium in sea water, *Anal. Chim. Acta, 51*, 455-562, 1970.

Olafsson, J., and J. P. Riley, Some data on the marine geochemistry of rhenium, *Chem. Geol.*, *9*, 227-230, 1972.

Scadden, E. M., Rhenium: Its concentration in Pacific Ocean surface waters, *Geochim. Cosmochim. Acta*, *33*, 633-637, 1969.

Schaule, B. K., and C. C. Patterson, Lead concentrations in the northeast Pacific: Evidence for global anthropogenic perturbations, *Earth Planet. Sci. Lett.*, *54*, 97-116, 1981.

Völkening, J., T. Walczyk, and K. G. Heumann, Osmium isotope ratio determinations by negative thermal ionization mass spectrometry, *Intl. J. Mass Spectrom. Ion Proc.*, *105*, 147-159, 1991.

Wasserburg, G. J., D. A. Papanastassiou, E. V. Nenow, and C. A. Bauman, A programmable magnetic field mass spectrometer, *Rev. Sci. Instrum.*, *40*, 288-295, 1969.

Whitfield, M., and D. R. Turner, The role of particles in regulating the composition of sea water, in *Aquatic Surface Chemistry*, edited by W. Stumm, pp. 457-493, J. Wiley & Sons, New York, 1987.

Zeininger, H., Ph.D. Thesis, University of Regensburg, 1984.

Table 2.1. Re concentrations in the Pacific Ocean

Sample Depth (m)	Re (ng/kg)	Re_N (ng/kg)	2σ	Salinity (‰)	Oxygen (μmol/kg)
6(a)	7.70	7.70	0.07	35.002	205.4
(b)	7.68	7.68	0.06		
45	7.38		0.03		
51	7.35	7.35	0.03	35.006	205.4
100	7.34	7.33	0.03	35.089	205.4
402(a)	7.20	7.39	0.03	34.104	156.3
(b)	7.24	7.43	0.04		
749	7.30	7.44	0.03	34.354	26.8
1499	7.31	7.40	0.03	34.561	62.5
2198	7.32	7.40	0.03	34.622	84.8
2800(a)	7.34	7.41	0.06	34.653	111.6
(b)	7.36	7.44	0.03		
4705	7.34	7.41	0.03	34.645	138.4

Re_N is the Re concentration normalized to 35‰ salinity. The uncertainty of each measurement is derived from uncertainties in the measured 249/251 ratio, tracer concentration, and all gravimetric determinations, (see text). Replicate samples (6, 402 and 2800 m) were processed separately, and indicate that the analytical variability was within the uncertainties of the individual measurements. Samples 6 (a), (b) and 2800 (b) were spiked using the Dil-2 tracer. All other samples were spiked with Dil-1.

Table 2.2. Estimates of Re in seawater

Location	Re (ng/kg)	Reference
Pacific Ocean	7.42 ± 0.04	(a) This study
Pacific Ocean	9.1 ± 4.4	(b) Koide *et al.*, 1987
Pacific Ocean	8.4 ± 2.4	(c) Scadden, 1969
Atlantic Ocean	4.0 ± 2.1	(d) Olafsson & Riley, 1972
Atlantic Ocean	6.9 ± 2.1	(e) Matthews & Riley, 1970
Average Ocean	8.19 ± 0.37	(f) Colodner (1991)

Depth profiles were measured in all studies except (c), which included only surface samples. In (b) and (e), no data at depths shallower than 200 m were obtained. Studies (b), (c), (d) and (f) included samples from more than one location. Uncertainties in (b), (c) and (f) were reported by the authors as ± 1σ of the measurements, but have been converted to ± 2σ for comparison with this study. No uncertainty estimates were included in (d) and (e); by analogy to (b) and (c), we have calculated their uncertainties as ± 2σ. Our average, (a), includes all measurements below 400 m, and the uncertainty is reported as ± 2σ of these values. Average values from studies (a) and (f) are reported on a salinity-normalized basis.

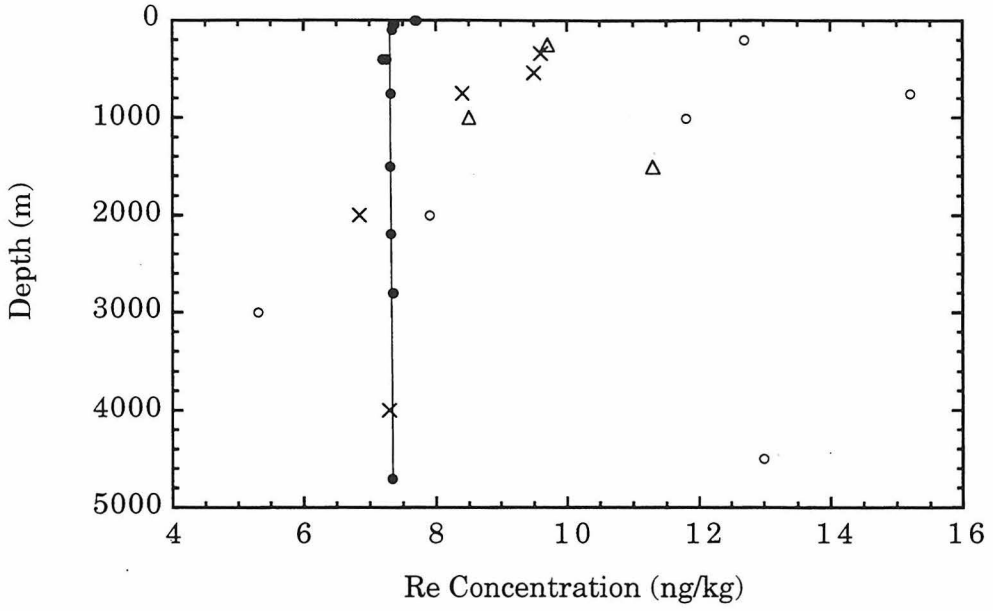

Fig. 2.1. The concentration of rhenium at various depths in the Pacific Ocean. The solid circles are data from this study; other points are from Koide *et al.* (1987). Our samples were taken at 22°N 158°W. Other samples were taken at 33°N 139°W (open circles); 35°N 122°W (triangles) and 35°N 138°W (crosses).

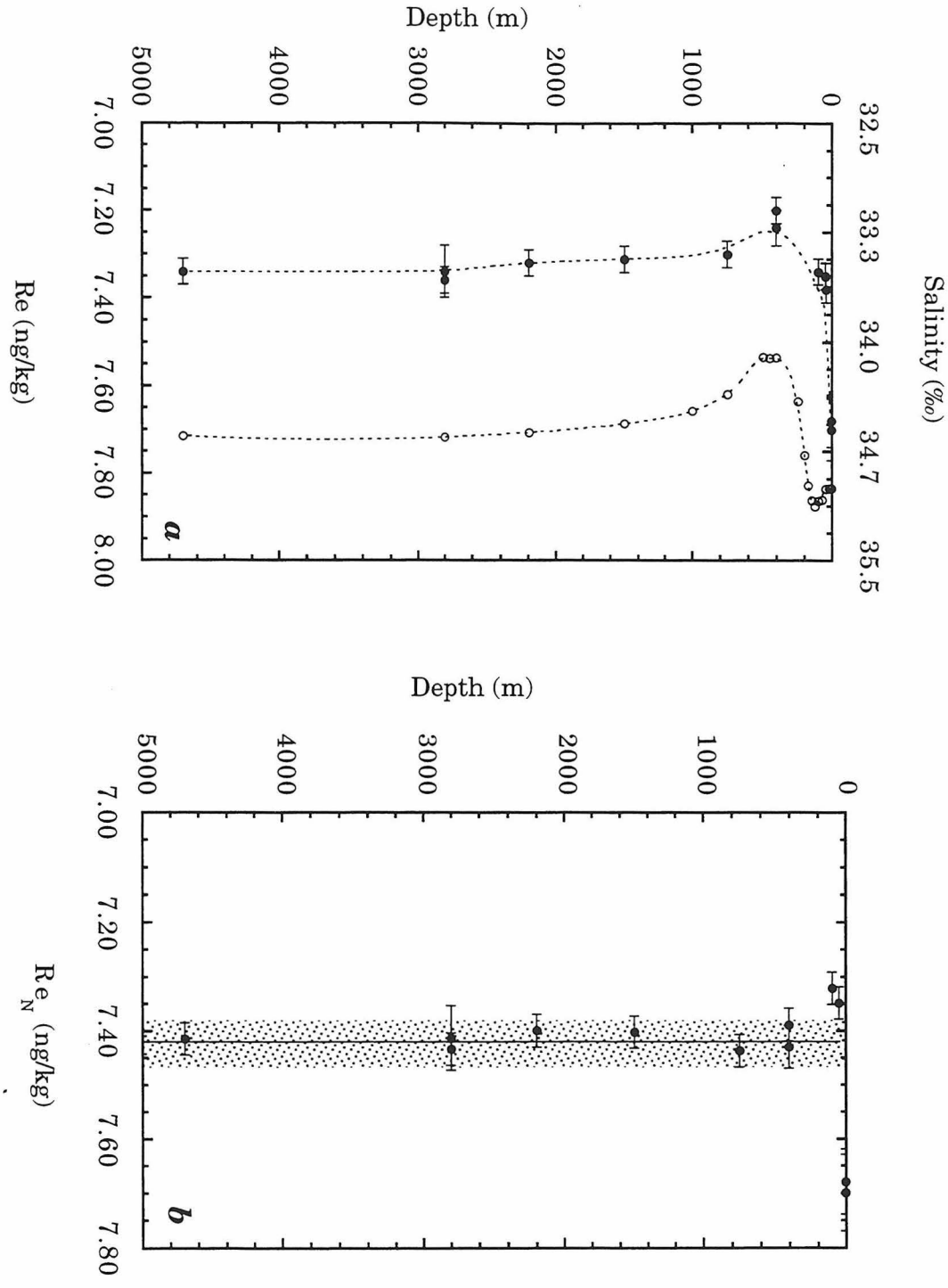

Fig. 2.2. (a) Depth profiles of salinity (open circles) and rhenium (solid circles) measured in this study. (b) Depth profile of rhenium normalized to 35‰ salinity. The vertical line represents the average Re concentration of the samples below 400 m (7.42 ng kg^{-1}), and the shaded area denotes the 95% confidence limits of this value (± 0.04 ng kg^{-1}).

Appendix 2.A.

The Filament Loading Blank

This Appendix describes experiments conducted to characterize the filament loading contamination (blank). This includes contamination from the filament itself, as well as any contamination from the loading procedure and materials. The results were summarized in Chapter 2. However, since blanks have been problematic in NTIMS analysis of Re, a more detailed presentation is warranted. This discussion focuses on the size of the blank as a function of elapsed time and filament temperature.

2.A.1. Procedures

The general approach for blank determination was to load small quantities of Re spike (typically ≈ 35 pg) on filaments, and determine the $^{185}Re/^{187}Re$ ratio in the mass spectrometer using a secondary electron multiplier (SEM) operated in analog mode. This ratio reflects the mixture of the Re spike and the normal Re coming from the filament and any contamination during loading. Prior work (Creaser *et al.*, 1991) indicated that a combination of Pt metal filaments and Ba salts as activators yielded high ionization efficiencies for Re. In the present study, the lowest blanks were attained with 99.999% purity Pt metal (ESPI) and $BaSO_4$ activator. The details of Re loading on the filament were critical; when the Re spike solution was loaded on top of the $BaSO_4$, rather than directly on the filament followed by deposition of $BaSO_4$, blanks were typically reduced by ≈ 2x, and the ionization efficiency increased substantially. Possibly, this loading procedure physically separates the loaded Re from Re which is diffusing from the filament, which minimizes mixing of the load and the blank. The high

solubility of Ba salts other than $BaSO_4$ makes them unsuitable for this technique, since they will dissolve when solutions are loaded on top of them.

2.A.2. Variation with time

Ratios determined using these procedures varied systematically as a function of time when operating conditions were held constant (*e.g.*, Fig. 2.A.1). *A priori,* it was not clear if this variation was due to depletion of the spike over time, an increase of the filament blank contribution with time, or some combination of these effects. This was of some concern. The precise determination of Re concentrations by isotope dilution requires tight control of the blank contribution from the filament or activator. If this contribution varies during the analysis of a sample, the precision of the ratio measurement is degraded. Such variation could result from accumulation of Re at the filament surface as atoms diffuse from within the metal. Although the blanks calculated from the observed ratios (Fig. 2.A.1) are small relative to typical sample sizes (≈ 1 ng), the possibility of a variable blank which might grow to much larger values was troubling.

The effects of sample depletion and blank growth can be deconvolved by applying a simple model which assumes that the only contributions to the measured ratios come from the loaded material and the filament blank, and that these two reservoirs do not mix before emission. Thus:

$$^{249}I_M = {}^{249}I_S + {}^{249}I_B \text{ and } {}^{251}I_M = {}^{251}I_S + {}^{251}I_B \qquad (2.A.1)$$

where ${}^{n}I_M$ is the total number of ions of mass n which arrive at the detector per unit time, and ${}^{n}I_S$ and ${}^{n}I_B$ are the number of ions of mass n per unit time

which come from the spike and the blank, respectively. These are combined to obtain:

$$^{249}I_M = R_S(^{251}I_M - {}^{251}I_B) + {}^{249}I_B \qquad (2.A.2)$$

where $R_S = {}^{249}I_S / {}^{251}I_S$. Rearranging:

$$^{249}I_M = R_S{}^{251}I_M + (R_B{}^{251}I_B - R_S{}^{251}I_B) \qquad (2.A.3)$$

where $R_B = {}^{249}I_B / {}^{251}I_B$. If the blank contribution is constant, a plot of $^{249}I_M$ vs. $^{251}I_M$ will yield a straight line with $m = R_S$ and $b = (R_B{}^{251}I_B - R_S{}^{251}I_B)$. The data from Fig. 2.A.1 are plotted this way in Fig. 2.A.2. The model and data are in excellent agreement: The data are fit well by a straight line (R^2 = 0.99), and R_S derived from the slope (m = 37.08) is within 3‰ of the actual value (R_S = 37.14). The contribution from a constant filament blank of normal isotopic composition (R_B = 0.597) is 5.54 x 10^3 cps at mass 251, and 3.31 x 10^3 cps at mass 249. Integrating the total signal during the 5000 seconds of this experiment, we find that 3% of the loaded spike is detected. If the blank has comparable ionization efficiency to the spike, then the counts contributed by the blank correspond to ≈ 0.4 pg of normal Re on the filament. This value is close to that derived directly from the measured ratios.

The alternative possibility of a variable filament blank and a minimal effect from spike depletion can also be derived from Eqn. 2.A.1, and would predict a straight line relationship:

$$^{185}I_M = R_B{}^{187}I_M + (R_S{}^{187}I_S - R_B{}^{187}I_S) \qquad (2.A.4)$$

In this case, the slope would correspond to R_B. Clearly, this is not the case for the data in Fig. 2.A.2, since the isotopic composition of the blank must be

close to that of normal Re. Thus, the filament loading blank is constant as a function of time.

2.A.3. Variation with temperature

In the experiment described above, temperature was held constant. However, when analyzing real samples, data were typically collected over a range of temperatures during the course of a run due to variable amounts of organic residue from the chemistry. If the blank varies with temperature, then this effect would introduce uncertainty into the ratio determination. Such a temperature effect would also degrade reproducibility.

Fig. 2.A.3 shows the results of an experiment in which the blank was characterized at several filament temperatures. In this experiment, temperature was increased rapidly in order to minimize the effects of sample depletion on the measured ratio. No systematic variation of $^{185}Re/^{187}Re$ was observed, and all the calculated blanks were well far below typical sample sizes. Thus, the magnitude and variability of the blank were assumed negligible for $T < 900°C$.

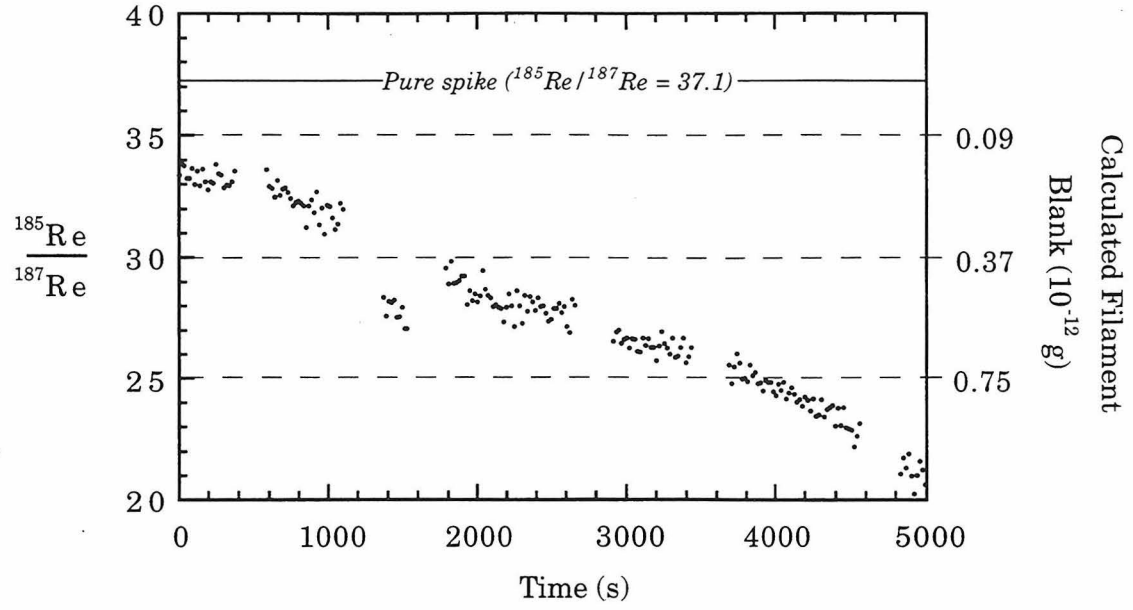

Fig. 2.A.1. The measured isotopic composition as a function of time for 36 pg of Re spike on a Pt filament. Re was detected as ReO_4^- at masses 249 and 251, and mass 251 was corrected for the contribution from $^{185}Re^{16}O_3{}^{16}O^-$ to derive $^{185}Re/^{187}Re$. Temperature was held at ≈ 850°C. Blank values (right axis) were determined using the isotope dilution equation and the ratios indicated by the dashed lines.

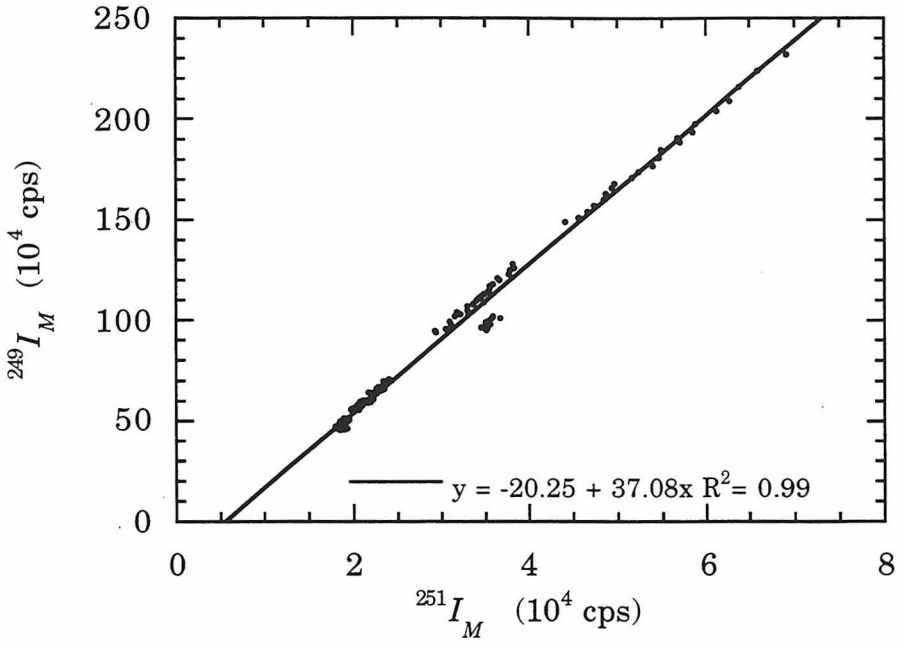

Fig. 2.A.2. $^{249}I_M$ vs. $^{251}I_M$, expressed as counts per second (cps) derived from ion currents measured at each mass. Data were collected using an SEM with a 10^9 Ω output resistor and amplification factor of 3300.

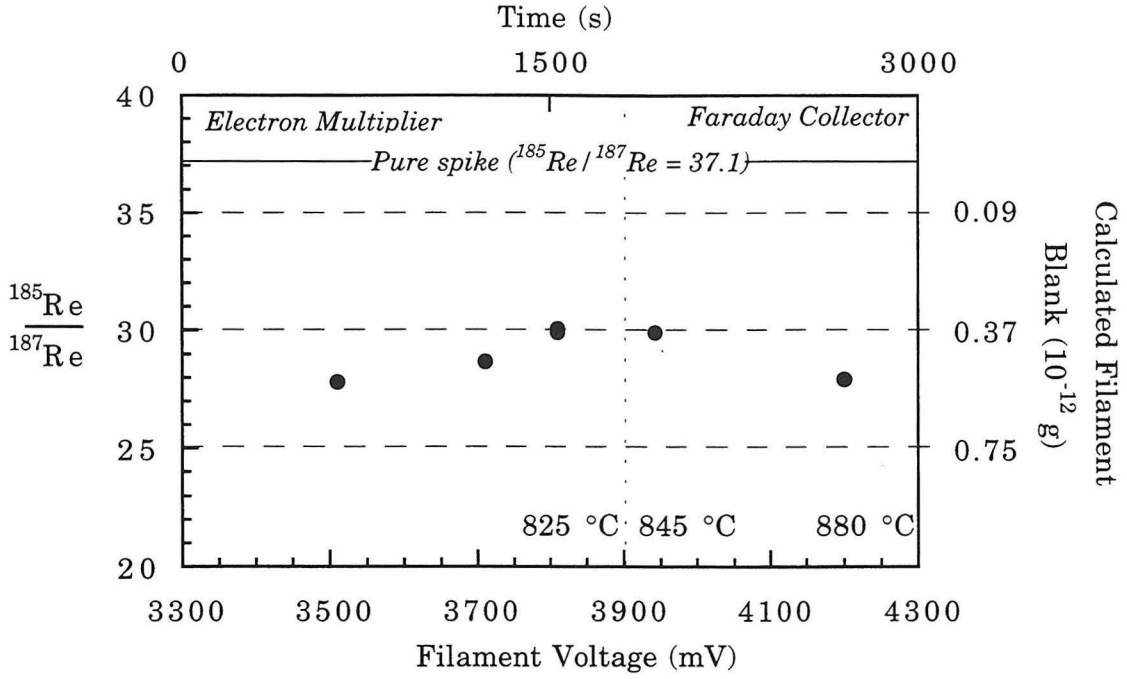

Fig. 2.A.3. Measured ratios and loading blanks as a function of filament temperature. 36 pg of Re spike were loaded on a Pt filament with $BaSO_4$. Filament voltages and corresponding temperatures are on the lower axis; elapsed time is indicated on the upper axis. Blanks (right axis) were calculated as in Fig. 2.A.1. The dotted vertical line denotes the boundary between data collected with the SEM and the Faraday collector.

Chapter 3.

Rhenium in Seawater II: Limits on Anoxia in the Glacial Deep Sea?

3.1. Abstract

A simple time-dependent model is used to quantify the variation of rhenium in seawater through time, and to place an upper limit on the area of anoxic sedimentation during glacial periods. Variations in seawater Re concentrations have attracted interest because the dominant sink of Re from seawater is believed to be deposition in organic-rich sediments (Colodner *et al.*, 1993; Goldberg *et al.*, 1988; Koide *et al.*, 1987; Ravizza *et al.*, 1991). It has been suggested that the oxygen content of deep ocean waters differs significantly between glacial and interglacial periods, resulting in changes in the area of the seafloor covered by such sediments (*e.g.,* Emerson, 1985). The concentration of Re in seawater may therefore change in response to climate conditions (Colodner, 1991). It is shown that, due to the long residence time of Re in seawater, variations of its seawater concentration in response to glacial cycle forcings are unlikely to exceed 10%, and are probably much smaller. Thus, useful paleoceanographic reconstructions of these variations will require an extremely faithful geochemical record, and precise analytical techniques. A further consequence of the long residence time of Re in seawater is that the present-day concentration represents the balance between riverine inputs and the *average* rate of removal over > 100,000 yr. Using this fact and observations of Re in modern seawater, sediments and riverwaters leads to an upper limit on the area of submarine anoxic sedimentation during glacial times of ≤ 3.6 times the present value.

3.2. Introduction

3.2.1. *The Rhenium Ocean Budget*

Understanding of the marine geochemistry of Re has advanced tremendously in the past decade. Much of this progress stems from the thesis work of D. C. Colodner (Colodner, 1991). The conservative behavior of Re in seawater has now been observed in three profiles (Anbar *et al.*, 1992; Colodner *et al.*, 1993). Two are in the North Pacific (22°45' N; 158°00' W and 24°16'N, 169°32'E), and one is in the North Atlantic (32°10'N, 64°30'W). There is no significant difference between the concentrations in each ocean, as expected for a conservative element. In the Amazon river estuary, Re appears to mix conservatively (Colodner *et al.*, 1993). Similarly, in this study, little deviation from conservative mixing was seen in the Baltic Sea (Fig. 3.1; Table 3.1). There appears to be little addition or loss of Re from solution in such environments.

Using measurements of Re in the waters of several major river systems, Colodner (1993) derived a flux-weighted average Re input of 83,000 mol yr^{-1} to the oceans. Although anthropogenic Re is believed to cause Re enrichment in some drainage systems (*e.g.,* Fig. 3.1, Colodner *et al.*, 1995), the major river systems appear to be dominated by non-anthropogenic inputs (Colodner *et al.*, 1993). Non-riverine inputs of Re to the ocean, such as from meteorites or aeolian dust, are insignificant by comparison. Thus, the riverine Re source is probably a reasonable estimate of the total input of Re to the oceans. Since the total ocean content of Re is $\approx 6.2 \times 10^{10}$ mol, a residence time of $\approx$ 750,000 yr is determined.

The distribution of Re in various geological materials is shown in Table 3.1. It is evident that Re is strongly enriched in reduced sediments, and depleted relative to its crustal abundance in pelagic clays and oxic sediments (*e.g.,* ferromanganese sediments). As noted by Koide *et al.* (1986), this fact makes Re a particularly sensitive paleoredox indicator. Thus, attention has focused on reducing environments as the dominant sink of Re from seawater.

A study of Re in the Black Sea (Colodner *et al.*, 1995) clearly indicates rapid removal of Re from anoxic waters; a residence time of 100 - 1000 yr is derived for Re in these waters. While particulate scavenging could account for some of the Re removal in the Black Sea, the strong correlation between Re and salinity in anoxic Black Sea waters suggests that this is not a major removal mechanism. It is probable that the dominant sink in the Black Sea is diffusion into sedimentary pore waters, followed by reduction and incorporation into insoluble phases, adsorption, or incorporation into organic materials in anoxic sediments. Analyses of pore waters in the reducing sediments of the Chesapeake Bay, the California Margin and the Black Sea provide evidence that this is a general process by which Re is removed from seawater, although the precise removal mechanism is not clear (Colodner *et al.*, 1994; Colodner *et al.*, 1993). The global Re removal flux can therefore be calculated from the concentration of Re in organic-rich sediments, and the burial flux of these sediments. A value of 36,000 mol yr^{-1} is derived (Colodner *et al.*, 1993). This is approximately 40% of the riverine input, implying an unidentified sink of $\approx$ 47,000 mol yr^{-1}. It has been suggested that this deficit can be accounted for by other removal processes, such as diffusion into suboxic sediments (defined as those sediments which have no oxygen, but also no H_2S; loss to these sediments has been observed for U), or precipitation

and/or adsorptive scavenging in hydrothermal systems (Colodner *et al.*, 1993). Even if this is the case, anoxic sediments are clearly a substantial Re sink.

3.2.2. *The Global Change Connection*

The important role of organic-rich sedimentation as a sink for marine Re has led to the suggestion that the Re concentration of seawater may be a function of the areal extent of anoxic sedimentation (Colodner, 1991). A similar suggestion has been made for the concentrations of Mo, V and U, which have marine chemistry similar to that of Re (Emerson and Huested, 1991). Presently, ≈ 0.3% of the seafloor is overlain by such sediments. This value may have been higher during glacial times, since a change in the concentration and/or distribution of deep water O_2 during glacial periods is indicated by a number of ocean-atmosphere models which seek to explain the change in atmospheric CO_2 between glacial and interglacial times (Boyle, 1988; Broecker, 1989; Knox and McElroy, 1984; Sarmiento and Toggweiler, 1984; Siegenthaler and Wenk, 1984). Depressed deep-water O_2 should expand the area of anoxic sedimentation (Emerson, 1985). However, these models produce different degrees of globally-averaged deep-water O_2 depletion compared to the present day, ranging from approximately twofold (Boyle, 1988; Broecker, 1989) to nearly 100% (Broecker, 1982; Knox and McElroy, 1984; Sarmiento and Toggweiler, 1984). Thus, any means of quantifying the extent of deep ocean anoxia during glacial times is of interest. In this context, it is worth exploring the impact of changes in the extent of anoxic sedimentation on Re in seawater, despite the remaining uncertainties in the geochemical budget. A simple model for this purpose is presented below. It will be shown that, even with the present uncertainties, the

observational data lead to constraints on the extent of anoxic sedimentation during glacial periods.

3.3. A Model of Rhenium in the Oceans

A simple, first-order differential equation can be used to describe the response of Re in the oceans to perturbations in the removal rate. To a first approximation:

$$\frac{dN}{dt} = R_{in} - R_{out}(t) \tag{3.1}$$

where N is the number of moles of Re in the ocean, R_{in} is the rate of input of Re to the oceans, and $R_{out}(t)$ is the time-dependent rate of removal. R_{in} is taken to be the observed riverine flux. $R_{out}(t)$ is modeled as:

$$R_{out}(t) = A(t) K_d \frac{dC}{dz} \tag{3.2}$$

where $A(t)$ is the area of anoxic sedimentation (m^2), which varies with time; K_d is the coefficient for diffusion into sediment pore waters ($m^2\ yr^{-1}$); and dC/dz is the concentration gradient in the sediments. The removal mechanism is assumed to produce a concentration gradient from $C = 0$ at some characteristic depth z_o, at which Re is removed from solution, to $C = C_o$ (the concentration of Re in the ocean) at the sediment/water interface. To first order, K_d is assumed constant. Thus, we derive:

$$R_{out}(t) = A(t) K_d \frac{C_o}{z_o} = k(t) N \tag{3.3}$$

$$k(t) = A(t) \frac{K_d}{V_o z_o} \tag{3.4}$$

where V_o is the total volume of the oceans. While this is an extremely simple parameterization of the removal process, it captures the essential features of removal of Re into anoxic sediments, as long as the diffusion coefficient and depth in the sediment at which Re is removed from solution are relatively constant through time.

Substituting Eqn. 3.4 back into Eqn. 3.1, we obtain:

$$\frac{dN}{dt} = R_{in} - k(t)N \tag{3.5}$$

Significant insights are obtained if we assume that $k(t)$ has the form of a square wave which jumps between two values of $k(t)$, k_1 and k_2. These are the values associated with glacial and interglacial climates. The timescale for the change of $A(t)$ from the glacial value to the interglacial value (A_2 and A_1, respectively) should be at least as fast as the 1,000 yr ocean mixing time; if deep water O_2 is consumed by transport of particulate-bound organic carbon to depth, then much faster changes are plausible. Such timescales are essentially instantaneous relative to the 750,000 yr residence time of Re in the oceans. Thus, the details of $k(t)$ variation during climate transitions are unlikely to have a significant impact on seawater Re, and are therefore ignored in this first approximation.

If $k(t)$ jumps between k_1 and k_2 at regular intervals and spends an equal span of time at each value, then the following relation must hold:

$$\frac{dN_{avg}}{dt} = R_{in} - \frac{(k_1 + k_2)}{2} N_{avg} \tag{3.6}$$

where N_{avg} is the time-averaged quantity of Re in seawater. Eventually, this system will evolve to a quasi-steady-state in which N is still varying, but

$dN_{avg}/dt = 0$. N must be bounded by the two steady-state solutions obtained when $k(t) = k_1$ and k_2. If k_1 and k_2 are the interglacial and glacial values, respectively ($k_1 = A_1(t)K_d/V_o z_o$; $k_2 = A_2(t)K_d/V_o z_o$), then $k_2 \geq k_1$, and:

$$\frac{R_{in}}{k_2} < N < \frac{R_{in}}{k_1} \tag{3.7}$$

This represents the full possible range of variation of Re in seawater. Since the area of anoxic sedimentation during glacial periods may be several times the present value, and since $k(t)$ is proportional to this area, it is apparent that the Re concentration could be highly variable. The *actual* variation of seawater Re is dictated by the relative magnitudes of the removal rate and the period of the oscillation of $k(t)$. If this period is long relative to the removal rate, then the full range will be approached. However, if the response time for Re is much longer than the oscillation period, then the variation may be highly attenuated. It is immediately obvious that the effects of the 100,000 yr periodicity in $k(t)$ expected from the dominant glacial cycle should be substantially attenuated in the case of Re, with its 750,000 yr residence time. Higher frequency cycles should have even less effect.

These relationships are considered quantitatively using a simple computer algorithm based on the equation:

$$N(t) = \frac{R_{in}}{k_n} + Be^{-k_n t} \tag{3.8}$$

where k_n is equal to either k_1 or k_2. This is the solution to Eqn. 3.5 for constant $k(t)$. Eqn. 3.8 is evaluated at fixed intervals of t, and the value of k_n is changed appropriately as time advances. The calculations are begun at the steady-state solution corresponding to $k_n = k_1$ and the constant B is evaluated for this condition. This constant is re-evaluated every time that k_n changes.

R_{in} is given as a fixed input to the model. The only other inputs to the model are the value of N at $t = 0$ (N_o), and the ratio k_2/k_1, from which k_1 and k_2 are calculated ($k_1 = R_{in}/N_o$; $k_2 = k_1 \times k_2/k_1$).

3.4. Results and Discussion

3.4.1. *Rhenium in Seawater Through Time*

This model was used to determine the variability of Re in seawater for $k_2/k_1 = 2$, and $k_2/k_1 = 10$. Larger ratios are precluded by the absence of sedimentological evidence for such extensive anoxic sedimentation. A range of N_o values was explored. These were chosen to result in N_{avg} within a factor of five of the present day value of N. In these models, k_n changed from k_1 to k_2 every 50,000 yr, corresponding to a glacial cycle with a 100,000 yr period, and time was advanced in 10,000 yr increments.

In all cases, Re in seawater falls from the interglacial steady-state solution to an intermediate value (N_{avg}) in 1 - 2 x 10^6 years (*e.g.*, Fig. 3.2). Thus, since the onset of modern glaciation $\approx$ 2.5 x 10^6 yr ago, Re in the oceans should have evolved from the interglacial steady-state solution ($N = R_{in}/k_1$) to the situation represented by $dN_{avg}/dt = 0$ at the present. Once this state is achieved, the variability of Re in seawater is rather small; no more than 10% variation is observed for $k_2/k_1 = 10$ (Fig. 3.2b), and < 5% variation is seen for $k_2/k_1 = 2$ (Fig. 3.2a). No relationship exists between the size of N_o and the magnitude of the Re variations. Perturbations by higher-frequency glacial cycles, such those with periods of 23,000 yr and 41,000 yr, have even less effect on Re in seawater (not shown).

These results differ from previous estimates which indicated substantially larger variabilities for Re, Mo, U and V when subject to a

tenfold increase in the area of anoxic sedimentation (Colodner, 1991; Emerson and Huested, 1991). Those estimates employed a linear approximation to the exponential solution used in this study, spanned only one transition from interglacial to glacial conditions, and took as a starting point a steady-state solution. Such calculations are analogous to a linear extrapolation of our results from $t = 0$ to $t \approx 5{,}000$ yr ($k_2/k_1 = 10$), in which the Re concentration falls ≈ 20% (Fig. 3.2b). Over a 10^6 year time span, however, the results presented here are a better representation of reality. Since the modern era of glacial oscillations began ≈ 2.5 x 10^6 years ago (*e.g.*, Raymo, 1994), this is the relevant interval.

The implications for paleoceanography are clear: The concentration of Re in seawater is unlikely to have changed substantially in response to the most recent Plio-Pleistocene glacial cycles, even if the perturbation of the removal rate was rather large. Useful reconstruction of Re concentrations in seawater over the past ≈ 10^6 years will require a geochemical record which is accurate to better than ± 10%, and analytical methods of better than 1% precision. While such analytical methods have been demonstrated (*e.g.*, ID-NTIMS, as described in Chapter 2), a geochemical record of the required fidelity has yet to be identified.

3.4.2. *Implications for Deep Sea Anoxia*

Some insight into the extent of deep sea anoxia during glacial periods can yet be made using this model and available data. From Fig. 3.2, it is apparent that at the present time, $N \approx N_{avg} = 6 \times 10^{10}$ mol (the amount of Re in the oceans today). Therefore, the Re budget may be unbalanced at most instances in time, reaching balance only in an average sense over a timescale

of $\approx 10^6$ yr. The "missing sink" of Re alluded to earlier may not be missing at all. This provides a means of placing an upper limit on the rate of Re removal during glacial periods. For $dN_{avg}/dt = 0$, Eqn. 3.6 reduces to:

$$k_2 = \frac{2R_{in}}{N_{avg}} - k_1 \tag{3.9}$$

Thus, if N_{avg}, R_{in} and k_1 are known, then k_2 is determined. Assuming that the model of Eqn. 3.4 is valid, the area of anoxic sedimentation in glacial times is directly obtained.

Two of the quantities needed to derive the value of k_2 from Eqn. 3.9 can be estimated from observations; N_{avg} (approximately equal to the present-day N) and R_{in} (the river input, which is assumed constant). The remaining unknown is k_1, the rate constant for Re removal during interglacial times. A lower limit on this quantity can be estimated from the measured rate of removal of Re into organic-rich sediments at the present time (R_{out}). As noted above, R_{out} = 36,000 mol yr^{-1}. It is probable that this quantity is typical of the interglacial removal rate, since the sediments used to arrive at this number all post-date the last deglaciation, $\approx$ 12,000 years ago. Allowing for the possibility of other sinks which have not yet been identified, $R_{out} \leq k_1 N(t)$. Since $N(t) \approx N_{avg}$, $k_1 \geq R_{out}/N_{avg}$. Thus, 3.9 is rewritten as:

$$k_2 \leq \frac{2R_{in} - R_{out}}{N_{avg}} \tag{3.10}$$

From this analysis, $k_1 \geq 5.8 \times 10^{-7} yr^{-1}$, and $k_2 \leq 2.1 \times 10^{-6}$ yr^{-1}. From Eqn. 3.4, it follows that k_2/k_1 is equal to A_2/A_1, the ratio of the area of anoxic sedimentation in glacial times to that during interglacial times. Thus, $A_2/A_1 \leq$

3.6. Since ≈ 0.3% of the seafloor is overlain with such sediments today, the glacial value must be less than or equal to ≈ 1%.

Recent analyses of pore waters in suboxic sediments suggests that these sediments may be a substantial Re sink (Colodner, personal communication). If the present-day Re budget is ever balanced by the identification of such sinks, then this analysis demands that the rate of Re removal changes very little in response to glacial forcings (*i.e.*, $k_2 \approx k_1$). This stems from the long residence time of Re, which prevents N from reaching a steady-state solution unless that solution is approximately constant over millions of years. A balanced Re budget would strongly suggest that the area of the seafloor covered by anoxic sediments is only slightly altered by glacial cycles and, hence, that deep water anoxia does not undergo drastic changes.

3.4.3. *Complications*

This analysis omits some possible complications. For example, the riverine flux of Re to seawater may also be perturbed by glaciation, due to altered weathering cycles. Both the magnitude and sign of such a perturbation are not immediately obvious. However, it is clear that to have a significant amplifying effect on the variability of seawater Re, the riverine flux would have to be smaller during the glacial maxima by nearly an order of magnitude relative to the present day. This is unlikely to have been the case, as it is generally thought that global chemical weathering rates are similar during glacial and interglacial times (*e.g.*, Kump and Alley, 1994).

Another complication is the possibility that re-oxidation of sediments during the transition from glacial to interglacial conditions could return substantial quantities of Re to the oceans. This would effectively raise the

input to seawater at the same time that the sink becomes smaller, increasing the magnitude of the post-glacial rise in seawater Re predicted by the model. However, the rates of sedimentation in the areas believed to dominate the Re burial flux are high, ranging from 0.1 - 1.0 cm yr^{-1} (Colodner *et al.*, 1993). Thus, tens of meters of Re-enriched sediment would accumulate during glaciation. Substantial remobilization of Re from such thick sections is unlikely.

Finally, the most serious assumption is that the values of k_1 and k_2 have remained the same through the entire glacial epoch, although the periodicity of climate change has clearly not remained constant (Imbrie *et al.*, 1993; Imbrie *et al.*, 1992). If, for example, the difference between k_1 and k_2 was smaller prior to the last half million years, when higher frequency modes dominated the climate system, then the arrival at N_{avg} may be delayed substantially. At the present level of understanding of global climate and the Re cycle, this remains an unconstrained assumption.

While further investigations of all these issues are clearly needed, the essential features of the model are certainly plausible.

3.5. Conclusions

Apparently, changes in the extent of anoxic sedimentation arising from glacial forcings during the past 10^6 years would have had little effect on the concentration of Re in seawater. This finding leads directly to an upper limit on the area of submarine anoxic sedimentation during glacial times of no more than 3.6 times the present value. This is a reassuring result. Observational evidence does not suggest widespread bottom water anoxia (Pederson *et al.*, 1988), and it is not clear if anoxic sediments identified with

glacial times are related to pervasive bottom-water anoxia or localized increases in the rate of organic carbon production (*e.g.,* Calvert *et al.*, 1992; Calvert and Pederson, 1993; Calvert *et al.*, 1995; Paropkari *et al.*, 1992; Pederson and Calvert, 1990; Sarkar *et al.*, 1993; Vonrad *et al.*, 1995). The fact that the Re budget requires, at most, a moderate increase over the present-day extent of anoxic sedimentation is in good agreement with these observations, and with models which minimize the glacial perturbations to dissolved oxygen in the deep sea (Boyle, 1988; Broecker, 1989).

Quantification of other likely Re sinks (*e.g.,* suboxic sediments and hydrothermal systems) is clearly a high priority. Future studies must also focus on the question of Re remobilization during the transition from glacial to interglacial conditions. Additionally, careful study of other long-lived species such as Mo, U and V may yield complimentary results; these elements are also removed largely into reducing sediments, and are therefore expected to behave similarly to Re (Emerson and Huested, 1991).

3.6. References

Anbar, A. D., R. A. Creaser, D. A. Papanastassiou, and G. J. Wasserburg, Rhenium in seawater: Confirmation of generally conservative behavior, *Geochim. Cosmochim. Acta*, *56*, 4099-4103, 1992.

Anders, E., and M. Ebihara, Solar System abundances of the elements, *Geochim. Cosmochim. Acta*, *46*, 2363-2380, 1982.

Boyko, T. F., G. N. Baturin, and A. D. Miller, Rhenium in recent ocean sediments, *Geochem. Int.*, *23*, 38-47, 1986.

Boyle, E. A., The role of vertical chemical fractionation in controlling late Quaternary atmospheric carbon dioxide, *J. Geophys. Res.*, *93*, 15,701-15,715, 1988.

Broecker, W. S., Ocean chemistry during glacial time, *Geochim. Cosmochim. Acta*, *46*, 1689-1705, 1982.

Broecker, W. S., The cause of the glacial to interglacial atmospheric CO_2 change: A polar alkalinity hypothesis, *Global Biogeochem. Cycles*, *3*, 215-239, 1989.

Calvert, S. E., R. M. Bustin, and T. F. Pederson, Lack of evidence for enhanced preservation of sedimentary organic-matter in the oxygen minimum of the Gulf of California, *Geology*, *20*, 757-760, 1992.

Calvert, S. E., and T. F. Pederson, Geochemistry of Recent oxic and anoxic marine sediments: Implications for the geological record, *Mar. Geol.*, *113*, 67-88, 1993.

Calvert, S. E., T. F. Pederson, P. D. Naidu, and U. Vonstackelberg, On the organic-carbon maximum on the continental-slope of the eastern Arabian Sea, *J. Mar. Res.*, *53*, 269-296, 1995.

Colodner, D., J. Edmond, and E. Boyle, Rhenium in the Black Sea: comparison with molybdenum and uranium, *Earth and Planet. Sci. Lett.*, *131*, 1-15, 1995.

Colodner, D., S. Natarajan, and B. Anderson, The ins and outs of rhenium in reducing sediments of the California margin and Black Sea, *EOS*, *75*, 56, 1994.

Colodner, D. C., The Marine Geochemistry of Rhenium, Iridium and Platinum, Ph.D. Thesis, MIT/WHOI, WHOI-91-30, 1991.

Colodner, D. C., J. Sachs, G. Ravizza, K. Turekian, J. Edmond, and E. Boyle, The geochemical cycle of rhenium: a reconnaissance, *Earth Planet. Sci. Lett.*, *117*, 205-221, 1993.

Emerson, S., Organic carbon preservation in marine sediments, in *Natural Variations in Carbon Dioxide and the Carbon Cycle, Archean to Present, Geophysical Monograph Series*, vol. 32, edited by E. T. Sundquist and W. S. Broecker, pp. 78-88, American Geophysical Union, Washington, D.C., 1985.

Emerson, S. R., and S. S. Huested, Ocean anoxia and the concentrations of molybdenum and vanadium in seawater, *Mar. Chem.*, *34*, 177-196, 1991.

Esser, B. K., and K. K. Turekian, The osmium isotopic composition of the continental crust, *Geochim. Cosmochim. Acta*, *57*, 3093-3104, 1993.

Goldberg, E. D., M. Koide, J. S. Yang, and K. K. Bertine, Comparative marine chemistries of platinum group metals and their periodic table neighbors, in *Metal Speciation: Theory, Analysis, and Application*, edited by J. R. Kramer and H. E. Allen, pp. 201-217, Lewis Publishers, Inc., Chelsea, MI, 1988.

Hauri, E. H., and S. R. Hart, Re-Os isotope systematics of HIMU and EMII oceanic island basalts from the south Pacific Ocean, *Earth Planet. Sci. Lett.*, *114*, 353-371, 1993.

Imbrie, J., A. Berger, E. A. Boyle, S. C. Clemens, A. Duffy, W. R. Howard, G. Kukla, J. Kutzbach, D. G. Martinson, A. McIntyre, A. C. Mix, B. Molfino, J. J. Morley, L. C. Peterson, N. G. Pisias, W. L. Prell, M. E. Raymo, N. J. Shackleton, and J. R. Toggweiler, On the structure and origin of major glaciation cycles 2. The 100,000-year cycle, *Paleoceanography*, *8*, 699-735, 1993.

Imbrie, J., E. A. Boyle, S. C. Clemens, A. Duffy, W. R. Howard, G. Kukla, J. Kutzbach, D. G. Martinson, A. McIntyre, A. C. Mix, B. Molfino, J. J. Morley, L. C. Peterson, N. G. Pisias, W. L. Prell, M. E. Raymo, N. J. Shackleton, and J. R. Toggweiler, On the structure and origin of major glaciation cycles 1. Linear responses to Milankovitch forcing, *Paleoceanography*, *7*, 701-738, 1992.

Knox, F., and M. B. McElroy, Changes in atmospheric CO_2: Influence of the marine biota at high latitude, *J. Geophys. Res.*, *89*, 4629-4637, 1984.

Koide, M., V. Hodge, J. S. Yang, and E. D. Goldberg, Determination of rhenium in marine waters and sediments by graphite furnace atomic absorption spectrometry, *Anal. Chem.*, *59*, 1802-1805, 1987.

Koide, M., V. F. Hodge, J. S. Yang, M. Stallard, and E. G. Goldberg, Some comparative marine chemistries of rhenium, gold, silver and molybdenum, *Appl. Geochem.*, *1*, 705-714, 1986.

Kump, L. R., and R. B. Alley, Global chemical weathering on glacial time scales, in *Material Fluxes on the Surface of the Earth, Studies in Geophysics*, edited by W. W. Hay, pp. 46-60, National Academy Press, Washington, D.C., 1994.

Martin, C. E., Osmium isotopic characteristics of mantle-derived rocks, *Geochim. Cosmochim. Acta*, *55*, 1421-1434, 1991.

Paropkari, A. L., C. P. Babu, and A. Mascarenhas, A critical evaluation of depositional parameters controlling the variability of organic-carbon in Arabian Sea sediments, *Mar. Geol.*, *107*, 213-226, 1992.

Pederson, T. F., and S. E. Calvert, Anoxia vs. productivity: What controls the formation of organic-carbon-rich sediments and sedimentary rocks?, *AAPG Bull.*, *74*, 454-466, 1990.

Pederson, T. F., J. S. Pickerzing, J. S. Vogel, J. N. Southon, and D. E. Nelson, The response of benthic foraminifera to productivity cycles in the eastern Equatorial Pacific: Faunal and geochemical constraints on glacial bottom-water oxygen level, *Paleoceanography*, *3*, 157-168, 1988.

Ravizza, G., and K. K. Turekian, Application of the ^{187}Re-^{187}Os system to black shale geochronometry, *Geochim. Cosmochim. Acta*, *53*, 3257-3262, 1989.

Ravizza, G., K. K. Turekian, and B. J. Hay, The geochemistry of rhenium and osmium in recent sediments from the Black Sea, *Geochim. Cosmochim. Acta*, *55*, 3741-3752, 1991.

Raymo, M. E., The initiation of Northern Hemisphere glaciation, *Annual Review of the Earth and Planetary Sciences*, *22*, 353-383, 1994.

Sarkar, A., S. K. Battacharya, and M. M. Sarin, Geochemical evidence for anoxic deep-water in the Arabian Sea during the last glaciation, *Geochim. Cosmochim. Acta*, *57*, 1109-1016, 1993.

Sarmiento, J. L., and J. R. Toggweiler, A new model for the role of the oceans in determining atmospheric P_{CO_2}, *Nature*, *308*, 621-624, 1984.

Siegenthaler, U., and T. Wenk, Rapid atmospheric CO_2 variations and ocean circulation, *Nature*, *308*, 624-626, 1984.

Vonrad, U., H. Schulz, A. A. Khan, M. Ansari, and U. Berner, Sampling the oxygen minimum zone off Pakistan- Glacial, interglacial variations of anoxia and productivity (preliminary results, Sonne-90 cruise), *Mar. Geol.*, *125*, 7-19, 1995.

Table 3.1. Rhenium in Geological Materials

Material	Re (ppb)	References
Modern anoxic sediments	2- 100	a, c
Black shales	50 - 300	b
Pelagic sediments	0.05 - 0.5	a, c, e
Chondritic meteorites	40	d
Basalts	0.1 - 1.6	f, g
Mn nodules	< 2	a, e
Avg. upper crust	0.4	h

(a) Koide *et al.* (1986, 1987); (b) Ravizza and Turekian (1989); (c) Colodner *et al.* (1993); (d) Anders and Ebihara (1982); (e) Boyko *et al.* (1985) (f) Hauri and Hart (1993); (g) Martin (1991); (h) Esser and Turekian (1993).

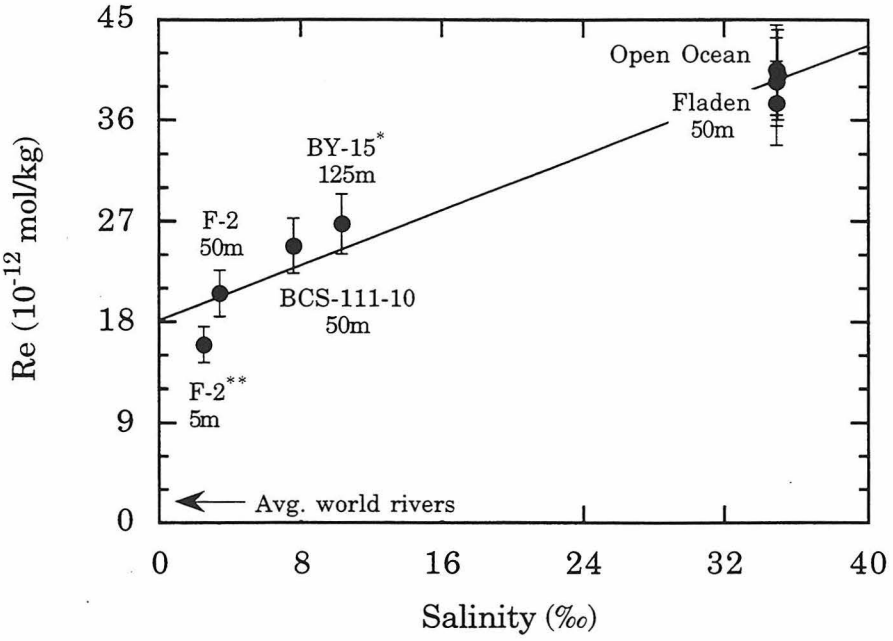

Fig. 3.1. The concentration of Re in the oceans and the Baltic Sea. The strong correlation with salinity is consistent with conservative behavior in the estuarine environment. The Re enrichment in the extrapolated freshwater end-member relative to average world rivers is probably due to anthropogenic contamination of the Baltic. A similar enrichment is observed in the Black Sea (Colodner *et al.*, 1995). The slight deviation from conservative mixing at station F-2 suggests that particles may play a role in Re transport in low salinity waters. Sample depths in the Baltic are as labeled. Open ocean values are average values from references cited in the text. These data were obtained using the chemical procedures described in Chapter 2. Isotope ratios were measured using a Perkin-Elmer Sciex ELAN 5000A ICP mass spectrometer with a standard torch and argon plasma, gas flow rates of 15 L/min (plasma), 1 L/min (auxiliary) and 1 L/min (nebulizer), and 1 kW applied power. Standard optical settings were selected. The rate of liquid sample uptake was ≈ 1 mL/min. Peak hopping was employed, with an integration time of 50 - 100 ms during a total data acquisition time of 30 - 60 s for 6 masses.

*Filtered to 0.10 μm; **Filtered to 0.45 μm.

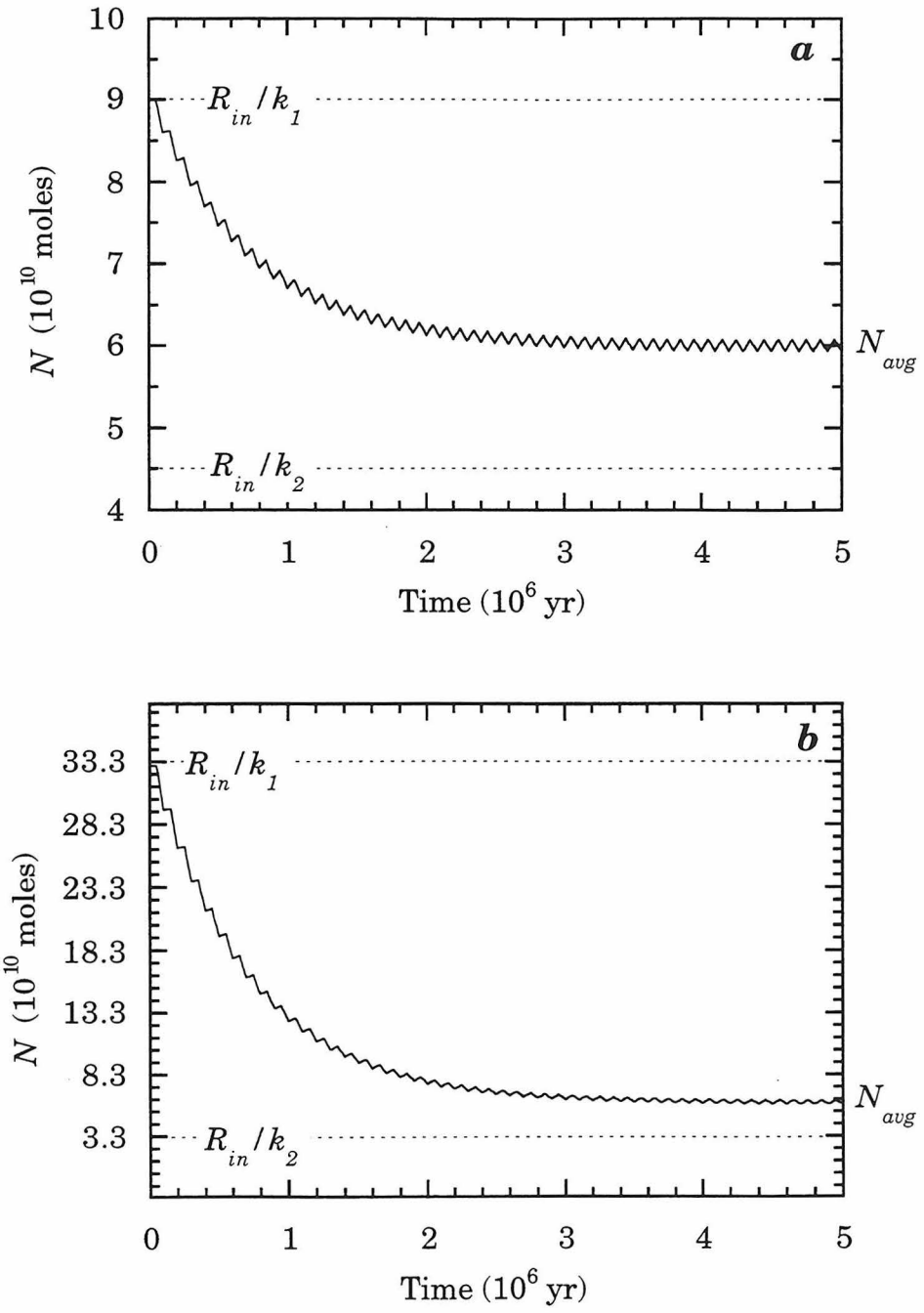

Fig. 3.2. Rhenium in seawater through time, calculated as described in the text to reach N_{avg} ≈ 6 x 10^{10} mol, the present-day Re content of the oceans. (a) k_2/k_1 = 2. (b) k_2/k_1 = 10. The dotted lines denote the steady-state solutions, R_{in}/k_n. Note that in both cases, $dN_{avg}/dt \approx 0$ within 2 x 10^6 yr.

Chapter 4.

Determination of Iridium at Sub-Femtomolar Concentrations in Natural Waters

4.1. Abstract

The chemistry of Ir in natural waters is poorly understood due to the extremely low abundance of this element at the Earth's surface. To address this problem, methods have been developed for the routine, precise measurement of Ir at sub-femtomolar concentrations (10^{-15} mol L^{-1}) using isotope dilution negative thermal ionization mass spectrometry (ID-NTIMS). After equilibration with a ^{191}Ir-enriched spike, Ir is separated from solution by coprecipitation with an Fe carrier, followed by anion exchange chromatography using a reductive elution technique. UV irradiation is employed for the clean decomposition of trace organics, which interfere with the NTIMS analysis. IrO_2^- ions are produced in the mass spectrometer by heating the sample on a Ni wire filament. These ions are detected by a secondary electron multiplier configured for ion-counting. The NTIMS analysis has a detection limit of $\approx 2 \times 10^6$ atoms. The practical detection limit is determined by a chemical blank of $(2 \pm 2) \times 10^8$ atoms. An Ir concentration of $(4.4 \pm 0.8) \times 10^8$ atoms kg^{-1} ($7.3 \pm 1.3 \times 10^{-16}$ mol kg^{-1}) has been determined in a 4 L sample of water from 1000 m depth in the Pacific Ocean.

4.2. Introduction

The measurement of the Platinum Group Elements (PGE) in natural materials is one of the more difficult challenges in trace element analysis. This is due to the extremely low concentrations of the PGE in most terrestrial materials. For example, Ir and Os rarely exceed the ppb range in rocks at the Earth's surface (ppb = 10^{-9} gm gm^{-1}; $\approx 3 \times 10^{12}$ atoms gm^{-1} for Ir and Os), and are present at ppt or lower abundances in many crustal materials (ppt = 10^{-12} gm gm^{-1}; $\approx 3 \times 10^{9}$ atoms gm^{-1} for Ir and Os) (Crocket and Kuo, 1979; Esser and Turekian, 1993; Fenner and Presley, 1984; Hodge *et al.*, 1986; Levinson, 1980; Ravizza and McMurtry, 1993; Taylor and McLennan, 1985). Thus, most PGE geochemical studies have focused on ore bodies, meteorites and mantle rocks, because of the higher abundances in these samples. The extreme enrichment of the PGE in meteorites ($\approx 10^{4}$ relative to crustal abundances) has led to their extensive use as tracers of extraterrestrial material, most spectacularly at the Cretaceous-Tertiary (K/T) boundary (Alvarez *et al.*, 1980; Ganapathy, 1980; Kyte *et al.*, 1980; Orth *et al.*, 1981). However, the distribution of the PGE in crustal materials is poorly known, and their transport by natural waters scarcely studied.

A variety of analytical techniques have previously been used to study these elements in natural samples, including: graphite furnace atomic absorption spectroscopy (GFAAS, Hodge *et al.*, 1986); inductively coupled plasma atomic emission spectroscopy (ICP-AES, Brown and Biggs, 1984); cathodic stripping voltammetry (van den Berg and Jacinto, 1988); instrumental and radiochemical neutron activation analysis (Crocket and Cabri, 1981; Keays *et al.*, 1974; Murali *et al.*, 1990); secondary ion mass

spectrometry (SIMS, Allègre and Luck, 1980); resonance ionization mass spectrometry (Blum *et al.*, 1990; Walker and Fassett, 1986); accelerator mass spectrometry (AMS, Teng *et al.*, 1987); and inductively-coupled plasma mass spectrometry (ICP-MS, Colodner *et al.*, 1993). Most of these methods lack the sensitivity needed for analysis of PGEs in many natural materials. A notable exception is ICP-MS, which has recently been shown to have PGE detection limits of $\approx 10^{10}$ atoms (Colodner *et al.*, 1993). This technology is undergoing rapid development, and recent advances in nebulization methods promise 10 - 100 fold improvements in this threshold.

In the case of Ir, the most commonly used analytical method is neutron activation analysis, due to the high neutron absorption cross section of ^{191}Ir. Samples containing as little as $\approx 6 \times 10^6$ atoms of Ir have been analyzed using the coincidence/anticoincidence counting method (Murali *et al.*, 1990), but sample sizes analyzed by RNAA are more typically in the range 5×10^9 - 10^{11} atoms (Alvarez *et al.*, 1990; Kyte *et al.*, 1993). Neutron activation has the advantage of low sensitivity to contamination following irradiation. However, materials such as seawater cannot be irradiated without chemical separation of Ir from solution (drying of seawater being problematic due to the high salt content of seawater). Additionally, the yields of any chemical separation procedures must be carefully controlled.

Recent advances in negative thermal ionization mass spectrometry (NTIMS, Creaser *et al.*, 1991; Völkening *et al.*, 1991; Zeininger, 1984) provide the sensitivity needed to analyze all the PGE in typical crustal materials (*e.g.*, sediments, granitic rocks, waters). An NTIMS procedure with a detection limit of $\approx 2 \times 10^6$ atoms of Ir is presented here, along with chemical methods allowing the routine, precise measurement of Ir in 1 - 10 L of water

at sub-femtomolar concentrations (10^{-15} mol L^{-1}). The clean separation of PGEs from other materials has been a substantial obstacle to routine PGE analysis with previous analytical methods. These methods required processing of large quantities of material to isolate enough PGE atoms. These quantities are often impractically large, and high levels of contamination may be introduced during processing. The high sensitivity of NTIMS makes this problem more manageable. Additionally, the use of isotope dilution methods minimizes uncertainties due to variable yields.

Similar techniques have been developed for rhenium analysis (Anbar *et al.*, 1992), and should be useful for the other PGE in a variety of samples. Application of this methodology should lead to the thorough characterization of the chemistry of Ir and the other PGE in natural waters, and a detailed examination of PGE distributions in typical rocks and sediments. These goals have long been elusive.

4.3. Experimental Section

The chemical procedures are outlined in Fig. 4.1, and described briefly below. Details presented in the following subsections include the preparation of ultra-clean reagents and materials (**4.2.1**), the preparation, calibration and equilibration of Ir spike solutions for isotope dilution (**4.2.2**), preconcentration procedures (**4.2.3**), and the NTIMS methodology (**4.2.4**). Yields, blanks, detection limits and concentration measurements are discussed in the subsequent section (**4.3**).

The procedures used here capitalize on the high affinity of $IrCl_6^{2-}$ for strongly basic anion exchange resin in dilute acid solutions ($K_d > 10^3$), and on the comparatively weak binding of $IrCl_6^{3-}$ to the same resin in strong HCl

solution (K_d < 1 in 6 M HCl) (Korkisch and Klakl, 1968; Kraus *et al.*, 1954). These complexes are expected to be the dominant forms of Ir in solutions acidified with HCl (Brajter *et al.*, 1979; Marcus, 1967). Ir in aqueous solution is easily converted to $IrCl_6^{2-}$ by chlorine gas (Hodge *et al.*, 1986), and resin-bound $IrCl_6^{2-}$ is readily reduced to $IrCl_6^{3-}$ by sulfur dioxide gas (Petrie and Morgan, 1982). In our procedure, acidified samples spiked with a ^{191}Ir-enriched tracer for isotope dilution are bubbled with Cl_2 (g), and passed over columns packed with anion exchange resin. Ir is eluted with solutions of SO_2 in water and HCl. The Ir from several liters of water can be separated in this manner using small quantities of resin. This scheme greatly reduces the quantity of acid needed for elution compared to other methods, minimizing blanks and the amount of organic residue resulting from degradation of the resin due to exposure to strong acids and Cl_2 (g).

Two approaches were used (Fig. 4.1). In Procedure I, prepared natural waters were directly loaded on columns. In Procedure II, Ir was preconcentrated from spiked solutions by coprecipitation with ferric oxyhydroxide, and then processed by anion exchange. Procedure I is not practical for solutions with high concentrations of dissolved organics, or of certain metals (*e.g.,* Mn), since these may form suspensions or precipitates which obstruct the resin bed or which interfere with Ir redox chemistry. Procedure I is also not practical for water samples with very low concentrations, which require larger volumes of solution and resin with concomitant increase in blanks. These problems are avoided in Procedure II. Only a fraction of the organic material is scavenged by the iron, and residual organics in the precipitate are easily decomposed with perchloric acid (Smith, 1953). The precipitate is then dissolved in a few tens of milliliters of acid,

from which Ir is easily separated by anion exchange. Since this procedure greatly reduces the volume of solution exposed to the column, Ir can be loaded from a solution acidic enough to prevent precipitation of other metals, without breakthrough of Ir. This procedure also reduces the blanks from column chemistry.

It must be stressed that these procedures are simple enough for the rapid analysis of a large number of samples. Ir can be separated from many samples in parallel, so that mass spectrometry becomes the rate-limiting step. Allowing 1 hour to analyze each sample, a throughput of as many as 12 samples per day is feasible using a mass spectrometer with a multiple-filament turret.

4.3.1. *Preparation of Reagents and Materials*

All reagents were ultra-high purity (Table 4.1). Concentrated hydrochloric and nitric acids were twice sub-boiling point distilled in quartz by a commercial supplier (Seastar Chemicals, Inc.) and stored in FEP bottles. Ultra-pure water was prepared in our laboratory by double distillation in quartz of 18 MΩ water produced by an ion exchange system (Millipore Super-Q) fed by water purified by reverse osmosis. This was the only water used in the chemistry. Water distilled once in quartz was used for some cleaning operations.

Solutions containing SO_2 (g) or Cl_2 (g) ("Cl_2-H_2O" or "SO_2-H_2O") were prepared by passing high purity gases through 0.2 μm Teflon filters and water scrubbers, and bubbling into water for 1 - 2 minutes. These solutions were prepared within 24 hours of use. Concentrated ammonium hydroxide solution was similarly prepared using NH_3 (g). Anion exchange resin (Bio-

Rad AG1-X8, 100-200 mesh) was cleaned by packing 100 mL (wet volume in H_2O) in a quartz column, and rinsing with the following sequence of ultra-pure reagents, added 100 mL at a time: 500 mL H_2O; 500 mL 12 M HCl; 300 mL H_2O; 250 mL ethanol; 200 mL H_2O; 500 mL 8 M HNO_3; 250 mL 12 M HNO_3; 400 mL 3 M HCl. The clean resin was stored in 3 M HCl in an FEP bottle.

Pure iron was prepared by solvent extraction with ether (Hillebrand *et al.*, 1953). Reagent-grade ferric chloride (25 gm of $FeCl_3 \bullet 6H_2O$; Mallinkrodt) was dissolved in ≈ 250 mL of 6 M HCl, and divided between three 250 mL Teflon FEP separatory funnels. The Fe in each funnel was then extracted in one pass with ≈ 150 mL of reagent-grade ethyl ether (Mallinkrodt), previously cleaned by water extraction. Although one-pass extraction does not recover all the Fe, it minimizes the Ir in the extracted Fe. Fe was then back-extracted into water, until the ether solution was colorless. The aqueous solution was dried almost to saturation (< 10 mL), whereupon it was dissolved in 250 mL 6 M HCl. This extraction procedure was repeated twice. The final aqueous extract was dried to < 10 mL to remove residual ether, and then diluted to ≈ 150 mL with H_2O. Approximately 75% of the original Fe was recovered by this procedure, while the Ir content fell from 3 x 10^{10} to 4.5 x 10^{8} atoms gm^{-1} (Table 4.1). It was found that reagent-grade $FeCl_3 \bullet 6H_2O$ had the lowest initial Ir content; other Fe salts were 2 - 10 times more contaminated, even if they were of higher purity. 99.9999% pure Fe metal (Johnson Matthey) was found to contain > 4.5 x 10^{11} atoms gm^{-1} of Ir.

Labware in contact with samples and reagents was exclusively polypropylene, polyethylene or Teflon (FEP or PFA), acquired commercially (*e.g.*, Nalgene, Savillex). All plastics were cleaned by degreasing in soap

solution. Teflon items were then sequentially boiled in aqua regia, 8 M HNO_3 and distilled water. Polyethylene and polypropylene were soaked in 3 M HNO_3 at room temperature, and then soaked in distilled water. The acids used during cleaning were all reagent grade (Baker). All labware was finally rinsed with double-distilled water.

4.3.2. *Isotopic Spike Preparation, Calibration and Equilibration*

Iridium metal powder enriched in ^{191}Ir (96.19%) was obtained from the Oak Ridge National Laboratory. Approximately 100 μg of the metal was introduced to a 0.5 mL quartz tube, along with 50 μL 12 M HCl and 5 μL 16 M HNO_3. The solution was cooled in liquid nitrogen, and the tube fused shut. This was encased in a steel jacket, and heated in an oven to 250°C (Wichers *et al.*, 1944). After 18 hours, most of the metal had dissolved. The resulting solution was decanted with 6 M HCl, dried to small volume, and passed through a 0.2 μm Teflon membrane filter. To separate Ir from the other PGE, the solution was passed over a 0.2 mL anion exchange column which was then rinsed with 3 mL 4 M HNO_3 and 3 mL SO_2-saturated 1 M HCl. The Ir was then eluted with 3 mL of 2.5 M HCl. The eluant was dried, taken up and dried in 1 mL aqua regia to oxidize the Ir, taken up and dried in 12 M HCl to convert to the chloride salt, and finally dissolved in 500 mL 4 M HCl in a FEP bottle. The isotopic composition of this spike solution was determined by NTIMS ($^{191}Ir/^{193}Ir = 28.54 \pm 0.03$).

The concentration of this solution was calibrated by isotope dilution against an Ir standard of normal isotopic composition ($^{191}Ir/^{193}Ir = 0.5930 \pm 0.0010$, also determined by NTIMS) made from ammonium hexachloroiridate salt (Johnson Matthey) dissolved in 4 M HCl. The Ir content of this salt is

43.59% according to stoichiometry, and 43.08% according to an Ir assay by the supplier. The average of these values is adopted here, and assigned a maximum uncertainty of ± 1%. This uncertainty is adequate for the purposes of this study. Spike and standard aliquots were weighed to ± 0.05 mg, mixed, agitated, and bubbled with Cl_2 (g) passed through a 0.2 μm Teflon filter and a water scrubber. This last step oxidizes all dissolved Ir to $IrCl_6^{2-}$ (Colodner, 1991; Hodge *et al.*, 1986), ensuring equilibration between spike and standard. At least 12 hours after chlorination, the mixture was dried and analyzed by NTIMS. The spike solution was found to have a concentration of 65.63 ± 0.68 ng gm^{-1}. Calibration of subsequent dilutions of this stock spike solution against dilutions of the standard solution yielded concentrations within 1% of the values expected from gravimetry, indicating no difficulty in equilibrating spikes and standards to this level of precision.

Natural water samples to be analyzed by isotope dilution were acidified with HCl to 0.025 M in the field, within hours of collection. In the lab, samples were weighed (typically ± 0.05 gm for a 4 kg sample), and spiked with 0.5-2 gm (± 0.05 mg) aliquots of a calibrated ^{191}Ir solution (3.51 pg gm^{-1}) to obtain $^{191}Ir/^{193}Ir \approx 2$, close to the optimal value needed to minimize uncertainties. The mixtures were agitated, and chlorinated. At least 24 hours were allowed to pass between chlorination and the Ir separation chemistry, to ensure complete conversion to $IrCl_6^{2-}$ and isotopic equilibration. Samples were repeatedly agitated during this time.

4.3.3. *Iridium Preconcentration*

As outlined above, Ir was preconcentrated either by passing samples directly over anion exchange columns ("Procedure I"), or by ferric

oxyhydroxide coprecipitation, followed by anion exchange separation of Ir from the precipitate ("Procedure II"). The preparation of the columns was identical in both cases. 1 mL (wet volume) of anion resin was packed in a 1 cm diameter polypropylene column (Bio-Rad). Fresh resin was used for every sample. Porous polyethylene frits at the top and bottom of the resin bed prevented disturbance. The resin was washed with 2 x 10 mL of 6 M HCl, and conditioned with 2 x 10 mL of Cl_2-H_2O.

In Procedure I, samples were spiked and chlorinated in 4 L polyethylene bottles with a molded 0.25" tubulation, and drip-loaded through corrugated FEP tubing attached to the tubulation and the column. Solutions were allowed to drip freely, with rates never exceeding 5 mL /minute.

In Procedure II, Fe was added to samples following equilibration with the spike. NH_4OH was then added dropwise, until a pH of 8.5 - 9.0 was reached and a fine Fe-oxyhydroxide precipitate developed. Typically, 300 mg of Fe and 20 mL of concentrated ammonium hydroxide solution were used for a 4 L acidified sample. The solution was agitated repeatedly over 5 - 7 days to maximize the scavenging yield, after which the precipitate was permitted to settle for 24 hours. Most of the solution was siphoned off, and the remaining Fe-rich slurry transferred to a pair of 250 mL wide-mouth polyethylene bottles. These were centrifuged at 3000 rpm for 20 minutes. The solution was carefully decanted, and the remaining precipitate transferred to a pair of 50 mL polypropylene centrifuge tubes. The precipitate was spun at 3000 rpm for 10 minutes, the solution decanted, and each tube filled with H_2O and vigorously shaken, in order to rinse residual salts and ammonia. The tubes were centrifuged again at 3000 rpm for 10 minutes, and the water decanted and monitored for pH. A second H_2O rinse was typically performed, after

which the pH was usually ≈ 8; lower pH was avoided to prevent desorption of Ir from the precipitate. The Fe slurry from both tubes (25 - 50 mL wet volume) was transferred to a 100 mL FEP beaker, and gently dried under an infrared lamp. At this stage, samples with large amounts of organic material were digested using 1 - 2 mL of a 2:1 $HClO_4$:HNO_3 mixture (Smith, 1953). All samples were then dissolved in 2.5 mL of 12 M HCl, which was then diluted to 0.6 M, and bubbled with Cl_2 (g). After ≥ 12 hours of equilibration, the sample was loaded on anion resin from a polyethylene reservoir attached to the column.

The same elution was used in both procedures. After loading, columns were rinsed with 2 x 10 mL Cl_2-H_2O, 3 x 2 mL H_2O and 5 mL 1N HNO_3 (to elute W and Mo). Ir was reduced to $IrCl_6^{3-}$ with SO_2-H_2O, added as a 2 mL cut, followed by two 5 mL cuts. Ir was finally recovered in a PFA vial with 10 mL of 6 M HCl, added 1 mL at a time. The 6 M HCl eluant was gently dried to 10 - 20 μL under an IR lamp in an N_2 atmosphere, and typically contained organic residues from the column and the sample. These darkened upon heating, due to polymerization in the presence of H_2SO_4 remaining from the SO_2 reduction. Some of these organics were resistant to treatment with aqua regia and $HClO_4$/HNO_3. Presumably, these were fragments of the vinyl benzene polymer backbone of the anion resin.

Organics were eliminated by UV photolysis with a 500 W xenon arc lamp (ILC Technology). This lamp has a sapphire window to maximize UV intensity, and a rear reflector integrated into the bulb, which collimates the beam. The lamp housing was mounted on a Teflon-coated aluminum stand, approximately 15 cm above the sample oriented to irradiate the sample below. In this orientation, the lamp's arc is vertical, which lengthens the

lifetime of the lamp. The high intensity radiation produced by this lamp must be regarded with caution; even brief exposure can damage the unprotected eye. The entire assembly was shielded with an 18" diameter PVC tube, with a hinged door and ports for gas lines and power cables. The sample vial was placed in a Teflon-coated water-cooled aluminum cooling jacket, which kept the temperature < 100°C. The cooling jacket was covered by a Teflon pot topped by a plate of UV-grade quartz. O_2 gas (filtered through a 0.1 μm Teflon membrane) was passed over the sample; the O_3 thus produced hastened organic decomposition. The gas flowing over the sample was exhausted to a fume hood. Adding 2 mL of 6 M HCl prior to irradiation greatly facilitated the reaction, presumably due to the photo-production of highly reactive Cl radicals in solution. Irradiation for 2 - 3 hours cleared even the murkiest samples, leaving 5 - 10 μL of H_2SO_4. This method proved so efficient and clean that it was used in lieu of any acid treatments for degradation of small amounts of organic matter.

To remove residual salts, a final anion separation was done using 5 - 10 μL resin in a Teflon needle (BoLab) attached to a polypropylene column used as a reservoir. This column was washed with 2 x 200 μL 6 M HCl and conditioned with 4 x 200 μL Cl_2-H_2O. The sample was taken up in 1 mL of 0.025 M HCl, chlorinated, and loaded on the column ≈ 12 hours later. The column was rinsed with 8 x 50 μL Cl_2-H_2O. Ir was reduced and eluted into a PFA vial, using 2 x 200 μL SO_2-H_2O, followed by 1 mL 6 M HCl added in thirds. The eluant was dried to ≈ 5 μL under N_2, UV-irradiated for 30 minutes in the presence of 50 - 100 μL 6 M HCl, and then heated intensely under N_2 until it was reduced to a sub-microliter droplet of H_2SO_4. An

additional UV treatment was performed if this droplet was strongly colored, with 50 - 100 μL 6N HCl.

4.3.4. *Mass Spectrometric Analysis*

Filaments consisted of 0.005" diameter 99.999% purity nickel wire (ESPI). A dimple was impressed in the center of each filament using a clean sapphire rod. This dimple extended the width of the wire, and was ≈ 0.010" long. The sample drop was picked-up with ≈ 0.5 μL 6 M HCl in polyethylene tubing attached to a microsyringe, loaded in the dimple, and carefully dried by passing 0.5 - 1.0 Amps through the filament. The sulfuric acid fumed during dry-down, and care was taken to prevent spattering due to overheating. Minor organic material was occasionally observed, although this was dramatically reduced once the UV procedure was adopted. Since ionization efficiency is inhibited by the presence of organics, these were ashed by heating the filament in air. Some discoloration of the dimple area due to reaction with acids was typical, as was slight oxidative discoloration of the entire wire. The dimple area was covered with $Ba(OH)_2$ (to enhance negative ion emission), and loaded as ≈ 1 μL of a saturated solution.

Separated samples were analyzed in a Lunatic mass spectrometer configured for negative thermal ionization (Creaser *et al.*, 1991; Wasserburg *et al.*, 1969), and equipped with a leak valve and UHP O_2 supply. A secondary electron multiplier (SEM) in ion-counting mode was used as the detector. Filaments were heated to 800 - 900°C (monitored using an optical pyrometer), and O_2 was bled into the ion source to maintain a pressure of ≈ 5 x 10^{-7} torr. Ir was analyzed as IrO_2^- at 223 and 225 amu. Beams at 35 and 37 amu (Cl^-) and 249 and 251 amu (ReO_4^-), observed at lower temperature, were

monitored to optimize focus conditions for IrO_2^-. Data collection began when counting rates > 75 cps were observed at either Ir mass, and continued as temperature increased to ≈ 975°C. The ratio 223/225 was measured repeatedly during the run, and the data collected and processed in real time. Beam intensities were measured at each peak top, and at one half mass to either side of each peak to monitor the background. A four second integration time was used at each mass. The ion intensity at mass 225 was corrected for the contribution from $^{191}Ir^{16}O^{18}O^-$ using $^{18}O/^{16}O = 0.002085$ (Creaser *et al.*, 1991) to obtain the ratio $^{191}Ir/^{193}Ir$ ($^{191}Ir/^{193}Ir = 1/[[1/I_{223}/I_{225}] - 2 \times {}^{18}O/^{16}O]$). The contribution from $^{191}Ir^{17}O^{17}O^-$ at mass 225 was negligible. The average of the measured $^{191}Ir/^{193}Ir$ ratios was then used to calculate the Ir content of the sample, using the isotope dilution equation:

$$N_{sample} = N_s \frac{(R_s - R_m)(1 + R_n)}{(R_m - R_n)(1 + R_s)} \qquad (4.1)$$

where N_s is the moles of spike, R_s, and R_n are the $^{193}Ir/^{191}Ir$ ratios in the spike and normal, respectively, and R_m is the ratio measured in the spiked sample.

4.4. Results and Discussion

4.4.1. *Yields*

Yields were initially determined by "doping" waters with nanogram quantities of isotopically normal Ir, and spiking aliquots separated at various stages of the chemistry with ^{191}Ir for isotope dilution analysis. ICP-MS was an efficient analytical tool for these experiments. Subsequently, yields for natural samples were determined using waters of known concentration and

NTIMS. ICP-MS analyses employed a Perkin-Elmer Sciex ELAN 5000A ICP mass spectrometer with a standard torch and argon plasma, gas flow rates of 15 L/min (plasma), 1 L/min (auxiliary) and 1 L/min (nebulizer), and 1 kW applied power. Standard optical settings were selected. The rate of liquid sample uptake was ≈ 1 mL/min. Peak hopping was employed, with an integration time of 50 - 100 ms during a total data acquisition time of 30 - 60 s for 6 masses.

Yields for various chemical steps are summarized in Tables 4.2 and 4.3. Nearly quantitative recovery of Ir was obtained with the 1 mL anion exchange columns. This high yield was observed for a wide range of solution compositions and volumes, including: 4 L of pure H_2O; seawater acidified to 0.025 M HCl (Fig. 4.2); and 50 - 100 mL Fe-rich solutions of 0.6 M HCl. Yields for the 5 - 10 μL columns were ≈ 75%. The use of freshly-prepared SO_2-H_2O was critical for reasonable recovery.

In Procedure II, nearly quantitative removal of Ir was attained with 1 gm Fe in a 4 L sample. Good yields were also achieved with $1/10^{th}$ this amount (≈ 75%). 300 mg of Fe was used for actual samples. Recovery of 85% was determined for one sample using Procedure II, by taking a split of the sample after elution from the 1 mL column. Overall yields for actual samples were 60 - 85% for both Procedure I and II.

Recovery by hydrolytic precipitation of Fe is a well-developed technique for a variety of trace elements, but has not previously been used for the recovery of Ir from natural samples. For most cations, pH > 8 is desired. This is consistent with adsorptive scavenging of cations attracted by electrostatic forces, since ferric oxyhydroxide surfaces are negatively charged in alkaline solution (Stumm and Morgan, 1981). Many cations will also

hydrolyze under these conditions, leading to coprecipitation with iron hydrolysis products. However, precipitation of Ir hydroxide begins as low as pH ≈ 5 (Hillebrand *et al.*, 1953), and adsorption of the $IrCl_6^{2-}$ and $IrCl_6^{3-}$ anionic complexes should be favored by acidic pH (when Fe surfaces are protonated). To determine the conditions for optimal iridium recovery, scavenging by Fe precipitates was characterized at several pH values, in both pure waters and seawater. In these experiments, 250 mL solutions in polyethylene bottles were doped to produce ppb concentrations of Ir. Fe was added and precipitated with NH_4OH at controlled pH. The Ir concentration of the residual solution was characterized by sampling 1 - 5 mL aliquots at discrete time intervals. These were spiked, and analyzed by ICP-MS. Additionally, two experiments of Ir scavenging from 4 L seawater samples were done. The results are shown in Table 4.3. Clearly, Ir removal is greatest at high pH, suggesting coprecipitation of Ir hydrolysis products. The slow kinetics are consistent with the literature on Ir ligand exchange (esp. Castillo-Blum and Sykes, 1987).

4.4.2. *Blanks*

A. Chemistry

Close attention was paid to Ir contamination. Total contamination from reagents for each procedure (including the HCl used to acidify the sample immediately after collection) is small relative to the ≈ 10^9 atoms of Ir in a typical 4 L sample (Table 4.1). To quantify the total procedural blank, three approaches were taken. First, blanks were determined for elutions from both the 1 mL columns and the 5 - 10 μL columns. In these experiments, small quantities of spike were dissolved in small volumes of dilute HCl

solution, with or without dissolved Fe. Ir was separated from these solutions using the elution procedures described above, and analyzed by NTIMS. The Ir observed in these experiments (Table 4.4) was comparable to that expected from reagent blanks, indicating no contribution from the resin during this procedure.

As a further constraint, 4 L of clean H_2O was spiked, chlorinated, and processed to separate Ir. This experiment was conducted for both Procedure I and Procedure II, and was intended to reveal the contribution from sources other than reagents (*e.g.*, from sample handling, NH_4OH, etc.). Thus, the H_2O was handled alongside samples (including shipboard filtration and acidification). The results are within 50% of the total reagent blanks, indicating no other sources of contamination (Table 4.4).

A more rigorous control is to use seawater containing no Ir. This was approximated as follows: Seawater samples (4 L) were spiked, chlorinated and processed to determine their Ir concentrations. The solutions remaining after the Ir separation should contain only the Ir remaining due to non-quantitative yields. These "stripped" solutions were spiked and passed through the separation procedure a second time. If the blank enters early in the chemistry, then the number of isotopically normal Ir atoms added during the second pass (N_{blank}) is determined by the relation:

$$N_{blank} = \left(N_{s,2} + (1-Y)N_{s,1}\right)\frac{\left(R_s - R_{m,2}\right)\left(1+R_n\right)}{\left(R_{m,2} - R_n\right)\left(1+R_s\right)} - (1-Y)N_{s,1}\frac{\left(R_s - R_{m,1}\right)\left(1+R_n\right)}{\left(R_{m,1} - R_n\right)\left(1+R_s\right)} \quad (4.2)$$

where N_s is the moles of spike added in each pass, Y is the stripping yield, R_s, and R_n are the $^{193}Ir/^{191}Ir$ ratios in the spike and normal, respectively, R_m is

the ratio of the spiked sample, and the index numbers refer to the first or second passes through the chemistry. An upper limit is obtained when $Y = 1$.

Results for Procedure I were variable, and surprisingly large. For example, using Pacific seawater from 400 m depth, the $^{191}Ir/^{193}Ir$ ratio changed from 4.72 in the original sample to 6.63 in the stripped solution. The same quantity of spike (3.03×10^9 atoms) was added before each pass. This corresponds to 9.44×10^8 atoms of Ir in the original sample, and an upper limit of 5.97×10^8 blank atoms. The blank falls only slightly for likely yields of 80 - 90% (Table 4.2). Even if the yield in this experiment was as low as 50%, the blank is still $> 4 \times 10^8$ atoms. A nominal blank correction of $5 \pm 3 \times 10^8$ atoms is applied to all data determined with Procedure I. This value is substantially higher than the H_2O procedural blank.

The analogous experiment for Procedure II resulted in substantially lower blanks. In an experiment using Baltic near-surface seawater, the $^{191}Ir/^{193}Ir$ ratio changed from 2.50 in the original sample to 10.4 in the stripped solution, again adding the same quantity of spike (6.01×10^9 atoms) each time. This determines an upper limit of 6.0×10^8 Ir atoms. The actual blank is certainly substantially lower than this, since the scavenging efficiency is not 100%. A strict lower bound on this efficiency is 85% (Table 4.2), determined during the same experiment, which corresponds to a blank of $< 1.5 \times 10^7$ using Eqn. 2. The probable range of stripping efficiencies for Fe coprecipitation is 85 - 95% (Tables 4.2 and 4.3), corresponding to a blank of $2 \pm 2 \times 10^8$ atoms. This is a conservative estimate of the Procedure II blank. Most probably, the blank is at the lower end of this range, consistent with the sum of all reagent contributions to the chemistry (Table 4.2). Since Procedure II produces unambiguously lower blanks than Procedure I, it is preferred for

Ir determination in small samples., although Procedure I is adequate for many samples.

The source of the higher Procedure I blank is unknown. It is possible that the high Cl^- content of seawater leads to exchange with a reservoir of Ir in the resin which does not otherwise interact with the solution, due either to the high ionic strength of seawater, or the tendency of Ir to form strong chloro-complexes. To test this hypothesis, reagent-grade NaCl (Mallinkrodt) was dissolved in 4 L of ultrapure water to produce a 0.5 M saline solution, which was processed repeatedly through the anion exchange chemistry. The Ir content fell from an initial level of 9×10^8 to $\approx 2 \times 10^8$ atoms after two strippings. This value is intermediate between the pure water and the stripped seawater blanks, suggesting that chloride content accounts for some of the blank. This is not an entirely satisfactory explanation, since the Cl^- content of the 6 M HCl used in all elutions is an order of magnitude higher than in seawater, while elution blanks are $<< 10^8$ atoms. However, since only 10 mL of this acid are passed over the columns during elution, compared to 4 L of seawater in Procedure I, dramatically different results are plausible. This could also explain the lower Procedure II blank, since only 50 mL are passed over the column following ferric oxyhydroxide precipitation.

B. Filament Loading

High purity Ni wire filaments (ESPI, 99.999%) in combination with $Ba(OH)_2$ produced loading blanks of $< 6 \times 10^5$ Ir atoms (Fig. 4.3; Table 4.4). Blank experiments were repeated many times during the course of the study, and no larger blanks were ever seen using Ni wire.

Several filament metals were tested before settling on Ni. Small quantities of ^{191}Ir spike (1.6×10^8 - 1.6×10^9 atoms) were loaded directly on filaments along with barium salts, and the isotopic composition determined by NTIMS. Blanks are reported as the apparent quantity of Ir determined using this composition and the quantity of spike. The relationship between this value and the actual concentration of Ir in the filament material is not known, and no doubt varies depending on the type of metal (Shen *et al.*, 1995).

Platinum is widely used for NTIMS, since high ionization efficiencies are easily obtained in combination with barium salts (Creaser *et al.*, 1991). However, even the highest purity Pt (ESPI, 99.9999%) gave unacceptably high blanks (3×10^6 - 1.5×10^7 atoms), despite 0.5 - 5% ionization efficiencies. This result is not surprising, given the difficulty of separating Pt from Ir.

Filaments made from high-purity gold wire (Johnson Matthey, 99.9999%) produced the highest ionization efficiency for Ir ($\approx$ 10%) of any metal tested, and acceptable blanks in the range 3×10^7 - 3×10^8 atoms. However, since the temperature of IrO_2^- emission approached the melting point of Au, intense beams of Au^- were generated. These produced a reflected interference in the SEM across the mass range of interest. Even after insertion of a series of baffle plates, which reduced the reflection efficiency to $\approx 10^{-6}$, thousands of counts were still observed. Since this background was variable with mass and time, and more intense than the IrO_2^- beams, the resulting uncertainties were unacceptably large. None of these problems appeared when using Ni filaments (see below).

4.4.3. *Mass Spectrometry*

IrO_2^- emission using Ni filaments typically began slightly above 800°C. Beam intensities increased with temperature. For clean, separated samples of ≈ 4 x 10^9 Ir atoms, counting rates of several hundred cps at both masses were typically observed near 850°C (Fig. 4.4), increasing to 1000 - 2000 cps above 900°C. These intensities were maintained for 30 - 60 minutes. At 975 - 1000°C, emission abruptly dropped, and could not be recovered by lowering the temperature.

No significant background counts were observed using Ni filaments when running either samples or standards (Figs. 4.2 and 4.3). However, in some samples (fewer than 1 in 5), weak ion beams (< 50 cps) were seen at masses 226, 227 and 228, as well as in the range 230 - 240, and a stronger beam (< 500 cps) was seen at mass 245. These fell below detection thresholds as temperature increased and as Ir began to ionize efficiently. Although PtO_2^- emission is expected at masses 226, 227 and 228, these transient ions do not have the isotopic composition expected from unenriched platinum. A small interference at mass 225, observed by systematic increase in the 223/225 ratio over time during the early stages of Ir emission, was strongly correlated with the intensities at 226, 227 and 228. Therefore, these beams were carefully monitored until they fell to zero, or until the relative intensities expected from Pt emissions were observed. Data obtained prior to these conditions was rejected. The 223/225 ratio remained constant within uncertainties once the transient peaks were gone. For typical natural samples, this ratio was determined to a precision of 1 - 10%. Most of this uncertainty derives from counting statistics. No systematic variation was observed, indicating negligible mass fractionation.

The effective ionization efficiency (EIE) is defined as the ratio of ions counted to atoms loaded on the filament. For separated samples this value ranged from 0.1 - 0.3%, and ≈ 0.3% for Ir spikes and standards. The variation in ionization efficiencies and operating temperatures depends on the amount of organic material and residual salt in the final load; dirtier samples require higher temperature and ionize less efficiently. Ionization efficiencies for processed samples increased by an order of magnitude after the UV procedure was adopted for organic decomposition.

The ratio of ions generated in the ion source to atoms loaded on the filament is somewhat higher than the EIE, since ions are lost during transit through the instrument, and due to limitations of the detection system. While the transmission efficiency of the Lunatic mass spectrometers approaches unity, the conversion efficiency of the SEM for IrO_2^- ions was only ≈ 30%, due to the low impact energy (≈ 5 kV) in our system.

4.4.4. *Detection Limits*

Absolute detection limits can be derived using these observations. Conservatively, a beam of 5 cps intensity for 10 minutes is required to collect meaningful data. This corresponds to 3,000 ions. For clean samples with 0.1 - 0.2% effective ionization efficiency, this translates to a minimum sample size of 1.5 - 3 x 10^6 atoms. This limit is comparable to the smallest samples analyzed by neutron activation (Murali *et al.*, 1990; Rocchia *et al.*, 1990). It is ≈ 10^3 - 10^4 times lower than typically obtained with RNAA (*e.g.,* Kyte *et al.*, 1993). A further factor of three improvement is possible with NTIMS, by using higher energy ions to improve conversion efficiency on the SEM.

At present, detection limits are determined by chemical blanks. Given a blank of $2 \pm 2 \times 10^8$ Ir atoms (Procedure II), $\approx 2 \times 10^9$ Ir atoms are needed to achieve precision of 10% or better. For a 4 L water sample, this requires concentrations $\geq 2.5 \times 10^8$ atoms/kg. Samples approximately three times larger are needed to achieve similar precision with Procedure I.

4.4.5. *Analytical Results*

Ir concentrations have been measured in a suite of water samples from the Pacific Ocean and the Baltic Sea system. The results are presented in detail in Chapter 5. Typical mass spectra are presented in Fig. 4.4. The data in Fig. 4.4a demonstrate that the procedures described above can be applied to water from the Pacific Ocean to determine Ir concentrations as low as $(4.4 \pm 0.8) \times 10^8$ atoms kg^{-1} (7×10^{-16} mol kg^{-1}). Much higher precision is attained in the more concentrated river waters which drain into the Baltic Sea (Fig. 4.4b).

4.5. Acknowledgments

Thanks are owed to M. Anbar and G. R. Rossman for many helpful conversations, especially those pertaining to the UV photolysis procedure. ICP-MS analyses were performed at the Bank of America Environmental Analysis Center at the California Institute of Technology. P. G. Green's assistance with this instrument was invaluable. T-L. Ku and J. Chen provided an initial sample of solvent-extracted iron for testing.

4.6. References

Allègre, C.-J., and J.-M. Luck, Osmium isotopes as petrogenic and geological tracers, *Earth Planet. Sci. Lett.*, *48*, 148-154, 1980.

Alvarez, L. W., W. Alvarez, F. Asaro, and H. V. Michel, Extraterrestrial cause for the Cretaceous-Tertiary extinction: Experimental results and theoretical interpretation, *Science*, *208*, 1095-1108, 1980.

Alvarez, W., F. Asaro, and A. Montanari, Iridium profile for 10 million years across the Cretaceous-Tertiary boundary at Gubbio (Italy), *Science*, *250*, 1700-1702, 1990.

Anbar, A. D., R. A. Creaser, D. A. Papanastassiou, and G. J. Wasserburg, Rhenium in seawater: Confirmation of generally conservative behavior, *Geochim. Cosmochim. Acta*, *56*, 4099-4103, 1992.

Blum, J. D., M. J. Pellin, W. F. Calaway, C. E. Young, D. M. Gruen, I. D. Hutcheon, and G. J. Wasserburg, Resonance ionization mass spectrometry of sputtered osmium and rhenium atoms, *Anal. Chem.*, *62*, 209-215, 1990.

Brajter, K., K. Slonawaska, and Z. Vorbrodt, Separation of rhodium(III)-platinum(IV) and iridium(III)-platinum(IV) on Varion AT-400 and Varion AT-600 exchangers, *Chem. Anal. (Warsaw)*, *24*, 763, 1979.

Brown, R. J., and W. R. Biggs, Determination of platinum and palladium in geologic samples by ion exchange chromatography with inductively coupled plasma emission spectrometric detection, *Anal. Chem.*, *56*, 646-649, 1984.

Castillo-Blum, S. E., and A. G. Sykes, Substitution inertness of $[Ir(H_2O)_6]^{3+}$, *Polyhedron*, *6*, 101-103, 1987.

Colodner, D. C., The Marine Geochemistry of Rhenium, Iridium and Platinum, Ph.D. Thesis, MIT/WHOI, WHOI-91-30, 1991.

Colodner, D. C., E. A. Boyle, and J. M. Edmond, Determination of rhenium and platinum in natural-waters and sediments, and iridium in sediments by flow-injection isotope-dilution inductively coupled plasma-mass spectrometry, *Anal. Chem.*, *65*, 1419-1425, 1993.

Creaser, R. A., D. A. Papanastassiou, and G. J. Wasserburg, Negative thermal ion mass spectrometry of osmium, rhenium, and iridium, *Geochim. Cosmochim. Acta*, *55*, 397-401, 1991.

Crocket, J. H., and L. J. Cabri, Analytical methods for the Platinum-Group Elements, in *Platinum Group Elements: Mineralogy, Geology, Recovery*, edited by L. J. Cabri, Canadian Institute of Mining and Metallurgy, Montreal, 1981.

Crocket, J. H., and H. Y. Kuo, Sources for gold, palladium and iridium in deep-sea sediments, *Geochim. Cosmochim. Acta*, *43*, 831-842, 1979.

Esser, B. K., and K. K. Turekian, The osmium isotopic composition of the continental crust, *Geochim. Cosmochim. Acta*, *57*, 3093-3104, 1993.

Fenner, F. D., and B. J. Presley, Iridium in Mississippi River suspended matter and Gulf of Mexico sediment, *Nature*, *312*, 260-262, 1984.

Ganapathy, R., A major meteorite impact on the Earth 65 million years ago: Evidence from the Cretaceous-Tertiary boundary clay, *Science*, *209*, 921-923, 1980.

Hillebrand, W. F., G. E. F. Lundell, H. A. Bright, and T. I. Hoffman, *Applied Inorganic Analysis-2nd Ed.*, Wiley, New York, 1953.

Hodge, V., M. Stallard, M. Koide, and E. D. Goldberg, Determination of platinum and iridium in marine waters, sediments and organisms, *Anal. Chem.*, *58*, 606-620, 1986.

Keays, R. R., R. Ganapathy, J. C. Laul, U. R. S. Krahenbuhl, and J. W. Morgan, The simultaneous determination of 20 trace elements in terrestrial, lunar and meteoritic material by radiochemical neutron activation analysis, *Anal. Chim. Acta*, *72*, 1-29, 1974.

Korkisch, J., and H. Klakl, Anion exchange behavior of the platinum metals and gold in hydrochloric acid-organic solvent media, *Talanta*, *15*, 339-346, 1968.

Kraus, K. A., F. Nelson, and G. W. Smith, Anion-exchange studies. IX. Adsorbability of a number of metals in hydrochloric acid solutions, *J. Phys. Chem.*, *58*, 11, 1954.

Kyte, F. T., K. Leinen, R. G. Heath, and L. Zhou, Cenozoic sedimentation history of the central North Pacific: Inferences from the elemental geochemistry of core LL44-GPC3, *Geochim. Cosmochim. Acta*, *57*, 1719-1740, 1993.

Kyte, F. T., Z. Zhou, and J. T. Wasson, Siderophile-enriched sediments from the Cretaceous-Tertiary boundary, *Nature*, *288*, 651-656, 1980.

Levinson, A. A., *Introduction to Exploration Geochemistry-2nd Ed.*, Applied Publishing, Wilmette, IL, 1980.

Marcus, Y., Metal-chloride complexes studied by ion-exchange and solvent extraction methods. II. Transition metal elements and the hexavalent actinides, *Coord. Chem. Rev.*, *2*, 257, 1967.

Murali, A. V., P. P. Parekh, and J. B. Cumming, On the determination of iridium in diverse geological samples employing HPGe-

coincidence/NaI(Tl)-anticoincidence spectrometry, *Geochim. Cosmochim. Acta*, *54*, 889-894, 1990.

Orth, C. J., J. S. Gilmore, J. D. Knight, C. L. Pillmore, R. H. Tschudy, and J. E. Fassett, An iridium abundance anomaly at the palynological Cretaceous-Tertiary boundary in northern New Mexico, *Science*, *214*, 1341-1343, 1981.

Petrie, R. K., and J. W. Morgan, Anion-exchange separation of platinum and iridium using perchloric and hydrochloric acid solutions, *J. Radioanal. Chem.*, *74*, 15, 1982.

Ravizza, G., and G. McMurtry, Osmium isotopic variations in metalliferous sediments from the East Pacific Rise and the Bauer Basin, *Geochim. Cosmochim. Acta*, *57*, 4301-4310, 1993.

Rocchia, R., P. Bonté, C. Jéhanno, E. Robin, M. de Angelis, and D. Boclet, Search for Tunguska event relics in the Antarctic snow and new estimation of the cosmic iridium accretion rate, 1990.

Shen, J. J., D. A. Papanastassiou, and G. J. Wasserburg, Precise Re-Os determinations and systematics of iron meteorites, *Geochim. Cosmochim. Acta*, Submitted., 1995.

Smith, G. F., The wet ashing of organic matter employing hot concentrated perchloric acid: The liquid fire reaction, *Anal. Chim. Acta*, *8*, 397-421, 1953.

Stumm, W., and J. J. Morgan, *Aquatic Chemistry- 2nd Edition*, John Wiley & Sons, Inc., New York, 1-780, 1981.

Taylor, S. R., and S. M. McLennan, *The Continental Crust: Its Composition and Evolution*, Blackwell Scientific Publications, Oxford, 1985.

Teng, R. T. D., U. Fehn, D. Elmore, T. K. Hemmick, P. W. Kubik, and H. E. Gove, Determination of Os isotopes and Re/Os using AMS, *Nucl. Instr. and Meth. in Phys. Res.*, *B29*, 281-285, 1987.

van den Berg, C. M. G., and G. S. Jacinto, The determination of platinum in sea water by adsorptive cathodic stripping voltammetry, *Anal. Chim. Acta*, *211*, 129-139, 1988.

Völkening, J., T. Walczyk, and K. G. Heumann, Osmium isotope ratio determinations by negative thermal ionization mass spectrometry, *Intl. J. Mass Spectrom. Ion Proc.*, *105*, 147-159, 1991.

Walker, R. J., and J. D. Fassett, Isotopic measurement of subnanogram quantities of rhenium and osmium by resonance ionization mass spectrometry, *Anal. Chem.*, *58*, 2923-2927, 1986.

Wasserburg, G. J., D. A. Papanastassiou, E. V. Nenow, and C. A. Bauman, A programmable magnetic field mass spectrometer, *Rev. Sci. Instrum.*, *40*, 288-295, 1969.

Wichers, E., W. G. Schlecht, and C. L. Gordon, Attack of refractory platiniferous materials by acid mixtures at elevated temperatures-RP#1614, *Journal of Research of the National Bureau of Standards*, *33*, 363-381, 1944.

Zeininger, H., Ph.D. Thesis, University of Regensburg, 1984.

Table 4.1. Reagent Blanks.

Reagent	Ir Content (atoms/gm)
H_2O:	$< 8.0 \times 10^4$
HCl (12 M):	$\approx 3.2 \times 10^6$
HNO_3 (16 M):	$< 1.2 \times 10^6$
$HClO_4$ (70%):	$\approx 1.0 \times 10^8$
NH_4OH (10 M):	$\approx 2.0 \times 10^6$
Fe	
Starting Material:	3×10^{10}
Ether-extracted:	$\approx 1.5 \times 10^8$
	Ir Content (atoms)
Total Reagents	
Procedure I:†	$\approx 8.5 \times 10^7$
Procedure II:††	$\approx 1.8 \times 10^8$

Reagents prepared as described in the text.

†10 mL 12 M HCl to acidify samples, 10 mL 12 M HCl to wash columns, 5 mL 12 M HCl and 0.3 mL 16 M HNO_3 for elution, and H_2O from various solutions.

††Same reagents as Procedure I, plus 0.3 gm Fe and 20 mL 10 M NH_4OH.

Chemical decomposition of organics introduces another $\approx 10^8$ atoms from 1 mL of 70% $HClO_4$ and 1 - 5 mL of 16 M HNO_3.

Table 4.2. Chemical Yields.

Procedure	Yield
Anion resin elution (1 mL):[a]	80 - 90%
Anion resin elution (5 μL):[a]	75 - 85%
Fe precipitation[b]	
1.0 gm:	90%
0.3 gm:[c]	85%
0.1 gm:	75%
Total Procedure I:	60 - 80%
Total Procedure II:	60 - 80%

(a) Elution yields apply to a wide range of sample sizes and compositions, as discussed in the text; (b) yields from 4 L of seawater using the indicated quantity of Fe; (c) includes rinsing of precipitate and separation with 1 mL resin.

Table 4.3. Fe Coprecipitation.

pH	Fe (ppm)†	*t* (hrs)	$Ir(t)/Ir_0$
Fresh Water			
1.5	-	36	1.06
5.5	40	36	0.30
		144	0.31
		210	0.19
7.5	40	2	0.69
		36	0.54
		72	0.32
		120	0.23
9.5	40	2	0.71
		36	0.38
		72	0.34
		120	0.31
Seawater			
1.5	-	48	1.12
		240	1.07
6.0	40	120	0.86
9.5	25††	168	0.25
9.5	40	48	0.51
		240	0.17
9.5	250††	168	0.10

Ir_0 = Ir initially in solution

†mg Fe/kg solution.
††Scavenging from 4 L;
all others from 250 mL.

Table 4.4. Procedural Blanks.

Procedure	Ir Blank (atoms)
Anion resin elution (1 mL):[a]	$\approx 1.5 \times 10^7$
Anion resin elution (5 μL):[a]	$\approx 6.0 \times 10^6$
Anion resin elution w/Fe (1 mL):[b]	$\approx 4.0 \times 10^7$
Total Procedure I	
H_2O:	$\approx 6.3 \times 10^7$
Seawater:	$5 \pm 3 \times 10^8$
Total Procedure II	
H_2O:	$\approx 1.0 \times 10^8$
Seawater:	$2 \pm 2 \times 10^8$
Filament Loading:[c]	$\approx 6.3 \times 10^5$

(a) Determined by loading small quantities of spike on resin, followed by rinses and elution procedure discussed in text; (b) spike loaded on resin from 25 mL of 0.6 N HCl solution containing 300 mg dissolved Fe; (c) Ni wire filament w/$Ba(OH)_2$ activator.

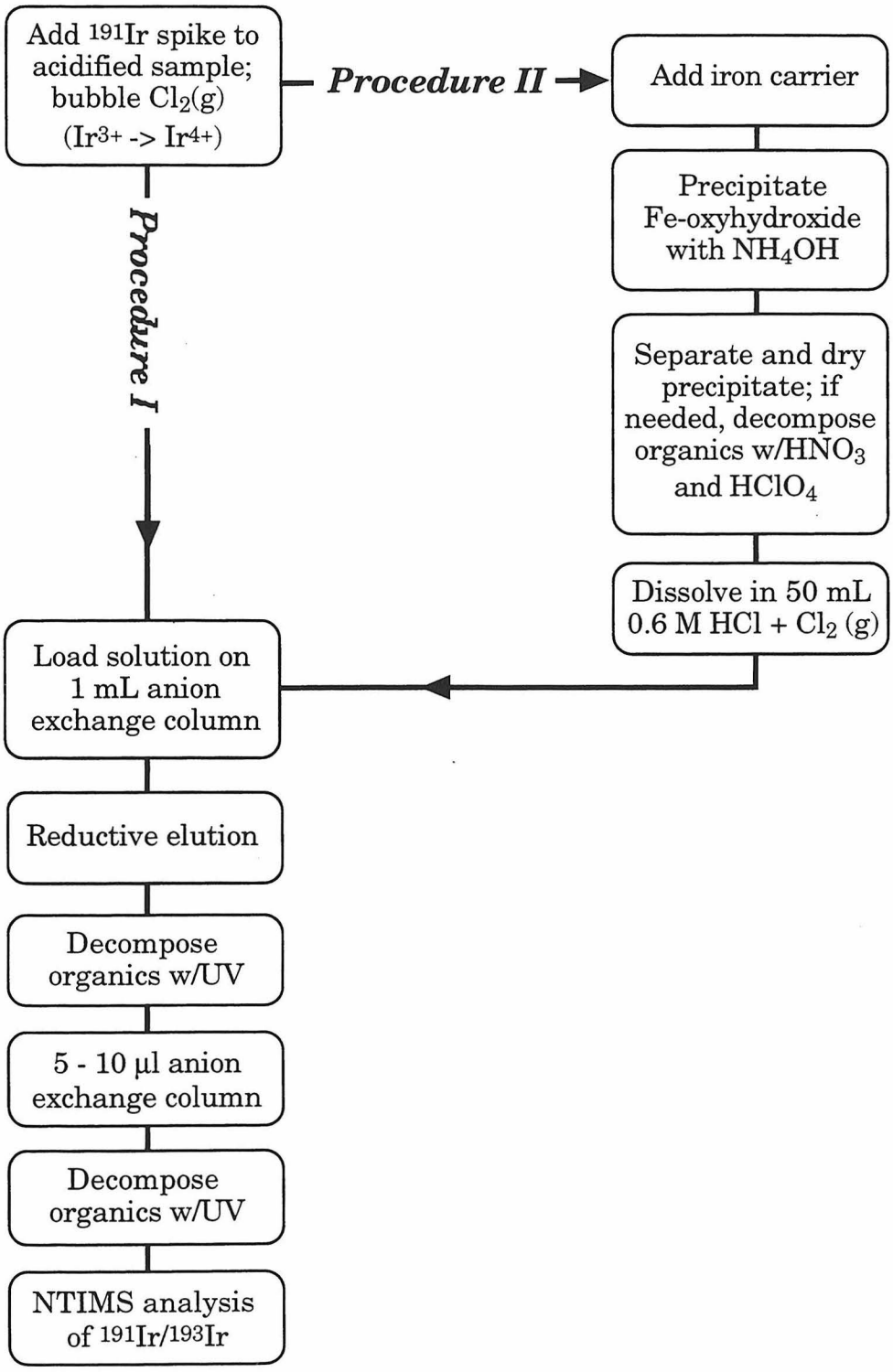

Fig. 4.1. Outline of the procedures used to separate Ir from natural water samples. Typical starting sample size was ≈ 4 L.

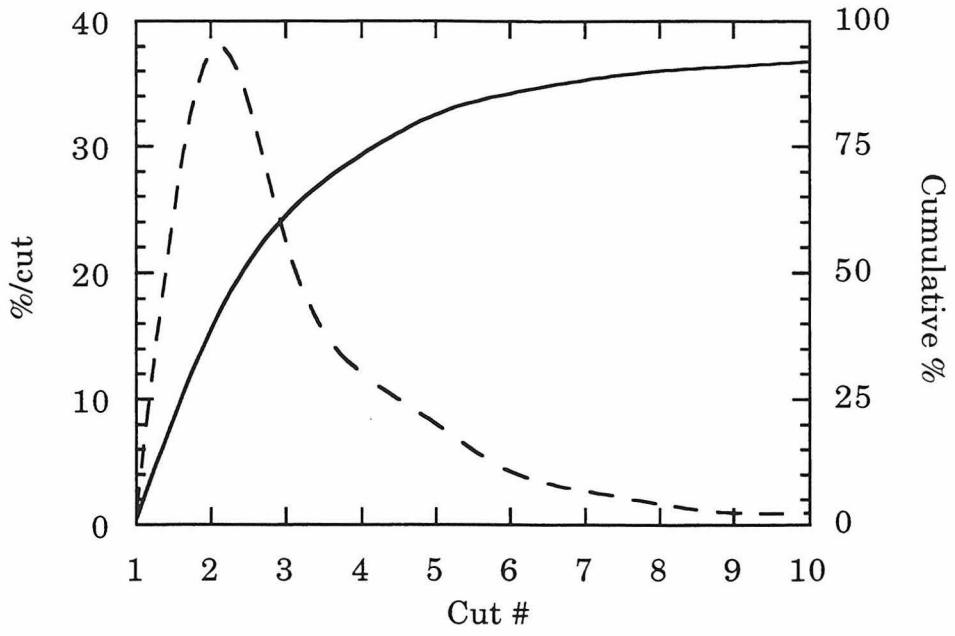

Fig. 4.2. Iridium recovery using the reductive elution procedure. In this experiment, a two liter seawater sample was "doped" with ≈ 4 x 10^{12} atoms of isotopically normal iridium, and passed over a 1 mL anion exchange column (Bio-Rad AG 1X8). Following reduction with SO_2-saturated water, the HCl eluant was collected in 1 mL cuts, spiked with ^{191}Ir, and analyzed by ICP-MS. The figure shows the cumulative recovery of Ir (solid line), and the percent of the total Ir recovered in each cut (dashed line). Similar results were obtained with seawater samples as large as 4 L, and with smaller samples of various compositions.

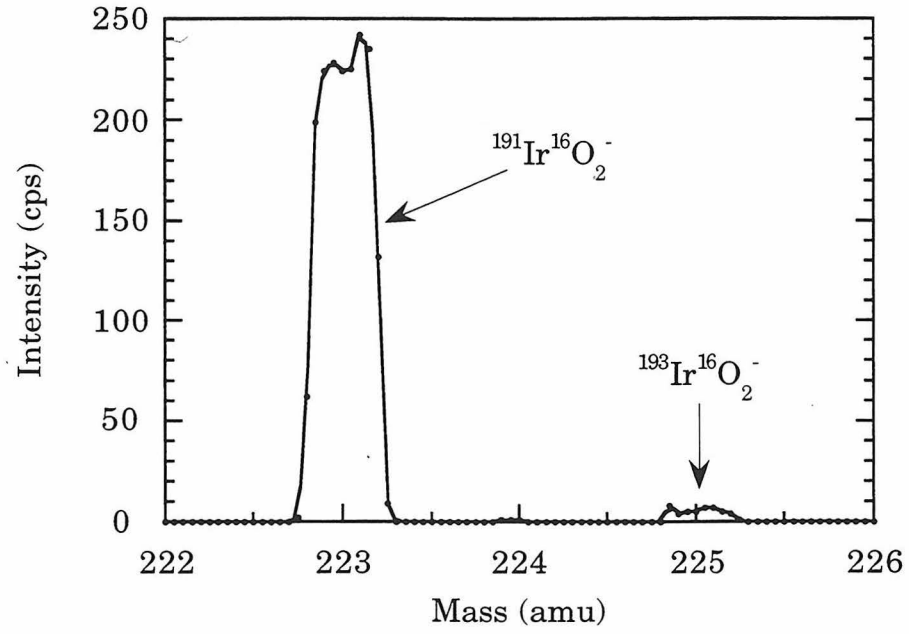

Fig. 4.3. Mass spectrum of 5.5 x 10^8 atoms of ^{191}Ir spike (^{191}Ir/^{193}Ir = 28.54 ± 0.03) loaded on a nickel wire filament, and analyzed by NTIMS. Data were collected at intervals of 0.05 amu with a two second integration time. The measured ratio (after correction for the contribution from $^{191}Ir^{18}O^{16}O^-$ at mass 225) is indistinguishable from pure spike, indicating a negligible loading blank, and no significant isobaric interferences.

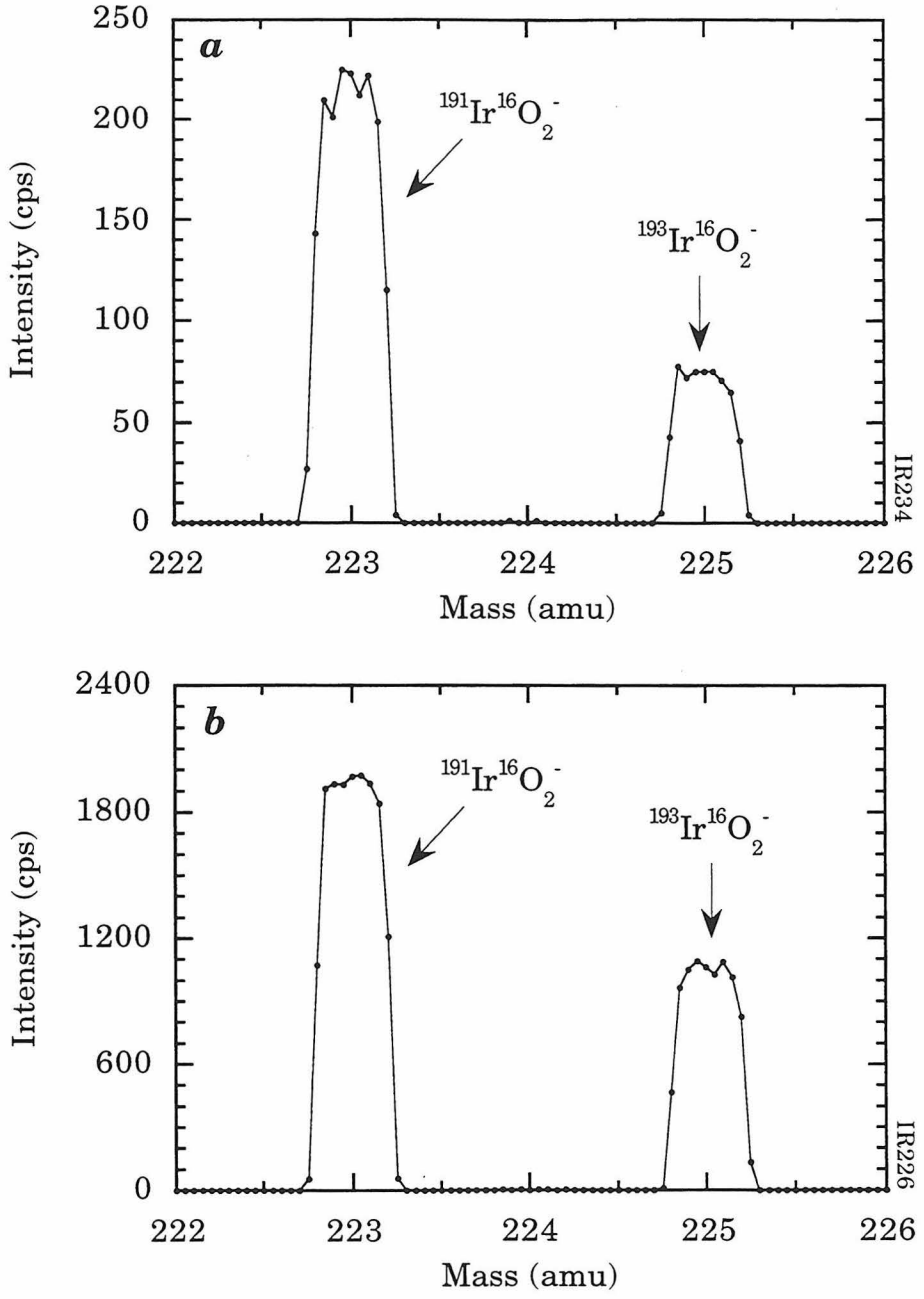

Fig. 4.4. Typical mass spectra observed during analysis of separated samples. Data were collected at intervals of 0.05 amu with a two second integration time. T ≈ 880°C. a) Ir separated from 4 L of water from the Pacific Ocean (1000 m depth). The concentration was determined to be (4.4 ± 0.6) x 10^8 atoms kg^{-1}. b) Ir separated from 4 L of water from the Kalixälven River, northern Sweden. The concentration was determined to be (17.4 ± 0.9) x 10^8 atoms kg^{-1}.

Chapter 5.

Iridium in Natural Waters

5.1. Abstract

The concentration of Ir has been measured in the Pacific Ocean, the North Sea and the Baltic Sea by isotope dilution negative thermal ionization mass spectrometry (ID-NTIMS) following the clean chemical separation of Ir from 4 L of seawater. The concentration of Ir in the oceans is fairly uniform, ranging from 2.9 to 5.7 x 10^8 atoms kg^{-1}, making Ir the least abundant stable element in seawater. No significant difference is seen between the concentrations in the mixed layer and 1000 m in the Pacific Ocean, or between the Pacific Ocean and the North Sea. The concentrations in the rivers draining into the Baltic Sea are much higher. The lowest river concentration was measured in the Kalixälven river ((20 ± 2) x 10^8 atoms kg^{-1}), which is presumed pristine. Higher concentrations are seen in the Neva and Wistula rivers ((49.7 ± 1.3) and (92.9 ± 2.2) x 10^8 atoms kg^{-1}, respectively), presumably due to anthropogenic inputs. In the Baltic Proper, Ir does not follow conservative mixing. The average concentration is (10 ± 1) x 10^8 atoms kg^{-1}. A simple mass balance model indicates that ≈ 75% of the riverine input is removed rapidly from solution. Under oxidizing conditions, Ir is scavenged by Fe-Mn oxyhydroxides. The enrichment of Ir in anoxic waters relative to overlying oxic waters demonstrates that anoxic sediments are not a major sink for Ir. It is proposed that Ir in the Baltic Sea is removed into the ferromanganese sediments deposited beneath oxic waters. These observations are used to construct a preliminary marine geochemical budget of Ir, along with published measurements of total Ir in marine pelagic

sediments. Despite considerable uncertainties, global riverine inputs of ≈ 75 mol yr^{-1} may be balanced by a sink of 50 - 100 mol yr^{-1} of hydrogenous Ir in marine sediments, after the sediment data are corrected for inputs from aeolian dust and extraterrestrial Ir. Other inputs of dissolved Ir are apparently negligible, with the possible exception of deep-ocean hydrothermal systems. The residence time of Ir in the oceans is 10^3 - 10^4 yr. These findings place new constraints on events at the Cretaceous/Tertiary boundary.

5.2. Introduction

Iridium is the PGE most often analyzed in natural samples. Yet, the low-temperature geochemistry of Ir is poorly understood. This fact is not altogether surprising, since analytical limitations have confined most studies to samples enriched in Ir, such as the sediments at the Cretaceous/Tertiary (K/T) and some other stratigraphic boundaries (Alvarez *et al.*, 1980; Alvarez *et al.*, 1982; Crocket *et al.*, 1988; Ganapathy, 1980; Gostin *et al.*, 1989; Holser *et al.*, 1989; Hsü *et al.*, 1985; Kyte *et al.*, 1980, 1981; McLaren and Goodfellow, 1990; Orth *et al.*, 1988a; Orth *et al.*, 1981; Orth *et al.*, 1988b; Playford *et al.*, 1984, Wang *et al.*, 1993; Wilde *et al.*, 1986), meteoritic materials (*e.g.*, Baedecker and Ehmann, 1965; Ganapathy *et al.*, 1971; Morgan *et al.*, 1975; Palme *et al.*, 1978), and ultramafic rocks (Crocket, 1981). The abundance of Ir in these materials is controlled by the chemistry of Ir at high temperatures and pressures. There are comparatively few measurements of Ir in the materials typical of the Earth's surface environment, due to the much lower abundance of Ir in these samples (*e.g.*, Barker and Anders, 1968; Colodner *et al.*, 1992; Crocket and Kuo, 1979; Fenner and Presley, 1984; Fresco, 1985; Hodge *et al.*, 1986; Keays and Scott, 1976; Kyte *et al.*, 1993; Wells *et al.*, 1988). Some of these studies hint at a fairly reactive chemistry in low temperature systems, in which Ir may be dissolved, mobilized and scavenged into authigenic phases. Measurements of Ir in natural waters can help transform these hints into a quantitative understanding of the low temperature geochemistry of Ir. This has obvious implications for the interpretation of Ir enrichments in the sedimentary record, which may or may not be related to the input of extraterrestrial Ir.

On thermodynamic grounds, Ir in seawater is expected to exist as the anionic chloro-complex $IrCl_6^{3-}$, with the Ir cation in the trivalent oxidation state (Baes and Mesmer, 1986; Cotton and Wilkinson, 1988; Goldberg *et al.*, 1986). Since Ir also forms strong hydroxy complexes (Gamsjäger and Beutler, 1979), it has the potential to be particle reactive (*e.g.,* Dzombak and Morel, 1990; Erel and Morgan, 1991). The only published measurements of Ir in natural waters come from two pioneering studies. Goldberg and coworkers used ion exchange chemistry to separate Ir from 100 L of seawater for analysis by graphite furnace atomic absorption spectrometry (Goldberg *et al.*, 1986; Hodge *et al.*, 1986). They determined a value of $\approx$ 1 pg kg^{-1} (3.1 x 10^9 atoms kg^{-1}). Fresco (1985) determined a concentration approximately ten times higher using neutron activation and a reductive precipitation procedure. Goldberg *et al.* (1986) estimated a residence time of $\approx$ 40,000 yr with respect to removal in marine sediments, similar to the residence times of nickel and palladium. This is a plausible result, since the chemistry of Ir in seawater should reflect a balance between its affinity for the chloride ion and a strong tendency to hydrolyze (Goldberg *et al.*, 1986). However, both these studies were limited to a handful of samples collected very near the California coast. Their relation to the bulk ocean is uncertain. No seawater profiles are available, nor are there any measurements of dissolved Ir in river waters. The behavior of Ir in the estuarine environment, where much can be learned about chemical reactivity and transport phenomena, is completely unknown.

In this study, Ir concentrations have been determined in a suite of water samples from the Pacific Ocean, the North Sea, the Baltic Sea, and several rivers draining into the Baltic. The seawater samples include waters

from the Pacific Ocean at depths of 25 m (the mixed layer), 400 m and 1000 m, and from the North Sea at 80 m depth. In the Baltic Sea, most samples are from above 100 meters, where the waters are oxygenated. Waters were also sampled in anoxic waters at one location.

These samples include a range of water types. The location chosen for the Pacific Ocean study is the subject of a long-term monitoring project in which salinity, temperature, dissolved oxygen and nutrients are routinely analyzed (Karl and Winn, 1991). It is therefore a benchmark location for oceanographic studies. Both conservative and highly particle-reactive trace elements have recently been characterized at this location (Anbar *et al.*, 1992; Roy-Barman *et al.*, 1996), making it an ideal location for the first determination of Ir in the open ocean. The Baltic Sea, North Sea and rivers provide a first look at the behavior of Ir in an estuarine environment, and at the effects of redox chemistry on dissolved Ir. Additionally, the Ir content of the rivers may reflect contrasting rock types, as well as the effects of anthropogenic inputs. Finally, the ongoing characterization of other trace elements and of hydrology in the Baltic system (Andersson *et al.*, 1995; Andersson *et al.*, 1992; Andersson *et al.*, 1994; Bergström and Carlsson, 1994; Boström *et al.*, 1983; Boström *et al.*, 1981; Falkenmark and Mikulski, 1975) makes it possible to gain insights by comparing Ir with other trace metals. In many ways, the Baltic Sea and its drainage system are an excellent "natural laboratory" for studies of trace element aqueous geochemistry.

5.3. Description of Field Sites

5.3.1. *The Pacific Ocean*

Pacific Ocean seawater was sampled at Station ALOHA, one of two locations selected for long-term oceanographic study as part of the Joint Global Ocean Flux Study (JGOFS) and the Hawaiian Ocean Time series program (HOT). A complete description of the HOT program and Station ALOHA is found in Karl and Winn (1991). This station is in the North Pacific Subtropical Gyre, 100 km north of Oahu, HI, and ≈ 50 km upwind of the Hawaiian Ridge (22°45' N; 158°00' W; Fig. 5.1). It is therefore a deep water location, bottoming at 4750 m, and is believed to be well removed from biogeochemical perturbation from the Hawaiian Islands. The gyre is bounded by the northeastward motion of the Kuroshio current along the east coast of the Asian continent, which merges into the eastward-trending North Pacific Current. Most of these waters turn southward upon reaching the west coast of North America, forming the California Current which, in turn, flows south to meet the westward-moving North Equatorial Current. This circulation pattern produces the largest uniform body of water on the Earth's surface (Karl and Winn, 1991). The oligotrophic surface waters are characterized by low nutrient concentrations, temperatures in excess of 24°C, and a mixed layer which varies in depth seasonally, from 40 to 100 m. An oxygen minimum is typically observed at 400 - 800 m depth, reaching dissolved O_2 values well below 100 μmol kg^{-1}. As part of the JGOFS/HOT program, the waters at Station ALOHA are sampled every 4 - 6 weeks, and a wide range of biogeochemical parameters are studied.

5.3.2. *The Baltic Sea, North Sea and Rivers*

Much of the following description is adapted from the reviews of Andersson *et al.* (1992, 1994, 1995), and from the hydrological studies of Bergström and Carlsson (1994) and Falkenmark and Mikulski (1975).

The Baltic Sea is an intracontinental sea in northern Europe. A map of the region, the sampling stations and the rivers sampled in this study is shown in Fig. 5.2. It is typically divided into at least four sub-basins: the Gulf of Bothnia (including the Bothnian Bay and the Bothnian Sea), the Gulf of Finland, the Gulf of Riga, and the Baltic Proper. The Kattegat, Danish Sounds, Belt Sea, Öresund and the Skagerrak are generally not considered part of the same system, although these areas are important for the regional hydrology.

A drainage basin of 1,729,000 km^2 is the dominant source of fresh water to the Baltic Sea; subsurface runoff is minimal, while annual precipitation and evaporation are nearly balanced (Falkenmark and Mikulski, 1975). The mean annual volume of fresh water entering this system from 1950 to 1990 was ≈ 446 km^3, excluding the Kattegat/Danish Sounds where another 37 km^3 of fresh water enter each year (Bergström and Carlsson, 1994). The geographic distribution of these waters is shown in Fig. 5.2. The inputs are almost equally divided between waters draining Precambrian crystalline basement to the west, north and northeast (≈ 45% of the drainage area, corresponding to ≈ 50% of the water), and waters draining a terrain of diverse Phanerozoic sediments to the south and southeast (Winterhalter *et al.*, 1981). These waters enter the Baltic Sea through dozens of individual rivers. The two largest rivers are the Neva (78 $km^3\ yr^{-1}$) and the Wistula (34 $km^3\ yr^{-1}$).

Major centers of population and industry are located along both of these rivers (*e.g.,* Leningrad and Gdansk), and a total population of nearly 70 million people live within the entire drainage basin. Thus, the fresh waters entering the Baltic, especially those from the south and southeast, are subject to substantial anthropogenic contamination. Evidence of increasing trace metal contamination of the Baltic Sea in the last 50 yr is seen in the concentrations of anthropogenic trace metals in sediment cores from the Baltic Proper (Hallberg, 1991). These inputs are concentrated in the southern latitudes. It is not clear how much of this input is riverine, and how much is airborne. Most of the rivers carry substantial quantities of organic pollutants due to sewage and agricultural industries (Dybern and Fonselius, 1981). One of the least contaminated rivers is the Kalixälven River, believed to be one of the few substantial rivers in Scandinavia which remains pristine (Pontér *et al.*, 1992).

The river waters mix with seawater in a basin of 21,000 km^3 volume and 377,400 km^2 area to produce the largest body of brackish water in the world (brackish water is defined as water of salinity between 0.5‰ and 17‰, Parker, 1984). The residence time of water in the Baltic Proper, with respect to fresh water inputs, is ≈ 45 yr. The overall residence time is closer to 35 yr, reflecting the input of seawater, which enters from the North Sea, via the Skagerrak (*e.g.,* Andersson *et al.*, 1992). Most of the mixing takes place in a transition region comprised of the Kattegat, Danish Sounds, Belt Sea and Öresund (hereafter referred to collectively as the Kattegat). This is a narrow, shallow region of average 40 m depth, forming a sill as shallow as 10 m which is an effective a barrier to free flow between the North Sea and the Baltic Proper. The mixing in this region is complex. On short time scales, the water

moves back and forth, driven largely by weather conditions. This produces complex currents and salinity gradients. Thus, estimations of the fluxes in and out of the Baltic Proper through the Kattegat, which typically use salinity as a conservative tracer, are somewhat variable, since they depend on which area in the Kattegat is chosen to represent the incoming waters (Ehlin, 1981). Most incoming seawater, however, remains in the transition region, and never enters the Baltic Proper. The net flow clearly carries brackish waters out to the North Sea. On longer time scales, this gentle mixing is punctuated by episodes of intense inflow associated with persistent westerly winds. Such events, which can bring in more water than delivered annually by the rivers, are separated by intervals of at least several years (Falkenmark and Mikulski, 1975).

The continuous input of fresh waters to the surface of the Baltic Proper generates a two-layer flow, in which a permanent halocline separates surface waters of 7 - 8‰ salinity flowing out from the Baltic Proper from 10 - 13‰ bottom waters flowing inward. The stability of the halocline sharply restricts convective mixing between the two layers. Since the bottom waters are renewed slowly, primarily during the irregular inflow events, stagnant conditions develop in the bottom water. While the surface layer is fully oxygenated, the bottom layer is frequently below saturation with respect to O_2, and some deep basins become anoxic between renewal episodes (Falkenmark and Mikulski, 1975; Grasshoff and Voipio, 1981). This is the case at station BY-15, where a stable redoxcline separates H_2S-bearing waters below 150 m from the oxygenated waters above. These waters were most recently renewed in 1995 and in 1979.

Surface salinities in the Gulf of Bothnia and the Gulf of Finland are substantially lower than in the Baltic Proper, due to the proximity of massive fresh water sources. These gulfs are also shallower than the Baltic Proper (average depths of ≈ 55 m and 40 m, respectively, compared to ≈ 70 m for the Baltic Proper), and lack the deep (> 100 m) basins found in the Baltic Proper. The penetration of seawater to these gulfs is therefore minimal, and the salinity stratification is much less pronounced. As a result, these waters rarely become anoxic, which contributes to the high abundance of ferromanganese concretions in the sediments of these gulfs.

5.4. Sampling and Analytical Procedures

5.4.1. *Sampling*

A. The Pacific Ocean

Waters from the Pacific Ocean were collected in collaboration with the Hawaiian Ocean Time series project in September, 1994 (HOT-57; R/V *Moana Wave*). Pressure, temperature, conductivity and dissolved oxygen were monitored continuously with depth using a conductivity-temperature-depth probe (CTD). The mixed layer depth was ≈ 50 m. Samples were recovered using PVC Niskin bottles, with Teflon-coated internal springs, lowered on a steel cable. Upon collection, waters were immediately transferred to 12 L acid-cleaned polyethylene bottles and acidified with 20 mL of ultrapure 12 N HCl (Seastar). The samples were stored in these bottles until analysis. The same sampling procedures have been used successfully in our lab to study the marine chemistry of Re and Th. No contamination problems have been observed.

B. The Baltic Sea, North Sea and Rivers

Water samples from the Baltic Proper, the Kattegat, the Gulf of Bothnia and the North Sea were collected aboard the R/V *Argos* (Fishery Board of Sweden) from 1991 to 1995 in collaboration with the Swedish Meteorological and Hydrological Institute (Andersson *et al.*, 1995; Andersson *et al.*, 1992; Andersson *et al.*, 1994). Sampling was done with PVC Niskin-type bottles with Teflon-lined 60 L GO-FLO bottles. Pressure, temperature, conductivity and dissolved oxygen were determined at all stations and depths. Upon recovery, waters were immediately transferred to polyethylene containers for storage before filtration. Filtration of most samples was performed in the field, within 3 hours of sample collection, before acidification. Anoxic waters containing H_2S were filtered immediately after recovery to minimize oxidation. A peristaltic pump with silicon tubing was used to pressurize the filtration system. The filters were acid-cleaned using 1 M HNO_3 and rinsed before use. Samples were either passed through 0.45 μm and 0.10 μm filters mounted in a series of polycarbonate filter holders, or through 0.45 μm filters only. The filters were 142 mm diameter, and made of cellulose nitrate. Following filtration, samples were acidified to ≈ 0.025 M (pH < 2) with 12 M HCl (Seastar), and stored in acid-cleaned polyethylene bottles. Typically, 10 - 20 L were collected from each site, with 4 L used for Ir determination.

River water samples were filtered *in situ,* using a portable peristaltic pump to pump water through silicon tubing submerged ≈ 0.3 m below the river surface. These waters were passed through 0.45 μm cellulose nitrate filters, and acidified using 25 mL of ultrapure 12 M HCl in each 10 L sample.

A few samples from the Baltic Proper were acidified without filtration. These were later filtered in the laboratory, through 0.45 μm Teflon filters mounted in an acid-cleaned cartridge made of Teflon PFA. North Sea waters were acidified to 0.025 M HCl, but not filtered.

5.4.2. *Analytical Procedures*

Ir concentrations were determined using ultra-clean chemical separation techniques and isotope dilution negative thermal ionization mass spectrometry (ID-NTIMS). This method permits the rapid, routine and precise analysis of Ir in as little as four liters of seawater. The analytical procedures were described in detail in Chapter 4, and are summarized below.

All reagents used were ultrapure, acquired commercially or prepared in the laboratory using standard techniques. The spike solution for isotope dilution analysis was prepared by dissolving ^{191}Ir-enriched metal (Oak Ridge National Laboratory) in 4 M HCl. The concentration of the spike solution was calibrated against a gravimetrically-prepared solution made from high-purity NH_4IrCl_6 salt. The uncertainty of the Ir content of this salt is ≈ 1%, based on the difference between stoichiometry and an Ir assay by the manufacturer. The isotopic composition of the spike, and of normal Ir, were determined by NTIMS.

Samples were spiked with an accurately-weighed ^{191}Ir-enriched spike solution, and bubbled with Cl_2 (g) to convert all dissolved Ir to $IrCl_6^{2-}$ (Hodge *et al.*, 1986). All sample volumes were ≈ 4 L, except for two determinations in the Pacific mixed layer, for which 8 L were processed. The spiked samples were repeatedly agitated over a 24 hour period. Separation of Ir was accomplished using one of two procedures. In Procedure I, water was loaded

directly onto anion exchange resin columns (Bio-Rad AG1-X8; 1 mL wet volume). In Procedure II, an iron oxyhydroxide coprecipitation method was used as an initial separation step. Ultraclean iron was prepared by repeated ether extraction of $FeCl_3 \bullet 6H_2O$, and precipitated by neutralization with NH_4OH prepared by bubbling NH_3 (g) into pure water. Approximately 300 mg of iron and 20 mL of NH_4OH (added dropwise to achieve pH $\approx$ 8.5) resulted in > 85% recovery of Ir from a 4 L seawater sample. The precipitate was separated by centrifugation, dried, and treated with $HNO_3/HClO_4$ to decompose organics. The precipitate was then dissolved in 2 mL 12 M HCl, and loaded on a 1 mL anion exchange column from 0.6 M HCl bubbled with Cl_2 (g). Subsequent chemistry was identical for both procedures. After Ir was loaded, the column was rinsed with chlorinated water (20 mL), pure water (6 mL), and 1 M HNO_3 (5 mL) to elute Re, W and Mo. Ir was reduced on the column to $IrCl_6^{3-}$ using 17 mL of pure water bubbled with SO_2 (g), and finally eluted with 10 mL of 6 M HCl. Recovery through the column chemistry was nearly quantitative. The eluant was dried, redissolved in 2 mL 6 M HCl, and irradiated under a high-intensity UV lamp to decompose residual organics. A second anion exchange procedure using a 5 µL column removed residual salts, and a second UV step eliminated organics introduced by this column. Overall yields ranged from 50 - 75%. For the separation of Ir from a 4 L sample, the blank corrections were $5 \pm 3 \times 10^8$ atoms for Procedure I, and $2 \pm 2 \times 10^8$ atoms for Procedure II. An additional correction of 10^8 atoms was applied for every mL of $HClO_4$ used to decompose organics. This treatment was needed only for river water samples, and for one sample from anoxic waters in the Baltic. The amount of $HClO_4$ used in this treatment was typically 0.5 mL. The determination of these blanks is discussed in detail in

Chapter 4. Procedure II is preferred for large volume samples bearing little Ir, as well as for samples with large amounts of dissolved organics or metals; these tend to precipitate upon chlorination, rendering Procedure I impractical. These blank corrections were applied to all samples, and were assumed to scale with the quantity of reagents used.

The chemically separated Ir was loaded on a high-purity Ni wire filament (ESPI) along with $Ba(OH)_2$, and analyzed in a Lunatic mass spectrometer configured for negative ions (Creaser *et al.*, 1991; Wasserburg *et al.*, 1969). The filament was heated to 850 - 950°C, and Ir analyzed as $^{191}Ir^{16}O_2^-$ (223 amu) and $^{193}Ir^{16}O_2^-$ (225 amu). Concentrations were calculated from the ratio 223/225, after correction for the contribution of $^{191}Ir^{16}O^{18}O^-$ at mass 225 ($^{18}O/^{16}O$ = 0.002085, Creaser *et al.*, 1991). Ion beam intensities of 1000 - 2000 counts per second (cps) were typically sustained for at least 30 min. Ionization efficiencies for separated samples ranged from 0.1 - 0.3%. No background was observed, nor were there any interferences at the measured masses. Filament loading blanks were < 10^6 atoms.

5.5. Results and Discussion

Iridium concentrations in waters from the Pacific Ocean and the Baltic Sea system are presented in Tables 5.1, 5.2 and 5.3. Ir concentrations were determined in seawater and other natural waters using 4 L samples. This sample size is 25 times smaller than that required by Hodge *et al.* (1986). These results demonstrate that ID-NTIMS is an analytical method well suited to the study of PGE low-temperature geochemistry, when coupled to ultra-clean chemical procedures.

Samples are classified according to filtration and acidification procedures. Seawater samples were acidified upon collection, but not filtered, raising the possibility of desorption of Ir from particle surfaces. Following the convention applied to manganese in seawater (Klinkhammer and Bender, 1980; Landing and Bruland, 1980), data from these waters are said to reflect "total dissolvable Ir" (Ir_{td}). Most samples from the Baltic Sea and all river waters were filtered in the field to 0.45 μm or 0.10 μm prior to acidification. Following standard conventions, this procedure defines "dissolved Ir" (Ir_d).

The quality of the data is briefly assessed in section **5.5.1**, followed by detailed presentation and discussion of the observations in sections **5.5.2** through **5.5.5**. The chemical scavenging of Ir by Fe-Mn oxyhydroxides is considered in section **5.6**. Implications for the geochemical cycle of Ir and the interpretation of Ir abundances in sediments are discussed in sections **5.7** and **5.8**.

5.5.1. *Data Quality*

Analytical precision was limited by counting statistics ($\sigma = n^{1/2}$) and by uncertainties in the correction for the chemical blank, with the former accounting for no more than half of the total uncertainty. Uncertainties ($\pm 2\sigma$) were ± 5% to 10% for sample sizes of ≈ 4 x 10^9 atoms, such as typical samples from the Baltic Sea. Significantly lower uncertainties were obtained in Ir-rich river waters. Uncertainties for ocean data are somewhat higher due to the lower concentration of Ir in seawater.

Strong evidence for the reproducibility of both Procedure I and Procedure II in determining Ir_d is found in the uniformity of the data from waters above the halocline in the Baltic proper (samples BY-15 A, B and C,

and BY-28 A; note that sample BY-28 B was analyzed for Ir_{td}). The pooled standard deviation of these samples (σ) is 0.65 atoms kg^{-1}. This is comparable to the uncertainties from the blank correction and counting statistics. The uniformity observed in two samples below the redoxcline at station BY-15, determined by Procedure II (Ir_d; samples BY-15 D and BY-15 E), is further evidence that this method produces reliable data. Good reproducibility is seen in the determination of Ir_{td} in Pacific surface waters, although there is some difference between the values determined with Procedure I and Procedure II. A significant difference between the two procedures is also seen in the river water data. These differences are discussed below.

Two samples used for blank determinations consisted of pure water from an 18 MΩ water purification system, and were handled alongside samples for all manipulations. This included shipboard filtration during a Baltic sampling expedition in 1992, acidification, and storage in acid-clean polyethylene bottles. The blank content in these samples was negligible (Table 5.3).

5.5.2. *The Oceans*

This study reveals that Ir is the least abundant stable element in the oceans, with a deep water concentration of $4.4 \pm 0.6 \times 10^8$ atoms kg^{-1}. This concentration is lower than that of any other PGE determined to date (Anbar *et al.*, 1992; Bertine *et al.*, 1993; Colodner *et al.*, 1993a; Colodner *et al.*, 1993b; Hodge *et al.*, 1986; Jacinto and van den Berg, 1989; Lee, 1983). The concentrations in the Pacific Ocean and the North Sea are an order of magnitude lower than observed by Hodge *et al.* (1986), and a hundred times lower than determined by Fresco (1985). As noted above, these earlier studies

were in near-shore Pacific surface waters. The tenfold decrease in Ir concentration from the California coast to the open Pacific is similar to the Mn distribution observed in a transect from Santa Cruz, CA to the Hawaiian Islands (Landing and Bruland, 1980). In the case of Mn, aeolian and riverine sources were suggested, with some evidence for both (Klinkhammer and Bender, 1980; Landing and Bruland, 1980). Similar sources probably account for the distribution of Ir.

The average concentration of Ir in the Pacific Ocean mixed layer ($4 \pm 2 \times 10^8$ atoms kg^{-1}) is very close to that at 1000 m depth ($4.4 \pm 0.6 \times 10^8$ atoms kg^{-1}). This profile is different from those of the other PGE. Pt in the Indian Ocean decreases by about a factor of six from the surface to 1000 m (Jacinto and van den Berg, 1989), while a Pt profile in the eastern Pacific Ocean had the opposite trend, indicating nutrient-like behavior (Goldberg *et al.*, 1986). Roughly uniform depth profiles have been seen in one study of Pt in seawater, in both the Atlantic and Pacific oceans (Colodner, 1991). Pd and Rh in the Pacific ocean both have nutrient-like trends (Bertine *et al.*, 1993; Lee, 1983). The closest analog for Ir in seawater may be Au, which has some chemical similarities to the PGE. Like Ir, Au shows only modest variation in the water column (Falkner and Edmond, 1990). Falkner and Edmond (1990) also saw no difference between Atlantic and Pacific Ocean Au abundances to within a factor of two. The concentrations of Ir in the open Pacific and the North Sea are similarly uniform. Additional insight is gained by comparing crustal and marine abundances of Ir, Au and the other PGEs (Table 5.4). While the ratios Ir/Pt, Ir/Pd and Ir/Rh show profound fractionation between the elements when going from crustal sources to seawater, the ratio Ir/Au changes only by a factor of 3. Falkner and Edmond (1990) estimated a

residence time of $\approx 10^3$ yr for Au in the oceans. On these grounds, a residence time of similar magnitude is likely for Ir.

The small but statistically significant difference observed between surface seawater values determined with Procedure II and Procedure I ($2.6 \pm 1.2 \times 10^8$ atoms kg^{-1}) may indicate that complexation with organic compounds is important in Ir speciation. In Procedure I, only Ir chloro-complexes are recovered, including those formed from chloride substitution of Ir hydroxy complexes following acidification and chlorination of the samples. The ferric hydroxide precipitation in Procedure II will scavenge organic complexes as well. If organo-iridium species exist in seawater and do not equilibrate with the isotopic spike, then the Ir in these complexes will only appear in Procedure II. Apparently, slightly less than half the dissolvable iridium in the mixed layer exists in these forms, the rest consisting of inorganic complexes. This explanation is plausible, given the apparent affinity of the PGE for organics in natural waters at near-neutral pH (Li and Byrne, 1990; Wood, 1990; Wood *et al.*, 1994), and the extreme enrichment of Ir in both zooplankton and phytoplankton (average content $\approx 6 \times 10^{13}$ atoms kg^{-1} dry weight) (Wells *et al.*, 1988). This result should be regarded as an upper limit, however, due to the magnitude of the blank correction relative to the size of the samples.

5.5.3. *The Baltic Rivers*

The concentration of Ir in the riverwater supplying the Baltic (Table 5.2) is an order of magnitude higher than in seawater, and comparable to previous determinations of Ir in coastal waters (Fresco, 1985; Hodge *et al.*, 1985). The Wistula has the highest concentration, approximately 25 times

that of seawater, while the Kalixälven shows a quarter of this enrichment. The Wistula is enriched in a variety of dissolved components relative to the world river average (Andersson *et al.*, 1994). Some of this is due to the terrain being weathered, but anthropogenic sources are generally believed to account for a large fraction.

The difference between Ir_d measured in May '92 and June '95 in the Kalixälven is consistent with the large variability of the dissolved metal load in this river during these months. In early May, for example, snowmelt can increase the water flow by nearly an order of magnitude over a period of days, resulting in short-term variability in trace metal concentrations (Pontér *et al.*, 1992). Thus, a 25% change in Ir_d is not surprising. At the time these samples were collected, the Mn concentrations were within a factor of two of their annual average values. Therefore, the Ir concentrations are believed to be a reasonable representation of the annual average value for the Kalixälven.

The value of Ir_d determined in the Kalixälven using Procedure I is ≈ 20% lower than the value determined by Procedure II on the same waters. As discussed above in the case of the surface Pacific Ocean, it is likely that this difference provides information on the speciation of Ir in the Kalixälven river. These waters had much higher concentrations of dissolved organics than any other samples. Organic residues were recovered with the Fe precipitates, and required digestion with $HNO_3/HClO_4$. Apparently, a substantial fraction of the total dissolved Ir is bound to this material.

A flux-weighted average river concentration of Ir can be estimated from the data presented here. It is assumed that the Kalixälven is representative of all the rivers draining Precambrian terrain (226 $km^3\ yr^{-1}$).

The Neva and Wistula are taken to represent the average riverwater in their drainage basins (112 km^3 yr^{-1} and 114 km^3 yr^{-1}), and the remaining drainage from Phanerozoic terrain (32 km^3 yr^{-1}) is assumed similar to the Neva. The result, $\approx$ 46 x 10^8 atoms kg^{-1}, is similar to the Ir concentration of the Neva (49.7 $\pm$ 1.3 x 10^8 atoms kg^{-1}). The actual average river concentration is probably somewhat higher, since we have neglected anthropogenic inputs from heavily industrialized southern Sweden.

5.5.4. *The Oxic Waters of the Baltic Sea*

In the O_2-bearing waters of the Baltic Proper and the Gulf of Bothnia, the Ir concentrations are notable for their uniformity (Table 5.3). There are no variations with depth, salinity or date of collection. The concentration in these waters is approximately half that in the Kalixälven, and nearly a fifth of the average Baltic river value. The concentration in the North Sea is lower still, by approximately a factor of three. In the transitional waters of the Kattegat (the Anholt sampling station; Fig. 5.2), the concentration is comparable to the Kalixälven, although the salinity of the sampled waters (20‰) indicates only a small contribution from fresh waters. Clearly, the Ir concentration in the Kattegat is not the result of mixing between water from the Baltic Proper and the North Sea.

These results can be compared with the distribution expected if Ir behaved conservatively during estuarine mixing. If the Baltic Sea is described as a simple two-component mixture of average river inputs and seawater, then it follows that:

$$C_{Ir}^{M} = fC_{Ir}^{SW} + (1-f)C_{Ir}^{RW} \qquad (5.1)$$

where C_{Ir}^{M} is the concentration of Ir in mixture M, C_{Ir}^{SW} and C_{Ir}^{RW} are the concentrations in seawater and average river water, respectively, and f is the mass fraction of seawater in the mixture. Since salinity (S) is conservative and well determined in both endmembers, it can be used to obtain f. Thus, we derive:

$$C_{Ir}^{M} = \frac{C_{Ir}^{SW} - C_{Ir}^{RW}}{S^{SW} - S^{RW}} S^{M} + C_{Ir}^{RW} \tag{5.2}$$

This is the equation of a straight line when the Ir concentration is plotted against salinity, with an intercept equal to C_{Ir}^{RW}. Such a mixing line can be drawn between the North Sea and the average river water source (Fig. 5.3, line ***a***). The waters from the Kattegat fall very close to this line. The average river endmember determined by the line connecting the Kattegat and the North Sea (Fig. 5.3, line ***b***) is within 20% of the value derived from the river water measurements. Therefore, the Ir concentration in the Kattegat appears to be the product of conservative mixing of average Baltic river water and the water from the North Sea.

This statement does not apply to the other oxic waters. These data fall well below the conservative mixing line (Fig. 5.3), and are strikingly uniform across a factor of two variation in salinity. The simplest explanation of this result is that a large fraction of the riverine Ir input is removed from solution in the Baltic Proper. It is proposed that Ir is adsorbed onto ferromanganese particles in solution and/or is oxidatively scavenged into ferromanganese oxide minerals. Rapid flocculation of Fe-Mn oxyhydroxides is observed at the river mouths, and rapidly-accumulating ferromanganese crusts and nodules are common in the Gulf of Bothnia and the Gulf of Finland (Ingri, 1985).

Scavenging of Ir would be most rapid in the low salinity waters of these gulfs, where Ir speciation shifts from soluble chloro-complexes to more readily scavenged hydroxy complexes. This process would produce Ir-depleted, low-salinity water emerging from the Gulf of Bothnia and the Gulf of Finland which would be the effective end-member mixing with seawater in the Baltic Proper. The mixing line between this water and water from the North Sea would have a very shallow slope, which probably explains the uniformity of the Ir concentrations in the Baltic Proper despite the variation in salinity. Other trace metals which exhibit uniform concentrations in the Baltic Proper are known to be scavenged by ferromanganse phases (Boström *et al.*, 1983; Boström *et al.*, 1981; Magnusson and Westerlund, 1980). Scavenging of Ir by oxyhydroxide phases is discussed in more detail in section **5.6**.

At the Anholt station, the Ir concentration reflects a mixture of seawater and average river inputs, with little or no contribution from waters flowing out of the Baltic Sea. Presumably, the sample analyzed here is a parcel of inflowing North Sea water which has mixed only with local river waters (the runoff directly into the Kattegat is $\approx$ 37 km^3 yr^{-1}). The local river input must have an Ir content similar to average river water. It is likely that Ir is not significantly depleted in these waters because the residence time of water in the Kattegat is short; a rough estimate of $\approx$ 1 yr is obtained on the basis of surface area, average depth and the rate of flow through the Baltic system. This is probably an overestimate, since 37 km^3 of fresh water pour each year directly into the Kattegat, in addition to the 433 km^3 yr^{-1} which flow through the Baltic Proper (Bergström and Carlsson, 1994). The seawater flowing into the Baltic also passes through this region, further reducing the turnover time. Thus, the freshly mixed waters in the Kattegat would not have

time to become significantly depleted if Ir removal is not instantaneous. This is in contrast to the Baltic Proper, which has a mixing time of ≈ 30 yr. Additionally, while Mn and Fe oxides are a major component of the recent sediments in most of the Baltic Sea, the sediments in the Kattegat are dominated by $CaCO_3$ and aluminosilicates (Belmans *et al.*, 1993). Therefore, there is no local reservoir of Mn and Fe oxides to scavenge Ir from solution.

5.5.5. *The Anoxic Waters of the Baltic Sea*

The Ir content of anoxic waters from the Gotland Deep (station BY-15) is fourfold higher than in the overlying O_2-saturated waters (Table 5.3; Fig. 5.4). These waters lie below a well-developed redoxcline at ≈ 150 m. They contain no dissolved oxygen, and as much as 110 mL L^{-1} H_2S. This anoxic basin is renewed periodically, when meteorological conditions drive large volumes of oxygen-rich North Sea water below the halocline in the Baltic Proper. The basin had been anoxic for 13 yr when the samples were collected.

The composition of these waters may be determined by conservative mixing in the Kattegat; as shown in Fig. 5.3, the anoxic samples fall perfectly on the conservative mixing line with the North Sea and Kattegat waters. These waters were transported from the mixing zone to their present location during the last intrusion from the North Sea, in 1979. Mixing with Ir-depleted Baltic Proper waters was minimal due to the salinity stratification, which confines incoming waters below the halocline. During these massive influx events, water moves from the Kattegat across the bottom of the Baltic in a matter of months, oxygenating the Gotland Deep. Stagnant conditions return fairly soon, and the basin typically returns to the anoxic state within a year or two (Falkenmark and Mikulski, 1975). The deep waters are then

trapped until the next renewal event. Since the incoming waters travel rapidly and have little or no contact with the oxic, low-salinity regions where Ir scavenging presumably occurs, they reach the basin without loss of Ir.

Evidently, little or no loss of Ir occurs in anoxic waters. This is consistent with observations in marine sediments. There is no correlation of Ir with black carbon in pelagic sediments (Goldberg *et al.*, 1986), and Ir is only modestly enriched in anoxic sediments relative to its average crustal abundance (Colodner *et al.*, 1992; Goldberg *et al.*, 1986). Ir is apparently not removed by incorporation into insoluble sulfide phases under these conditions. The thermodynamics of Ir sulfides in the presence of chloride and water are not well known. It is possible that $IrCl_6^{3-}$ is favored over Ir sulfides in high salinity systems, or that soluble complexes with HS^- are important (Stumm and Morgan, 1981). Organo-Ir complexes may also stabilize the solution concentration. Alternatively, the reaction kinetics may be too slow to allow much Ir loss. Some Ir complexation reactions have extremely slow kinetics. For example, in 40°C aqueous solutions, the rate of chloride substitution of the $Ir(H_2O)_6^{3+}$ aquo ion is $< 2 \times 10^{-9}$ M^{-1} s^{-1} (Castillo-Blum and Sykes, 1987).

A number of other elements are enriched in these waters by downward transport on Mn oxyhydroxide particles. These include Th, Sr, Nd, and Sm (Andersson *et al.*, 1995; Andersson *et al.*, 1992; Andersson *et al.*, 1994). Insoluble Mn(IV) oxides are produced at the redox boundary, when Mn(II) from the anoxic waters diffuses and/or advects across the redoxcline. The oxides dissolve shortly after they fall back into the anoxic layer, releasing any bound trace metals. This Mn redox cycle "pumps" particle-reactive trace elements across the redoxcline. Such Mn and Fe oxide particle cycles are well

known in anoxic waters (Bacon *et al.*, 1980; Boström *et al.*, 1988; Emerson *et al.*, 1979; Spencer and Brewer, 1971). Apparently, this mechanism results in little or no accumulation of Ir, or these anoxic waters would not remain on the mixing line. This is considered quantitatively in the next section.

5.6. Iridium Scavenging

5.6.1. *General Considerations*

Scavenging of Ir by ferromanganese phases, proposed above to account for the depletion of Ir in the oxic waters of the Baltic Proper and Gulf of Bothnia, is not surprising. Ferromanganese oxyhydroxides influence the transport and removal of other trace metals in the Baltic (Andersson *et al.*, 1995; Andersson *et al.*, 1992; Boström *et al.*, 1983; Boström *et al.*, 1981; Boström *et al.*, 1988; Boström *et al.*, 1982). In the oceans, the enrichment of Ir and Os in seafloor Mn nodules is well known; concentrations of ≈ 1 ppb are typical, compared to the average crustal value of ≈ 0.05 ppb (Goldberg *et al.*, 1986; Goldberg *et al.*, 1988; Hodge *et al.*, 1986). Hydrogenous scavenging clearly plays a role in the incorporation of Os in Mn nodules (Esser and Turekian, 1988; Palmer *et al.*, 1988), and is suspected for Ir, since Ir concentrations in these sediments generally covary with Os and Pt (Goldberg *et al.*, 1986; Koide *et al.*, 1991). In pelagic sediments, Ir content correlates strongly with Mn content, and with Co and Ni, elements which are known to be removed by hydrogenous scavenging (Goldberg *et al.*, 1986; Kyte *et al.*, 1993). An association of Pt and Ir with Fe-Mn oxyhydroxides is also seen in oxic turbiditic sediments (Colodner *et al.*, 1992).

Ir may be incorporated into these phases by oxidative uptake from the trivalent to tetravalent state, as suggested by Goldberg *et al.* (1986). An

analogous mechanism has been suggested to explain the abundances of Pt, Os and Ce in ferromanganese nodules (Goldberg *et al.*, 1963; Goldberg *et al.*, 1988). Ir may also be removed by adsorption to the surfaces of Fe and Mn oxyhydroxide precipitates. Equilibrium constants for adsorption of divalent cations scale with cation hydroxide binding constants (Dzombak and Morel, 1990). The hydroxide binding constants of Ir^{3+} are large; $\log \beta^{o}_{1IrOH} = 9.63$ and $\log \beta^{o}_{2IrOH} = 8.80$ (Gamsjäger and Beutler, 1979). These values are only one to two orders of magnitude smaller than those of Th^{4+} (Baes and Mesmer, 1986). Th is known to be rapidly removed from seawater by adsorptive scavenging (*e.g.,* Roy-Barman *et al.*, 1996). The difference between Ir_{td} and Ir_{d} at station BY-28 indicates that a sizable fraction of Ir is adsorbed to detrital or authigenic particles, which include a substantial Mn oxyhydroxide component (Boström *et al.*, 1981).

5.6.2. *Scavenging Experiments*

To test the hypothesis that Ir is efficiently scavenged into ferromanganese phases, a series of experiments were conducted to determine the scavenging efficiency of Ir by Mn and Fe oxyhydroxides.

These experiments were conducted at several pH values, and in both pure water and seawater solutions. Mn or Fe oxyhydroxide precipitates were generated in solutions containing $\approx 5 \times 10^{-6}$ M Ir. The solutions were prepared using Fe, Mn and Ir chloride salts dissolved in either pure water or seawater, acidified to pH 2 - 4. These solutions were titrated with NH_4OH to generate precipitates. The titration was stopped at the pH of interest. The solutions were agitated repeatedly over 2 - 240 hours, and the pH adjusted with additional base to compensate for acidification due to cation hydrolysis.

Aliquots drawn over this period were filtered, spiked with a ^{191}Ir-enriched tracer, and the Ir concentration was determined by isotope dilution ICP-MS (see Chapter 4 for a description of ICP-MS procedures). Pt and Re were also included in these experiments, since they are expected to show different affinities for oxide surfaces. In the case of Pt, the high affinity of Pt^{2+} for the chloride ion should result in much weaker adsorption in seawater than in freshwater. Re should show little affinity for surfaces at neutral or alkaline pH, since the Re^{7+} cation is strongly bound to oxygen in the ReO_4^- anion.

The results are presented in Tables 5.5 and 5.6. Clearly, Ir is readily removed by both types of particles at alkaline pH, in either fresh water or seawater. Ir is also efficiently scavenged by Fe at near-neutral pH. A large fraction of the Ir is removed rapidly, although scavenging may continue for many days. Since Fe and Mn are completely oxidized within minutes to hours, this late loss of Ir is presumably due to adsorption rather than oxidative uptake during formation of Fe or Mn oxides. The reduced scavenging by Fe at low pH in seawater is also consistent with an adsorptive process, since $pH_{zpc} \approx 7$ for Fe oxyhydroxide. This is the pH at which the surface has a net zero charge; at lower pH the surface is protonated, creating electrostatic repulsion between the Ir^{3+} cation and the surface (Dzombak and Morel, 1990; Stumm and Morgan, 1981). The situation is somewhat more complex for Mn oxyhydroxide, since the pH_{zpc} of Mn oxides range from ≈ 3 - 7.

In fresh water at low pH, Fe oxyhydroxide is still a good scavenger of Ir because the O^- surface ligands have no competition from chloride for the Ir^{3+} cation. Adsorption of anionic hydroxide complexes may also explain this result.

As expected, Re is not significantly removed from solution under any conditions. The largest Re loss is on Fe oxyhydroxide at pH = 5.5. Since this is below the pH_{zpc}, the positively charged surfaces have some affinity for the ReO_4^- anion. Pt is stripped rapidly and efficiently from fresh water, but loss is negligible in seawater. This is a dramatic demonstration of the stabilizing influence of chloride complexes on Pt in solution. This effect is modest for Ir, which has smaller chloride binding constants (Goldberg *et al.*, 1986).

The pH in the Baltic Proper is usually ≥ 7.3, and values > 8 are not uncommon. In the Gulf of Bothnia, pH ≈ 8 is typical. Therefore, extrapolating from the experimental results presented here, Ir should be efficiently scavenged by Fe and Mn oxyhydroxides in the Baltic Sea. This scavenging should be most efficient in the low salinity waters near the river mouths and in the gulfs.

5.6.3. *Baltic Scavenging Flux*

The considerable depletion of Ir in the oxic waters of the Baltic Sea demands that a large fraction of the riverine Ir input to the Baltic is removed before these waters leave the estuarine environment. This flux can be quantified using a simple steady-state box model (Fig. 5.5). Following Falkenmark and Mikulski (1975), the Baltic Sea is divided into an upper and lower box, each with an average salinity. These represent the waters separated by the permanent halocline. River water flows into Box 1 (M_{rw}), and seawater into Box 2 (M_{sw}). Recognizing that salinity (S_i) is a conservative quantity, we write:

$$\text{Box 1: } M_{rw}S_{rw} + M_{21}S_2 = M_{out}S_1 + M_{12}S_1 \qquad (5.3)$$

$$\text{Box 2: } M_{sw}S_{sw} + M_{12}S_1 = M_{21}S_2 \tag{5.4}$$

Given $S_{rw} \approx 0‰$, $S_{sw} = 35‰$, $S_1 = 8‰$, $S_2 = 12‰$ and $M_{rw} = 446$ km^3 yr^{-1}, and imposing mass conservation (*i.e.*, $M_{sw} + M_{12} = M_{21}$; $M_{rw} + M_{21} = M_{out} + M_{12}$), the remaining mass fluxes can be calculated.

The analogous equations can be written for Ir, with the addition of a term representing the flux into sediments (F_{sed}):

$$\text{Box 1: } M_{rw}C_{rw} + M_{21}C_2 = M_{out}C_1 + M_{12}C_1 + F_{sed} \tag{5.5}$$

$$\text{Box 2: } M_{sw}C_{sw} + M_{12}C_1 = M_{21}C_2 \tag{5.6}$$

The concentrations of Ir in seawater, river water and in Box 1 are derived from the observations presented earlier ($C_{sw} = 3.4 \times 10^8$ atoms kg^{-1}; $C_{rw} \approx 50 \times 10^8$ atoms kg^{-1}; $C_1 = 10.5 \times 10^8$ atoms kg^{-1}), and M_{sw}, M_{out}, M_{12} and M_{21} are determined from Eqns. 5.7 and 5.8.

These equations are solved to obtain $F_{sed} = 1.7 \times 10^{24}$ atoms yr^{-1}, vs. a riverine flux of $\approx 2.2 \times 10^{24}$ atoms yr^{-1}. Thus, $\approx 75\%$ of the riverine Ir flux is removed in the Baltic Sea, and never reaches the ocean. Similar behavior is likely in many major estuaries, where the flocculation of ferromanganese phases is common (Boyle *et al.*, 1977; Sholkovitz, 1976; Turekian, 1977).

5.6.4. *Particle Transport in the Gotland Deep*

The fact that the anoxic waters of station BY-15 fall on, or close to, the conservative mixing line (Fig. 5.3) is strong evidence that the rate at which Ir is transported across the redoxcline is not large enough to significantly perturb the Ir concentration of these waters over the 13 yr that this basin was anoxic prior to sampling. A first-order estimate of the downward flux

from the oxic waters is derived by assuming that the Ir removal rate calculated in the preceding section (1.7 x 10^{24} atoms yr^{-1}) is evenly distributed across the entire Baltic Proper (377,400 km^2). The resulting value is 14.3 atoms cm^{-2} s^{-1}. Over 4.1 x 10^8 s (13 yr), this amounts to 5.9 x 10^9 atoms cm^{-2}. This calculation is probably an overestimate, since it does not include the Gulf of Bothnia and the Gulf of Finland, where much of the removal probably occurs. The column density of Ir in the anoxic waters of BY-15 is 3.9 x 10^{10} atoms cm^{-2}. Therefore, it is likely that ≤ 15% of the Ir in the anoxic waters comes from particle scavenging. This small degree of deviation from conservative behavior can be accommodated by the analytical uncertainties in the Ir concentration measurements, and by uncertainties in the actual composition of the riverine endmember.

This simple calculation can be compared to a more rigorous estimate derived as follows. The rate of transport of cation C by adsorption on settling oxyhydroxide particles can be modeled as:

$$F_C = C_p M_p V_p \tag{5.7}$$

where F_C is the flux (mol cm^{-2} s^{-1}), C_p is the concentration on particles (mol gm^{-1}), M_p is the particle concentration (gm cm^{-3}), and V_p is the particle settling velocity (cm s^{-1}). C_p is related to the solution concentration, C_s, by:

$$C_p = [H^+]^{-1} K_C C_s S_p \tag{5.8}$$

where S_p is the concentration of $^-$O-donor adsorption sites on the particle surfaces (mol gm^{-1}), Here, C_s is the concentration of the free cation in the solution from which C is being scavenged (mol cm^{-3}), and we presume that H^+ competes with cation C for the adsorption sites. The unitless equilibrium

constant K_M is defined by the reaction: C^{n+} + HO-S <=> H^+ + CO-$S^{(n-1)+}$ ($[C^{n+}] = C_s$; [HO-S] = S_p; [CO-$S^{(n-1)+}$] = C_p). It follows that:

$$F_C = [H^+]^{-1} K_C M_p C_s S_p V_p \tag{5.9}$$

These parameters are not all known. However, we can eliminate M_p, V_p, $[H^+]$ and S_p by assuming an analogy with Th. ^{232}Th was measured above and below the redoxcline by Andersson *et al.* (1995), and has a profile similar to that of Ir. If Th and Ir react with the same adsorption sites on the same particles, and if we neglect other complexation reactions which compete with the surface groups for the free cations, we may write:

$$F_{Ir} = F_{Th} \frac{K_{Ir}}{K_{Th}} \frac{C_s^{Ir}}{C_s^{Th}} \tag{5.10}$$

K_{Ir}/K_{Th} is estimated from the relation:

$$\frac{K_{M_1}}{K_{M_2}} \cong \left(\frac{\beta^o_{1M_1OH}}{\beta^o_{1M_2OH}} \right)^{1.2} \tag{5.11}$$

where $\beta^o_{1M_nOH}$ is the first hydroxide binding constant of metal M_n (Dzombak and Morel, 1990). This relationship was originally developed for the adsorption of divalent cations, but appears to also provide a first-order guide to the adsorption of trivalent and quadravalent cations on particle surfaces in natural waters (*e.g.,* Clegg and Sarmiento, 1989; Erel and Morgan, 1991). In the present case, we use $\log\beta^o_{1IrOH} = 9.63$ and $\log\beta^o_{1ThOH} = 10.80$ (Baes and Mesmer, 1986; Gamsjäger and Beutler, 1979). F_{Th} is obtained by assuming that the ^{232}Th profile at BY-15 is initially well-mixed, and that the deep

waters have reached their present concentration over time t_o (13 yr = 4.1 x 10^8 s):

$$F_{Th} = \frac{\left(C_{Th}^{Anoxic} - C_{Th}^{Oxic}\right)}{t_o} z_o \qquad (5.12)$$

where C_{Th}^{Anoxic} and C_{Th}^{Oxic} are the concentrations in the anoxic and oxic waters, respectively, and z_o is the height of the anoxic zone (10^4 cm). For C_{Th}^{Anoxic} = 0.396 ng kg^{-1} and C_{Th}^{Oxic} = 0.088 ng kg^{-1} (Andersson *et al.*, 1995), F_{Th} = 1.95 x 10^4 atoms cm^{-2} s^{-1}, and F_{Ir} = 3.37 atoms cm^{-2} s^{-1}. Over 13 yr, this flux would increase the Ir column density in the anoxic waters by ≈ 1.4 x 10^9 atoms cm^{-2}. This result is ≈ 4% of the observed column density (3.9 x 10^{10} atoms cm^{-2}), in good agreement with the ≤ 15% limit determined above. An even lower value is likely, since the treatment above ignores the effect of competing ligands for the free cations in solution. In the case of Ir, complexation with chloride should lower the concentration of the free cation. Since Th forms much weaker complexes with chloride than does Ir, this effect will reduce the magnitude of C_{Ir}/C_{Th}. Unfortunately, good estimates of the chloride complexation constants of Ir^{3+} are lacking, which prevents a more rigorous calculation.

Particle scavenging *could* account for the concentration observed in the anoxic waters if $K_{Ir}/K_{Th} \approx 1$. This is unlikely given the nearly tenfold difference in the hydroxide binding constants of these elements. Evidence for weaker scavenging of Ir than Th in the Baltic is indicated when the simple box model of Eqns. 5.3 - 5.6 is applied to Th. ^{232}Th was determined by Andersson *et al.* (1995) in the Wistula and Kalixälven rivers, in the Baltic Proper, and in the North Sea. Taking an average riverine concentration of 10

ng kg^{-1}, and concentrations of 0.2 ng kg^{-1} and 0.15 ng kg^{-1} in the North Sea and Baltic Proper, respectively, F_{sed} = 1.90 mol yr^{-1} *vs.* a riverine flux of 1.92 mol yr^{-1}. Therefore, ≈ 99% of the riverine Th is apparently scavenged, compared to ≈ 75% of the river-borne Ir.

Scavenging of Ir on Mn particles is unlikely to produce a large enough flux to substantially perturb the concentration of Ir in the anoxic waters of the Gotland Deep. However, the possibility that the enrichment of these waters is the result of scavenging cannot be completely excluded in the absence of direct measurements of Ir in the particles settling across the redoxcline. Reliable determinations of K_{Ir} would also be helpful.

5.7. A Preliminary Geochemical Budget

The observations presented above allow consideration of the Ir ocean budget for the first time. Below, quantitative estimates of the sources and sinks of Ir are discussed. Although considerable uncertainties remain in some key terms, upper and lower limits are placed on the residence time of Ir in seawater.

5.7.1. *Riverine Source*

The Ir content of the world's major rivers is unknown, but may be similar to that of the Kalixälven. As noted above, this river is relatively unperturbed by man. The annual average dissolved load of Mn in the Kalixälven is nearly identical to the average world river (Andersson *et al.*, 1994; Martin and Whitfield, 1983). To the extent that Ir and Mn have some geochemical coherence, this suggests that the Kalixälven can be used for a first approximation. Using a concentration of 20 x 10^8 atoms kg^{-1} and an annual river influx of 4.2 x 10^4 km^3 yr^{-1} (Lvovitch, 1973), an input of 140 mol

yr^{-1} is obtained. This is probably an upper limit, as scavenging on Fe-Mn oxyhydroxides and other particle surfaces in estuaries should reduce this figure substantially. Using transport through the Baltic Sea as a rough guide, it is reasonable to assume that approximately half of this riverine flux reaches the open ocean.

5.7.2. *Aerosol Source*

Dust derived from continental crust is a significant source of many trace elements to the oceans (*e.g.*, Hydes, 1979; Klinkhammer and Bender, 1980; Schaule and Patterson, 1981). An upper limit to this contribution can be calculated from estimates of the mineral aerosol flux to the ocean, assuming that this aerosol has approximately the Ir content of average continental crust. This is a typical assumption for non-anthropogenic trace elements (Duce *et al.*, 1991). It is particularly justified in the case of Ir by analyses of Os in loess samples. These reveal concentrations close to those of average crust, and suggest a coherence between Ir and Os during weathering and aeolian transport (Esser and Turekian, 1993). Taking a global aerosol flux of 9.1×10^{14} gm yr^{-1} (Duce *et al.*, 1991) and an Ir content of 4.8×10^{-11} gm gm^{-1} (Esser and Turekian, 1993; Fenner and Presley, 1984), a source of 227 mol yr^{-1} is derived. The fraction of this input which dissolves is likely to be small due to the insolubility of suspected Ir carrier phases, which include native metal and sulfides. Laboratory studies of Ir dissolution from aeolian dust are completely lacking. Falkner and Edmond (1990) inferred that approximately 3% of aerosol-born Au is dissolved in the Mediterranean Sea. Similar dissolution percentages are reported for other metals delivered to the oceans in mineral aerosols (Duce *et al.*, 1991). Therefore, it is reasonable to

assume that ≈ 5% of aerosol-borne Ir is dissolved. Thus, ≈ 10 mol yr^{-1} of dissolved Ir is derived from continental dust sources, and ≈ 217 mol yr^{-1} reaches the seafloor in particulate form.

Trace metals in atmospheric aerosols can also be derived from volcanic sources, and could be a significant intermittent source of Ir to the oceans. Ir enrichments in aerosols derived from hot-spot volcanism are well known (Olmez *et al.*, 1986; Toutain and Meyer, 1989; Zoller *et al.*, 1983). Osmium isotopic analysis suggests a mantle source (Krähenbühl *et al.*, 1992). Ir-enriched volcanic aerosols are apparently transported substantial distances (Koerberl, 1989). The identity of the volatile species is a subject of debate; IrF_6 has been suggested (Zoller *et al.*, 1983), but is apparently not stable in the presence of water (Wood, 1987).

Olmez *et al.* (1986) estimated that Ir emissions from Kilauea are ≈ 1.5 x 10^{-8} mol per cubic meter of erupted magma. The total magma output of hotspot volcanism is estimated as ≈ 0.15 km^3 yr^{-1} (Gerlach, 1990; Olmez *et al.*, 1986), which extrapolates to 2.5 mol yr^{-1} of Ir, assuming the Kilauea results are typical. The fraction of this input which enters seawater in dissolved form is unknown, but is unlikely to be 100%. Thus, eruption rates more than an order of magnitude higher than presently observed are required for this input to rival the riverine source. Volcanic activity of this magnitude is not unprecedented in the geologic record, but is not typical of the Plio-Pleistocene. Given the ≈ 10^3 yr residence time estimated earlier for Ir in seawater, volcanogenic sources are unlikely to be an important term in the present-day global ocean budget. However, the marine Ir budget may be strongly perturbed by episodes of intense volcanism, such as those which generate continental flood basalts.

5.7.3. *Extraterrestrial Source*

The extreme enrichment of Ir in extraterrestrial material relative to crustal sources is well established. An Ir concentration of 4.81×10^{-7} gm gm^{-1} is commonly accepted for average chondritic meteorites (Anders and Grevesse, 1989). The best constraint on the mass of such material accreted by the Earth is $40 \pm 20 \times 10^6$ kg yr^{-1}, based on direct measurement of the micrometeorite flux above the atmosphere (Love and Brownlee, 1993). Micrometeorites dominate the extraterrestrial mass flux, although larger objects will periodically overwhelm this background accretion. Assuming that this mass flux is predominately chondritic, the extraterrestrial Ir flux is 100 ± 50 mol yr^{-1}. The fraction of this input which dissolves in the oceans is probably small, particularly if the PGE are in metal phases. Some insight into this problem is gained by considering Os isotope systematics in marine sediments, since Os and Ir should dissolve similarly from meteorite sources. Based on the $^{187}Os/^{186}Os$ ratios in bulk marine sediments and leachates presumed to recover only hydrogenous Os, Esser and Turekian (1988) estimated that 20% of the meteoritic Os input could be dissolved in the oceans. This input was invoked to lower the $^{187}Os/^{186}Os$ of seawater from 12.5 (the average crustal composition) to 8.4 (the inferred composition of seawater). However, since the isotopic compositions of meteorite Os and mantle-derived Os are identical, this model cannot distinguish between these sources. Recent findings suggest that rivers draining ophiolitic terrains supply the oceans with mantle-derived Os (Pegram *et al.*, 1994). Additionally, recent work has revised the $^{187}Os/^{186}Os$ of the average continental crust to $\approx$ 10.5, so a smaller input of non-radiogenic Os may be required to generate the observed isotopic composition of Os in seawater (Esser and Turekian, 1993).

Therefore, ≈ 20 mol yr^{-1} should be considered an upper limit on the extraterrestrial source of dissolved Ir to the oceans. It is likely that the actual contribution is much smaller than this, and is not significant to the ocean Ir budget.

5.7.4. *Hydrothermal Source*

There are no measurements of Ir in hydrothermal fluids. Crocket (1990) has reviewed the literature on trace metals in these fluids, and concludes that the noble metals should reflect the composition of the MORB wall rock interacting with these high temperature, saline waters. Thus, he predicts Au/Ir ≈ 20 in the fluid. Falkner and Edmond (1990) estimated an upper limit of 2 x 10^4 mol yr^{-1} for hydrothermal input of Au, based on measurements of Au in such fluids. Thus, as much as 1000 mol of Ir may be supplied annually by hydrothermal sources. Seafloor hydrothermal sulfides are strongly depleted in the PGE relative to Au, exhibiting Au/Ir values of 10^3 - 10^4 (Crocket, 1990). This is presumably the result of preferential removal of Au into sulfide phases formed in the hydrothermal plume. Ir is apparently not removed by this process. The ultimate fate of the Ir remaining in solution is unknown. However, there is extensive evidence that many trace elements are scavenged on Fe oxyhydroxides which form rapidly as hydrothermal plumes cool and mix with oxygenated seawater (Coale *et al.*, 1991; Edmond *et al.*, 1979; Edmond *et al.*, 1982; Trefry and Metz, 1989). Ir should be among these elements, given the observations in the Baltic Sea and the laboratory results presented in Tables 5.5 and 5.6. Indirect evidence that this is the case comes from observations of $^{187}Os/^{186}Os$ in metalliferous sediments from the East Pacific Rise (EPR) (Ravizza and McMurtry, 1993). These sediments are

believed to scavenge Os directly from seawater. Hydrothermal fluids should carry a mantle-like $^{187}Os/^{186}Os$. The measured ratios at the EPR are identical to those measured in pelagic sediment leachates, which record $^{187}Os/^{186}Os$ of seawater. Therefore, there is no evidence of a localized contribution of mantle-derived dissolved Os to these sediments. Presumably, such Os is scavenged on Fe oxyhydroxides close to the ridge. Although the analogy between the solution chemistries of Os and Ir is imperfect, and Os/Ir in MORB is < 0.2 (Crocket, 1990; Martin, 1991), a similar fate is suggested for hydrothermal Ir. Therefore, the magnitude of the hydrothermal source is likely to be much smaller than 1000 mol yr^{-1}. A more quantitative estimate is not possible at this time.

5.7.5. *Sedimentary Sink and a Rough Ocean Budget*

From the preceding discussion, out of a total Ir input of ≈ 400 mol yr^{-1}, roughly 75 mol yr^{-1} is expected to enter the oceans in dissolved form. These totals assume no significant hydrothermal input. Fe-Mn oxyhydroxide phases are likely to be the dominant sink of dissolved Ir from seawater. This statement is based on several observations, discussed above in detail: a) the apparent hydrogenous enrichment of Ir in pelagic sediments (relative to average continental crust); b) evidence of Ir removal in oxic waters of the Baltic Sea; c) laboratory evidence of Ir scavenging by Fe and Mn oxyhydroxides from seawater solutions; d) the negligible loss of Ir from anoxic waters in the Baltic Sea; e) the absence of an Ir enrichment in reducing sediments (Colodner, 1992). While none of these observations are convincing on their own, they make a compelling case when taken together. Therefore, a

sedimentary sink of ≈ 75 mol yr^{-1} must be found to balance the Ir ocean budget.

The flux of hydrogenous Ir into a sediment (F_H) can be calculated by subtracting the Ir contribution from undissolved aeolian dust (F_A) and extraterrestrial sources (F_{ET}) from the total Ir accumulation rate (F_T). The remainder represents the hydrogenous flux, *i.e.,*:

$$F_H = F_T - F_M - F_A \tag{5.13}$$

Since the aeolian flux is spatially heterogeneous, the value applied to any particular sediment must be the appropriate regional estimate of mineral aerosol deposition of Duce *et al.* (1991). These aerosols are assumed to have the average crustal abundance of most trace elements (Duce *et al.*, 1991), and we presume the same is true of Ir. In this calculation, none of the extraterrestrial flux enters solution, and hydrothermal inputs are minimal.

The Ir concentration of marine ferromanganese crusts and nodules ranges from 1 - 7 ppb (Koide *et al.*, 1991), a fraction of which is surely hydrogenous. These sediments accumulate slowly and with substantial discontinuities, making their growth rates highly uncertain (Bender *et al.*, 1970; McMurtry *et al.*, 1994). Therefore, it is difficult to correct F_T for the extraterrestrial flux to these sediments in a meaningful way. Additionally, it is not plausible to correct for the aerosol flux in a sediment which has accumulated over tens of millions of years using present day dust measurements. Thus, while ferromanganese crusts may constitute a sizable sink for hydrogenous Ir, quantification of this sink is not presently feasible.

However, the concentration of Ir in pelagic sediments is well characterized in cores from the North Pacific (GPC-3, Kyte *et al.*, 1993; Kyte

and Wasson, 1986) and the South Pacific (DSDP hole 596, Zhou and Kyte, 1992). These sediments have high concentrations of hydrogenous Mn, presumably as Mn oxyhydroxide and oxide phases. Although both data sets span more than 70 million years, only the uppermost sections of these cores (≤ 1 million years) are used in these calculations to minimize uncertainties in the aerosol flux. Thus, in core GPC-3, a total Ir flux of 1.8×10^{-16} mol cm^{-2} yr^{-1} is corrected for an aerosol Ir contribution of 5.3×10^{-4} gm cm^{-2} yr^{-1} x 2.5×10^{-13} mol Ir gm^{-1} = 1.3×10^{-16} mol yr^{-1}, and a meteorite Ir flux of 2.0×10^{-17} mol cm^{-2} yr^{-1}, to yield $F_H = 2.8 \times 10^{-17}$ mol cm^{-2} yr^{-1}. A similar exercise for DSDP 596 (where $F_T = 4.2 \times 10^{-17}$ mol cm^{-2} yr^{-1}, and the aerosol flux is only 3.5×10^{-5} gm cm^{-2} yr^{-1}) produces $F_H = 1.3 \times 10^{-17}$ mol cm^{-2} yr^{-1}. These F_H values must be regarded cautiously, due to the considerable uncertainties associated with the estimates of the aerosol and meteorite fluxes. However, if taken at face value, these estimates correspond to a sink of ≈ 50 - 100 mol yr^{-1} when averaged over a total ocean area of 3.61×10^{18} cm^2 (Linde, 1990).

This result is encouraging. Despite considerable uncertainties, it suggests that riverine inputs can be roughly balanced by removal into pelagic sediments. This implies that the quantity of Ir released from hydrothermal systems is not large enough to dominate the marine Ir budget. A rough estimate of the residence time of Ir in the oceans (τ) can now be made. Assuming an average concentration of 4×10^8 atoms kg^{-1} in an ocean of mass 1.35×10^{21} kg (Speidel and Agnew, 1982), ≈ 9×10^5 mol Ir are contained in the world's ocean. If 50 - 100 mol pass through the oceans annually at steady-state, then the residence time of Ir in seawater is ≈ 10^4 yr.

5.7.6. *Limits on the Ocean Residence Time*

Strong upper and lower limits can be placed on τ by making some plausible extrapolations from our observations. If the total burial flux of Ir in sediments is F_T, then $\tau = ({}^{sw}C_{Ir}M_o)/(f_T F_T A_o)$, where f_T is the fraction of total buried Ir which is hydrogenous. M_o and A_o are the mass and area of the oceans, respectively. ${}^{sw}C_{Ir}$ is the average concentration of Ir in seawater (4 x 10^8 atoms kg^{-1}). Based on the analyses of cores GPC-3 and DSDP-596, $F_T \approx 10^{-16}$ mol cm^{-2} yr^{-1} over the past 10^6 yr. Since some fraction of the Ir in deep sea sediments must be in the form of undissolved aeolian dust and micrometeorites, $f_T < 1$. Therefore, $\tau > 2500$ yr.

An upper limit on τ is derived from the inputs of dissolved Ir to the ocean. In this case, $\tau = ({}^{sw}C_{Ir}\, M_o)/(f_R F_R + f_A F_A + f_M F_M + F_{HT})$ where: F_R is the flux of dissolved riverine Ir; f_R is the fraction of this source which reaches the deep ocean; F_A and F_M are the fluxes of Ir on aeolian dust and meteorites, respectively; f_A and f_M are the fractions of these inputs which dissolve; and F_{HT} is the flux of Ir from deep-sea hydrothermal systems. We assume that the world's major rivers and the Kalixälven have similar C_{Ir}. This similarity holds for Mn, which has some geochemical coherence with Ir based on the preceding discussions. In the Baltic, 25% of riverine Ir survives scavenging. This value is probably larger in typical estuaries, since the residence time of water in the Baltic Sea is unusually long, which provides more opportunity for scavenging. Therefore, $f_R > 0.25$, and $f_R F_R > 35$ mol yr^{-1}. Limits on the values of F_A, f_A, F_M, f_M and F_{HT} were discussed in sections **5.7.2**, **5.7.3** and **5.7.4**. Using these constraints, $(f_R F_R + f_A F_A + f_M F_M + F_H) > 42$ mol yr^{-1}, with rivers likely to be the dominant source of dissolved Ir to the oceans. Thus,

2500 yr < τ < 21,000 yr. This range is similar to the values for many trace metals which are moderately particle-reactive (Bruland, 1983).

5.8. Implications for the Sedimentary Record

The first-order observations of the natural water chemistry of Ir presented here have significant implications for the interpretation of Ir abundances in the sedimentary record.

The Ir enrichment found globally in sediments at the K/T boundary is believed to arise from the impact of an asteroid 10 km in diameter (Alvarez *et al.*, 1980; Alvarez *et al.*, 1995). This event is linked to the terminal Cretaceous mass extinctions (Alvarez *et al.*, 1980). The impact/extinction hypothesis was initially based on the high concentration of Ir in the boundary clays. This concentration is on the order of 10^{-8} gm gm^{-1} (*e.g.*, Alvarez *et al.*, 1980; Kyte *et al.*, 1993; Zhou and Kyte, 1992). Since the typical crustal abundance of Ir is 5 x 10^{-11} gm gm^{-1}, while that of meteorites is 4.81 x 10^{-7} gm gm^{-1}, the interest in an extraterrestrial source is obvious.

The low abundance of Ir in seawater makes this argument even more compelling. While some elements are accumulated in seawater, Ir clearly is not one of them. The Ir content of the ocean determined here is $\approx 10^6$ mol. This is a factor of 10^3 smaller than the quantity of Ir deposited at the boundary, assuming global coverage of a layer containing 60 - 70 ng cm^{-2} (Alvarez *et al.*, 1980; Officer *et al.*, 1987). It is $\approx 10^4$ times smaller than the total quantity of Ir in a 10 km diameter chondrite. Thus, even if an unidentified mechanism caused all the Ir in the oceans to be deposited in a single sedimentary layer, the K/T boundary Ir signature would not be reproduced.

A number of smaller Ir enrichments have been found in the geologic record (*e.g.,* Alvarez *et al.*, 1982; Dao-Yi *et al.*, 1985; Orth *et al.*, 1988a; Playford *et al.*, 1984; Wang *et al.*, 1991; Wilde *et al.*, 1986). Although the connection of these enrichments to impacts and extinctions is much more tenuous than at the K/T, attempts have been made to draw such connections (*e.g.,* Rampino and Caldeira, 1993; Sepkoski, 1986). Such minor anomalies must be regarded with great care. Despite being a "noble metal", Ir is apparently chemically reactive when dissolved in natural waters. Ir can be scavenged from solution by common sedimentary materials, and its mobility is apparently a function of redox conditions, pH and salinity. Thus, changes in the chemical conditions of groundwaters, porewaters or the water column overlying a sedimentary bed can remobilize and/or concentrate Ir, producing Ir-enriched horizons. Similar conclusions have been drawn from studies of Ir in sediments (Colodner *et al.*, 1992; Wallace *et al.*, 1990). Additionally, the marine geochemical cycle of Ir could be easily perturbed by changes in volcanogenic or hydrothermal inputs, or by changes in the flux of terrigenous dust. Thus, minor Ir "anomalies" with no connection to extraterrestrial inputs may be common in the sedimentary record.

The magnitude of the residence time of Ir also has implications for the debate over the ultimate source of Ir at the K/T boundary. It has been suggested that the impact-related features of the boundary sediments can be explained by massive volcanic activity 65 million years ago, such as that associated with the formation of the Deccan Traps flood basalts (*e.g.,* Officer *et al.*, 1987). Extrapolating from the observations of Ir in Kilauea aerosols, it has been estimated that such an event could release as much Ir as found at the K/T boundary (Olmez *et al.*, 1986). A critical consequence of this

volcanogenic hypothesis is that the Ir anomaly at the K/T should span a considerable period of time, corresponding to the duration of intense volcanic activity (*e.g.*, Crocket *et al.*, 1988; Officer *et al.*, 1987).

A simple model of the Ir ocean budget demonstrates that an enrichment spanning 10^4 - 10^5 years can be produced in marine sediments in response to a massive impact event if a fraction of the extraterrestrial Ir is dissolved in the oceans. We assume that riverine inputs are balanced by hydrogenous scavenging of dissolved Ir before the impact ($t = 0$), and that this is the condition to which the system will return as $t \rightarrow \infty$. If a substantial fraction of the Ir in the impactor dissolved rapidly into seawater, then the return of Ir in seawater to steady-state conditions can be written as:

$$C_{sw}(t) = \left(C_{sw}(0) - \frac{R_{in}}{KSV} \right) e^{-KSt} + \frac{R_{in}}{KSV} \qquad (5.14)$$

where: $C_{sw}(t)$ is the concentration of Ir in seawater at time t; R_{in} is the rate of riverine input; K is an equilibrium constant relating C_{sw} to the concentration of Ir in sediments; and S is the sedimentation rate. $C_{sw}(0)$ is the concentration of Ir in seawater immediately following the impact. The Ir content of seawater will fall exponentially with time following the impact, with an "e-folding" timescale equal to $(KS)^{-1}$, the steady-state residence time of Ir in seawater. Since the residence time of Ir is 10^3 - 10^4 yr, a substantial enrichment could persist for tens of thousands of years. This would be reflected in the sedimentary record as a "tail" of hydrogenous Ir decaying exponentially upsection from the K/T boundary, persisting for as long as $\approx$ 10^5 years.

It is not known what fraction of the Ir borne by the impactor entered seawater in dissolved form soon after the impact. However, there are

indications that this fraction was substantial. These include: a) the probable vaporization of the projectile by shock heating upon impact (O'Keefe and Ahrens, 1982); b) the perturbation in seawater $^{187}Os/^{186}Os$ at the K/T boundary, which indicates that PGE marine chemistry was strongly perturbed by an extraterrestrial input at the boundary (Peucker-Ehrenbrink *et al.*, 1995); c) the correlation between chalcophile elements and Ir in marine boundary clays, but not in continental boundary clays, consistent with the notion that these elements and Ir were scavenged together from seawater into the marine clays (Schmitz, 1992). Additionally, detailed analyses of the mineralogical associations of the PGEs at the boundary reveal that these elements are associated with clay minerals (Evans *et al.*, 1994). If this association is primary, then it is evidence in favor of a scavenging model. If these clays were formed by alteration of phases formed during condensation from an impact fireball, as suggested by Evans *et al.* (1994), then a large fraction of the PGE apparently entered seawater in easily weathered minerals, rather than as highly insoluble metal nuggets. Either way, the results of Evans *et al.* (1994) strongly suggest that impact-derived PGEs were available for dissolution in seawater.

Most well-studied K/T boundary sections are too bioturbated to derive a meaningful chronology at a time scale of 10^4 - 10^5 years (Kyte *et al.*, 1993; Zhou and Kyte, 1992). The action of bioturbation on an instantaneous spike in sediment composition results in an exponentially-decaying distribution qualitatively similar to that produced by Eqn. 5.14 (Guinasso and Schink, 1975; Officer and Lynch, 1983). However, some locations are believed to be adequately preserved. This is the case in the Gubbio, Italy boundary section, where Alvarez *et al.* (1990) observe a periodic variation in the clay/carbonate

ratio which they attribute to climatic forcing by the 22,000 yr Milankovitch cycle. This signal would not survive extensive bioturbation. The Ir anomaly spans 10^4 - 10^5 yr in this section, distributed above and below the K/T boundary. This has been invoked as evidence of volcanogenesis (Crocket *et al.*, 1988; Officer *et al.*, 1987; Rocchia *et al.*, 1990). The presence of Ir downsection of the K/T boundary is ascribed to increasing volcanic activity prior to 65 million years ago. The highest resolution Ir profile across this section is that of Alvarez *et al.* (1990). Examined in detail, the Ir anomaly appears to be distributed asymmetrically about the K/T boundary; the upsection tail is significantly larger than the downsection tail. Rather than volcanism, it is possible that extraterrestrial Ir introduced during an impact event was hydrogenously scavenged to produce an exponentially decreasing tail upsection. Subsequent diffusion of this signal produced the downsection signal, but was not extensive enough to erase the asymmetric distribution. Obviously, this model includes many simplifying assumptions, and is somewhat *ad hoc*. However, it demonstrates that an Ir anomaly of $\approx 10^5$ yr duration can be explained in the context of an accretionary event without invoking diagenetic modifications of the primary signal or an extended period of Ir input to the oceans.

An analysis of the PGE, Os isotopes and other trace elements at high stratigraphic resolution across the K/T boundary at Gubbio, Italy could be revealing. If the seawater residence time controls the PGE abundances in these sediments, then the distribution of these elements through the section should differ according to their residence times. Bioturbation would act uniformly on all the elements. Coupled to knowledge of the marine geochemistries of these elements, such a study could lead to a chronology of

the events at the boundary, and would provide information on the perturbations to ocean chemistry resulting from the impact. This mechanism could also help explain the PGE inter-element ratios in K/T boundary sediments, which are not always chondritic, and which vary from site to site (Evans *et al.*, 1993; Tredoux *et al.*, 1989). The methodology used in the present study is well suited for such a project.

5.9. Summary

Direct measurements of Ir in seawater and in the Baltic Sea reveal that Ir is the least abundant stable element in seawater, with an average ocean concentration of $\approx 4 \times 10^8$ atoms kg^{-1}. There is little variation in the concentration of Ir between the surface and 1000 m.

In the Baltic Sea, ≈ 75% of the riverine input is apparently scavenged in the Baltic Proper. This loss does not occur in reducing waters, where Ir behaves conservatively. Laboratory experiments indicate that rapid uptake of Ir by Fe and Mn oxyhydroxides occurs in seawater under alkaline conditions. This is consistent with data from marine sediments, in which Ir is strongly associated with Mn and with other hydrogenous elements. Ir scavenging is enhanced at lower salinity. Therefore, it is proposed that Ir in the Baltic Sea is sequestered in the extensive ferromanganese sediments formed in the oxic waters of the Gulf of Bothnia and the Gulf of Finland.

A preliminary marine geochemical budget of Ir balances a dissolved riverine input of ≈ 75 mol yr^{-1} against a sink of 50 - 100 mol yr^{-1} of hydrogenous Ir in marine pelagic sediments. The input is estimated from measurements of Ir in the pristine Kalixälven river, which is taken to represent global average riverwater. Other inputs of dissolved Ir are

negligible, with the possible exception of Ir from deep-ocean hydrothermal systems. The sink is estimated from measurements of Ir in two pelagic sediment cores, after correction for inputs from aeolian dust and micrometeorites. The surprisingly close balance of inputs and outputs suggests that the hydrothermal source does not dominate the marine Ir budget. The residence time of Ir in seawater is 2500 - 21,000 yr.

The total amount of Ir in seawater is 10^3 times smaller than the quantity of Ir observed at the K/T boundary. This eliminates terrestrial Ir dissolved in the oceans as a possible source of this anomaly. A truly extraordinary input of Ir is called for. However, the chemistry of Ir in natural waters is apparently characterized by sensitivity to redox conditions, pH and salinity. This indicates that Ir can be remobilized and concentrated into certain types of sediments. This could lead to modest Ir enrichments in the sedimentary record without invoking exogenous Ir. The same chemical processes govern the rate at which Ir is removed from seawater. A simple model of this process indicates that the time interval spanned by the K/T boundary anomaly in marine sediments should be 10^4 - 10^5 yr if a significant fraction of the impactor's Ir was dissolved in the oceans. This eliminates one of the arguments used in support of volcanism as the source of the K/T boundary Ir anomaly.

5.10. Acknowledgments

P. S. Andersson, D. Porcelli and M. Roy-Barman are thanked for their assistance in sample collection. P. S. Andersson's help in interpreting the Baltic Sea data is greatly appreciated. D. Porcelli provided valuable advice and support at critical stages of this project.

5.11. References

Alvarez, L. W., W. Alvarez, F. Asaro, and H. V. Michel, Extraterrestrial cause for the Cretaceous-Tertiary extinction: Experimental results and theoretical interpretation, *Science*, *208*, 1095-1108, 1980.

Alvarez, W., F. Asaro, H. V. Michel, and L. W. Alvarez, Iridium anomaly approximately synchronous with terminal Eocene extinctions, *Science*, *216*, 886-888, 1982.

Alvarez, W., P. Claeys, and S. W. Kieffer, Emplacement of Cretaceous-Tertiary boundary shocked quartz from Chicxulub crater, *Science*, *269*, 930-935, 1995.

Anbar, A. D., R. A. Creaser, D. A. Papanastassiou, and G. J. Wasserburg, Rhenium in seawater: Confirmation of generally conservative behavior, *Geochim. Cosmochim. Acta*, *56*, 4099-4103, 1992.

Anders, E., and N. Grevesse, Abundances of the elements: Meteoritic and solar, *Geochim. Cosmochim. Acta*, *53*, 197-214, 1989.

Andersson, P. S., G. J. Wasserburg, J. H. Chen, D. A. Papanastassiou, and J. Ingri, ^{238}U-^{234}U and ^{232}Th-^{230}Th in the Baltic Sea and in river water, *Earth Planet. Sci. Lett.*, *130*, 217-234, 1995.

Andersson, P. S., G. J. Wasserburg, and J. Ingri, The sources and transport of Sr and Nd isotopes in the Baltic Sea, *Earth and Planetary Sciences Letters*, *113*, 459-472, 1992.

Andersson, P. S., G. J. Wasserburg, J. Ingri, and M. C. Stordal, Strontium, dissolved and particulate loads in fresh and brackish waters: the Baltic Sea and Mississippi Delta, *Earth Planet. Sci. Lett.*, *124*, 195-210, 1994.

Bacon, M. P., P. G. Brewer, D. W. Spencer, J. W. Murray, and J. Goddard, Lead-210, polonium-210, manganese and iron in the Cariaco Trench, *Deep-Sea Res.*, *27A*, 119-135, 1980.

Baedecker, P. A., and W. D. Ehmann, The distribution of some noble metals in meteorites and natural materials, *Geochim. Cosmochim. Acta*, *29*, 329-342, 1965.

Baes, C. F., and R. E. Mesmer, *The Hydrolysis of Cations*, Robert Krieger Publishing Company, Inc., Malabar, FL, 1986.

Barker, J. L., and E. Anders, Accretion rate of cosmic matter from iridium and osmium contents of deep-sea sediments, *Geochim. Cosmochim. Acta*, *32*, 627-645, 1968.

Belmans, F., R. van Grieken, and L. Brügmann, Geochemical characterization of recent sediments in the Baltic Sea by bulk and electron microprobe analysis, *Mar. Chem.*, *42*, 223-236, 1993.

Bender, M. L., T.-L. Ku, and W. S. Broecker, Accumulation rates of manganese in pelagic sediments and nodules, *Earth Planet. Sci. Lett.*, *8*, 143-148, 1970.

Bergström, S., and B. Carlsson, River runoff to the Baltic Sea: 1950-1990, *Ambio*, *23*, 280-287, 1994.

Bertine, K. K., M. Koide, and E. D. Goldberg, Aspects of rhodium marine chemistry, *Mar. Chem.*, *42*, 199-210, 1993.

Boström, K., J.-O. Burman, and J. Ingri, A geochemical massbalance for the Baltic, *Ecol. Bull.*, *35*, 39-58, 1983.

Boström, K., J.-O. Burman, C. Pontér, and J. Ingri, Selective removal of trace elements from the Baltic by suspended matter, *Mar. Chem.*, *10*, 335-354, 1981.

Boström, K., J. Ingri, and C. Pontér, Origin of iron-manganese-rich suspended matter in the Landsort Deep, NW Baltic Sea, *Mar. Chem.*, *24*, 93-98, 1988.

Boström, K., L. Wiborg, and J. Ingri, Geochemistry and origin of ferromanganese concretions in the Gulf of Bothnia, *Mar. Geol.*, *50*, 1-24, 1982.

Boyle, E. A., J. M. Edmond, and E. R. Sholkovitz, The mechanism of iron removal in estuaries, *Geochim. Cosmochim. Acta*, *41*, 1313-1324, 1977.

Bruland, K. W., Trace elements in sea-water, in *Chemical Oceanography*, vol. 8, edited by J. P. Riley and R. Chester, pp. 157-220, Academic Press, London, 1983.

Castillo-Blum, S. E., and A. G. Sykes, Substitution inertness of $[Ir(H_2O)_6]^{3+}$, *Polyhedron*, *6*, 101-103, 1987.

Clegg, S. L., and J. L. Sarmiento, The hydrolytic scavenging of metal ions by marine particulate matter, *Prog. Oceanog.*, *23*, 1-21, 1989.

Coale, K. H., C. S. Chin, G. J. Massoth, K. S. Johnson, and E. T. Baker, In situ chemical mapping of dissolved iron and manganese in hydrothermal plumes, *Nature*, *352*, 325-328, 1991.

Colodner, D. C., The Marine Geochemistry of Rhenium, Iridium and Platinum, Ph.D. Thesis, MIT/WHOI, WHOI-91-30, 1991.

Colodner, D. C., E. A. Boyle, and J. M. Edmond, Determination of rhenium and platinum in natural-waters and sediments, and iridium in sediments

by flow-injection isotope-dilution inductively coupled plasma-mass spectrometry, *Anal. Chem.*, *65*, 1419-1425, 1993a.

Colodner, D. C., E. A. Boyle, J. M. Edmond, and J. Thomson, Postdepositional mobility of platinum, iridium and rhenium in marine sediments, *Nature*, *358*, 402-404, 1992.

Colodner, D. C., J. Sachs, G. Ravizza, K. Turekian, J. Edmond, and E. Boyle, The geochemical cycle of rhenium: a reconnaissance, *Earth Planet. Sci. Lett.*, *117*, 205-221, 1993b.

Cotton, F. A., and G. Wilkinson, *Advanced Inorganic Chemistry-5th edition*, J. Wiley & Sons, New York, 1988.

Creaser, R. A., D. A. Papanastassiou, and G. J. Wasserburg, Negative thermal ion mass spectrometry of osmium, rhenium, and iridium, *Geochim. Cosmochim. Acta*, *55*, 397-401, 1991.

Crocket, J. H., Geochemistry of the platinum-group elements, in *Platinum-Group Elements: Mineralogy, Geology, Recovery*, edited by L. J. Cabri, pp. 47-64, Canadian Institute of Mining and Metallurgy, Montreal, 1981.

Crocket, J. H., Noble metals in seafloor hydrothermal mineralization from Juan de Fuca and Mid-Atlantic ridges: A fractionation of gold from platinum metals in hydrothermal fluids, *Canad. Mineral.*, *28*, 639 - 648, 1990.

Crocket, J. H., and H. Y. Kuo, Sources for gold, palladium and iridium in deep-sea sediments, *Geochim. Cosmochim. Acta*, *43*, 831-842, 1979.

Crocket, J. H., C. B. Officer, F. C. Wezel, and G. D. Johnson, Distribution of noble metals across the Cretaceous/Tertiary boundary at Gubbio, Italy: iridium variation as a constraint on the duration and nature of Cretaceous/Tertiary boundary events, *Geology*, *16*, 77-80, 1988.

Dao-Yi, X., M. Shu-Lan, C. Zhi-Fang, M. Xuo-Ying, S. Yi-Ying, Z. Qin-Wen, and Y. Zheng-Zhong, Abundance variation of iridium and trace elements at the Permian/Triassic boundary at Shangsi in China, *Science*, *314*, 154-156, 1985.

Duce, R. A., P. S. Liss, J. T. Merrill, E. L. Atlas, P. Buat-Menard, B. B. Hicks, J. M. Miller, J. M. Prospero, R. Arimoto, T. M. Church, W. Ellis, J. N. Galloway, L. Hansen, T. D. Jickells, A. H. Knap, K. H. Reinhardt, B. Schneider, A. Soudine, J. J. Tokos, S. Tsunogai, R. Wollast, and M. Zhou, The atmospheric input of trace species to the world ocean, *Global Biogeochem. Cycles*, *5*, 193-259, 1991.

Dybern, B. I., and S. H. Fonselius, Pollution, in *The Baltic Sea, Elsevier Oceanography Series*, vol. 30, edited by A. Voipio, pp. 351-381, Elsevier Scientific Publishing Company, Amsterdam, 1981.

Dzombak, D., and F. M. M. Morel, *Surface Complexation Modeling*, John Wiley & Sons, New York, 1-393, 1990.

Edmond, J. M., C. Measures, R. E. McDuff, L. H. Chan, R. Collier, and B. Grant, Ridge crest hydrothermal activity and the balances of the major and minor elements in the ocean: The Galapagos data, *Earth Planet. Sci. Lett.*, *46*, 1-18, 1979.

Edmond, J. M., K. L. Von Damm, R. E. McDuff, and C. I. Measures, Chemistry of hot springs on the East Pacific Rise and their effluent dispersal, *Nature*, *297*, 187-191, 1982.

Ehlin, U., Hydrology of the Baltic Sea, in *The Baltic Sea, Elsevier Oceanography Series*, vol. 30, edited by A. Voipio, pp. 123-134, Elsevier Scientific Publishing Company, Amsterdam, 1981.

Emerson, S., R. E. Cranston, and P. S. Liss, Redox species in a reducing fjord: Equilibrium and kinetic considerations, *Deep-Sea Res.*, *26A*, 859-878, 1979.

Erel, Y., and J. J. Morgan, The effect of surface reactions on the relative abundances of trace metals in deep-ocean water, *Geochim. Cosmochim. Acta*, *55*, 1991.

Esser, B. K., and K. K. Turekian, Accretion rate of extraterrestrial particles determined from osmium isotope systematics of Pacific pelagic clay and manganese nodules, *Geochim. Cosmochim. Acta*, *52*, 1383-1388, 1988.

Esser, B. K., and K. K. Turekian, The osmium isotopic composition of the continental crust, *Geochim. Cosmochim. Acta*, *57*, 3093-3104, 1993.

Evans, N. J., D. C. Gregoire, W. D. Goodfellow, B. I. McInnes, N. Miles, and J. Veizer, Ru/Ir ratios at the Cretaceous-Tertiary boundary: Implications for PGE source and fractionation within the ejecta cloud, *Geochim. Cosmochim. Acta*, *57*, 3149-3158, 1993.

Evans, N. J., D. C. Gregoire, W. D. Goodfellow, N. Miles, and J. Veizer, The Cretaceous-Tertiary fireball layer, ejecta layer and coal seam: Platinum-group element content and mineralogy of size fractions, *Meteoritics*, *29*, 223-235, 1994.

Falkenmark, M., and Z. Mikulski, The Baltic Sea- A semi-enclosed sea, as seen by the hydrologist, *Nord. Hydrol.*, *6*, 115-136, 1975.

Falkner, K. K., and J. M. Edmond, Gold in seawater, *Earth Planet. Sci. Lett.*, *98*, 208-221, 1990.

Fenner, F. D., and B. J. Presley, Iridium in Mississippi River suspended matter and Gulf of Mexico sediment, *Nature*, *312*, 260-262, 1984.

Fresco, J., Iridium in sea-water, *Talanta*, *32*, 830-831, 1985.

Gamsjäger, H., and P. Beutler, The hydrolysis of iridium(III), *J. Chem. Soc. Dalton Trans.*, 1415-1418, 1979.

Ganapathy, R., A major meteorite impact on the Earth 65 million years ago: Evidence from the Cretaceous-Tertiary boundary clay, *Science*, *209*, 921-923, 1980.

Ganapathy, R., R. R. Keays, J. C. Laul, and E. Anders, Trace elements in Apollo 11 lunar rocks: Implications for meteorite influx and origin of the moon, *Proc. Lunar Sci. Conf.*, *2*, 1117-1142, 1971.

Gerlach, D. C., Eruption rates and isotopic systematics of ocean islands: Further evidence for small-scale heterogeneity in the upper mantle, *Tectonophys.*, *172*, 273-289, 1990.

Goldberg, E. D., V. Hodge, P. Kay, M. Stallard, and M. Koide, Some comparative marine chemistries of platinum and iridium, *Appl. Geochem.*, *1*, 227-232, 1986.

Goldberg, E. D., M. Koide, R. A. Schmitt, and R. H. Smith, Rare earth distributions in the marine environment, *J. Geophys. Res.*, *68*, 4209-4217, 1963.

Goldberg, E. D., M. Koide, J. S. Yang, and K. K. Bertine, Comparative marine chemistries of platinum group metals and their periodic table neighbors, in *Metal Speciation: Theory, Analysis, and Application*, edited by J. R. Kramer and H. E. Allen, pp. 201-217, Lewis Publishers, Inc., Chelsea, MI, 1988.

Gostin, V. A., R. R. Keays, and M. W. Wallace, Iridium anomaly from the Acraman impact ejecta horizon: Impacts can produce sedimentary iridium peaks, *Nature*, *340*, 542-544, 1989.

Grasshoff, K., and A. Voipio, Chemical oceanography, in *The Baltic Sea, Elsevier Oceanography Series*, vol. 30, edited by A. Voipio, pp. 183-218, Elsevier Scientific Publishing Company, Amsterdam, 1981.

Guinasso, N. L., and D. R. Schink, Quantitative estimates of biological mixing rates in abyssal sediments, *J. Geophys. Res.*, *80*, 3032-3043, 1975.

Hallberg, R. O., Environmental implications of metal distribution in Baltic Sea sediments, *Ambio*, *20*, 309-316, 1991.

Hodge, V., M. Stallard, M. Koide, and E. D. Goldberg, Determination of platinum and iridium in marine waters, sediments and organisms, *Anal. Chem.*, *58*, 606-620, 1986.

Hodge, V. F., M. Stallard, M. Koide, and E. D. Goldberg, Platinum and the platinum anomaly in the marine environment, *Earth Planet. Sci. Lett.*, *72*, 158-162, 1985.

Holser, W. T., H.-P. Schonlaub, M. Attrep, K. Boeckelmann, P. Klein, M. Magaritz, C. J. Orth, A. Fenninger, C. Jenny, M. Kralik, H. Mauritsch, E. Pak, J.-M. Schramm, K. Stattegger, and R. Schmoller, A unique geochemical record at the Permian/Triassic boundary, *Nature*, *337*, 39-44, 1989.

Hsü K. J., H. Oberhänsli, J. Y. Gao, S. Shu, C. Haihong, and V. Krähenbühl, "Strangelove ocean" before the Cambrian explosion. *Nature 316*, 809-811, 1985.

Hydes, D. J., Aluminum in seawater; control by inorganic processes. *Science*, *205*, 1260, 1979.

Ingri, J., Geochemistry of Ferromanganese Concretions and Associated Sediments in the Gulf of Bothnia, Ph.D. Thesis, Lulea University of Technology, 1985.

Jacinto, J. S., and C. M. G. van den Berg, Different behavior of platinum in the Indian and Pacific Oceans, *Nature*, *338*, 332-334, 1989.

Karl, D. M., and C. D. Winn, A sea of change: Monitoring the oceans' carbon cycle, *Environ. Sci. Tech.*, *25*, 1977-1981, 1991.

Keays, R. R., and R. B. Scott, Precious metals in ocean ridge basalts: Implications for basalts as source rocks for gold mineralization, *Econ. Geol.*, *71*, 705-720, 1976.

Klinkhammer, G. P., and M. L. Bender, The distribution of manganese in the Pacific Ocean, *Earth Planet. Sci. Lett.*, *46*, 361-384, 1980.

Koerberl, C., Iridium enrichment in volcanic dust from blue ice fields, Antarctica, and possible relevance to the K/T boundary event, *Earth Planet. Sci. Lett.*, *92*, 317-322, 1989.

Koide, M., E. D. Goldberg, S. Niemeyer, D. Gerlach, V. Hodge, K. K. Bertine, and A. Padova, Osmium in marine sediments, *Geochim. Cosmochim. Acta*, *55*, 1641-1648, 1991.

Krähenbühl, U., M. Geissbühler, F. Bühler, P. Eberhardt, and D. L. Finnegan, Osmium isotopes in the aerosols of the mantle volcano Mauna Loa, *Earth Planet. Sci. Lett.*, *110*, 95-98, 1992.

Kyte, F. T., K. Leinen, R. G. Heath, and L. Zhou, Cenozoic sedimentation history of the central North Pacific: Inferences from the elemental geochemistry of core LL44-GPC3, *Geochim. Cosmochim. Acta*, *57*, 1719-1740, 1993.

Kyte, F. T., and J. T. Wasson, Accretion rate of extraterrestrial matter: Iridium deposited 33 to 67 million years ago, *Science*, *232*, 1225-1229, 1986.

Kyte, F. T., Z. Zhou, and J. T. Wasson, Siderophile-enriched sediments from the Cretaceous-Tertiary boundary, *Nature*, *288*, 651-656, 1980.

Kyte F. T., Z. Zhou, and J. T. Wasson. High noble metal concentrations in a late Pliocene sediment. *Nature 292*, 417-420, 1981.

Landing, W. M., and K. W. Bruland, Manganese in the North Pacific, *Earth Planet. Sci. Lett.*, *49*, 45-56, 1980.

Lee, D. S., Palladium and nickel in north-east Pacific waters, *Nature*, *305*, 47-48, 1983.

Levinson, A. A., *Introduction to Exploration Geochemistry-2nd Ed.*, Applied Publishing, Wilmette, IL, 1980.

Li, J., and R. H. Byrne, Amino acid complexation of palladium in seawater, *Environ. Sci. Tech.*, *24*, 1038-1041, 1990.

Linde, D. R., *CRC Handbook of Chemistry and Physics- 71st edition*, CRC Press, Inc., Boca Raton, 1990.

Love, S. G., and D. E. Brownlee, A direct measurement of the terrestrial mass accretion rate of cosmic dust, *Science*, *262*, 550-553, 1993.

Lvovitch, M. I., The global water balance, *EOS*, *54*, 28-42, 1973.

Magnusson, B., and S. Westerlund, The determination of Cd, Cu, Fe, Ni, Pb and Zn in Baltic Sea water, *Mar. Chem.*, *8*, 231-244, 1980.

Martin, C. E., Osmium isotopic characteristics of mantle-derived rocks, *Geochim. Cosmochim. Acta*, *55*, 1421-1434, 1991.

Martin, J.-M., and M. Whitfield, The significance of the river input of chemical elements to the ocean, in *Trace Metals in Sea Water*, edited by C. S. Wong, pp. 265-296, Plenum Press, New York, 1983.

McLaren D. J. and W. D. Goodfellow, Geological and biological consequences of giant impacts. In *Annual Reviews of Earth and Planetary Science*, Vol. 18, pp. 123-171, 1990.

McMurtry, G. M., D. L. VonderHaar, A. Eisenhauer, J. J. Mahoney, and H.-W. Yeh, Cenozoic accumulation history of a Pacific ferromanganese crust, *Earth Planet. Sci. Lett.*, *125*, 105-118, 1994.

Morgan, J. W., H. Higuchi, R. Ganapathy, and E. Anders, Meteoritic material in four terrestrial meteorite craters, *Proc. Lunar Sci. Conf.*, *6*, 1609-1623, 1975.

O'Keefe, J. D., and T. J. Ahrens, The interaction of the Cretaceous-Tertiary extinction bolide with the atmosphere, ocean and solid earth, 1982.

Officer, C. B., A. Hallam, C. L. Drake, and J. D. Devine, Late Cretaceous and paroxysmal Cretaceous/Tertiary extinctions, *Nature*, *326*, 143-148, 1987.

Officer, C. B., and D. R. Lynch, Determination of mixing parameters from tracer distributions in deep-sea sediment cores, *Mar. Geol.*, *52*, 59-74, 1983.

Olmez, I., D. L. Finnegan, and W. H. Zoller, Iridium emissions from Kilauea volcano, *J. Geophys. Res.*, *91*, 653-663, 1986.

Orth, C. J., M. Attrep, and X. Y. Mao, Iridium abundance maxima in the upper Cenomanian extinction interval, *Geophys. Res. Lett.*, *15*, 346-349, 1988a.

Orth, C. J., J. S. Gilmore, J. D. Knight, C. L. Pillmore, R. H. Tschudy, and J. E. Fassett, An iridium abundance anomaly at the palynological Cretaceous-Tertiary boundary in northern New Mexico, *Science*, *214*, 1341-1343, 1981.

Orth, C. J., L. R. Quintana, J. S. Gilmore, J. E. Barrick, J. N. Haywa, and S. A. Spesshardt, Pt-group metal anomalies in the Lower Mississippian of southern Oklahoma, *Geology*, *16*, 627-630, 1988b.

Palme, H., M.-J. Janssens, H. Takahashi, E. Anders, and J. Hertogen, Meteoritic material at five large impact craters, *Geochim. Cosmochim. Acta*, *42*, 313-323, 1978.

Palmer, M. R., K. K. Falkner, K. K. Turekian, and S. E. Calvert, Sources of osmium isotopes in manganese nodules, *Geochim. Cosmochim. Acta*, *52*, 1197-1202, 1988.

Parker, S. P., *McGraw-Hill Dictionary of Scientific and Technical Terms-Third Edition*, McGraw-Hill Book Company, New York, 1984.

Pegram, B. J., B. K. Esser, S. Krishnaswami, and K. K. Turekian, The isotopic composition of leachable osmium from river sediments, *Earth Planet. Sci. Lett.*, *128*, 591-599, 1994.

Peucker-Ehrenbrink, B., G. Ravizza, and A. W. Hofmann, The marine $^{187}Os/^{187}Os$ record of the past 80 million years, *Earth Planet. Sci. Lett.*, *130*, 155-167, 1995.

Playford, P. E., D. J. McLaren, C. J. Orth, J. S. Gilmore, and W. D. Goodfellow, Iridium anomaly in the Upper Devonian of the Canning Basin, Western Australia, *Science*, *226*, 437-439, 1984.

Pontér, C., J. Ingri, and K. Boström, Geochemistry of manganese in the Kalix River, northern Sweden, *Geochim. Cosmochim. Acta*, *56*, 1485-1494, 1992.

Rampino, M. R., and K. Caldeira, Major episodes of geologic change: correlations, time structure and possible causes, *Earth Planet. Sci. Lett.*, *114*, 215-227, 1993.

Ravizza, G., and G. McMurtry, Osmium isotopic variations in metalliferous sediments from the East Pacific Rise and the Bauer Basin, *Geochim. Cosmochim. Acta*, *57*, 4301-4310, 1993.

Rocchia, R., D. Boclet, P. Bonté, C. Jéhanno, C. Yan, V. Courtillot, C. Mary, and R. Wezel, The Cretaceous-Tertiary boundary at Gubbio revisited: Vertical extent of the Ir anomaly, *Earth Planet. Sci. Lett.*, *99*, 206-219, 1990.

Roy-Barman, M., J. H. Chen, and G. J. Wasserburg, ^{230}Th-^{232}Th systematics in the Central Pacific Ocean: The sources and fates of thorium, *Earth Planet. Sci. Lett.*, *Submitted*, 1996.

Schaule, B. K., and C. C. Patterson, Lead concentrations in the northeast Pacific: Evidence for global anthropogenic perturbations, *Earth Planet. Sci. Lett.*, *54*, 97-116, 1981.

Schmitz, B., Chalcophile elements and Ir in continental Cretaceous-Tertiary boundary clays from the western interior of the USA, *Geochim. Cosmochim. Acta*, *56*, 1695-1703, 1992.

Sepkoski, J. J. J., Phanerozoic overview of mass extinction, in *Pattern and Process in the History of Life*, edited by D. M. Raup and D. Jablonski, pp. 277-295, Springer, Berlin, 1986.

Sholkovitz, E. R., Flocculation of dissolved organic and inorganic matter during the mixing of river water and seawater, *Geochim. Cosmochim. Acta*, *40*, 831-845, 1976.

Speidel, D. H., and A. F. Agnew, *The Natural Geochemistry of our Environment*, Westview Press, Boulder, CO, 1982.

Spencer, D. W., and P. G. Brewer, Vertical advection diffusion and redox potentials as controls on the distribution of manganese and other trace metals dissolved in waters of the Black Sea, *J. Geophys. Res.*, *76*, 5877-5892, 1971.

Stumm, W., and J. J. Morgan, *Aquatic Chemistry- 2nd Edition*, John Wiley & Sons, Inc., New York, 1-780, 1981.

Toutain, J.-P., and G. Meyer, Iridium-bearing sublimates at a hot-spot volcano (Piton de la Fournaise, Indian Ocean), *Geophys. Res. Lett.*, *16*, 1391-1394, 1989.

Tredoux, M., M. J. De Wit, R. J. Hart, N. M. Lindsay, B. Verhagen, and J. P. F. Sellschop, Chemostratigraphy across the Cretaceous-Tertiary boundary and a critical assessment of the iridium anomaly, *J. Geol.*, *97*, 585-605, 1989.

Trefry, J. H., and S. Metz, Role of hydrothermal precipitates in the geochemical cycling of vanadium, *Nature*, *342*, 531-533, 1989.

Turekian, K. K., The fate of metals in the oceans, *Geochim. Cosmochim. Acta*, *41*, 1139-1144, 1977.

Wallace, M. W., V. A. Gostin, and R. R. Keays, The Acraman impact ejecta and host shales: Evidence for low-temperature mobilization of iridium and other platinoids, *Geology*, *18*, 132-135, 1990.

Wang, K., C. J. Orth, M. J. Attrep, B. D. E. Chatterton, H. Hou, and H. H. J. Geldsetzer, Geochemical evidence for a catastrophic biotic event at the Frasnian/Famennian boundary in south China, *Geology*, *19*, 776-779, 1991.

Wang K., M. Attrep, and C. J. Orth, Global iridium anomaly, mass extinction, and redox change at the Devonian-Carboniferous boundary. *Geology 21*, 1071-1074, 1993.

Wasserburg, G. J., D. A. Papanastassiou, E. V. Nenow, and C. A. Bauman, A programmable magnetic field mass spectrometer, *Rev. Sci. Instrum.*, *40*, 288-295, 1969.

Wells, M. C., P. N. Boothe, and B. J. Presley, Iridium in marine organisms, *Geochim. Cosmochim. Acta*, *52*, 1737-1739, 1988.

Wilde, P., W. B. N. Berry, M. S. Quinby-Hunt, C. J. Orth, L. R. Quintana, and J. S. Gilmore, Iridium abundances across the Ordovician-Silurian stratotype, *Science*, *233*, 339-341, 1986.

Winterhalter, B., T. Flodén, H. Ignatius, S. Axberg, and L. Niemistö, Geology of the Baltic Sea, in *The Baltic Sea*, *Elsevier Oceanography Series*, vol. 30, edited by A. Voipio, pp. 1-121, Elsevier Scientific Publishing Company, Amsterdam, 1981.

Wood, S. A., Thermodynamic calculations of the volatility of the platinum group elements (PGE): The PGE content of fluids at magmatic temperatures, *Geochem. Cosmochim. Acta*, *51*, 3041-3050, 1987.

Wood, S. A., The interaction of dissolved platinum with fulvic acid and simple organic acid analogues in aqueous solutions, *Can. Min.*, *28*, 665-673, 1990.

Wood, S. A., C. D. Tait, and D. Vlassopoulos, Solubility and spectroscopic studies of the interaction of palladium with simple carboxylic-acids and fulvic-acid at low-temperature, *Geochim. Cosmochim. Acta*, *58*, 625-637, 1994.

Zhou, L., and F. T. Kyte, Sedimentation history of the South Pacific pelagic clay province over the last 85 million years inferred from the geochemistry of Deep Sea Drilling Project hole 596, *Paleoceanography*, *7*, 441-465, 1992.

Zoller, W. H., J. R. Parrington, and J. M. Phelan Kotra, Iridium enrichment in airborne particles from Kilauea volcano: January 1983, *Science*, *222*, 1118-1121, 1983.

Table 5.1. Iridium in the Oceans.

Sample	Date	Depth (m)	Salinity (‰)	O_2 (μmol kg^{-1})	Procedure	Iridium (10^8 atoms kg^{-1})
Pacific Ocean						
(22°45' N, 158°00' W)						
Aloha A†	Sept. '94	25	34.82	198	I	2.9 ± 0.9
Aloha A†	Sept. '94	25	34.82	198	I	3.3 ± 0.9
Aloha A	Sept. '94	25	34.82	198	II	5.7 ± 0.8
Aloha C	Sept. '94	1000	34.46	47	II	4.4 ± 0.6
North Sea						
(57°30' N, 6°59' E)						
H6	May '91	80	35.18	6.15*	II	3.4 ± 0.6

All samples unfiltered and acidified (Ir_{td})

†8 L sample volumes; all others ≈ 4 L.
*mL kg^{-1}

Table 5.2. Iridium in the Baltic Rivers.

Sample	Date	Procedure	Iridium (10^8 atoms kg^{-1})
Rivers			
Kalix A	May '92	I	18.2 ± 1.2
Kalix A	May '92	II	23.5 ± 1.4
Kalix B	June '95	II	17.4 ± 0.9
Neva	May '93	II	49.7 ± 1.3
Wistula	Feb '93	II	92.9 ± 2.2

All samples filtered (0.45 μm) and acidified (Ir_d)
All sample volumes ≈ 4 L

Table 5.3. Iridium in the Baltic Sea.

Sample	Date	Depth (m)	Salinity (‰)	O_2 (mL kg^{-1})	Procedure	Iridium (10^8 atoms kg^{-1})
Baltic Proper						
(57°20' N, 20°03' E)						
BY-15 A[a]	May '92	5	7.30	9.95	I	10.0 ± 1.0
BY-15 A[a]	May '92	5	7.30	9.95	II	11.8 ± 1.2
BY-15 B[b]	May '95	30	7.23	8.74	II	10.7 ± 1.0
BY-15 C[a]	May '92	125	9.89	0.67	I	10.9 ± 1.2
BY-15 D[a]	May '92	150	10.45	0	II	38.6 ± 2.1
BY-15 E[a]	May '92	225	11.16	0	II	38.9 ± 2.2
(59°02' N, 21°05' E)						
BY-28 A[b]	May '91	75	7.93	5.81	I	10.9 ± 1.1
BY-28 B[c]	May '90	50	7.31	8.43	I	14.2 ± 2.0*
Gulf of Bothnia						
(65°23' N, 23°30' E)						
F-2[b]	June '91	50	3.55	9.01	I	11.3 ± 1.2
Kattegat and Danish Sounds						
(56°40' N, 12°07' E)						
Anholt[b]	June '95	15	19.92	7.23	II	25.5 ± 1.5
Blanks						
Blank A	May '92	-	-	-	I	≈ 0.2
Blank B	May '92	-	-	-	II	≈ 0.3

Filtration and acidification: (a) Filtered to 0.10 μm, then acidified (Ir_d)
(b) Filtered to 0.45 μm, then acidified (Ir_d)
(c) Acidified, then filtered to 0.45 μm (Ir_{td})

All sample volumes ≈ 4 L
*Average of two analyses.

Table 5.4. Ir, Pt, Pd, Rh and Au in Continental Crust and in Seawater.

	Ir	Pd	Pt	Rh	Au	Ir/Pd	Ir/Pt	Ir/Rh	Ir/Au
Avg. Crust* (ppb):	0.05	1	2	0.4	1.5	0.050	0.025	0.125	0.033
Seawater** (fmol L^{-1}):	0.5	500	300	1000	50	0.0010	0.0017	0.0005	0.0100

*Ir: Fenner and Presley (1984), Esser and Turekian (1993); Pd, Au: Crocket and Kuo (1979); Pt, Rh: Levinson (1980)

**Ir: This study; Pd: Lee (1983); Pt: Hodge *et al.,* (1986), Jacinto and van den Berg (1989), Colodner (1991); Rh: Bertine *et al.,* (1993); Au: Falkner and Edmond (1990)

Table 5.5. Mn Coprecipitation of Ir, Pt and Re.

pH	Mn(ppm)†	T (hr.)	*fraction in solution after T hr.* Ir	Pt	Re
Fresh Water					
9.5	40	36	0.22	0.30	0.97
		144	0.12	0.12	0.95
		210	0.09	0.07	0.97
Seawater					
9.5	10	48	0.48	0.83	0.82
		72	0.32	0.85	1.00
		120	0.47	0.85	1.05
		240	0.37	0.64	1.03
9.5	40	48	0.48	0.78	0.95
		168	0.41	0.60	0.98
9.5	200	48	0.20	0.25	0.98
		240	0.08	0.21	0.97
6.0	40	48	1.04	1.06	1.01
		240	1.04	0.99	0.98

Initial concentrations of ≈ 5 μg kg^{-1}, in 250 mL solutions.

†mg kg^{-1} solution.

Table 5.6. Fe Coprecipitation of Ir, Pt and Re.

			fraction in solution after T hr.		
pH	Fe (ppm)†	T (hr.)	Ir	Pt	Re
Fresh Water					
9.5	40	2	0.71	0.81	1.00
		36	0.38	0.21	0.99
		72	0.34	0.07	0.97
		120	0.31	0.05	0.99
7.5	40	2	0.69	0.90	1.07
		36	0.54	0.28	1.02
		72	0.32	0.21	0.99
		120	0.23	0.18	1.04
5.5	40	36	0.30	0.16	0.88
		144	0.31	0.14	0.91
		210	0.19	0.09	0.89
Seawater					
9.5	25††	168	0.25	-	-
9.5	40	48	0.51	1.12	1.05
		240	0.17	0.81	0.99
9.5	250††	168	0.10	-	-
6.0	40	120	0.86	0.76	1.02

Initial concentrations of ≈ 5 μg kg^{-1}, in 250 mL solutions.

†mg kg^{-1} solution.
††Scavenging from 4 L; all others from 250 mL.

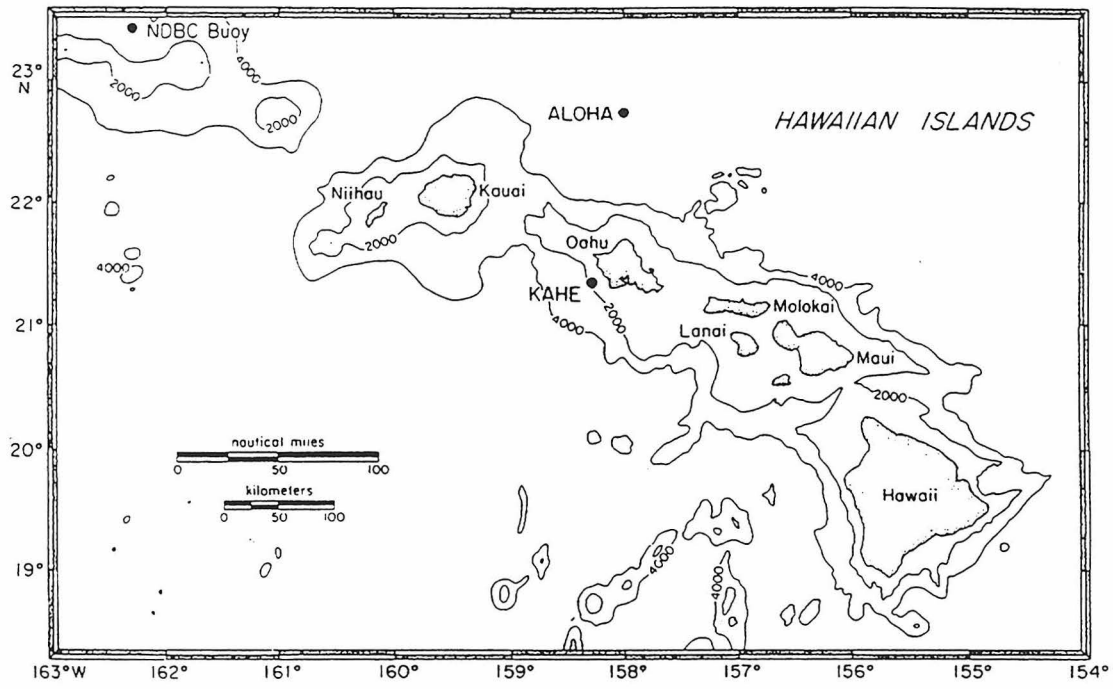

Fig. 5.1. Map showing the location of the Pacific Ocean sampling site, station ALOHA. Adapted from Karl and Winn (1991).

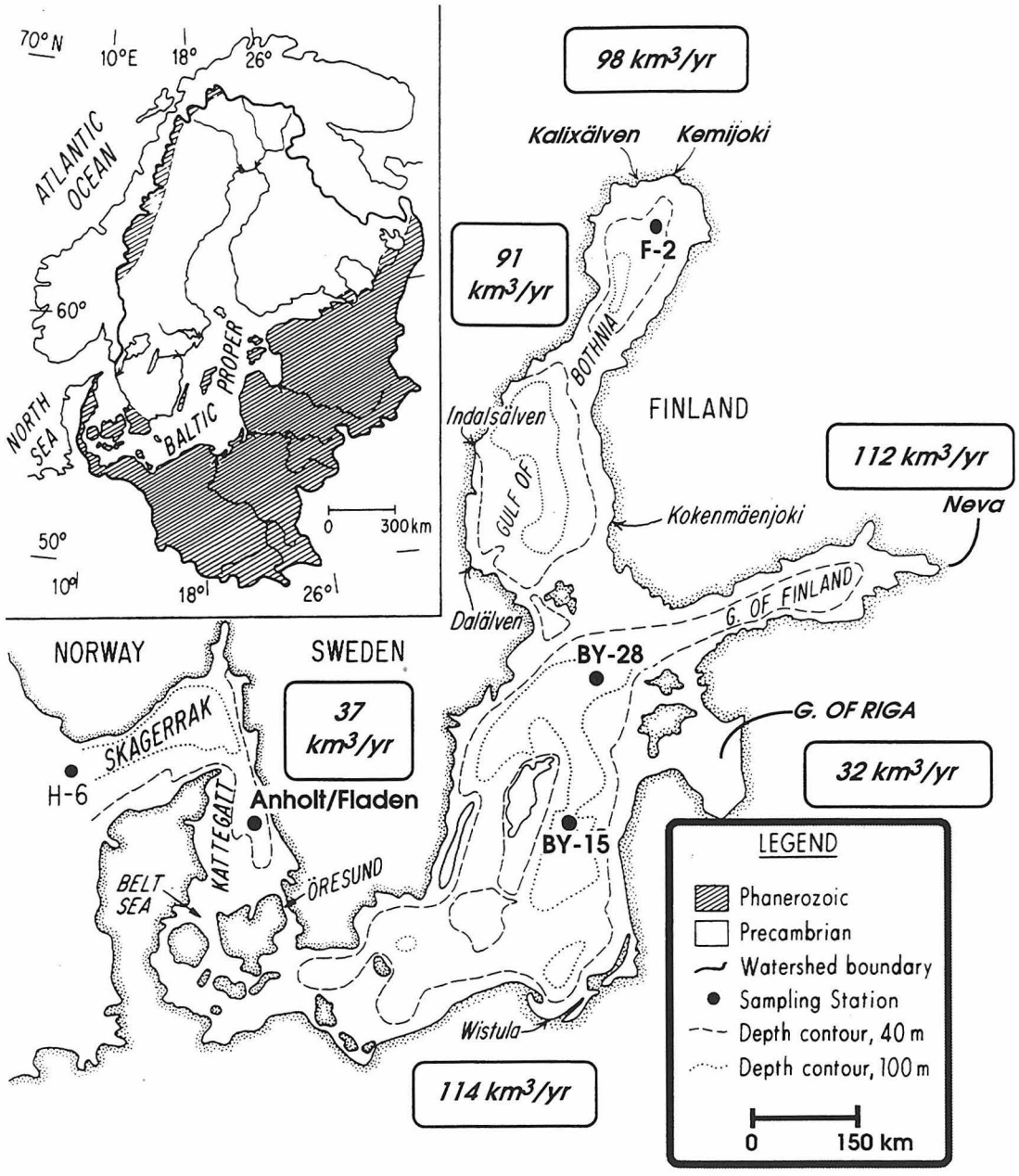

Fig. 5.2. Map of the Baltic Sea, showing the sampling stations and the geographic distribution of fresh water inputs. The inset map illustrates the major lithologies and the watershed boundaries. The map is adapted from Andersson *et al.* (1995). Hydrological data are from Bergström and Carlsson (1994).

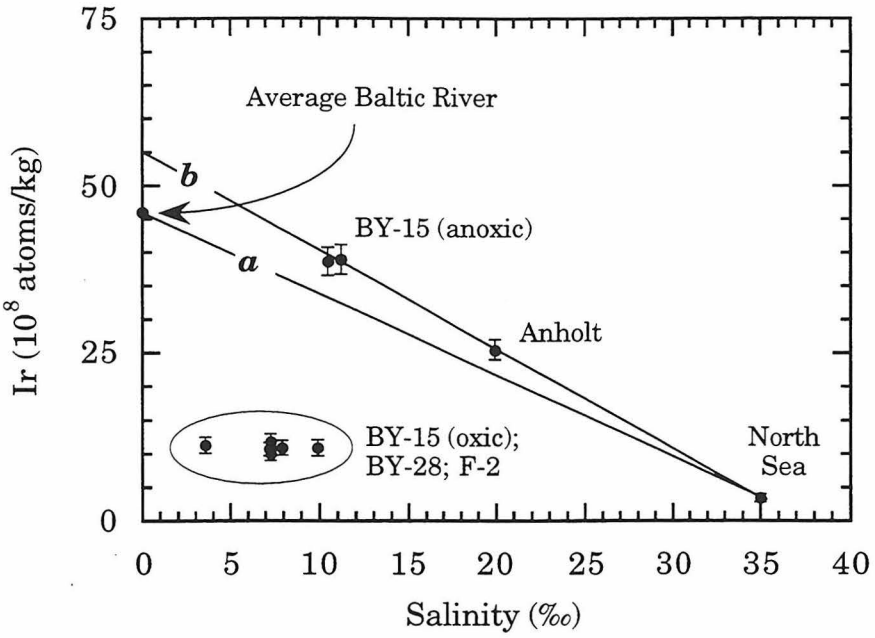

Fig. 5.3. Iridium in the Baltic Sea. Curve *a*: Conservative mixing line between the North Sea and average Baltic river inputs (flux-weighted average, as described in the text). Curve *b*: Conservative mixing line defined by the samples from the North Sea, Kattegat and BY-15 anoxic waters. Samples from oxic waters in the Baltic Proper (stations BY-15 and BY-28) and from oxic waters in the Gulf of Bothnia (station F-2) fall far below these mixing lines.

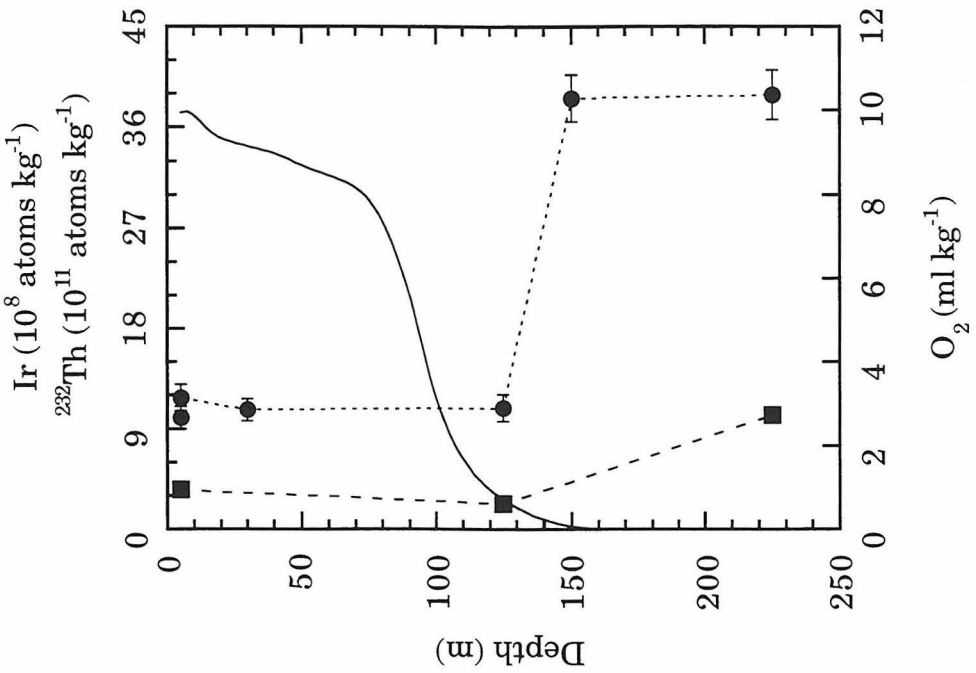

Fig. 5.4. Ir (circles, dotted line), ^{232}Th (squares, dashed line) and O_2 (solid line) in the Gotland Deep (station BY-15).

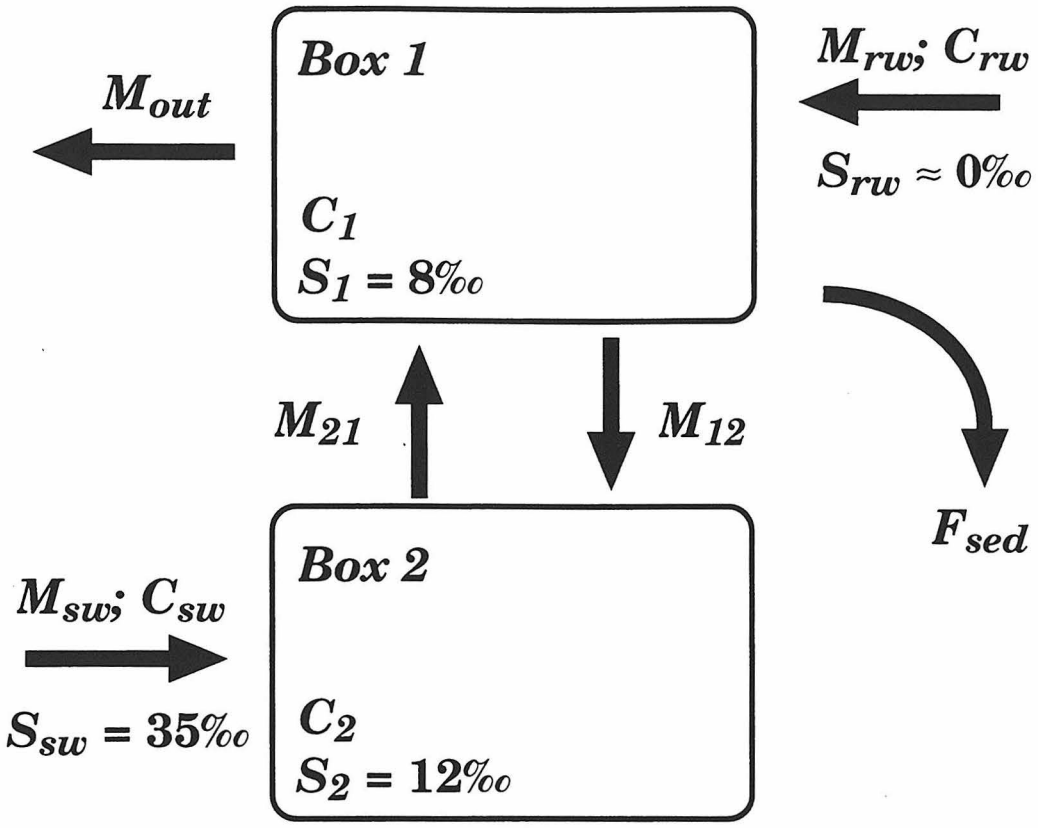

Fig. 5.5. A simple box model of the Baltic Sea, as described in the text. Boxes 1 and 2 are separated by a permanent halocline. M_i are water mass fluxes. S_i and C_i represent salinity and Ir concentration, respectively. Ir is removed into sediments from the upper box by flux F_{sed}. C_1, C_{sw}, C_{rw} and all salinities are set equal to observed values.

Part II.

Methyl Bromide: Ocean Sources, Ocean Sinks and Climate Sensitivity

Published as:

A. D. Anbar, F. Chavez and Y. L. Yung (1996).
Global Biogeochemical Cycles, **10**: 175-190.

1. Abstract

The oceans play an important role in the geochemical cycle of methyl bromide (CH_3Br), the major carrier of O_3-destroying bromine to the stratosphere. The quantity of CH_3Br produced annually in seawater is comparable to the amount entering the atmosphere each year from natural and anthropogenic sources. The production mechanism is unknown, but may be biological. Most of this CH_3Br is consumed *in situ,* by hydrolysis or reaction with chloride. The size of the fraction which escapes to the atmosphere is poorly constrained; measurements in seawater and the atmosphere have been used to justify both a large oceanic CH_3Br flux to the atmosphere, and a small net ocean sink.

Since the consumption reactions are extremely temperature-sensitive, small temperature variations have large effects on the CH_3Br concentration in seawater, and therefore on the exchange between the atmosphere and the ocean. The net CH_3Br flux is also sensitive to variations in the rate of CH_3Br production. We have quantified these effects using a simple, steady-state, mass-balance model. When CH_3Br production rates are linearly scaled with seawater chlorophyll content, this model reproduces the latitudinal variations in marine CH_3Br concentrations observed in the East Pacific Ocean by Singh *et al.* (1983) and by Lobert *et al.* (1995). The apparent correlation of CH_3Br production with primary production explains the discrepancies between the two observational studies, strengthening recent suggestions that the open ocean is a small net sink for atmospheric CH_3Br, rather than a large net source. The Southern Ocean is implicated as a possible large net source of CH_3Br to the atmosphere.

Since our model indicates that both the direction and magnitude of CH_3Br exchange between the atmosphere and ocean are extremely sensitive to temperature and marine productivity, and since the rate of CH_3Br production in the oceans is comparable to the rate at which this compound is introduced to the atmosphere, even small perturbations to temperature or productivity can modify atmospheric CH_3Br. Therefore, atmospheric CH_3Br should be sensitive to climate conditions. Our modeling indicates that climate-induced CH_3Br variations can be larger than those resulting from small (± 25%) changes in the anthropogenic source, assuming that this source comprises less than half of all inputs.

Future measurements of marine CH_3Br, temperature and primary production should be combined with such models to determine the relationship between marine biological activity and CH_3Br production. Better understanding of the biological term is especially important to assess the importance of non-anthropogenic sources to stratospheric ozone loss, and the sensitivity of these sources to global climate change.

2. Introduction

The observation that bromine plays a significant role in the depletion of polar ozone (Anderson *et al.*, 1989; McElroy *et al.*, 1986; Salawitch *et al.*, 1988) has stimulated interest in the importance of bromine compounds in the destruction of stratospheric ozone at mid-latitudes (World Meteorological Organization, 1992), a possibility first noted in the 1970's (Wofsy *et al.*, 1975). As much as a third of Antarctic ozone loss is believed due to bromine, which implies that a bromine atom is ≈ 50 times as efficient as a chlorine atom in destroying O_3 (Salawitch *et al.*, 1988; Solomon *et al.*, 1992; Wofsy *et al.*, 1975). In the mid-latitude lower stratosphere, recent data indicate that bromine accounts for ≈ 15% of total ozone loss (Wennberg *et al.*, 1994). Methyl bromide is of special importance because it is the major carrier of bromine to the stratosphere (Schauffler *et al.*, 1993; Wofsy *et al.*, 1975; Yung *et al.*, 1980), and because the magnitudes of the natural and anthropogenic sources of CH_3Br may be comparable (Khalil *et al.*, 1993; Reeves and Penkett, 1993; Singh and Kanakidou, 1993; Singh *et al.*, 1983; World Meteorological Organization, 1992). However, since the lifetime of CH_3Br with respect to atmospheric loss processes is only ≈ 1.7 yr (Mellouki *et al.*, 1992), its emissions are not limited by existing international agreements on anthropogenic halocarbons, which were intended to minimize long-term ozone loss. As a result, CH_3Br has only recently become a focus of both regulatory and scientific attention (World Meteorological Organization, 1992).

The fate of CH_3Br in the atmosphere, where the most likely sink is reaction with OH radical, has been well studied. Measurements of CH_3Br have been combined with 1-D and 2-D gas-phase kinetic models to estimate the rate of destruction in the atmosphere (Reeves and Penkett, 1993; Wofsy *et*

al., 1975; Yung *et al.*, 1980), which in turn can be used to constrain the flux of CH_3Br to the atmosphere under steady-state conditions. These studies converge on a total source strength of 0.8 to 1.0 Gmol yr^{-1}. The total source is somewhat higher if other sinks are considered (*e.g.*, 0.9 - 1.2 Gmol yr^{-1}; (Lobert *et al.*, 1995)). The goal of most current methyl bromide research is to determine the relative magnitudes of various natural and anthropogenic sources, about which there are large uncertainties. These include industrial and agricultural sources of CH_3Br, biogenic emissions (such as from marine organisms), and pyrogenic CH_3Br from biomass burning.

Characterization of methyl bromide in the marine environment is particularly important, since the oceanic flux is a critical unknown in the CH_3Br atmospheric budget. While the first observational studies suggested that the ocean is a large net source of CH_3Br (Khalil *et al.*, 1993; Singh *et al.*, 1983), more recent work indicates a small net sink (Lobert *et al.*, 1995). Constraining the oceanic flux is critical to a rational regulatory approach to industrial use of CH_3Br, since it is necessary to know how the size of the anthropogenic source compares to natural sources. Additionally, the magnitude of the gross flux of CH_3Br into the ocean affects the atmospheric lifetime of CH_3Br and, hence, the ozone depletion potential (ODP) of this compound (Lobert *et al.*, 1995; Mellouki *et al.*, 1992). Finally, the variability of the oceanic flux in response to the changing atmospheric burden of CH_3Br may "buffer" atmospheric CH_3Br against changes in the magnitude of anthropogenic sources (Butler, 1994).

The conflicting conclusions of the observational studies of marine methyl bromide arise primarily from differences in the observed concentrations of CH_3Br in seawater, and the assumptions used to

extrapolate measurements made in limited geographic areas to the global oceans. Below, using a simple, steady-state model, we re-examine the data of Singh *et al.* (1983) ("Cruise *A*") and Lobert *et al.* (1995) ("Cruise *B*") to evaluate the hypothesis of a large ocean source. When we carefully consider the marine chemistry of CH_3Br, substantial spatial and temporal variations in the seawater concentration and oceanic flux appear inevitable due to the temperature sensitivity of CH_3Br inorganic chemistry, and the apparent role of biological activity in CH_3Br production. These effects can be modeled with some confidence, and account for most of the observational discrepancies; we find that the data of Singh *et al.* (1983) are consistent with the small ocean sink determined by Lobert *et al.* (1995) when these data are reinterpreted. Since marine temperature and productivity are both functions of climate, the possible effects of climate change on atmospheric CH_3Br are also explored, using a coupled ocean/atmosphere model.

3. Marine Chemistry of CH_3Br

All studies of methyl bromide in seawater reveal concentrations too high to be the simple result of invasion from the atmosphere balanced in steady-state against the known marine loss processes, indicating a large rate of CH_3Br production in the water column (*e.g.,* Khalil *et al.*, 1993; Lobert *et al.*, 1995; Singh *et al.*, 1983). This production process is poorly understood, although it has been assumed to be biological in the absence of other explanations (*e.g.,* Singh and Kanakidou, 1993), and because biogenesis of halogenated organics in natural waters is well known (*e.g.,* Gschwend *et al.*, 1985; Itoh and Shinya, 1994; Manley and Dastoor, 1986; Moore and Tokarczyk, 1993). Production of CH_3Br by marine kelp and phytoplankton

has been observed, although not at rates sufficient to support the observed seawater concentrations (Manley and Dastoor, 1986; Moore *et al.*, 1995). Quantitative identification of the CH_3Br production mechanism is of obvious importance.

CH_3Br is also *consumed* in the ocean, by nucleophilic substitution by Cl^- and by hydrolysis (Elliott and Rowland, 1993; Zafiriou, 1975):

$$CH_3Br + Cl^- \rightarrow CH_3Cl + Br^-$$
$$CH_3Br + H_2O \rightarrow CH_3OH + H^+ + Br^-$$

Using available kinetic data (Bathgate and Moelwyn-Hughes, 1959; Elliott and Rowland, 1993; Mabey and Mill, 1978; Moelwyn-Hughes, 1938; Moelwyn-Hughes, 1953), the rate constants for these reactions are $k_{Cl} = 9.5 \times 10^{12} e^{(-12679/T)}$ liters mol^{-1} s^{-1} and $k_{H_2O} = 1.0 \times 10^{12} e^{(-13348/T)}$ s^{-1}. At a typical open-ocean surface temperature of 21.9°C (Lobert *et al.*, 1995), and $[Cl^-] = 0.56$ mol $liter^{-1}$, the pseudo first-order rate constant for CH_3Br loss can be estimated as $\approx 10^{-6}$ s^{-1}. This value is comparable to the air-sea exchange constant estimated for methyl halides (Liss and Slater, 1974; Zafiriou, 1975). *A priori,* this suggests that the rate of CH_3Br destruction in the water column should be of comparable magnitude to the escape flux to the atmosphere. This is an important point: Assuming steady-state in the upper oceans, the net flux between the atmosphere and ocean (F_{net}) must equal the difference between the rate of CH_3Br production (P_o) and the rate at which CH_3Br is destroyed in the water column (D_o), i.e. $F_{net} = P_o - D_o$. If D_o is as large as, or larger than, F_{net}, then moderate perturbations to either P_o or D_o will have a non-trivial impact on F_{net}. This can impact atmospheric CH_3Br .

The magnitudes of P_o, D_o and F_{net} on a global average basis have been constrained using measurements of CH_3Br in the atmosphere and ocean. Determinations of tropospheric CH_3Br all converge on a global average abundance of ≈ 10 ppt (Atlas *et al.*, 1993; Cicerone *et al.*, 1988; Khalil *et al.*, 1993; Lal *et al.*, 1994; Lobert *et al.*, 1995; Penkett *et al.*, 1985; Singh and Kanakidou, 1993; Singh *et al.*, 1983). A decreasing concentration gradient from the northern to southern hemisphere is typically observed, possibly due to higher anthropogenic emissions in the north (Reeves and Penkett, 1993). A slight global increase was reported from 1983 to 1991, possibly due to increasing anthropogenic use over this time, and uncorrelated short-term variations of less than ≈ 2 ppt have been reported at various latitudes (Khalil *et al.*, 1993). However, observations of variations in atmospheric CH_3Br concentrations through time are complicated by analytical artifacts (Montzka *et al.*, 1995). Recent work indicates that the actual variations may be much smaller (Miller and Weiss, 1995).

Although few measurements have been made, CH_3Br in seawater (c_o) is apparently more variable, reflecting the ≈ 10 day residence time with respect to chemical loss. Singh *et al.* (1983) (recalibrated by Singh and Kanakidou (1993) determined an average value of ≈ 5.2 x 10^{-9} mol m^{-3} in the near-shore eastern Pacific, with site-to-site variations as large as a factor of six (Cruise *A*). Lobert *et al.* (1995), following a ship track 10 - 20° further west, found substantially lower concentrations, ranging from ≈ 1 to 2.5 x 10^{-9} mol m^{-3} (Cruise *B*). Khalil *et al.* (1993) observed an average value intermediate between these two across a larger area of the Pacific, as well as a trend of CH_3Br increasing by a factor of two in seawater from southern to northern latitudes.

When combined with the atmospheric data, these marine data sets have been used to justify a wide range of F_{net} estimates. Singh *et al.* (1983) originally determined a global source of 2.3 - 3.2 Gmol yr^{-1}, based on a straightforward extrapolation of observations of CH_3Br supersaturation in the eastern Pacific. If correct, such values require the existence of a large, unidentified sink for atmospheric CH_3Br. In a recent re-evaluation of these data, Singh and Kanakidou (1993) assumed that the magnitude of the CH_3Br flux is proportional to marine primary production, and/or to the CH_3Cl flux, and thereby estimated a global source of 0.42 - 0.84 Gmol yr^{-1}. This approaches the findings of Khalil *et al.* (1993), who estimated a source of 0.32 - 0.42 Gmol yr^{-1} based on a more geographically representative sampling of Pacific Ocean waters. However, it is not apparent why the CH_3Br flux should be proportional to primary production, even if biological sources dominate. Since the flux is a function of the difference between CH_3Br production and loss ($F_{net} = P_o - D_o$), proportionality will only occur if the loss rate is negligibly small ($F_{net} \approx P_o$), or if the rate of CH_3Br loss is directly proportional to the rate of production, with a proportionality constant that is insensitive to temperature or other variables ($F_{net} = P_o - \alpha P_o$; α = constant). Neither assumption is justified *a priori*. As for the correlation between the fluxes of CH_3Br and CH_3Cl, this does not appear to be a consistent relationship (*e.g.,* Lobert *et al.*, 1995).

More recently, Lobert *et al.* (1995) estimated a net CH_3Br ocean *sink* of $\approx$ 0.13 Gmol yr^{-1}, based on c_o measurements lower than those observed previously, as well as on a more realistic extrapolation to the global oceans. The reason(s) for the lower measured CH_3Br concentrations has not been explained in the literature, although it has been suggested that analytical

artifacts led to erroneously high seawater measurements in the previous studies (Lobert *et al.*, 1995).

Despite the divergence of F_{net} estimates, as well as a variety of other uncertainties in making global extrapolations (*e.g.*, average seawater temperature), all studies indicate that most of the CH_3Br produced in the oceans is consumed in the oceans. For example, Singh and Kanakidou (1993) estimate $F_{net} \approx 0.42$ - 0.84 Gmol yr^{-1}, against a total marine production rate of 2.1 - 3.2 Gmol yr^{-1}, and losses of 1.7 - 2.4 Gmol yr^{-1}. The data of Lobert *et al.* (1995) extrapolate to $F_{net} \approx$ - 0.13 Gmol yr^{-1}, $D_o \approx 1.7$ Gmol yr^{-1}, and $P_o \approx$ 1.6 Gmol yr^{-1} for the global ocean. Thus, F_{net} accounts for at most $\approx 40\%$ of the CH_3Br production in the ocean, and it is possible that all the CH_3Br produced in seawater is consumed *in situ.* As a result, c_o and F_{net} should be quite sensitive to perturbations of the rates of D_o and P_o, as suggested above. The response time to such changes is on the order of weeks, reflecting the short residence time of CH_3Br in seawater. Therefore, variations of c_o should be readily apparent if such perturbations exist. Since measurements of c_o reveal substantial, unexplained variations with depth and location (Khalil *et al.*, 1993; Lobert *et al.*, 1995; Singh *et al.*, 1983), it appears that the rates of CH_3Br production and/or chemical loss are, indeed, highly variable.

We suggest that substantial variability in the rate of CH_3Br consumption arises from the extreme temperature-dependence of the rates of hydrolysis and the reaction with chloride; the Arrhenius activation energies, E_a, are $\approx$ 100 kJ/mol, leading to an increase in the rate constants of nearly an order of magnitude as temperature is raised from 0°C to 22°C (Fig. 1). The potential impact of this effect in seawater is shown in Fig. 2a, where the combined rate constant for loss by hydrolysis and displacement by Cl^- has

been calculated using measured sea-surface temperatures (SSTs) as a function of latitude for Cruise *A* and Cruise *B* (Lobert *et al.*, 1995; Singh *et al.*, 1983). Along these transects, the potential for CH_3Br destruction at low northern latitudes, where temperatures are highest, is as much as four times that at 30°S. Thus, substantial variations in the exchange of CH_3Br between the atmosphere and ocean should arise from naturally-occurring temperature changes, such as those associated with latitudinal variations, seasonal cycles and global climate change.

Variations in the rate of production of CH_3Br, which could also lead to substantial variability in marine and atmospheric CH_3Br levels, are more difficult to quantify, largely because the CH_3Br *in situ* source has not yet been identified. Below, we explore the possibility that CH_3Br production is a function of primary production in the oceans (Singh and Kanakidou, 1993). To do this, we scale CH_3Br production rates to observed marine chlorophyll abundances (primary production and chlorophyll abundance are proportional under conditions of constant illumination (*e.g.,* Morel and Berthon, 1989)). Chlorophyll data are available from shipboard measurements (*in vivo* fluorescence or extracted chlorophyll), and from satellite observations of ocean color. Measurements from the Coastal Zone Color Scanner (CZCS) experiment on the Nimbus-7 satellite for the month of December (climatological average from 1979 - 86), the month of Cruise *A*, are presented in Fig. 2b (Feldman, 1989). Gaps in this data set along the shiptrack are minimal, and were filled by linear extrapolation from adjacent pixels. Continuous measurements of *in vivo* phytoplankton fluorescence, a surrogate for chlorophyll concentration (Lorenzen, 1966), were made during the cruise of Lobert *et al.* (1995) in January - February of 1994 (Cruise *B*). These data

are also presented in Fig. 2b. These observations indicate that during Cruise *A*, production rates near 10°S along the shiptrack were more than twice the regional average, while productivity near 25°S was particularly low. Chlorophyll variations during Cruise *B* were much more subdued. This reflects that the later cruise sampled waters more representative of the open ocean, where productivity is uniformly low relative to coastal waters. Clearly, if CH_3Br production correlates with primary production, substantial latitudinal and longitudinal variations in CH_3Br abundances and ocean/atmosphere exchange should result from this effect, as well as from temperature.

4. Marine CH_3Br: A Steady-State Ocean Model

4.1. General Model Description

Since the residence time of CH_3Br in the oceans is much less than the atmospheric residence time, we can quantify the short-term response of c_o to ocean temperature variations by assuming a constant value of CH_3Br in the atmosphere, and considering a simple steady-state model of the upper ocean. In this system, the rate of biological CH_3Br production per unit area (P) is balanced by chemical loss in the mixed layer, removal by eddy mixing to, and chemical loss in, deeper waters, and escape to the atmosphere:

$$\frac{dc_o}{dt} = \frac{P}{z} - k_d(T)c_o - \frac{\left(k_d(T_{th})D_z\right)^{1/2}}{z}c_o - \frac{K_l \, x \, 10^{-12}}{zH(T)}\left(\frac{H(T)}{10^{-12}}c_o - p_a\right) \quad (1)$$

where $k_d(T)$ is the temperature-dependent rate constant for chemical loss ($k_d(T) = k_{Cl}(T) + k_{H_2O}(T)$); D_z (5.4 x 10^3 m^2 yr^{-1}) parameterizes the rate of vertical mixing from the mixed layer down to a thermocline of average

temperature T_{th}, where CH_3Br undergoes chemical loss (Butler, 1994; Butler *et al.*, 1991); K_l is the air-sea exchange coefficient expressed on a liquid-phase basis (1.2 x 10^3 m yr^{-1}, calculated by the method of Liss and Slater (1974)); $H(T)$ is the Henry's Law constant (1.2 x 0.251 x 0.029 x $e^{(0.0334(T - 25))}$ m^3 atm mol^{-1}, where 0.251 = H(25°C) in pure water, 1.2 accounts for the salting-out effect in seawater, and 0.029 converts from the unitless partition coefficient to the units used here (Singh *et al.*, 1983)); c_o is the concentration of CH_3Br in the ocean (mol m^{-3}); p_a is the partial pressure of CH_3Br in the atmosphere (ppt); and the factor of 10^{-12} converts units between ppt and atm.

Solving for c_o at steady state, we obtain:

$$c_o = \left[P + \frac{K_l p_a \, x \, 10^{-12}}{H(T)} \right] \times \left[\frac{1}{z k_o(T) + K_l} \right] \tag{2}$$

where:

$$k_o(T) = k_d(T) + \frac{\left(k_d(T_{th}) D_z\right)^{1/2}}{z} \tag{3}$$

We have used Eqn. (2) to examine the effect of T and P on c_o along the shiptracks of Cruise *A* (Singh and Kanakidou, 1993; Singh *et al.*, 1983) and Cruise *B* (Lobert *et al.*, 1995). The data of Khalil *et al.* (1993) are not considered because chlorophyll data, used below to model variations of P, are not available for this shiptrack.

4.2. Constant Production Model: Results and Comparison with Observations

Initially, we assume a uniform value of P across the sampled waters (P_{avg}). Although this is unlikely to be a valid assumption (Fig. 2b), it allows us to isolate the effects of temperature, since any latitudinal variations in the

calculated c_o will arise exclusively from the effect of temperature on k_d. Productivity effects are considered in the next section. P_{avg} for each cruise was determined by re-expressing Eqn. 2 to solve for P in terms of measured values of c_o and T at each point along the shiptrack, and then averaging these P values (Cruise A: P_{avg} = 1.5 x 10^{-14} Gmol m^{-2} yr^{-1}; Cruise B: P_{avg} = 3.8 x 10^{-15} Gmol m^{-2} yr^{-1}). p_a is fixed at 11 and 8.5 ppt in the northern and southern hemispheres, respectively. A mixed layer depth of 30 meters is assumed for Cruise A, and 75 meters for Cruise B. The temperature in the mixed layer is considered equal to the measured SST, falling to an average thermocline value of 15°C. These parameters are consistent with oceanographic data from the sampled regions (*e.g.,* Lobert *et al.*, 1995; Pazen, 1993).

Some averaging of the observational data is necessary to smooth-over the effects of horizontal circulation, which can be significant during the lifetime of CH_3Br in seawater. Data used in the models (*e.g.,* temperature, chlorophyll abundance) were averaged at the indicated resolution prior to calculation. In the case of Cruise B, 1° latitudinal bins were chosen. Bins of 10° width were employed in the case of Cruise A, due to the coarseness of the CH_3Br observations to which model results were compared.. Data collected from 16°S to 10°S during Cruise A, as well as those from Cruise B north of 30°N and south of 40°S, were omitted to exclude anthropogenic and/or near-shore effects. For Cruise A, the data of Singh *et al.* (1983) were divided by a factor of 2.3, following the recalibration of Singh and Kanakidou (1993).

The results of this constant production model are a reasonable qualitative and quantitative fit to the Cruise A observations from 10°S to 30°N, which exhibit c_o variations of nearly a factor of two (Fig 3a). Model predictions and observations agree to within ≈ 30% in this region. Notably,

the model reproduces the observed minimum in the low-latitude northern hemisphere, a reflection of the SST maximum in this region (Fig. 2a). The discrepancies between the model results and observations are greatest at the southern latitudes, where the model deviates from observations by as much as 115%. This is likely due to a flaw in the assumption that CH_3Br production rates are uniform across the sampled waters, a particularly implausible assumption for southern waters in which chlorophyll abundances are typically low during December (Fig. 2b).

The model results for Cruise *B* are a markedly better fit to the observational data (Fig. 3b). Most points agree to well within 30% (the average deviation is 25%), and the general trend of increasing concentrations at higher latitudes is reproduced. This good agreement presumably results from the fact that this cruise sampled waters more representative of the open oceans, where productivity is low and relatively uniform (Fig. 2b). Temperature should be the dominant control on CH_3Br concentrations in such waters. The greatest deviations are seen where primary production varies strongly from the regional average (Fig. 2b), i.e. between 20°S and 30°S, ± 10° of the equator, and at latitudes higher than 20°N.

4.3. Variable Production Model: Results and Comparison with Observations

The variability in CH_3Br production rates can be easily parameterized by scaling the CH_3Br production rate to chlorophyll concentration, assuming a linear correlation exists between these variables. Heretofore, this was an unproved assumption. However, its validity is demonstrated by the highly linear relationship seen when regressing *Chl* against P_{model} (Fig. 4a), where P_{model} is obtained by substituting *observed* c_o and T into Eqn. 2, to calculate a

model P at each latitude. When using the Cruise B data, the correlation coefficient, r, is 0.82. Thus, it is reasonable to conclude that chlorophyll concentration and CH_3Br production rates are strongly correlated and, in turn, that CH_3Br production and primary production are related. We note that the correlation coefficient increases to > 0.90 if these data are averaged to 10° latitudinal resolution, suggesting that mixing effects may still be significant at 1° resolution.

A similar analysis using Cruise A data also shows a generally linear trend (Fig. 4a), but with noticeably poorer correlation (r = 0.66), slightly different slope, and a much larger intercept. Analytical artifacts in the CH_3Br data from Cruise A may account for some of the scatter (Montzka *et al.*, 1995). Additionally, discrepancies arise from at least two problems with the satellite-based ocean color observations used to derive Chl along the Cruise A shiptrack. First, because of gaps in the satellite data, we have been forced to use the climatological average data for the month of the cruise. This is bound to degrade the correlation, particularly for a species with as dynamic a marine cycle as CH_3Br's. Second, the satellite data have been found to significantly underestimate chlorophyll when compared to shipboard observations in the Eastern Pacific (Chavez, 1995) and elsewhere (Balch *et al.*, 1992). It is likely that this accounts for the offset between the regression lines. When the satellite data are adjusted by the empirical relation $Chl_{ship} = 1.104 \times 10^{((\log(Chl_{sat}) + 0.4393) / 0.8058)}$ (Chavez, 1995), the Cruise A chlorophyll data are more typical of the sampled waters, and both data sets fall along a single regression line similar to that obtained from the Cruise B data alone, with r = 0.86 (Fig. 4b).

This linear relationship was incorporated into the CH_3Br model. In the case of Cruise *A* (Fig. 5a), the northern hemisphere results are not changed substantially by the inclusion of the productivity effect, since chlorophyll abundances at these latitudes did not deviate far from the regional mean. However, the results for the southern latitudes are improved considerably. In this case, the model results are within ≈ 50% of the observations for every bin. Although the constant production model fits the Cruise *B* data fairly well, inclusion of the productivity effects leads to a significantly better fit (Fig. 5b). In particular, the depression between 30°S and 20°S is reproduced, as are many of the small-scale variations from 20°S to 20°N. The model still overestimates the observations north of 20°N, but to a lesser degree. Overall, the model results and observational data now agree to within 15% for nearly all latitudes.

These results clearly indicate a connection between CH_3Br and overall biological productivity in seawater, despite the crudeness of the calculations (especially the assumptions of uniform mixed-layer temperature and depth, and the omission of any corrections for variable surface windspeed). This accounts for a large fraction of the observed latitudinal variation in seawater CH_3Br. Previous, unsuccessful examinations of CH_3Br marine data for this relationship (Khalil *et al.*, 1993) may have been complicated by temperature effects; simple comparisons of c_o and chlorophyll will not show a high degree of correlation unless all sampled waters are at uniform temperature. Variations in *both* $k_d(T)$ and P must be considered when modeling c_o.

This correlation, observed across a range of productivities, has serious implications for future observational studies. Since marine primary production is highly variable both geographically and temporally (*e.g.*,

Feldman, 1989; Michaels *et al.*, 1994), it is likely that the same is true of marine CH_3Br production rates. Thus, estimates of the global average CH_3Br flux based on extrapolation of measurements made in limited geographic areas over short periods of time may err substantially, unless appropriate corrections are made for these effects. Although geographic variations in the rate of CH_3Br production are sometimes considered explicitly (*e.g.,* Singh and Kanakidou, 1993), or implicitly (*e.g.,* Lobert *et al.*, 1995), seasonal or other short-term productivity variations typically are not. Since the residence time of CH_3Br in the oceans is short, this effect should not be overlooked.

While our findings suggest that CH_3Br is a general product of the marine biota, identification of the ultimate CH_3Br seawater source remains an outstanding area of research. Studies of phytoplankton in the laboratory cannot easily account for the necessary rate of CH_3Br production, and at least one small-scale field study revealed no connection between methyl halide concentrations and phytoplankton abundance (Moore *et al.*, 1995; Tokarczyk and Moore, 1994). It is possible that CH_3Br production rates are extremely species specific, much like that of another important trace species, dimethylsulfide (DMS) (Keller, 1991). Further complications would arise if CH_3Br production in the oceans were not a direct function of cell division or photosynthesis, as observed in some laboratory cultures (Scarratt and Moore, 1995). Combined, these effects would make direct correlation of CH_3Br production and primary production particularly difficult in the laboratory and in limited field studies. This situation is not without precedent. For example, over small scales, correlation of DMS concentration and chlorophyll have been difficult to make. However, over larger scales, similar to those used here, such correlations have been observed (Falkowski *et al.*, 1992).

4.4. Extrapolations to the Global Ocean: Cruises *A* and *B* Compared

Cruise *A* and Cruise *B* observations have been used to justify a large net CH_3Br ocean source, and a small net ocean sink, respectively (Lobert *et al.*, 1995; Singh and Kanakidou, 1993; Singh *et al.*, 1983). The difference arises largely from the different seawater CH_3Br concentrations observed in the two studies. These have led to different estimates of CH_3Br production rates and/or saturation anomalies, which have then been extrapolated to the entire ocean. However, as demonstrated above, the variations of CH_3Br concentrations measured during each cruise can be predicted simply on the basis of observed temperature and chlorophyll along each shiptrack. The same simple model can be used to reconcile the two studies.

When extrapolating the Cruise *B* observations, Lobert *et al.* (1995) included temperature and productivity variations implicitly, since they determined mean saturation anomalies (saturation anomaly = $(H(T)c_o - p_a \times 10^{-12})/(p_a \times 10^{-12})$) for characteristic ocean regions sampled during the cruise (*i.e.*, "open ocean", "coastal", and "upwelling"). These were summed in proportion to the area of the ocean represented by each region. To the extent that temperature and CH_3Br production rates in each characteristic region are truly representative, this approach is valid. Their open ocean results are summarized in Table 1, along with the mean sea surface temperature observed for this region (21.9°C). Since it accounts for 80% of ocean area, the open ocean region dominates the CH_3Br budget. Although a mean value of 17°C has been widely used as an average upper ocean temperature (Sverdrup *et al.*, 1942), open ocean SSTs are substantially higher than this. The value of 21.9°C is more representative.

Singh *et al.* (1983) inferred a large global ocean source of CH_3Br, but did not account for either temperature or production variations in extrapolating Cruise *A* results. Singh and Kanakidou (1993) made the significant observation that Cruise *A* sampled waters close to the continental margins, where marine productivity is much higher than is typical of the open ocean. However, they accounted for this variation in a simplistic manner, as discussed earlier, and did not account for temperature effects. Using Eqn. 2, and the exchange model of Liss and Slater (1972), we have extrapolated the Cruise *A* data to the open oceans. We have assumed that the rate of CH_3Br production in the open ocean is 1/4 of the average rate in the waters sampled by Cruise *A*. This is consistent with the ratio of the mean chlorophyll abundance along the Cruise *A* shiptrack to the mean abundance in the open ocean (derived from the CZCS data set). For consistency, the mean open ocean temperature used by Lobert *et al.* (1995) is also incorporated here, as are their average open ocean values for H (6.7×10^{-3} m^3 atm mol^{-1}) and K_l (1.8×10^3 m yr^{-1}). Note that this value of H is the average of the values calculated at individual data points along the portions of the shiptrack in open ocean waters. Since H is not a linear function of T, the open ocean value cannot be simply calculated from the mean open ocean temperature. This extrapolation of the Cruise *A* observations (Table 1) predicts a net sink of $\approx$ 0.14 Gmol yr^{-1}, D_o = 1.22 Gmol yr^{-1} and P_o = 1.08 Gmol yr^{-1}. We consider this surprisingly good agreement with the results of Lobert *et al.* (1995), considering the simplicity of the model. Apparently, the Cruise *A* data set does not contradict the Cruise *B* observations.

However, it should be recognized that these extrapolations are extremely sensitive to the assumed temperature of the upper ocean. A 12%

increase in the average open ocean SST doubles the magnitude of the net sink, to ≈ 0.28 Gmol yr^{-1}. Conversely, a 12% decrease in the mean open ocean SST decreases the rate of CH_3Br loss in seawater such that F_{net} reverses direction. Combined with the small net evasion of CH_3Br observed in coastal and upwelling waters (Lobert *et al.*, 1995), this would result in a small net CH_3Br ocean source. Thus, although a large open ocean source for CH_3Br now seems unlikely, a small source is still possible, if average open ocean temperatures are slightly different from those observed by Lobert *et al.* (1995). Regardless, the elimination of a large open ocean source is problematic for the CH_3Br atmospheric budget, since known sinks of ≥ 100 Gmol yr^{-1} are not balanced by the remaining known sources.

One source which may have been overlooked is evasion from polar oceans. In particular, the Southern Ocean, which comprises approximately 10% of ocean area, is a region of high primary production and very low sea surface temperature. These factors may combine to produce a high rate of CH_3Br production, a low rate of *in situ* consumption and, hence, a large net flux to the atmosphere. Using available chlorophyll and temperature data for the Southern Ocean (Comiso *et al.*, 1993), a simple extrapolation based on the relationship in Fig. 4b and our model (Eqns. 1-3) predicts an extremely high contribution from these waters to the total CH_3Br source (Table 2). This contribution may have an extremely large seasonal variability.

The contribution from extreme northern latitudes is likely to be a smaller fraction of the total source since there is less exposed ocean at these latitudes. However, CH_3Br from these waters could have an important regional effect, since organo-bromides have been strongly implicated in Arctic ozone loss.(*e.g.,* Leaitch *et al.*, 1994; Li *et al.*, 1994)

Such extrapolations should be regarded cautiously, as they are subject to all the uncertainties inherent in the CZCS data set discussed above. Additionally, we have assumed that the relationship between chlorophyll and CH_3Br production rates observed in low-latitude waters can be directly applied to extreme latitudes. Since the agent responsible for CH_3Br production has not been identified, this assumption may be flawed. Clearly, there is an urgent need for characterization of CH_3Br in high-latitude seawater.

The sensitivity of marine CH_3Br to temperature suggests that climate change can affect the direction and magnitude of the net CH_3Br ocean/atmosphere flux. Since the amount of CH_3Br produced in seawater each year ($\approx$ 1.1 Gmol) is comparable to the amount of CH_3Br emitted from all sources to the atmosphere (0.80 - 1.2 Gmol), even small perturbations to this flux may significantly alter the atmospheric partial pressure of CH_3Br. A coupled ocean-atmosphere model is needed to explore this problem. Such a model is discussed below.

5. Atmospheric CH_3Br: A Coupled Ocean-Atmosphere Model

5.1. Model Description

Variations in c_o such as those modeled above translate directly into variations in the ocean-atmosphere flux, which are reflected in the average atmospheric abundance of CH_3Br if the system is permitted to equilibrate over timescales greater than the atmospheric residence time, τ_{CH_3Br}. This effect can be studied using a simple, two-box model which couples the upper ocean and troposphere (Fig. 6), following the treatment of Butler (1994). This approach assumes that the upper ocean and troposphere are well-mixed.

Thus, geographic heterogeneities, such as those discussed in the previous section, are not considered. Instead, this model lets us examine the global average abundance of CH_3Br in the atmosphere and ocean for different values of upper ocean temperature and/or different rates of CH_3Br production.

The upper ocean budget is again described by Eqn. (1). The atmospheric budget balances destruction by reaction with OH (and possible land sinks) against inputs from the oceans, anthropogenic sources (R_{anthro}), and other sources, such as biomass burning (R_{other}):

$$\frac{dp_a}{dt} = \frac{R_{anthro} + R_{other}}{N_T \, x \, 10^{-12}} + \frac{K_l A \, x \, 10^{-12}}{N_T H(T)} \left(\frac{H(T)}{10^{-12}} c_o - p_a \right) - k_a p_a \qquad (4)$$

where k_a is the rate of loss from the atmosphere (≈ 0.56 yr^{-1} (Mellouki *et al.*, 1992)), N_T is the total number of moles in the atmosphere (1.8×10^{20} mol), and A is the global ocean surface area (3.61×10^{14} m^2). Although the rate of CH_3Br evasion to the stratosphere dominates the stratospheric bromine budget, this is a negligible sink for the troposphere and is therefore not included in k_a.

The coupled model is solved by assuming that steady-state conditions exist in each box. Eqns. (1) and (4) can be simplified by using Eqn. (3), and by replacing the net exchange coefficient, K_l, with separate coefficients ($k_\alpha(T) = K_l A / H(T) N_T$; $k_\beta = K_l / z$). We can then solve for c_o or p_a :

$$c_o = \frac{P_o + (R_{anthro} + R_{other})(1-\alpha)}{Az\left(k_o(T) + k_\beta \alpha\right)}; \quad \alpha = \frac{k_a}{k_a + k_\alpha(T)} \qquad (5)$$

$$p_a = \frac{R_{anthro} + R_{other} + P_o(1-\beta)}{N_T\left(k_a + k_\alpha \beta\right)} \, x \, 10^{12}; \quad \beta = \frac{k_o(T)}{k_o(T) + k_\beta} \qquad (6)$$

where $P_o = PA$, for convenient comparison of the total marine production term with R_{anthro} and R_{other}. These equations can be used to explore the effects of global-scale variations in P_o and T on c_o and p_a. A complete model built on these equations requires a multi-box approach, to account for the wide variations of temperature and productivity in different waters. However, the intent of this study is to point the way for future work in as simple and illustrative a manner as possible. Thus, in the calculations below, we have modeled only the interaction of the atmosphere with the open ocean (therefore, A = 0.8 x 3.61 x 10^{14} m^2). Since these waters appear to dominate the CH_3Br system (Lobert *et al.*, 1995), this is a reasonable first-order approach.

The utility of these equations is somewhat hampered by uncertainties in the estimates of R_{anthro} and R_{other} (*e.g.*, Albritton and Watson, 1992; Manö and Andreae, 1994). Since R_{anthro} and R_{other} are assumed to be independent of temperature, and are by definition independent of P_o, these sources "dilute" the atmospheric impact of variations in F_{net}; the resulting variation of p_a will correlate inversely with the magnitude of these sources relative to F_{net}. Thus, rigorous modeling of the global response of p_a to perturbations in the anthropogenic source is not possible until the relative magnitudes of these sources are determined. Below, we illustrate the effects of temperature and productivity changes in a semi-quantitative fashion, using reasonable literature values for R_{anthro} and R_{other}. Our intent is to point out some general implications of temperature and productivity effects which should be contemplated as better source estimates become available in coming years. For the purpose of this exercise, we adopt R_{anthro} = 0.40 Gmol yr^{-1}, well

within the latest range of published estimates (*e.g.*, Butler, 1995). By subtraction from a total source of 1.05 Gmol yr^{-1} (Lobert *et al.*, 1995), R_{other} = 0.65 Gmol yr^{-1}.

Although there are undoubtedly feedbacks between variations in temperature and variations in CH_3Br production, for simplicity we will begin by considering the effects of these variables separately. The complications are addressed further below.

5.2. Temperature Effects

Fig. 7 illustrates the effects of temperature over a 10°C range, centered at an average open ocean mixed-layer temperature of 21.9°C (Lobert *et al.*, 1995). This model also incorporates a mixed layer of 75 meters depth, and T_{th} = 15°C. P_o is assumed invariant with temperature, and is equal to the value in Table 1. As temperature increases, the rate constant for CH_3Br loss rises, so that D_o rises from ≈ 1.1 to 1.3 Gmol yr^{-1} (Fig. 7a), and c_o falls from 2.0 x10^{-9} to 6.3 x 10^{-10} mol m^{-3} (Fig. 7b). The drop in c_o is reflected in F_{out}, the gross flux of CH_3Br out of the ocean (Fig. 7a). F_{in}, the gross rate of CH_3Br invasion, also falls with increasing temperature, due to decreasing solubility. However, this effect is not large enough to compensate for the drop in F_{out}, causing F_{net} to decrease and change direction, from 0.03 to - 0.17 Gmol yr^{-1} over the 10°C range. The impact on p_a is substantial; a decrease of ≈ 20% is predicted, from 11 to 8.9 ppt.

These findings have important implications for the response of atmospheric CH_3Br to changes in the size of the anthropogenic source. Since p_a is sensitive to temperature, climatological temperature variations may have more effect on atmospheric CH_3Br than small changes in the source

strength. As shown in Fig. 8 (Region *a*), in the case of a 5°C temperature rise, p_a does not climb above the present level even if anthropogenic emissions increase by 25% relative to the assumed present value of 0.40 Gmol yr^{-1}. Since surface ocean warming of 1 to 5°C has been predicted to result from CO_2-induced global warming in coming decades (*e.g.,* Bretherton *et al.*, 1990), it is plausible to suggest that such warming will reduce the level of CH_3Br in the atmosphere even if anthropogenic emissions are not changed, or increase slightly. Ironically, the consequences of anthropogenic emissions of CH_3Br may be lessened by anthropogenic CO_2. Conversely, atmospheric CH_3Br can actually increase, in spite of substantial reductions in the anthropogenic source, if mean temperatures decrease (Region *b*).

Additionally, Figure 8 illustrates that even the complete elimination of anthropogenic CH_3Br does not reduce atmospheric levels to zero; 7 ppt is the lower limit in our model, neglecting temperature effects. This is in part due to the existence of large non-anthropogenic sources in our model; this remains an active area of research. However, the "buffering" of p_a by changes in F_{net} also plays a role, as first suggested by Butler (1994). Even if all non-marine sources were eliminated, ≈ 2 ppt of atmospheric CH_3Br would be supported by evasion from the oceans.

These results also suggest that there may be substantial, natural variations in the atmospheric burden of CH_3Br. For example, the 2 - 5°C global cooling experienced during glacial periods (Folland *et al.*, 1990) would have exerted an upward pressure on CH_3Br levels. The absence of anthropogenic sources would have led to lower pre-industrial values of p_a, but would also have increased the relative importance of marine chemistry for the atmosphere, since the marine source would have been a larger fraction of

total CH_3Br input. We calculate that under such conditions, upper open ocean temperatures 5°C lower than the modern mean would have resulted in a 20% increase of p_a (7.0 vs. 8.3 ppt), assuming constant P_o and non-anthropogenic, non-marine sources of 0.65 Gmol yr^{-1}.

5.3. Productivity Effects

An analogous set of calculations can be made for constant temperature but variable P_o (Fig. 9). Here, T is held constant at 21.9°C while P_o is varied ± 50% of the present value. Even over a fraction this range, the effects are significant. For example, a 20% rise in P_o from the present global average would cause an increase in F_{net} of more than a third (Fig 9a). At P / P_{avg} = 1.5, F_{net} changes sign, and the open ocean becomes a small net CH_3Br source. Over the full range of P_o values considered, p_a varies by nearly 25% (Fig. 9b).

Unfortunately, the applicability of these results is uncertain. Although marine productivity varies markedly in most regions on seasonal and longer timescales, the variability of mean open ocean productivity is unclear. Therefore, we are reluctant to speculate on the implications of variable P_o to the same degree as with variable T. We do note, however, that glacial periods are often thought to be times of *heightened* overall marine productivity, possibly by as much as a factor of two (*e.g.,* Gingele and Dahmke, 1994; Herguera and Berger, 1991). This would tend to push CH_3Br levels up during glaciation. If R_{anthro} = 0, a 50% increase in P_o would increase p_a by ≈ 15 %, from 6.8 to 7.8 ppt. Thus, during glacial periods, productivity changes and temperature changes could have acted in concert to raise tropospheric CH_3Br from inter-glacial, pre-industrial values.

While more sophisticated models and a better accounting of CH_3Br sources and sinks are needed to quantify these effects, it is clear that the geochemistry of CH_3Br is complex, and that this compound is not directly comparable to other halocarbons, which have only anthropogenic sources and no significant marine chemistry. This complexity must be considered during the formulation of CH_3Br regulatory guidelines.

5.4. Model Validation?

Ideally, this simple open ocean model would be tested by comparison of model results with measurements of atmospheric CH_3Br made during periods of multi-year variation in SSTs and/or marine productivity. Although global productivity changes are poorly constrained, sufficiently large global SST variations have occurred in the past: an average increase of ≈ 1°C is associated with climatic warming since the late 19^{th} century, and glacial surface waters are estimated to have been 2 to 5 °C cooler than at present (*e.g.,* Folland *et al.*, 1990). Unfortunately, CH_3Br data exist only for the past decade. During this time, the only significant SST changes have been those associated with seasonal cycles and El Niño events. Seasonal cycles are too short to expect a large global perturbation to p_a; with $\tau_{CH_3Br} \approx 1.8$ yr, and a total mass of ≈ 2.1 Gmol, average atmospheric CH_3Br is quite insensitive to 10 to 30% fluctuations of a small marine sink (or source) on a 1/2 yr timescale. A similar argument can be made for the insensitivity of p_a to plausible seasonal-scale variations in global or hemispheric P_o.

El Niño events are unlikely to cause global perturbations for similar reasons. However, since the elevated SSTs and depressed productivities associated with El Niño conditions typically persist for ≈ 1.5 yr (Cane, 1983;

Folland *et al.*, 1990; Philander, 1990), these events might cause an observable *regional* perturbation of CH_3Br in the tropical Pacific, where El Niño SST effects are localized. Qualitatively, SST warming and productivity retardation during El Niño years should work in concert to depress p_a. Quantitative modeling of the effect on p_a is beyond the scope of this paper.

Biomass burning, which is also highly variable geographically and with time, is expected to have similar regional effects on tropospheric CH_3Br. Comprehensive CH_3Br measurements in the tropical Pacific during future El Niño events, and at locations close to biomass burning sources, could reveal much about CH_3Br geochemistry.

5.5. Other Biological Complications?

Simulations of global CH_3Br response to temperature change are dependent on assumptions about the response of biology to such change. Above, we have assumed that the rate of CH_3Br production is not strongly coupled to temperature. This is unlikely to be the case. However, the direction of any feedback between CH_3Br production and temperature is unclear.

During El Niño, for example, warmer SSTs are a signature of reduced nutrient flux into the euphotic zone. This reduction is due to a combination of upwelling of water with lower nutrient content as a result of a deeper nutricline and to reduced upwelling intensity. The corollary is a depression in biological productivity of surface waters. (Barber and Chavez, 1983; Halpern and Feldman, 1994). If CH_3Br production scales with primary productivity, then El Niño's could result in *decreased* CH_3Br production and escape to the

atmosphere. In this case, the effects of temperature and primary production should work in concert to depress the CH_3Br flux.

On the other hand, a positive correlation has been observed between temperature and primary production when nutrient supply is not limiting (Eppley, 1972; Keller, 1989; Malone, 1982). Eppley (1972) quantified this effect ($P(T_1)/P(T_2) = 10^{0.0275(T_2-T_1)}$), which would lead to *enhanced* rates of CH_3Br production under warmer conditions. However, when incorporated into our model, this effect is strong enough to counteract the influence of temperature on inorganic loss processes. The result is little net change in p_a over a 10°C range (Fig. 10). Thus, it is difficult to determine whether, on balance, feedbacks between temperature and biological activity dampen or amplify the effects of temperature on the flux of CH_3Br from the modern oceans, let alone from the oceans of the past or future.

6. Summary and Conclusions

Our examination of the marine geochemistry of CH_3Br indicates that the rates of loss and production in the water column control the concentration of CH_3Br in seawater, and the direction and magnitude of the CH_3Br flux between the atmosphere and ocean. Large variations in the rate of chemical loss result from modest temperature variations. Linear scaling of CH_3Br production rates to chlorophyll content brings models and observations into agreement, which strongly suggests a high rate of biological production of CH_3Br in seawater. A simple mass-balance model which accounts for temperature and biological production can successfully reproduce the latitudinal variations of marine CH_3Br observed in the Eastern Pacific Ocean in two separate studies. When temperature and primary productivity effects

are carefully considered, global extrapolations of the open ocean flux from both these data sets can be brought into good agreement. These results demonstrate that the data of Singh *et al.* (1983), Singh and Kanakidou (1993) and Lobert *et al.* (1995) are not in conflict, and support Lobert *et al.'s* (1995) conclusion that the open ocean constitutes a small net sink for CH_3Br, rather than a large net source. This finding presents a new challenge, since anthropogenic emissions and biomass burning are believed to total only $\approx$ 60 - 80 Gmol yr^{-1}, out of the 90 - 120 Gmol yr^{-1} total source estimated by Lobert *et al.* (1995). Either the magnitudes of these sources have been underestimated, or a large CH_3Br source remains unidentified. This deficit may be filled by large emissions from the Southern Ocean, a result of the combination of low temperature and high productivity in these waters.

Since temperature and marine productivity are sensitive to climate, both the direction and magnitude of the oceanic flux should be sensitive to global climate change. Since the total amount of CH_3Br produced and destroyed annually in the ocean is comparable to the flux to the atmosphere from non-marine sources, even small perturbations of the marine cycle can produce significant atmospheric effects. Changes in tropospheric CH_3Br due to changes in the ocean term are somewhat buffered by the longer residence time of CH_3Br in the atmosphere. Thus, seasonal variations should be minor, and perturbations due to El Niño conditions would be, at best, apparent only at the local or regional level. However, temperature and productivity variations large enough to impact the atmospheric budget have occurred in the past, and are predicted to occur in the future due to anthropogenic global warming. These effects should be taken into account during the formulation of CH_3Br regulatory policies.

A large area of uncertainty in modeling the natural geochemical cycle of CH_3Br is the variability of the marine production rate. We suggest that one means of quantifying this term is to compare the CH_3Br abundances predicted by models such as ours with *in situ* or satellite-based chlorophyll data. Our simple modeling of CH_3Br in the eastern Pacific is a first step in this direction. Further progress requires more measurements of CH_3Br, temperature and primary productivity in the oceans, with wide geographic and seasonal coverage. Satellite estimates of chlorophyll concentration from the upcoming SeaWiFS experiment (SeaWiFS Working Group, 1987) will be particularly useful. These observations will be incorporated into 3-D extensions of our model, which will include the effects of horizontal transport in the ocean and atmosphere, as well as seasonal and climatic effects on atmospheric chemistry, to improve our understanding of the role of CH_3Br in stratospheric O_3 loss.

7. Acknowledgments

The authors are grateful to J. Butler and J. Lobert for providing CH_3Br and temperature data in electronic format, and for many helpful comments. Thanks to G. Feldman and S. Pazen for providing CZCS data and Pacific oceanographic data, respectively, in electronic format. D. Halpern's suggestions in the early stages of this project are appreciated, as are those of A. Meinrat and an anonymous reviewer.

8. References

Albritton, D. L., and R. T. Watson, Methyl bromide and the ozone layer: A summary of current understanding, in *Methyl Bromide: Its Atmospheric Science, Technology and Economics, Montreal Protocol Assessment Supplement*, edited by R. T. Watson, D. L. Albritton, S. O. Anderson and S. Lee-Bapty, pp. 3-18, United Nations Environment Programme, Nairobi, Kenya, 1992.

Anderson, J. G., W. H. Brune, S. A. Lloyd, D. W. Toohey, S. P. Sander, W. L. Starr, M. Loewenstein, and J. R. Podolske, Kinetics of O_3 destruction by ClO and BrO within the Antarctic vortex-An analysis based on *insitu* ER-2 data, *J. Geophys. Res.*, *94*, 11480-11520, 1989.

Atlas, E., W. Pollock, J. Greenberg, and L. Heidt, Alkyl nitrates, nonmethane hydrocarbons, and halocarbon gases over the equatorial Pacific ocean during Saga 3, *J. Geophys. Res.*, *98*, 16933-16947, 1993.

Balch, W., R. Evans, J. Brown, G. Feldman, C. McClain, and W. Esias, The remote sensing of ocean primary productivity: Use of a new data set compilation to test satellite algorithms, *J. Geophys. Res.*, *97*, 2279-2293, 1992.

Barber, R. T., and F. P. Chavez, Biological consequences of El Niño, *Science*, *222*, 1203-1210, 1983.

Bathgate, R. H., and E. A. Moelwyn-Hughes, The kinetics of certain ionic exchange reactions of the four methyl halides in aqueous solution, *J. Chem. Soc.*, 2642-2648, 1959.

Bretherton, F. P., K. Bryan, and J. D. Woods, Time-dependent greenhouse-gas-induced climate change, in *Climate Change: The IPCC Scientific Assessment*, edited by J. T. Houghton, G. J. Jenkins and J. J. Ephraums, pp. 173-194, Cambridge University Press, Cambridge, 1990.

Butler, J. H., The potential role of the ocean in regulating atmospheric CH3Br, *Geophys. Res. Lett.*, *21*, 185-188, 1994.

Butler, J. H., Methyl bromide under scrutiny, *Nature*, *376*, 469-470, 1995.

Butler, J. H., J. W. Elkins, T. M. Thompson, and B. D. Hall, Oceanic consumption of CH_3CCl_3: Implications for tropospheric OH, *J. Geophys. Res.*, *96*, 22347-22355, 1991.

Cane, M. A., Oceanographic events during El Niño, *Science*, *222*, 1189-1210, 1983.

Chavez, F. P., A comparison of satellite and ship chlorophyll from California and Peru, *J. Geophys. Res.*, *In Press*, 1995.

Cicerone, R. J., L. E. Heidt, and W. H. Pollock, Measurements of atmospheric methyl bromide and bromoform, *J. Geophys. Res.*, *93*, 3745-3749, 1988.

Comiso, J. C., C. R. McClain, C. W. Sullivan, J. P. Ryan, and C. L. Leonard, Coastal Zone Color Scanner pigment concentrations in the Southern Ocean and relationships to geophysical surface features, *J. Geophys. Res.*, *98*, 2419-2451, 1993.

Elliott, S., and F. S. Rowland, Nucleophilic substitution rates and solubilities for methyl halides in seawater, *Geophys. Res. Lett.*, *20*, 1043-1046, 1993.

Eppley, R. W., Temperature and phytoplankton growth in the sea, *Fish. Bull.*, *70*, 1063-1085, 1972.

Falkowski, P. G., Y. Kim, Z. Kolber, C. Wilson, C. Wirick, and R. Cess, Natural versus anthropogenic factors affecting low-level cloud albedo over the North Atlantic, *Science*, *256*, 1311-1313, 1992.

Feldman, G. C., Ocean color: Availability of the global data set, *EOS Trans. AGU*, *70*, 634-636, 1989.

Folland, C. K., T. Karl, and K. Y. Vinnikov, Observed climate variations and change, in *Climate Change: The IPCC Scientific Assessment*, edited by J. T. Houghton, G. J. Jenkins and J. J. Ephraums, pp. 195-239, Cambridge University Press, Cambridge, 1990.

Gingele, F., and A. Dahmke, Discrete barite particles and barium as tracers of paleoproductivity in South Atlantic sediments, *Paleoceanography*, *9*, 151-168, 1994.

Gschwend, P. M., J. K. MacFarlane, and K. A. Newman, Volatile halogenated organics released to seawater from temperate marine macroalgae, *Science*, *227*, 1033-1035, 1985.

Halpern, D., and G. C. Feldman, Annual and interannual variations of phytoplankton pigment concentration and upwelling along the Pacific equator, *J. Geophys. Res.*, *99*, 7347-7354, 1994.

Herguera, J. C., and W. H. Berger, Paleoproductivity from benthic foraminifera abundance: Glacial to postglacial change in the west-equatorial Pacific, *Geology*, *19*, 1173-1176, 1991.

Itoh, N., and M. Shinya, Seasonal evolution of bromomethanes from coralline algae (Corallinaceae) and its effect on atmospheric ozone, *Mar. Chem.*, *45*, 95-103, 1994.

Keller, A. A., Modeling the effects of temperature, light, and nutrients on primary productivity: An empirical and a mechanistic approach compared, *Limnol. Oceanogr.*, *34*, 82-95, 1989.

Keller, M. D., Dimethylsulfide production and marine phytoplankton: The importance of species composition and cell size, *Biol. Oceanogr.*, *6*, 375-382, 1991.

Khalil, M. A. K., R. A. Rasmussen, and R. Gundawardena, Atmospheric methyl bromide: Trends and global mass balance, *J. Geophys. Res.*, *98*, 2887-2896, 1993.

Lal, S., R. Borchers, P. Fabian, P. K. Patra, and B. H. Subbaraya, Vertical distribution of methyl bromide over Hyderabad, India, *Tellus*, *46B*, 373-377, 1994.

Leaitch, W. R., L. A. Barrie, J. W. Bottenheim, S. M. Li, P. B. Shepson, K. Muthuramu, and Y. Yokouchi, Airborne observations related to ozone depletion at polar sunrise, *J. Geophys. Res.*, *99*, 25499-25517, 1994.

Li, S. M., Y. Yokouchi, L. A. Barrie, K. Muthuramu, P. B. Shepson, J. W. Bottenheim, W. T. Sturges, and S. Landsberger, Organic and inorganic bromine compounds and their composition in the arctic troposphere during polar sunrise, *J. Geophys. Res.*, *99*, 25415-25428, 1994.

Liss, P. S., and P. G. Slater, Flux of gases across the air-sea interface, *Nature*, *247*, 181-184, 1974.

Lobert, J. M., J. H. Butler, S. A. Montzka, L. S. Geller, R. C. Myers, and J. W. Elkins, A net sink for atmospheric CH_3Br in the East Pacific Ocean, *Science*, *267*, 1002-1005, 1995.

Lorenzen, C. J., A method for the continuous measurement of in vivo chlorophyll concentration, *Deep-Sea Res.*, *13*, 223-227, 1966.

Mabey, W., and T. Mill, Critical review of hydrolysis of organic compounds in water under environmental conditions, *J. Phys. Chem. Ref. Data*, *7*, 383-415, 1978.

Malone, T. C., Phytoplankton photosynthesis and carbon-specific growth: Light-saturated rates in a nutrient-rich environment, *Limnol. Oceanogr.*, *27*, 226-235, 1982.

Manley, S. L., and M. N. Dastoor, Methyl halide (CH_3X) production from the giant kelp, *Macrocystis,* and estimates of global CH_3X production by kelp, *Limnol. Oceanogr.*, *32*, 709-715, 1986.

Manö, S., and M. O. Andreae, Emission of methyl bromide from biomass burning, *Science*, *263*, 1255-1257, 1994.

McElroy, M. B., R. J. Salawitch, S. C. Wofsy, and J. A. Logan, Reductions of Antarctic ozone due to synergistic interactions of chlorine and bromine, *Nature*, *321*, 759-762, 1986.

Mellouki, A., R. K. Talukdar, A.-M. Schmoltner, T. Gierczak, M. J. Mills, S. Solomon, and A. R. Ravishankara, Atmospheric lifetimes and ozone depletion potentials of methyl bromide (CH_3Br) and dibromomethane (CH_3Br_2), *Geophys. Res. Lett.*, *19*, 2059-2062, 1992.

Michaels, A. F., A. H. Knap, R. L. Dow, K. Gunderson, R. J. Johnson, J. Sorensen, A. Close, G. A. Knauer, S. E. Lohrenz, V. A. Asper, M. Tuel, and R. Bidigare, Seasonal patterns of ocean biogeochemistry at the U.S. JGOFS Bermuda Atlantic Time-series Study site, *Deep-Sea Res. I*, *41*, 1013-1038, 1994.

Miller, B. R., and R. F. Weiss, Absolute calibration and measurement of tropospheric methyl bromide at La Jolla, California and Cape Grim, Tasmania, in *1995 Methyl Bromide State of the Science Workshop*, Monterey, CA, 1995.

Moelwyn-Hughes, E. A., The hydrolysis of the methyl halides, *Proc. Roy. Soc. London A*, *164*, 295-306, 1938.

Moelwyn-Hughes, E. A., The kinetics of hydrolysis, *Proc. Roy. Soc. London A, 220*, 386-396, 1953.

Montzka, S., J. H. Butler, J. Lobert, and J. Elkins, Difficulties associated with measuring methyl bromide in the atmosphere and results from global and regional studies, in *1995 Methyl Bromide State of the Science Workshop*, Monterey, CA, 1995.

Moore, R. M., M. Scarratt, and Z. Hu, Methyl chloride and bromide production by marine phytoplankton, *EOS, 76*, S161, 1995.

Moore, R. M., and R. Tokarczyk, Volatile biogenic halocarbons in the northwest Atlantic, *Global Biogeochem. Cycles, 7*, 195-210, 1993.

Morel, A., and J.-F. Berthon, Surface pigments, algal biomass profiles, and potential production of the euphotic layer: Relationships reinvestigated in view of remote-sensing applications, *Limnol. Oceanogr., 34*, 1545-1562, 1989.

Pazen, S., Oceanographic data from December, 1993 cruise of the *Polar Sea* (Oceanatlas digital format), 1993.

Penkett, S. A., B. M. R. Jones, M. J. Rycroft, and D. A. Simmons, An interhemispheric comparison of the concentrations of bromine compounds in the atmosphere, *Nature, 318*, 550-553, 1985.

Philander, S. G., *El Niño, La Niña, and the Southern Oscillation*, Academic Press, Inc., San Diego, 1-293, 1990.

Reeves, C. E., and S. A. Penkett, An estimate of the anthropogenic contribution to atmospheric methyl bromide, *Geophys. Res. Lett., 20*, 1563-566, 1993.

Salawitch, R. J., S. C. Wofsy, and M. B. McElroy, Chemistry of OClO in the Antarctic stratosphere: Implications for bromine, *Planet. Space Sci.*, *36*, 213-224, 1988.

Scarratt, M. G., and R. M. Moore, Production of methyl halides by axenic cultures of the marine diatom Phaeodactylum tricornutum, *EOS*, *76*, S169, 1995.

Schauffler, S. M., L. E. Heidt, W. H. Pollock, T. M. Gilpin, J. F. Vedder, S. Solomon, R. A. Lueb, and E. L. Atlas, Measurements of halogenated organic-compounds near the tropical tropopause, *Geophys. Res. Lett.*, *20*, 2567-2570, 1993.

SeaWiFS Working Group, Report of the joint EOSAT:NASA SeaWiFS working group, NASA Earth Observ. Satell. Co., NASA Earth Sci. and Applic. Div., Washington, D. C., 1987.

Singh, H. B., and M. Kanakidou, An investigation of the atmospheric sources and sinks of methyl bromide, *Geophys. Res. Lett.*, *20*, 133-136, 1993.

Singh, H. B., L. B. Salas, and R. E. Stiles, Methyl halides in and over the eastern Pacific (40°N-32°S), *J. Geophys. Res.*, *88*, 3684-3690, 1983.

Solomon, S., M. Mills, L. E. Heidt, W. H. Pollock, and A. F. Tuck, On the evaluation of ozone depletion potentials, *J. Geophys. Res.*, *97*, 825-842, 1992.

Sverdrup, H. U., M. W. Johnson, and R. H. Fleming, *The Oceans*, Prentice Hall, Englewood Cliffs, New Jersey, 1942.

Tokarczyk, R., and R. M. Moore, Production of volatile organohalogens by phytoplankton cultures, *Geophys. Res. Lett.*, *21*, 285-288, 1994.

Wennberg, P. O., R. C. Cohen, R. M. Stimpfle, J. P. Koplow, J. G. Anderson, R. J. Salawitch, D. W. Fahey, E. L. Woodbridge, E. R. Keim, R. S. Gao, C. R. Webster, R. D. May, D. W. Toohey, L. M. Avallone, M. H. Proffitt, M. Loewenstein, J. R. Podolske, K. R. Chan, and S. C. Wofsy, Removal of stratospheric O_3 by Radicals: Insitu measurements of OH, HO_2, NO, NO_2, ClO, and BrO, *Science*, *266*, 398-404, 1994.

Wofsy, S. C., M. B. McElroy, and Y. L. Yung, The chemistry of atmospheric bromine, *Geophys. Res. Lett.*, *2*, 215-218, 1975.

World Meteorological Organization, Scientific Assessment of ozone depletion: 1991, World Meteorological Organization Global Ozone Research and Monitoring Project, 25, 1992.

Yung, Y. L., J. P. Pinto, R. L. Watson, and S. P. Sander, Atmospheric bromine and ozone perturbations in the lower stratosphere, *J. Atmos. Sci.*, *37*, 339-353, 1980.

Zafiriou, O. C., Reaction of methyl halides with seawater and marine aerosols, *J. Mar. Res.*, *33*, 75-81, 1975.

Table 1. Estimates of F_{net}, D_o and P_o in the Open Ocean.

	T (°C)	F_{net} (Gmol yr^{-1})	D_o (Gmol yr^{-1})	P_o (Gmol yr^{-1})
	19.3	0.01	1.07	1.08
Cruise A[1]	**21.9**	**-0.14**	**1.22**	**1.08**
	24.5	-0.28	1.36	1.08
Cruise B[2]	**21.9**	**-0.17**	**1.28**	**1.11**

[1]Results of this study, based on the data of Singh *et al.* (1983) and Singh and Kanakidou (1993). F_{net} and D_o were derived from c_o, which was calculated from Eqn. 2, using the tabulated values of T and P_o. Mean open ocean P_o was derived by scaling to observed chlorophyll abundances, as described in the text.

[2]Results of Lobert *et al.* (1995). F_{net} was derived from the observed mean saturation anomaly, and D_o was calculated using observed mean $c_o$and T. P_o is the sum of F_{net} and D_o.

Table 2. Estimates of F_{net}, D_o and P_o in the Southern Ocean.

	T (°C)	CZCS *Chl* (mg m^{-3})	[CH_3Br] mol m^{-3}	F_{net} (Gmol yr^{-1})	D_o (Gmol yr^{-1})	P_o (Gmol yr^{-1})
January:	12	0.25	4.09×10^{-9}	0.14	0.14	0.27
July:	8	0.45	1.38×10^{-8}	0.74	0.27	1.01
Annual Avg:	10	0.35	8.93×10^{-9}	0.43	0.21	0.64

Based on seasonal *Chl* and T data from Comiso *et al.* (1993).

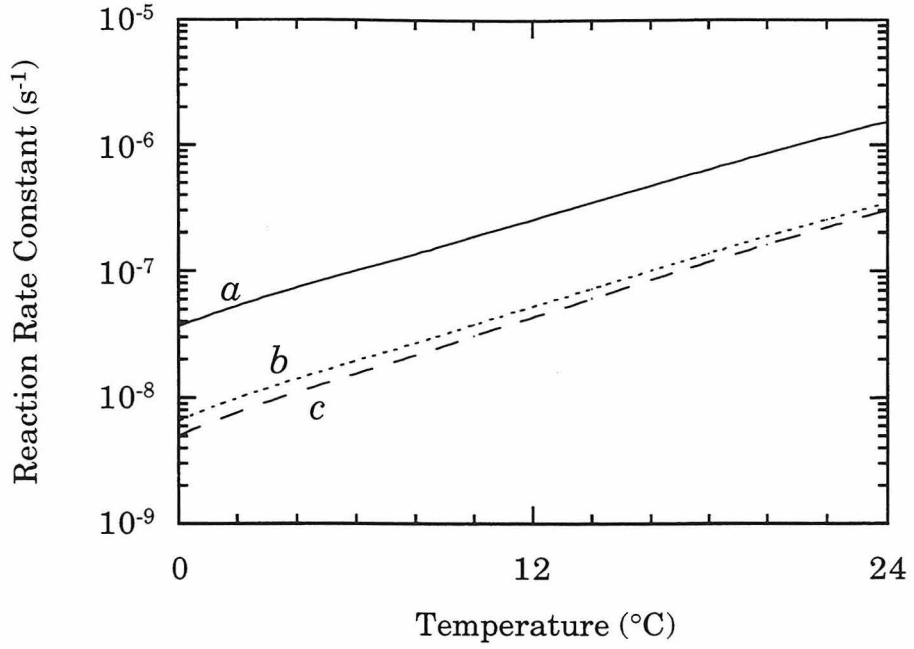

Fig. 1. The temperature sensitivity of the rate constants important for CH_3Br loss in seawater: (a) $CH_3Br + Cl^-$; (b) & (c) $CH_3Br + H_2O$; expressed as pseudo first-order constants for marine conditions ($[Cl^-]$ = 0.56 mol $liter^{-1}$). References: (a) Elliott and Rowland (1993); (b) Mabey and Mill (1978); (c) Moelwyn-Hughes (1938).

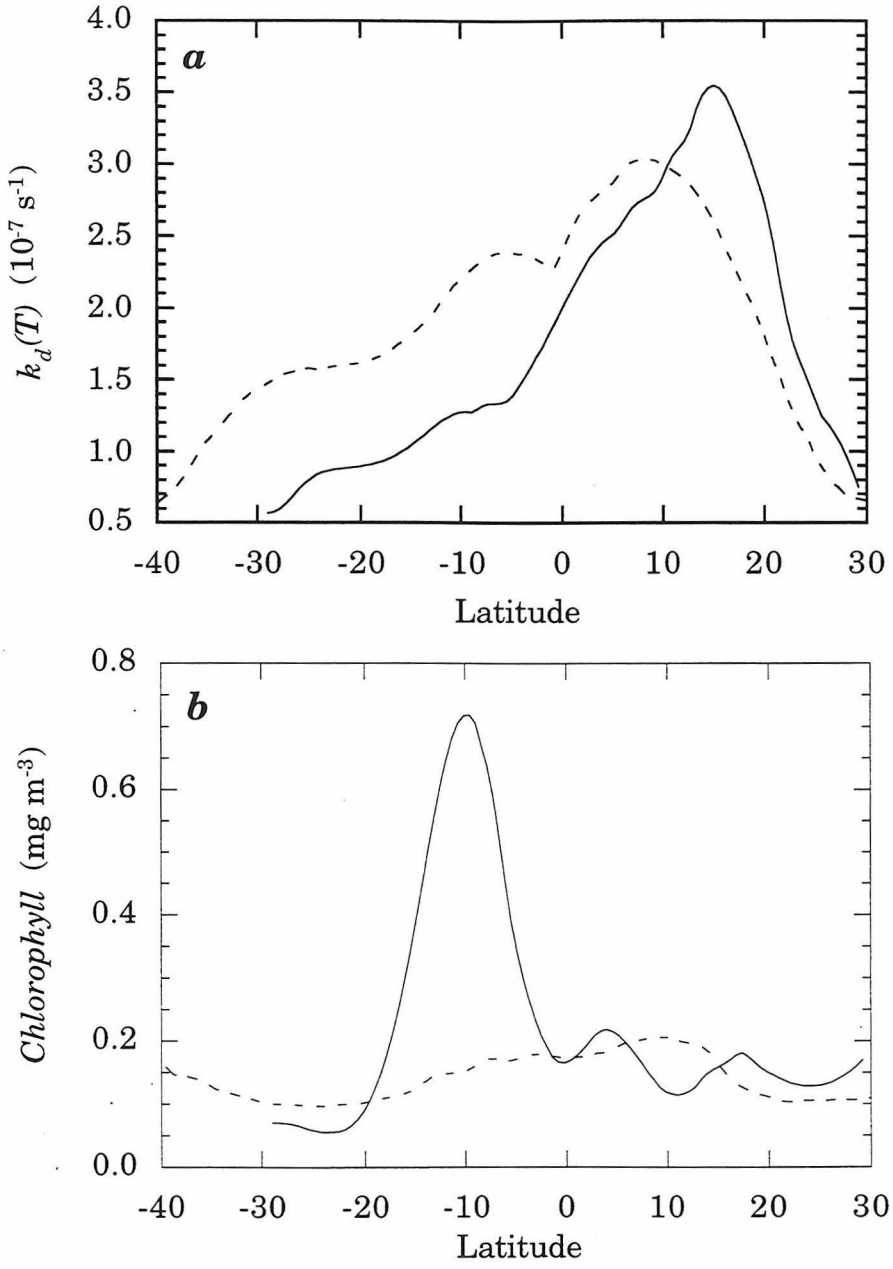

Fig. 2. Latitudinal variability of (a) the rate of CH_3Br destruction ($k_d(T) = k_{Cl}(T) + k_{H_2O}(T)$), and (b) the abundance of chlorophyll (mg m^{-3}), along the shiptracks of Singh *et al.* (1983) (Cruise *A*; solid lines) and Lobert *et al.* (1995) (Cruise *B*; dashed lines). $k_d(T)$ was calculated using the rate constants in Fig. 1, and temperature from SST measurements during the cruises. Chlorophyll data for Cruise *A* are drawn from CZCS observations, as described in the text (Feldman, 1989) . Cruise *B* chlorophyll data are based on shipboard fluorescence measurements made during the cruise (Chavez, 1995).

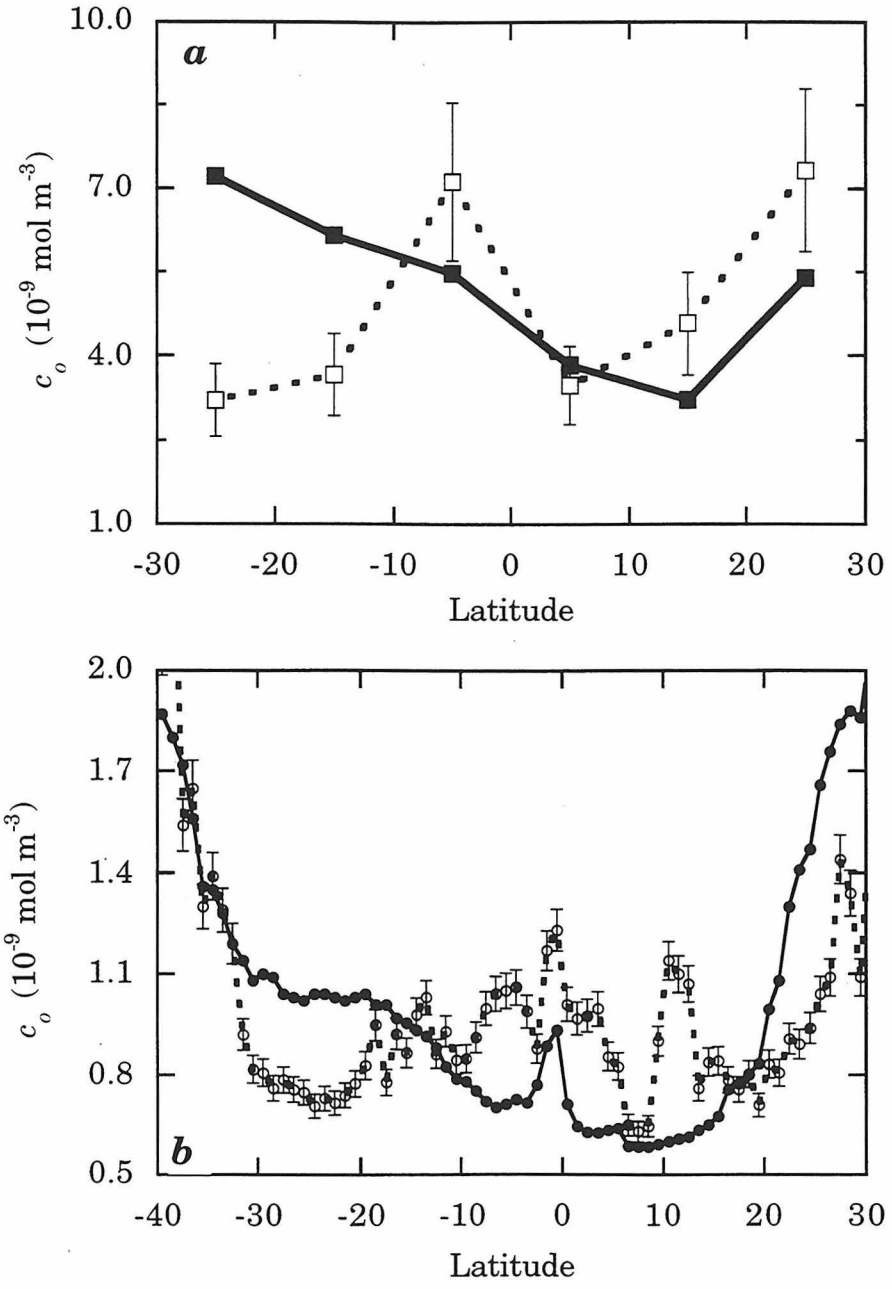

Fig. 3. Comparisons of model predictions (filled symbols) with observed CH_3Br concentrations (unfilled symbols). (a) Cruise *A*; (b) Cruise *B*. Data have been averaged as described in the text. Observational uncertainties are ± 2σ, as reported in Singh *et al.* (1983) and Lobert *et al.* (1995). This model includes only the effect of temperature on the kinetics of CH_3Br loss in seawater.

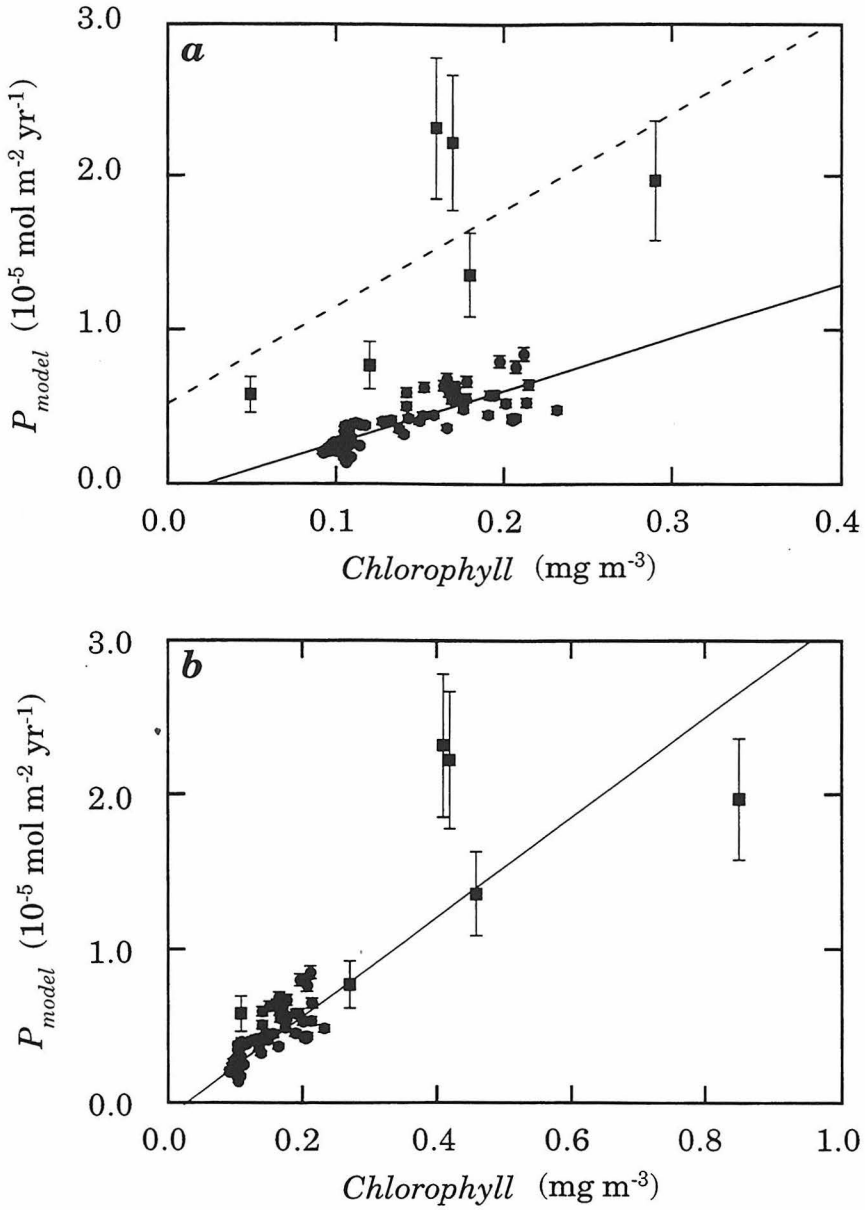

Fig. 4. (a) Comparison of the CH_3Br production rate needed to provide the observed levels of CH_3Br (P_{model}) with chlorophyll observations. P_{model} is calculated from c_o and T data from Cruiser A (squares) and Cruise B (circles). Chlorophyll data are from satellite (Cruise A) and ship-based (Cruise B) measurements. P_{model} uncertainties are based on the uncertainties for the c_o data used to calculate P_{model}. The best-fit line for each data set is indicated. r = 0.66 (Cruise A) and r = 0.82 (Cruise B). (b) Identical to (a), but satellite data are corrected to match ship-based chlorophyll measurements, as described in the text. The combined data set is fit by the line $y = mx + b$, $m = 3.2 \times 10^{-5}$, $b = -2.8 \times 10^{-7}$. r = 0.86.

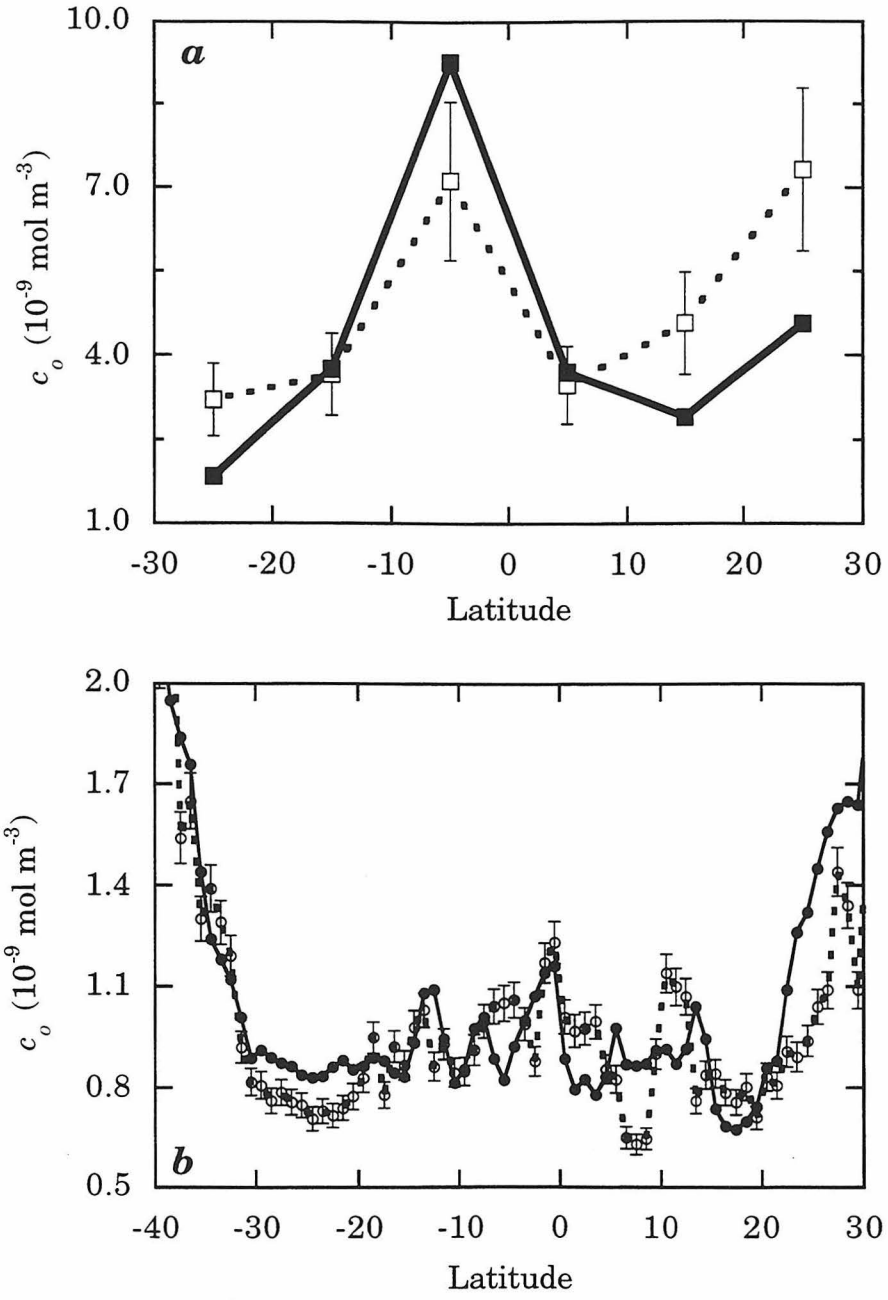

Fig. 5. Identical to Fig. 3, including the effect of temperature on CH_3Br loss rates, and latitudinal variation in CH_3Br production rates. Production rates are adjusted to follow chlorophyll observations, as described in the text.

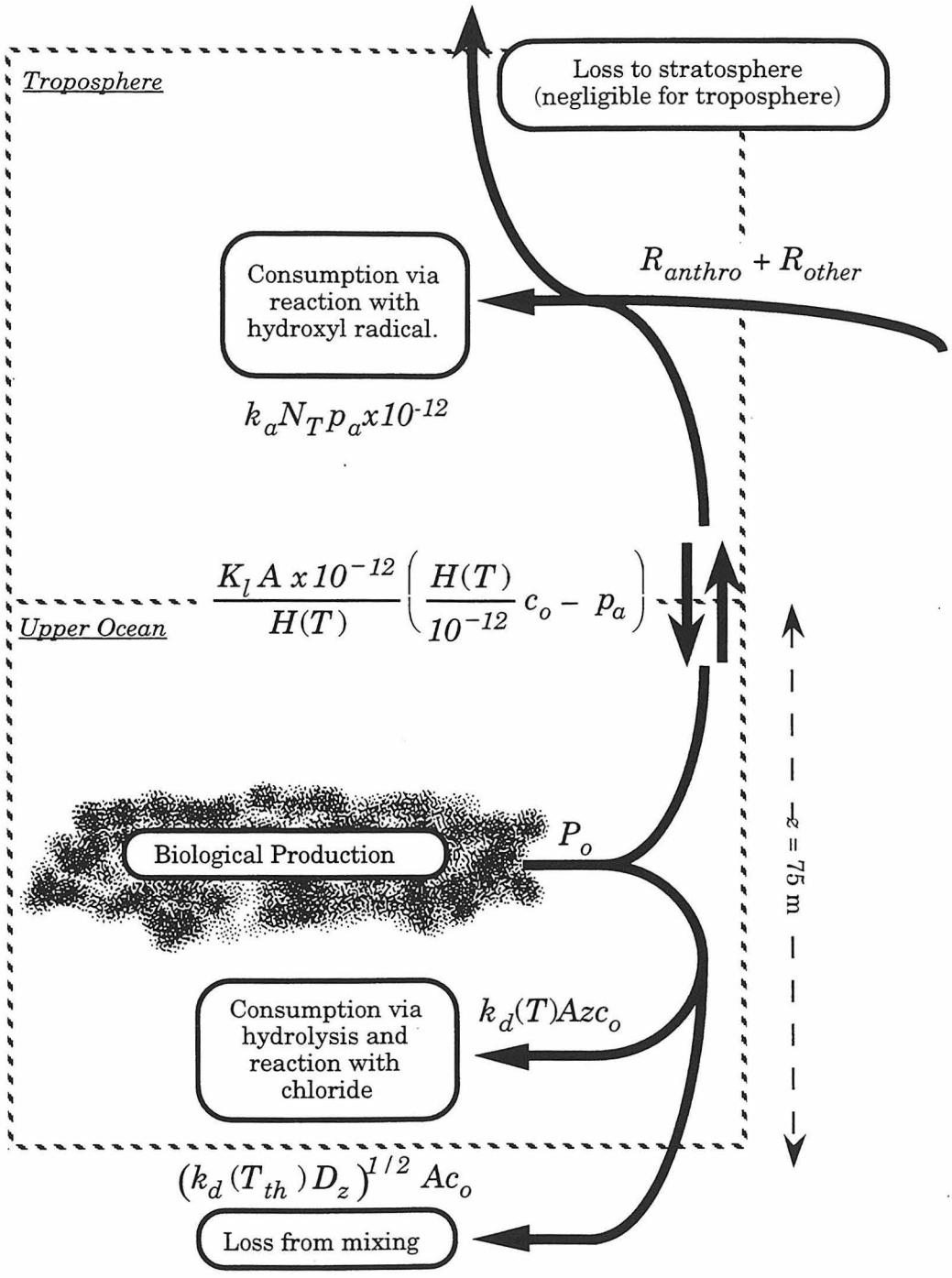

Fig. 6. Schematic presentation of the coupled ocean/atmosphere model. Variables are defined in the text. Inputs and outputs are expressed in units of mol yr^{-1}.

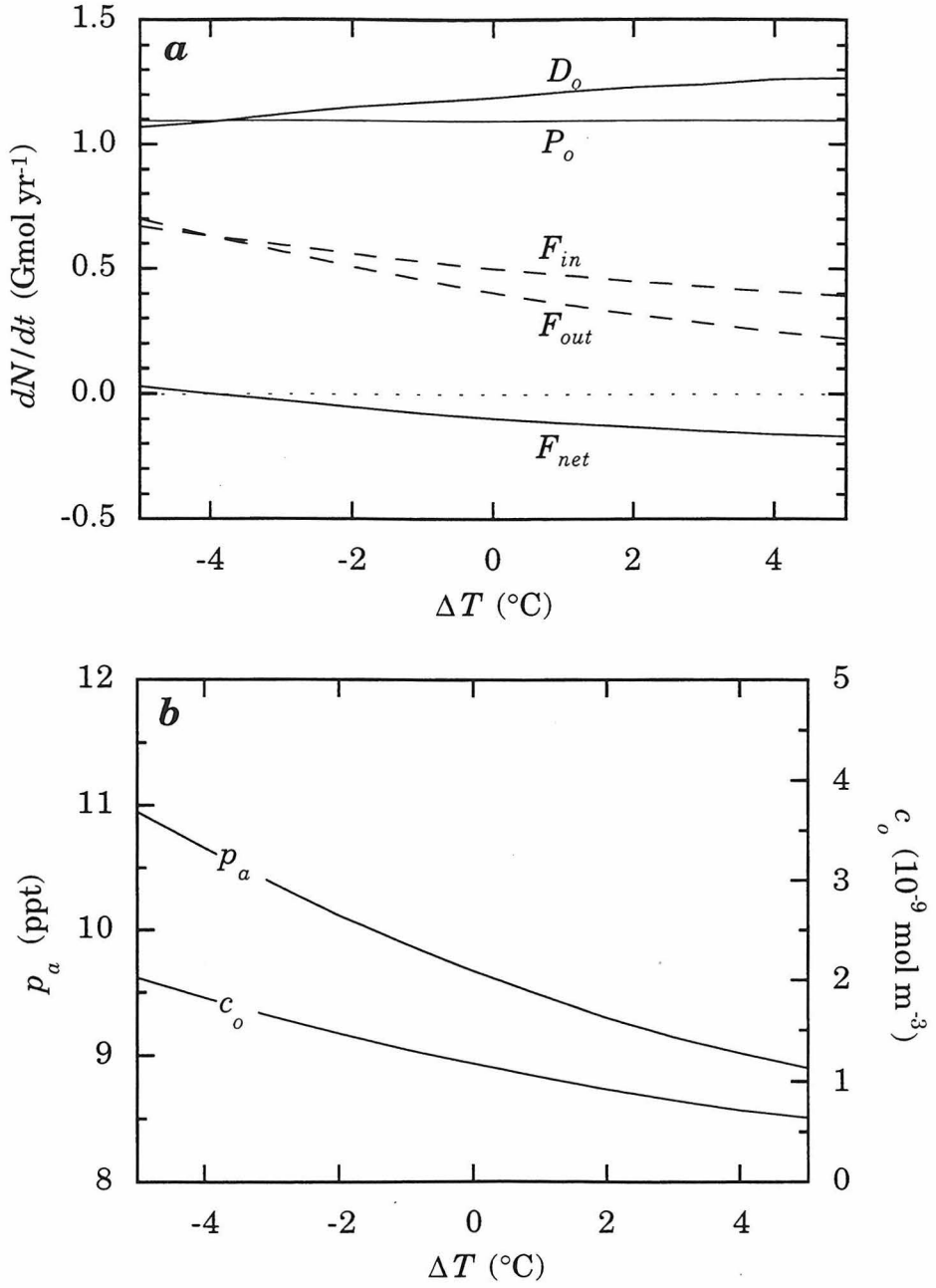

Fig. 7. The effect of temperature on the CH_3Br cycle in the present atmosphere and open ocean (R_{anthro} = 0.40 Gmol yr^{-1}, R_{other} = 0.65 Gmol yr^{-1}, P_o = 1.08 Gmol yr^{-1}, z = 75 m). $\Delta T = T$ - 21.9°C. (a) The rate of CH_3Br consumption in seawater (D_o), the gross fluxes in and out of the ocean (F_{in} and F_{out}) and the net oceanic flux (F_{net}); (b) the resulting variation of CH_3Br concentrations in seawater (c_o) and in the atmosphere (p_a).

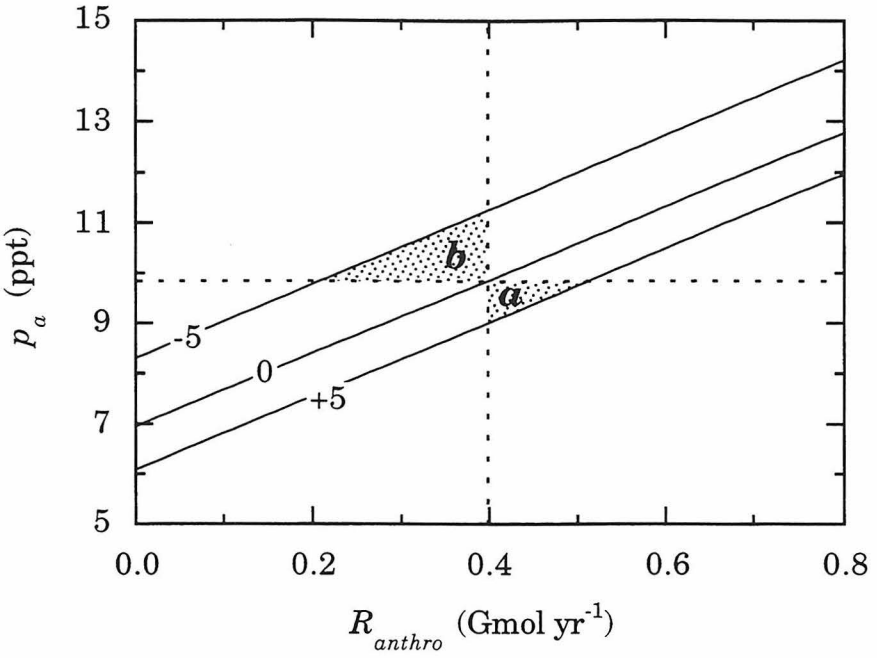

Fig. 8. The effect of the anthropogenic source strength (R_{anthro}) on atmospheric CH_3Br (p_a), using the same model as in Fig. 7. Results for ΔT = -5, 0, and +5 °C are presented. Dotted lines indicate present p_a (9.8 ppt) and R_{anthro} (0.4 Gmol yr^{-1}). The total non-marine source is assumed to be 0.65 Gmol yr^{-1}. The shaded regions are fields in which temperature effects rather than the source strength govern p_a. Region *a*: increasing temperature results in lower p_a despite small increases in R_{anthro}; Region *b*: decreasing temperature results in higher p_a despite small reductions in R_{anthro}. Note that for ΔT = 0 and R_{anthro} = 0, the pre-industrial condition, p_a = 7.0 ppt. At R_{anthro} = 0.8 Gmol yr^{-1}, a doubling of the current source, p_a =14.2 ppt.

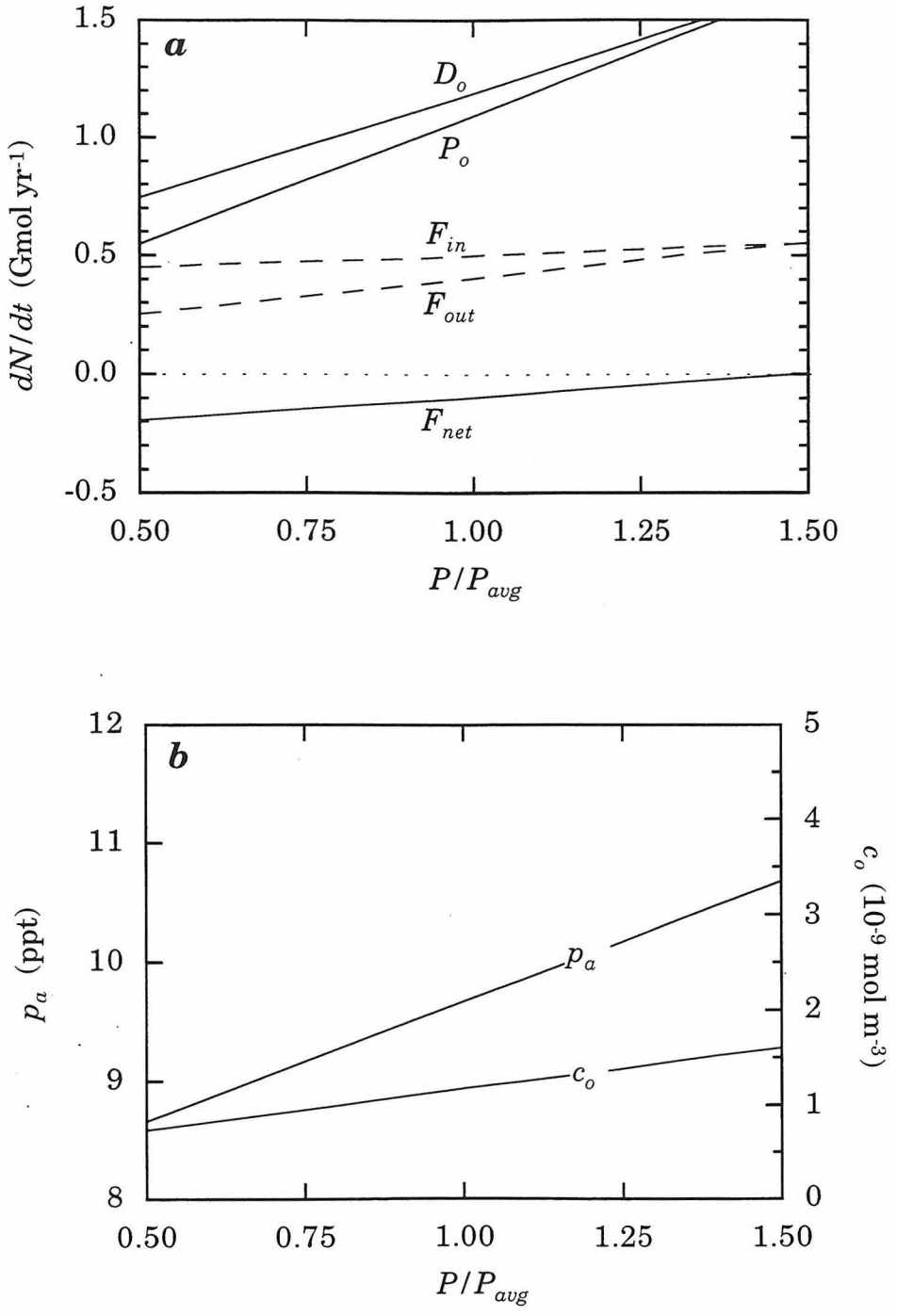

Fig. 9. The effect of changes in the rate of CH_3Br production on the CH_3Br cycle in the present atmosphere and ocean (R_{anthro} = 0.40 Gmol yr^{-1}, R_{other} = 0.65 Gmol yr^{-1}, P_o = 1.08 Gmol yr^{-1} z = 75 m, T_{avg} = 21.9°C). (a) and (b) are as described in Fig. 7.

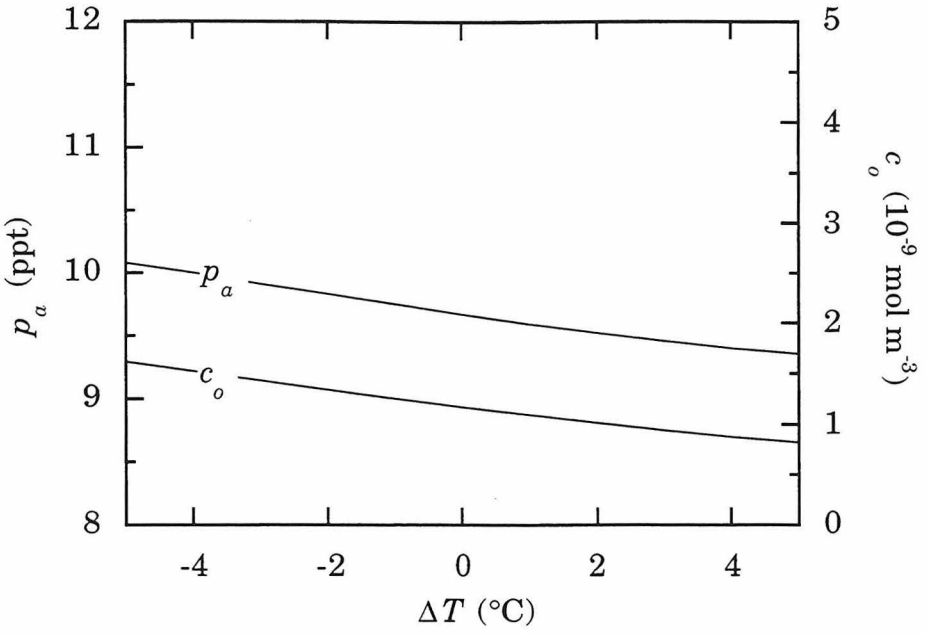

Fig. 10. The same as Fig. 7b, but including the effect of temperature-dependence on biological productivity, $P(T_1)/P(T_2) = 10^{0.0275(T_2-T_1)}$ (Eppley, 1972).

Part III.

Heterogeneous Chemistry and CO_2 Stability in the Atmosphere of Mars

Chapter 1.

Photodissociation in the Atmosphere of Mars: Impact of High Resolution, Temperature-Dependent CO_2 Cross Section Measurements

This chapter was previously published as Anbar, Allen, and Nair, 1993.

1.1. Abstract

We have investigated the impact of high resolution, temperature-dependent CO_2 cross section measurements (Lewis and Carver, 1983) on calculations of photodissociation rate coefficients in the Martian atmosphere. Since the cross section measurements exhibit large variations on a 10 - 20 Å scale, the calculations are sensitive to the wavelength resolution. We find that the adoption of 50 Å intervals for the purpose of computational efficiency results in errors in the calculated values for photodissociation of CO_2, H_2O, and O_2 which are generally ≤ 10%, but as large as 20% in some instances. These are acceptably small errors, especially considering the uncertainties introduced by the large temperature dependence of the CO_2 cross section. The inclusion of temperature-dependent CO_2 cross sections is shown to lead to a decrease in the diurnally-averaged rate of CO_2 photodissociation as large as 33% at some altitudes, and increases of as much as 950% and 80% in the photodissociation rate coefficients of H_2O and O_2, respectively. The actual magnitude of the changes depends on the assumptions used to model the CO_2 absorption spectrum at temperatures lower than the available measurements, and at wavelengths longward of 1970 Å. Given our current understanding, these results minimize or even reverse the sense of the CO_2 chemical stability problem.

1.2. Introduction

The ultraviolet (UV) absorption spectrum of carbon dioxide has a critical influence on the chemical stability of the atmosphere of Mars, which is predominantly CO_2. The UV transmissivity of the atmosphere, controlled primarily by CO_2 absorption, affects the photolysis rates of CO_2, H_2O, and other species. Since CO is produced by CO_2 photolysis, while H_2O photolysis provides the HO_x species considered necessary for rapid recombination of CO and O (McElroy and Donahue, 1972; Parkinson and Hunten, 1972), the CO_2 absorption spectrum governs the partitioning between CO and CO_2.

Most models of the Martian atmosphere have incorporated room temperature CO_2 cross sections, such as those measured by Shemansky (1972), Ogawa (1971) or Nakata *et al.* (1965). This is true of the classic pre-Viking studies dealing with the CO/CO_2 ratio, the "CO_2 stability problem" (McElroy and Donahue, 1972; Parkinson and Hunten, 1972), as well as the definitive post-Viking model of Kong and McElroy (1977). Even some of the most recent Mars models (*e.g.,* Yung *et al.,* 1988) and speculation on the CO_2 stability problem (Atreya and Blamont, 1990) have assumed that the CO_2 absorption spectrum is invariant with temperature.

However, the UV absorbtivity of CO_2 is actually temperature dependent, as first shown by DeMore and Patapoff (1972). Their data indicate a factor of 2 decrease near 1800 Å as temperature decreases from ≈ 300 to 200 K. Consequently, Shimazaki and Shimizu (1979), Shimazaki (1981; 1989) and Chassefière (1991) reduced the published room temperature cross sections of CO_2 by a factor of two in their photochemical models. Using a wavelength-dependent parameterization of the DeMore and Patapoff (1972) results, Parisot and Zucconi (1984) estimated that the inclusion of

temperature dependence increases the modeled H_2O photodissociation coefficient at the surface of Mars by a factor of 10. This finding is consistent with the conclusion of Shimazaki (1989) that the calculated CO/CO_2 ratio could be increased to match observed values only if the abundance of H_2O was one-tenth of the globally averaged value deduced from Viking data (Jakosky and Farmer, 1977).

The results of DeMore and Patapoff (1972), which were utilized in these studies, consist of measurements of the temperature-dependence of CO_2 absorption separated by 10 - 20 Å, covering temperatures from 223 - 323 K, and confined to a limited wavelength range (≈ 1740 - 1860 Å). Lewis and Carver (1983) provide a more complete data set, measuring the CO_2 cross section continuously between 1200 and 1970 Å at ≈ 200, 300 and 370 K with 0.5 Å resolution. These data show a weak temperature dependence at short wavelengths, but a significant increase with temperature longward of 1750 Å, in agreement with the DeMore and Patapoff (1972) results. In addition, the sensitivity to temperature is seen to continue to increase at wavelengths longward of the 1860 Å cutoff in DeMore and Patapoff (1972). Significantly, the high resolution of this data set reveals structure in the cross section variation with wavelength of ≈ 10 - 20 Å scale across the entire measured wavelength range. This structure in the spectrum becomes more pronounced at low temperatures, exhibiting changes in cross section values of up to a factor of four with small changes in wavelength.

Although the DeMore and Patapoff (1972) data are grossly consistent with the results of the Lewis and Carver (1983) study, the inclusion of the additional wavelength and temperature data in photochemical calculations is potentially important, particularly since the photolysis reactions of both CO_2

and H_2O near the Martian surface are sensitive to atmospheric transmissivity between 1860 and 1970 Å, a region not covered by the earlier measurements. The high spectral resolution of the newer data also allows more accurate modeling of the wavelength variation of the temperature dependence than that used by Parisot and Zucconi (1984).

The presence of structure in the temperature-dependent CO_2 absorption spectrum raises several additional questions. For the sake of computational efficiency, atmospheric models typically use cross section data averaged over 50 Å intervals in calculating photodissociation rate coefficients. In an atmosphere in which CO_2 absorption controls the penetration of solar radiation, does this allow the correct computation of atmospheric opacity? Does the structure in the CO_2 absorption spectrum correlate with structure in the solar flux and/or in the spectra of other species in such a way that the photochemical rate constants calculated for these species are sensitive to the scale of averaging?

Only one published model of the Martian atmosphere (Lindner, 1985; Lindner, 1988) has incorporated the Lewis and Carver (1983) CO_2 cross section data set, but without addressing these issues. In the present study, we utilize the Lewis and Carver (1983) data to consider the impact of the detailed structure measured in the CO_2 absorption spectrum, and its temperature dependence, on the calculation of various photodissociation rate constants. The potential implications for the stability of CO_2 are discussed.

1.3. Structure in the CO_2 Absorption Spectrum

To gauge the influence of the small-scale structure in the CO_2 spectrum on the calculated photolysis values, several photodissociation

coefficients computed with high resolution cross section data and a relatively high resolution solar flux spectrum were compared with the coefficients calculated from the same data averaged over 50 Å intervals. Differences between these two cases occur only if the structure in the spectrum, which is not resolved in the low averaged data, is quantitatively important in the calculations.

The computation of photodissociation coefficients for species x at altitude z, $J_x(z)$, involves a summation over wavelength λ:

$$J_x(z) = \sum_{\lambda} \sigma_x(\lambda) Q_x(\lambda) Tr(z,\lambda) F(\lambda) d\lambda \qquad (1.1)$$

where σ is the photoabsorption cross section, Q is the wavelength-dependent quantum yield for dissociation, Tr is the atmospheric opacity, and F is the solar flux impinging on the top of the atmosphere. The atmospheric opacity is determined by the column abundances of all species y, N_y, along the line of sight to the sun from altitude z, and by the total photoabsorption cross sections of these species:

$$Tr(z,\lambda) = \exp\left(-\sum_{y} \sigma_x(\lambda) N_y(z) \right) \qquad (1.2)$$

In both the high resolution and averaged cases, CO_2 was assumed to be the only species contributing to the atmospheric opacity. These test calculations were made between 1200 and 1970 Å, the wavelength range of the CO_2 measurements reported by Lewis and Carver (1983).

To most clearly determine if problems arise from the use of wavelength-averaged data, we consider a case in which the wavelength-dependent variation in the CO_2 cross sections is most extreme. Thus, an

isothermal atmosphere of ≈ 200 K has been assumed. B. R. Lewis kindly provided the Lewis and Carver (1983) measurements at 0.5 Å spacing in electronic format. The data fall into three groups, with mean temperatures of 202, 298, and 368 K. Cross sections obtained at temperatures slightly different (1 - 2 K) from these mean temperatures were adjusted for this difference by assuming that the cross sections vary linearly with temperature. Transmissivity values were calculated at this wavelength resolution for several different values of the CO_2 column density along the optical path (N_{CO2} between 1 x 10^{18} and 1 x 10^{24} cm^{-2}, these being selected values for the optical paths between the zenith angles 0° and 90° at the surface and at higher altitudes), and were then multiplied by equally high resolution absorption cross sections for CO_2, H_2O (Lee and Suto, 1986; Kley, 1984; Watanabe and Zelikoff, 1953; Thompson *et al.,* 1963) or O_2 (Ogawa and Ogawa, 1975; Lewis *et al.,* 1988b; Carver *et al.,* 1977; Kley, 1984; Wang *et al.,* 1987; Black *et al.,* 1985; Gibson *et al.,* 1983; Ackerman, 1971; Allen and Frederick, 1982; Yoshino *et al.,* 1991). The resulting values were averaged in 10 Å intervals, then multiplied by values of the solar flux available at 10 Å resolution (Mount and Rottman, 1983), and finally summed over wavelength to obtain J_{CO2}, J_{H2O}, or J_{O2}. A dissociation quantum yield of unity was adopted for all these calculations, consistent with available laboratory measurements (Okabe, 1978). In the averaged case, the transmissivity and photolysis calculations utilized species cross sections and solar fluxes averaged over the 50 Å intervals.

The calculations of J_{CO2}, J_{H2O}, and J_{O2} represent three very different situations. In the case of J_{CO2}, structure in the transmissivity of the atmosphere reflects (and is anticorrelated with) the CO_2 absorption cross

section (Eqn. 1.2). Thus, the sensitivity of the computed value of J_{CO2} (the product of atmospheric transmissivity and the CO_2 cross section; Eqn. 1.1) to structure in the transmissivity of the atmosphere is minimal. On the other hand, the highly structured O_2 spectrum has no *a priori* correlation with the structure in transmissivity; there is no compensation between atmospheric transmissivity and absorption by O_2. Finally, the J_{H2O} calculation represents a case in which the cross sections in Eqn. 1.1 are rapidly, and monotonically, decreasing at the longer wavelengths where the structure in the low-temperature CO_2 spectrum is largest.

In general, the results from the photodissociation rate coefficient calculations employing 50 Å-averaged input data agree to better than 10% with the results from the high spectral resolution (0.5 - 10 Å resolution) calculations. Exceptions are J_{O2} at $N_{CO2} \approx 2.5 \times 10^{22}$ cm^{-2}, in which case the value calculated from the averaged data is ≈ 20% smaller than the value derived at high resolution. For $N_{CO2} > 3 \times 10^{23}$ cm^{-2}, the computed coefficients for CO_2, H_2O and O_2 using the averaged input data were all systematically smaller than the high resolution values by ≥ 10%. However, it is important to note that the photodissociation between 1200 and 1970 Å (the region covered in these test calculations) often is much smaller than the total dissociation, to which all wavelengths contribute. In the cases of CO_2 and O_2, enough dissociation occurs longward of 1970 Å to minimize errors introduced by the spectral resolution adopted for the calculations, assuming that the CO_2 spectrum varies smoothly longward of 1970 Å at low temperatures; unfortunately, there are no laboratory data to test this assumption. In particular, near $N_{CO2} \approx 2.5 \times 10^{22}$ cm^{-2}, the differences in total J_{O2} between the two methods we have used is no larger than 15%, when the contribution

of absorption at longer wavelengths is included. For $N_{CO2} > 3 \times 10^{23}$ cm^{-2}, total J_{CO2} and J_{O2} agree in the two schemes to better than 10%. However, since the long wavelength limit for H_2O absorption is < 1970 Å, the large differences in J_{H2O} noted above remain. Fortunately, these values of J_{H2O} are $\leq 2 \times 10^{-10}$ s^{-1}, so that photodissociation becomes unimportant in these cases, neither influencing the vertical distribution of H_2O, nor being a significant source of HO_x species. Therefore, we conclude that using input data averaged over 50 Å intervals does not introduce significant errors in the calculation of photodissociation coefficients. Clearly, additional laboratory measurements of the CO_2 cross section longward of 1970 Å are highly desirable.

1.4. Temperature Dependence of CO_2 Cross Sections

We have parameterized the temperature dependence of CO_2 photoabsorption as follows: The Lewis and Carver (1983) CO_2 cross section measurements for 202, 298 and 368 K were averaged in 50 Å intervals, covering the wavelength range 1225 to 1975 Å (at some temperatures, the laboratory measurements exist only shortward of 1970 Å, so an extrapolation to 1975 Å was performed). In addition, there is an interval for 1200 - 1225 Å, and a 1 Å interval centered on 1215.67 Å to treat the solar hydrogen Lyman alpha emission separately from other UV emissions. These average cross section values are presented in Table 1.1.

The fractional change in the average absorption cross section per degree Kelvin change in temperature (denoted as P) was calculated for each interval by pairing the 202 and 298 K values, and the 298 and 368 K values:

$$P(\lambda) = \frac{\left(\sigma_T(\sigma) / \sigma_{298}(\sigma)\right) - 1}{T - 298} \qquad (1.3)$$

where T is either 202 K (P_L) or 368 K (P_H). The results for $P_L(\lambda)$ and $P_H(\lambda)$ are also shown in Table 1.1. These simple linear fits to the temperature sensitivity were found to best reproduce the available measurements; smooth functions fit to all three temperature data points in each interval systematically missed the 298 K value to an unacceptable degree. Even so, these smooth functions did not deviate significantly from a linear interpolation between the measurements.

To compare the temperature sensitivity of the CO_2 absorption spectrum, as revealed by the high resolution Lewis and Carver (1983) measurements, with previous treatments based on the DeMore and Patapoff (1972) data, we calculated the CO_2 cross sections for 202 K at 0.5 Å spacing from the Lewis and Carver (1983) 298 K data (Table 1.1) according to the equation (W. B. DeMore, private communication, as quoted in Allen *et al.*, 1981; Yung and DeMore, 1982):

$$\sigma(\lambda,T)/\sigma(\lambda,T_0) = (1 - S(\lambda)/100)^{(To-T)} \qquad (1.4)$$

where:

$$S(\lambda) = 0.5 + 5 \times 10^{-3} (\lambda-1740) \qquad \lambda \geq 1640 \text{ Å}$$

$$= 0 \qquad \lambda < 1640 \text{ Å}$$

and T = 202 K and T_0 = 298 K. Temperature sensitivity factors for this model spectrum (P_{DMP}) were calculated from Eqn. 1.3 and are listed in Table 1.1. Shortward of 1775 Å, P_{DMP} is systematically smaller than the P_L which we have computed. The largest difference occurs in the 1625 - 1675 Å interval, where P_{DMP} is a factor of ≈ 5 smaller than P_L. Longward of 1775 Å, P_{DMP} is systematically larger than P_L, by as much as ≈ 23% in the interval 1925 to 1975 Å.

These values of P_L and P_{DMP} both result in ≈ 50% reduction from the room temperature absorbtivity when the CO_2 cross section is calculated at 220 K (a characteristic temperature for the lower atmosphere of Mars) between 1825 and 1875 Å (a wavelength region which controls the photolysis of CO_2 and H_2O at low altitudes). Calculation of 220 K cross sections at longer wavelengths using the P_L values also results in absorbtivity reductions of ≈ 50%. However, the use of the P_{DMP} temperature sensitivities at these same wavelengths leads to an underestimation of the CO_2 cross section by as much as 25% relative to values calculated using P_L. This difference is of greatest importance near the ground, where long wavelength photons are most important. Thus, models of lower atmospheric photochemistry which assume a uniform 50% reduction at all wavelengths (*e.g.,* Shimazaki, 1989) are more accurate than those that use Eqn. 1.4 to determine the temperature sensitivity at long wavelengths (*e.g.,* Parisot and Zucconi, 1984).

The use of the P_{DMP} values to extrapolate CO_2 cross sections to temperatures below 200 K is also a potential source of error. For example, the predicted cross sections at 160 K between 1825 and 1875 Å are a factor of 3 smaller than those predicted using P_L. In modeling the middle of the atmosphere (between ≈ 50 and 150 km) where such low temperatures are encountered (Fig. 1.1), this difference may be significant.

1.5. Photodissociation Rate Coefficients

Photodissociation rate coefficients for CO_2, H_2O and O_2 appropriate for use in photochemical models were calculated from the surface to an altitude of 240 km in a realistic approximation of the Martian atmosphere. The

sensitivities of the calculated coefficients to specific models of the temperature dependence of the CO_2 cross section are explored below.

The hydrostatic atmosphere we have adopted is described in Fig. 1.1. The temperature profile was taken from the COSPAR model atmosphere below 100 km (Seiff, 1982), and the exospheric temperature was set to 365 K (Kong and McElroy, 1977). The temperature profile of the upper atmosphere was found by smoothly interpolating between these two regions using a spline function. We have assumed that the CO_2 mixing ratio is near unity at all altitudes, but also include the contribution to the opacity from absorption by O_2, O_3, and H_2O. For this purpose, we have adopted mixing ratios of 1.3 x 10^{-3}, 3.8 x 10^{-8} and 3 x 10^{-4}, respectively, which are based on a variety of observations (Barker, 1972; Carleton and Traub, 1972; Espenak *et al.,* 1991; Jakosky and Farmer, 1982; Rizk *et al.,* 1991). The calculations account for Rayleigh scattering (Hansen and Travis, 1974; Weast, 1986) and reflection from a Lambert surface with an albedo of 0.04 (Lindner, 1985 and references therein) using the method described in Michelangeli (1992).

We accounted for photodissociation due to solar radiation between the far ultraviolet and the long wavelength limit for O_2 absorption near $\approx$ 2500 Å. Solar flux values at 1 AU from Torr and Torr (1985), in addition to Mount and Rottman (1983), were scaled to 1.52 AU. In these calculations, we used the averaged values for $\sigma_{298}(\lambda)$ and the temperature sensitivities $P_L(\lambda)$ and $P_H(\lambda)$ from Table 1.1. Longward of 1975 Å, we used the CO_2 absorption cross sections reported by Shemansky (1972). We also assumed that the temperature sensitivities at longer wavelengths were the same as for the 1925 - 1975 Å interval. The cross sections for CO_2 shortward of 1200 Å came from Hitchcock and Brion (1980) and Nakata *et al.* (1965). For O_2, absorption

cross sections shortward of 1200 Å and longward of 1975 Å are from Samson *et al.* (1977; 1982), Hayaishi *et al.* (1986), Matsunaga and Watanabe (1967), Ogawa and Ogawa (1975), Lewis *et al.* (1988a), Black *et al.* (1985), Yoshino *et al.* (1988, 1991), Ditchburn and Young (1962), Johnston *et al.* (1984), and K. Yoshino (private communication). The H_2O cross sections shortward of 1200 Å were taken from Haddad and Samson (1986) and Lee and Suto (1986). The references for the O_3 cross sections are Tanaka *et al.* (1953), Ogawa and Cook (1957), W.M.O. Rep. 16 (1985) and DeMore *et al.* (1990); we accounted for the temperature dependence of these cross sections where given.

The photodissociation rate coefficients were computed with a diurnally-averaged radiation field for a spherical atmosphere at equinox for 30° latitude. The results for CO_2, H_2O, and O_2 are shown in figures 2, 3, and 4, respectively. Three cases were considered for each molecule. In case A, we assumed that the CO_2 cross sections were temperature-independent and employed only the 298 K values. In case B, CO_2 cross sections for temperatures lower than 202 K or higher than 368 K were equated to the values at 202 K and 368 K, respectively. In case C, we assumed that the values for $P_L(\lambda)$ and $P_H(\lambda)$ were valid for temperatures below 202 K and above 368 K, respectively. Cross sections were set equal to zero when extrapolations using $P_L(\lambda)$ resulted in negative values.

It is immediately apparent from Fig. 1.2 that, as in the Parisot and Zucconi (1984) study, J_{CO2} decreases at all altitudes when temperature-dependence is considered, with the largest change occurring several scale heights above the surface. Our results differ from the previous work in that, (1) the maximum decrease between cases A and B ($\approx$ 33%) is at $\approx$ 45 km, rather than at 30 km, and (2) the temperature-dependent calculation is

nearly equal to the temperature-independent value at the surface, rather than the earlier result of a significant increase. The first discrepancy arises from differences in the CO_2 cross sections used in the two studies, as well as minor differences in the temperature profiles and solar fluxes. Since the variation of J_{CO2} with altitude is a complex function of these factors, a discrepancy of this magnitude is not surprising.

The second discrepancy results from the over-estimation of the temperature sensitivity of the CO_2 cross section in the previous study. As noted above, extrapolations based on Eqn. 1.4 result in an under-estimation of the CO_2 absorption cross section in the longer-wavelength region, which becomes increasingly important at low altitudes. Thus, the work by Parisot and Zucconi (1984) may have overestimated the flux near the surface, resulting in an enhanced rate of CO_2 photodissociation. Our result is qualitatively similar to that of Lindner (1985), who also utilized the Lewis and Carver (1983) cross sections, but at polar temperatures and illumination conditions which are very different from those in our model.

The incorporation of the temperature dependence of the CO_2 cross sections in our calculations was found to have a larger impact on the calculation of J_{H2O} and J_{O2} than on J_{CO2}. While the anticorrelation between atmospheric transmissivity and CO_2 absorption discussed earlier limits the impact on J_{CO2}, the rates of H_2O and O_2 photodissociation are strongly enhanced by the increase of solar radiation in the middle and lower atmosphere which results from the incorporation of temperature-dependent CO_2 cross sections. The increases in J_{H2O} we observe when utilizing temperature-dependent CO_2 cross sections instead of the 298 K values (Fig. 1.3) are in qualitative agreement with the results of Parisot and Zucconi

(1984). We find a factor of 11 increase at the surface. This is somewhat smaller than the increase shown in Fig. 1.3 of Parisot and Zucconi (1984), an observation consistent with the larger temperature-sensitivity of CO_2 absorption incorporated in the earlier study (discussed above).

In the calculation of J_{O2}, an increase of as much as 79% occurs near 38 km when temperature-dependence is incorporated (Fig. 1.4). However, the effect on J_{O2} near the surface is minimal, due to the sizable contribution to the photodissociation of O_2 at low altitudes of wavelengths longward of the point at which CO_2 absorption makes a significant contribution to atmospheric opacity.

Since temperatures as low as 140 K are not unusual in the Martian atmosphere (*e.g.*, the altitude range 50 - 110 km; Fig. 1.1), the manner of estimating CO_2 cross sections below 202 K is an important issue in the calculation of J_{CO2}, J_{H2O} and J_{O2}. At these altitudes, the assumptions of case C lead to significantly lower values for the CO_2 cross-section than obtained in case B and, hence, a higher radiative flux. Thus, the case C values for J_{H2O} and J_{O2} in the middle atmosphere are larger than the case B results by as much as 93% and 57%, respectively (Figs. 1.3 and 1.4). The calculation of J_{CO2} is more complicated, because it is the product of the CO_2 cross section (Eqn. 1.1) and an exponential function describing atmospheric opacity in which the CO_2 cross section is again included explicitly (Eqn. 1.2). At these altitudes, where the atmosphere is optically thin, the pre-exponential term dominates. Thus, in contrast to the calculations of J_{H2O} and J_{O2}, the case C values for J_{CO2} are *lower* than the case B values, by as much as 39% at 65 km.

However, below ≈ 25 km, the temperatures are near 200 K (Fig. 1.1). Thus, the differences in J values arising from different low-temperature extrapolations of the CO_2 cross sections are small in this altitude region, and errors introduced by the adoption of different extrapolations in cases B and C are minimal. For example, the sensitivity of J_{CO2} to assumptions about the temperature dependence of the CO_2 absorption spectrum is limited between the surface and ≈ 25 km (Fig. 1.2). Similarly, below 10 km, the J_{H2O} values calculated for cases B and C are quite similar (Fig. 1.3). Significantly, since most of the water vapor in the Martian atmosphere is found below this altitude, the H_2O photolysis rate (and, hence, the HO_x production rate) is relatively insensitive to the details of the extrapolation to extreme temperatures.

Since the chemical stability of the predominantly CO_2 Martian atmosphere depends on the details of the photochemical processes occurring throughout the atmosphere, the differences we have noted between cases B and C will have a significant impact on calculated chemical rates. Thus, laboratory measurements of CO_2 photoabsorption cross sections at temperatures below 202 K are needed to improve the constraints on photochemical model computations.

1.6. Conclusions

The high resolution CO_2 spectra from 1200 to 1970 Å of Lewis and Carver (1983) show significant sensitivity to temperature and, at low temperatures, large variations in cross section values with small changes in wavelength. While the computed photodissociation rate coefficients for CO_2, H_2O, and O_2, species with significant absorption in this wavelength region,

are generally slightly sensitive to the wavelength intervals over which the cross section data are averaged for use in model calculations, the 50 Å intervals often used in models to increase the efficiency of photorate calculations seem adequate. However, the computed coefficients are quite sensitive to the adopted model for the temperature dependence of the CO_2 absorption cross sections, particularly when the temperature dependence is extrapolated to temperatures below those at which laboratory data are available. Relative to values from calculations utilizing only CO_2 cross sections at 298 K, the inclusion of temperature-dependent CO_2 cross sections results in decreases in diurnally-averaged values for J_{CO2} of as much as 33%, and respective increases of as much as 950% and 79% in J_{H2O} and J_{O2}, at temperatures characteristic of Mars.

These results are important in understanding the stability of CO_2 in the Martian atmosphere. The first models which considered this problem (McElroy and Donahue, 1972; Parkinson and Hunten, 1972) struggled to find a mechanism of CO oxidation rapid enough to balance the rate of CO_2 photolysis. The problem was resolved by invoking HO_x catalysis of CO oxidation. However, it has been suggested that to oxidize CO rapidly enough, these models require either eddy diffusion coefficients which may be unacceptably high, or H_2O abundances larger than those observed (Atreya and Blamont, 1990). Thus, Atreya and Blamont (1990) argued that HO_x chemistry alone is not adequate, and suggested that catalysis of CO oxidation on surfaces might be necessary to maintain CO_2 stability.

Our results, which are qualitatively similar to those of Parisot and Zucconi (1984), suggest that this problem may be lessened, or even reversed, when the temperature dependence of the CO_2 absorption spectrum is

considered. The decrease in J_{CO2} and, more importantly, the increase in J_{H2O} will tend to increase the abundance of HO_x species, while simultaneously decreasing the rate of CO_2 photolysis. Thus, qualitatively, the CO_2/CO ratio should shift toward CO_2, potentially reversing the sense of the CO_2 stability problem.

1.7. Acknowledgments

We thank B. R. Lewis for the electronic versions of his CO_2 measurements.

1.8. References

Ackerman, M., Ultraviolet solar radiation related to mesospheric processes, in *Mesospheric Models and Related Experiments*, edited by D. Reidel, pp. 149-159, Dordrecht-Holland, 1971.

Allen, M., and J. E. Frederick, Effective photodissociation cross sections for molecular oxygen and nitric oxide in the Schumann-Runge bands, *J. Atmos. Sci.*, *39*, 2066-2075, 1982.

Allen, M., Y. L. Yung, and J. W. Waters, Vertical transport and photochemistry in the terrestrial mesosphere and lower thermosphere, *J. Geophys. Res.*, *86*, 3617-3627, 1981.

Anbar, A. D., M. Allen, and H. A. Nair, Photodissociation in the atmosphere of Mars: Impact of high resolution, temperature-dependent CO_2 cross section measurements, *J. Geophys. Res., 98,* 1993.

Atreya, S. K., and J. E. Blamont, Stability of the Martian atmosphere: Possible role of heterogeneous chemistry, *Geophys. Res. Lett.*, *17*, 287-290, 1990.

Barker, E. S., Detection of molecular oxygen in the Martian atmosphere, *Nature*, *238*, 447-448, 1972.

Black, G., R. L. Sharpless, T. G. Slanger, and M. R. Taherian, The 1150-1300 Å absorption spectrum of O_2 at 930 K, *Chem. Phys. Lett.*, *113*, 311-313, 1985.

Carleton, N. P., and W. A. Traub, Detection of molecular oxygen on Mars, *Science*, *177*, 988-992, 1972.

Carver, J. H., H. P. Gies, T. I. Hobbs, B. R. Lewis, and D. G. McCoy, Temperature dependence of the molecular oxygen photoabsorption cross section near the H Lyman a line, *J. Geophys. Res.*, *82*, 1955-1960, 1977.

Chassefière, E., Photochemical regulation of CO on Mars, *Geophys. Res. Lett.*, *18*, 1055-1058, 1991.

DeMore, W. B., and M. Patapoff, Temperature and pressure dependence of CO_2 extinction coefficients, *J. Geophys. Res.*, *77*, 6291-6293, 1972.

DeMore, W. B., S. P. Sander, D. M. Golden, M. J. Molina, R. F. Hampson, M. J. Kurylo, C. J. Howard, and A. R. Ravishankara, *Chemical Kinetics and Photochemical Data for Use in Stratospheric Modeling*, JPL Publication 90-1, 1990.

Ditchburn, R. W., and P. A. Young, The absorption of molecular oxygen between 1850 and 2500 Å, *J. Atmos. Terr. Phys.*, *24*, 127-139, 1962.

Espenak, F., M. J. Mumma, T. Kostiuk, and D. Zipoy, Ground-based infrared measurements of the global distribution of ozone in the atmosphere of Mars, *Icarus*, *92*, 252-262, 1991.

Gibson, S. T., H. P. F. Gies, A. J. Blake, D. G. McCoy, and P. J. Rogers, Temperature dependence in the Schumann-Runge photoabsorption continuum of oxygen, *J. Quant. Spectrosc. Radiat. Transfer*, *30*, 385-393, 1983.

Haddad, G. N., and J. A. R. Samson, Total absorption and photoionization cross sections of water vapor between 100 and 1000 Å, *J. Chem. Phys.*, *84*, 6623-6626, 1986.

Hansen, J. E., and L. D. Travis, Light scattering in planetary atmospheres, *Space Sci. Rev.*, 16, 527-610, 1974.

Hayaishi, T., Y. Iida, Y. Morioka, M. Sasanuma, E. Ishiguro, and M. Nakamura, Photoionization mass spectrometry of O_2 in the VUV region, *At. Mol. Phys.*, *19*, 2861-2870, 1986.

Hitchcock, A. P., and C. E. Brion, Absolute oscillator strengths for valence-shell ionic photofragmentation of N_2O and CO_2 (8-75 eV), *Chem. Phys.*, *45*, 461-478, 1980.

Jakosky, B. M., and C. B. Farmer, The seasonal and global behavior of water vapor in the Mars atmosphere: Complete global results of the Viking atmospheric water detector experiment, *J. Geophys. Res.*, *87*, 2999-3019, 1982.

Johnston, H. S., M. Paige, and F. Yao, Oxygen absorption cross sections in the Herzberg continuum and between 206 and 327 K, *J. Geophys. Res.*, *89*, 11661-11665, 1984.

Kley, D., Ly(α) absorption cross-section of H_2O and O_2, *J. Atmos. Chem.*, *2*, 203-210, 1984.

Kong, T. Y., and M. B. McElroy, Photochemistry of the Martian atmosphere, *Icarus*, *32*, 168-189, 1977.

Lee, L. C., and M. Suto, Quantitative photoabsorption and fluorescence study of H_2O and D_2O at 50-190 nm, *Chem. Phys.*, *110*, 161-169, 1986.

Lewis, B. R., and J. H. Carver, Temperature dependence of the carbon dioxide photoabsorption cross section between 1200 and 1970 Å, *J. Quant. Spectrosc. Radiat. Transf.*, *30*, 297-309, 1983.

Lewis, B. R., S. T. Gibson, M. Emami, and J. H. Carver, Resonances in the photodissociation of isotopic molecular oxygen - I. The longest band, *J. Quant. Spectrosc. Radiat Transfer*, *40*, 1-13, 1988a.

Lewis, B. R., S. T. Gibson, M. Emami, and J. H. Carver, Resonances in the photodissociation of isotopic molecular oxygen - II. The second and third bands, *J. Quant. Spectrosc. Radiat. Transfer*, *40*, 469-477, 1988b.

Lindner, B. L., *The Aeronomy and Radiative Transfer of the Martian Atmosphere,* Ph.D. thesis, University of Colorado, 1985.

Lindner, B. L., Ozone on Mars: The effects of clouds and airborne dust, *Planet. Space Sci.*, *36*, 125-144, 1988.

Matsunaga, F. M., and K. Watanabe, Total and photoionization coefficients and dissociation continua of O_2 in the 580-1070 Å region, *Sci. Light*, *16*, 31-42, 1967.

McElroy, M. B., and T. M. Donahue, Stability of the Martian atmosphere, *Science*, *177*, 986-988, 1972.

Michelangeli, D. V., M. Allen, Y. L. Yung, R-L. Shia, D. Crisp, and J. Eluszkiewicz, Enhancement of atmospheric radiation by an aerosol layer, *J. Geophys. Res.*, 97, 865-874, 1992.

Mount, G. H., and G. J. Rottman, The solar absolute spectral irradiance 1150-3173 Å: 17 May 1982, *J. Geophys. Res.*, *88*, 5403-5410, 1983.

Nakata, R. S., K. Watanabe, and F. M. Matsunaga, Absorption and photoionization coefficient of CO_2 in the region 580-1670 Å, *Sci. Light*, *14*, 54-71, 1965.

Ogawa, M. and G. R. Cook, Absorption coefficients of O_3 in the vacuum ultraviolet region, *J. Chem. Phys.*, 28, 173-174, 1957.

Ogawa, S., and M. Ogawa, Absorption cross sections of O_2 ($a^1\Delta_g$) and O_2 ($X^3\Sigma_g^-$) in the region from 1087 to 1700 Å, *Can. J. Phys.*, *53*, 1845-1852, 1975.

Okabe, H., *Photochemistry of Small Molecules*, Wiley-Interscience, New York, 1978.

Parisot, J.-P., and J.-M. Zucconi, Temperature effect on the photodissociation rates in the atmospheres of Mars and Venus, *Icarus*, *60*, 327-331, 1984.

Parkinson, T. M., and D. M. Hunten, Spectroscopy and aeronomy of O_2 on Mars, *J. Atmos. Sci.*, *29*, 1380-1390, 1972.

Rizk, B., W. K. Wells, D. M. Hunten, C. R. Stoker, R. S. Freedman, T. Rouch, J. B. Pollack, and R. M. Haberle, Meridional Martian water abundance profiles during the 1988-1989 season, *Icarus*, *90*, 205-213, 1991.

Samson, J. A. R., J. C. Gardner, and G. N. Haddad, Total and partial photoionization cross-sections of O_2 from 100 to 800 Å, *J. Electron Spectrosc. Relat. Phenom.*, *12*, 281-292, 1977.

Samson, J. A. R., G. H. Rayborn, and P. N. Pareek, Dissociative photoionization cross sections of O_2 from threshold to 120 Å, *J. Chem. Phys.*, *76*, 393-397, 1982.

Seiff, A., Post-Viking models for the structure of the summer atmosphere of Mars, *Adv. Space Sci.*, *2*, 3-17, 1982.

Shemansky, D. E., CO_2 extinction coefficient 1700-1300 Å, *J. Chem. Phys.*, *56*, 1582-1587, 1972.

Shimazaki, T., A model of temporal variations in ozone density in the Martian atmosphere, *Planet. Space Sci.*, *29*, 21-33, 1981.

Shimazaki, T., Photochemical stability of CO_2 in the Martian atmosphere: Reevaluation of the eddy diffusion coefficient and the role of water vapor, *J. Geomag. Geoelectr.*, *41*, 273-301, 1989.

Shimazaki, T., and M. Shimizu, The seasonal variation of ozone density in the Martian atmosphere, *J. Geophys. Res.*, *84*, 1269-1276, 1979.

Tanaka, Y., E. C. Y. Inn, and K. Watanabe, Absorption coefficients of gases in the vacuum ultraviolet. Part IV. Ozone, *J. Chem. Phys.*, 21, 1651-1653, 1953.

Thompson, B. A., P. Harteck, and R. R. Reeves, Ultraviolet absorption coefficients of CO_2, CO, O_2, H_2O, N_2O, NH_3, NO, SO_2, and CH_4 between 1850 and 4000 Å, *J. Geophys. Res.*, *68*, 6431-6436, 1963.

Torr, M. R., and D. G. Torr, Ionization frequencies for solar cycle 21: Revised, *J. Geophys. Res.*, *90*, 6675-6678, 1985.

Wang, J., D. G. McCoy, A. J. Blake, and L. Torop, Effects of the close approach of potential curves in photoabsorption by diatomic molecules - II.

Temperature dependence of the O_2 cross section in the region 130-160 nm., *J. Quant. Spectrosc. Radiat. Transfer*, *38*, 19-27, 1987.

Watanabe, K., and M. Zelikoff, Absorption coefficients of water vapor in the vacuum ultraviolet, *J. Opt. Soc. Amer.*, *43*, 753-755, 1953.

World Meteorological Organization, Atmospheric Ozone, *World Meteorological Organization Report 16,* Global Research and Monitoring Project, Geneva, Switzerland, 1986.

Weast, R. C. (ed.), *Handbook of Chemistry and Physics, 67th ed.,* CRC Press, Boca Raton, p. E-374, 1986.

Yoshino, K., A. S.-C. Cheung, J. R. Esmond, W. H. Parkinson, D. E. Freeman, S. L. Guberman, A. Jenouvrier, B. Coquart, and M. F. Merienne, Improved absorption cross-sections of oxygen in the wavelength region 205-240 nm of the Herzberg continuum, *Planet. Space Sci.*, *36*, 1469-1475, 1988.

Yoshino, K., J. R. Esmond, A. S.-C. Cheung, D. E. Freeman, and W. H. Parkinson, High resolution absorption cross sections in the transmission window region of the Schumann-Runge bands and Herzberg continuum of O_2, *Planet. Space Sci.*, *in press*, 1991.

Yung, Y. L., and W. B. DeMore, Photochemistry of the stratosphere of Venus: Implications for atmospheric evolution, *Icarus*, *51*, 199-247, 1982.

Yung, Y. L., J. S. Wen, J. P. Pinto, M. Allen, K. K. Pierce, and S. Paulson, HDO in the Martian atmosphere: Implications for the abundance of crustal water, *Icarus*, *76*, 146-159, 1988.

Table 1.1. Temperature-Dependent CO_2 Cross Sections.

	Average Cross Section (cm^{-2})			T Sensitivity Factor (K^{-1})		
λ Interval (Å)	202 K	298 K	368 K	P_L	P_H	P_{DMP}
1200 - 1225	5.89E-20	6.40E-20	7.02E-20	8.22E-04	1.38E-03	0.00E+00
1215.2 - 1216.2	7.13E-20	7.45E-20	8.12E-20	4.42E-04	1.29E-03	0.00E+00
1225 - 1275	2.17E-19	2.28E-19	2.47E-19	5.03E-04	1.18E-03	0.00E+00
1275 - 1325	6.40E-19	6.73E-19	7.23E-19	5.08E-04	1.07E-03	0.00E+00
1325 - 1375	7.19E-19	7.34E-19	7.60E-19	2.19E-04	4.96E-04	0.00E+00
1375 - 1425	5.55E-19	5.54E-19	5.41E-19	-9.39E-06	-3.38E-04	0.00E+00
1425 - 1475	5.73E-19	5.77E-19	5.86E-19	7.40E-05	2.18E-04	0.00E+00
1475 - 1525	4.83E-19	5.06E-19	5.35E-19	4.85E-04	7.93E-04	0.00E+00
1525 - 1575	3.11E-19	3.46E-19	3.79E-19	1.05E-03	1.38E-03	0.00E+00
1575 - 1625	1.49E-19	1.80E-19	2.13E-19	1.77E-03	2.69E-03	0.00E+00
1625 - 1675	5.69E-20	7.50E-20	9.71E-20	2.51E-03	4.20E-03	5.46E-04
1675 - 1725	1.73E-20	2.66E-20	3.73E-20	3.64E-03	5.78E-03	2.61E-03
1725 - 1775	4.30E-21	7.67E-21	1.19E-20	4.58E-03	7.88E-03	4.33E-03
1775 - 1825	9.17E-22	1.91E-21	3.54E-21	5.42E-03	1.22E-02	5.76E-03
1825 - 1875	1.69E-22	4.16E-22	8.91E-22	6.19E-03	1.63E-02	6.85E-03
1875 - 1925	3.18E-23	9.39E-23	2.35E-22	6.89E-03	2.14E-02	7.67E-03
1925 - 1975	6.16E-24	1.72E-23	5.59E-23	6.70E-03	3.21E-02	8.23E-03

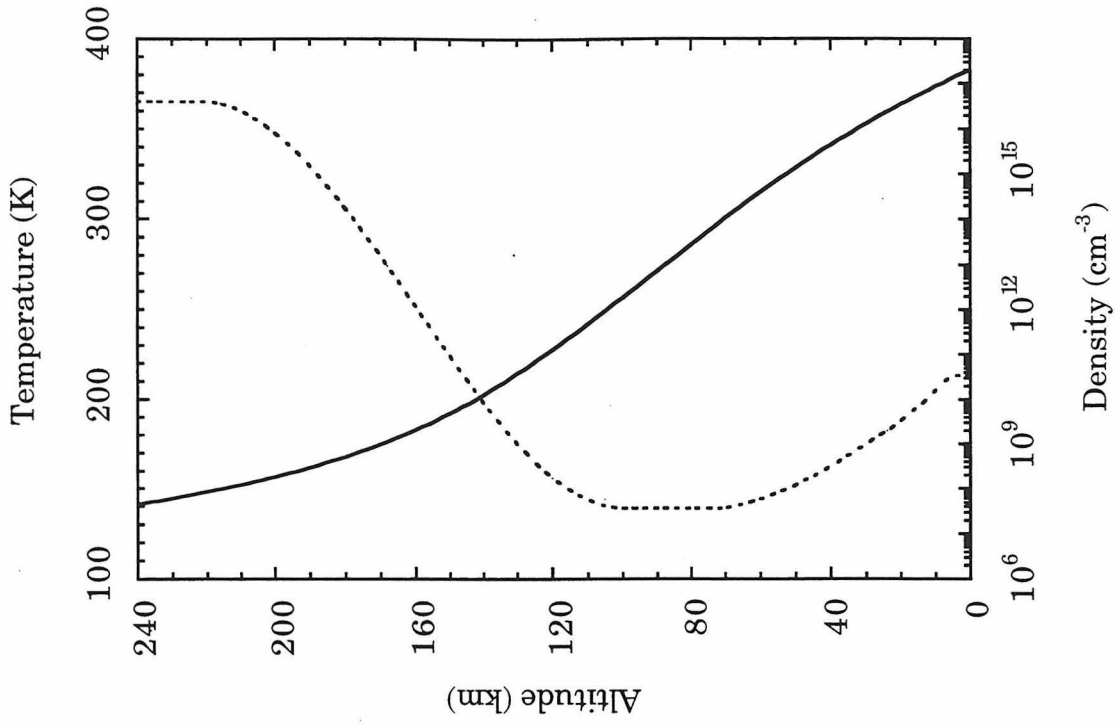

Fig. 1.1. Adopted hydrostatic atmosphere for Mars, showing total atmospheric density (solid line) and temperature (dotted line).

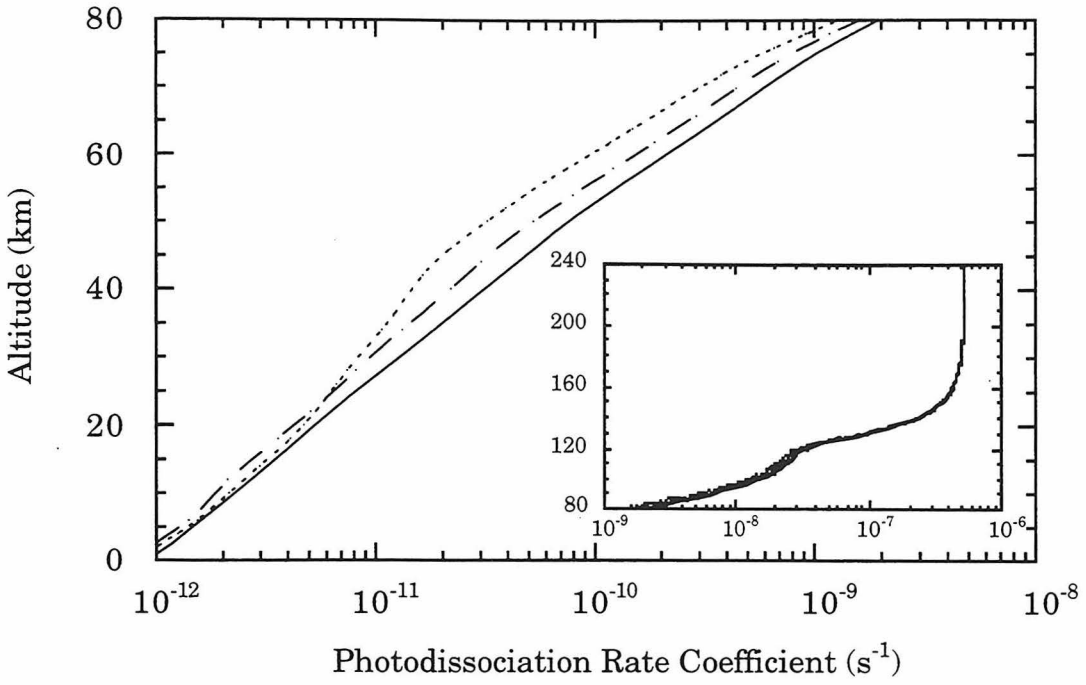

Fig. 1.2. Calculated photodissociation rate coefficients for CO_2 assuming (a) temperature-independent CO_2 cross sections (solid line), (b) temperature-dependent CO_2 cross sections, with cross section values for temperatures below 202 K and above 368 K set equal to the values at 202 K and 368 K, respectively (dashed line), and (c) temperature-dependent CO_2 cross sections, but with temperature sensitivities below 202 K and above 368 K assumed equal to the sensitivities in the 202 - 298 K and 298 - 368 K ranges, respectively (dotted line).

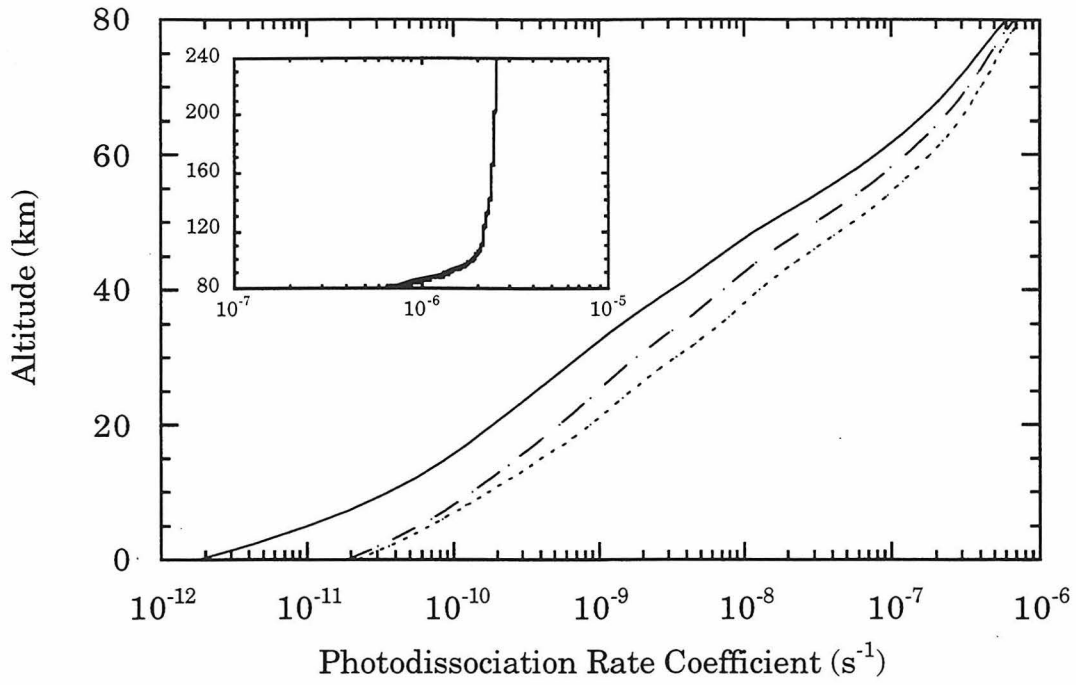

Fig. 1.3. Same as Fig. 1.2, except for H_2O.

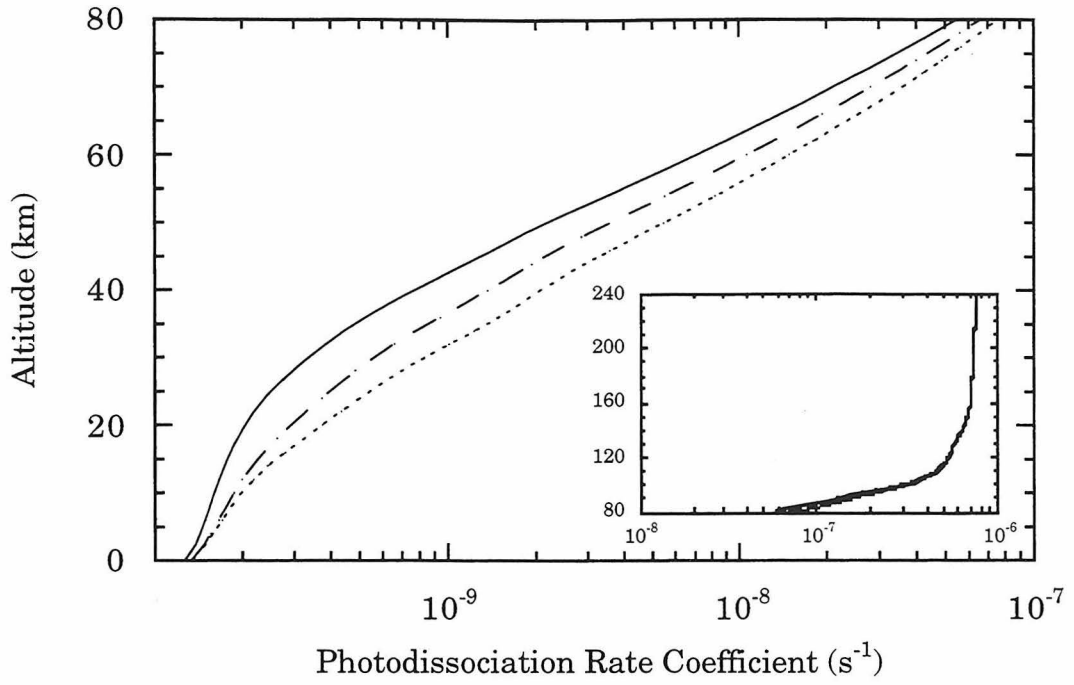

Fig. 1.4. Same as Fig. 1.2, except for O_2.

Chapter 2.

Adsorption of HO_x on Aerosol Surfaces: Implications for the Atmosphere of Mars

This chapter was previously published as Anbar, Leu, Nair and Yung, 1993.

2.1. Abstract

The potential impact of heterogeneous chemistry on the abundance and distribution of HO_x in the atmosphere of Mars has been assessed by combining observational data of dust and ice aerosol distributions with an updated photochemical model. Critical parameters include the altitude distributions of aerosols, and the surface loss coefficients (γ) of HO_2 on dust and ice in the lower atmosphere, and H on ice above 40 km. We find that adsorption on dust ($\gamma_{HO_2} \geq 0.01$), or ice near 30 km ($\gamma_{HO_2} \geq 0.1$), can deplete OH abundances in the lower atmosphere by $\approx$ 10% or more. Such depletions approach those obtained by lowering the water vapor abundance by an order of magnitude below the global average observed by Viking ($\approx$ 25%). Since the oxidation of CO is catalyzed by HO_x in the lower atmosphere via the reaction CO + OH --> CO_2 + H, loss of OH due to adsorption of HO_x on dust or ice at low altitudes could have a significant effect on the ratio CO : CO_2. The adsorption of H on ice at 50 km ($\gamma_H \geq 0.01$) can result in even larger OH depletions. However, this effect is localized to altitudes > 40 km, where CO oxidation is relatively unimportant. Laboratory data suggest that $\gamma_{HO_2} \approx$ 0.01 is a reasonable estimate for adsorption on dust. Larger values are plausible, but are not strongly supported by experimental evidence. The reactivity of HO_2 on ice is unknown, while γ_H on ice appears to be < 0.001.

There is a need for measurements of HO_x adsorption on surfaces representative of Martian aerosols at temperatures < 220 K.

2.2. Introduction

Carbon dioxide comprises over 95 % of the atmosphere of Mars, despite continuous photolysis of CO_2 by solar UV radiation. Since the direct recombination of CO and O is slow, the balance between CO_2 production and loss in the Martian atmosphere (the "stability of CO_2") is thought to be maintained by a HO_x-catalyzed CO oxidation scheme (McElroy and Donahue, 1972; Parkinson and Hunten, 1972). Thus, the rate of CO oxidation is sensitive to the abundance and altitude-distribution of the HO_x species (OH, H and HO_2).

Recent models of gas-phase chemistry in the Martian atmosphere predict ratios of CO to CO_2 lower than those observed, presumably due to an overabundance of HO_x (Shimazaki, 1989; Krasnopolsky, 1991; Nair *et al.*, 1991; Nair *et al.*, 1992). This is largely the result of two important factors which were not considered in the classic explanations of CO_2 stability (McElroy and Donahue, 1972; Parkinson and Hunten, 1972). First, the temperature dependence of the CO_2 absorption cross-section (*e.g.*, DeMore and Patapoff, 1972; Lewis and Carver, 1983) was not accounted for in earlier studies. This effect should decrease the calculated CO_2 photolysis rate, while increasing the rate of HO_x production via photolysis of H_2O (Parisot and Zucconi, 1984; Anbar *et al.*, 1992). Secondly, the water vapor profiles used in most of the earlier Mars models assumed that water was present primarily near the surface (the lower 5 - 10 km). In current models, the lower atmosphere is considered well-mixed with respect to water to altitudes as high as 20 - 40 km, consistent with observational data (Jakosky and Farmer,

1982; Clancy *et al.*, 1992). This increases the amount of H_2O exposed to photolysis at higher altitudes, thereby raising the rate of HO_x production.

In a recent study which accounted for these factors, Shimazaki (1989) was able to balance CO_2 production and loss only by imposing an upper limit on the water vapor abundance of 1 - 2 precipitable microns (prμm). This constraint limits the abundance of HO_x species, which are largely derived from photolysis of H_2O. However, this water vapor abundance is an order of magnitude lower than the globally-averaged abundance measured by Viking (Jakosky and Farmer, 1977), and is also substantially lower than the recent measurements of Clancy *et al.* (1992).

The adsorption of HO_x on aerosol surfaces is an alternative means of reducing HO_x abundances (Anbar *et al.*, 1991; Krasnopolsky *et al.*, 1991). Most Martian atmospheric models have assumed that HO_x abundances are governed entirely by gas-phase chemistry (*e.g.*, Yung *et al.*, 1988; Shimazaki, 1989). However, it is well established that reactive HO_x radicals are adsorbed by a wide variety of surfaces (Table 2.1). Adsorption of these species on the surfaces of Martian aerosols could decrease HO_x abundances significantly, thereby retarding CO oxidation.

Previous discussions of the influence of heterogeneous chemistry on the Martian atmosphere have largely focused on heterogeneous catalysis of CO oxidation (*e.g.*, Clark, 1971; Huguenin *et al.*, 1977; Atreya and Blamont, 1990; Leu *et al.*, 1992), although surface catalyzed CO oxidation has not yet been observed under Martian atmospheric conditions. HO_x adsorption has typically been overlooked, although this phenomenon has been studied in the laboratory at temperatures and pressures approaching those of the lower Martian atmosphere (Table 2.1). Hunten (1974) was the first to suggest that

"cold trapping" of water and HO_x species on surfaces could strongly perturb gas-phase HO_x catalytic chemistry. However, this was discussed as a low-temperature equilibrium condensation process, rather than as an adsorption reaction governed by the kinetics of gas-surface reactions, capable of occurring at temperatures typical of the Martian surface and lower atmosphere. Kong and McElroy (1977) made the only attempt to quantitatively consider the impact of heterogeneous destruction of HO_x, but considered only adsorption on the regolith at the Martian surface; reactions on aerosol surfaces (dust or ice) were not included, although the surface area available for reaction on aerosol particles in the Martian atmosphere is often comparable to the area of the planet's surface. Their study also did not account for the temperature-dependence of the CO_2 absorption cross section, and assumed that water in the atmosphere was present only very close to the surface.

In this study, we explore the suggestion that the adsorption and reaction of HO_x on aerosol surfaces is an alternative mechanism for suppressing HO_x abundances and retarding the rate of CO oxidation, without violating observational constraints on the abundance of H_2O. Our intent is not to rigorously quantify the effects on CO chemistry, but to determine the feasibility of heterogeneous chemistry as a significant HO_x-suppression mechanism. We assess the potential impact of heterogeneous processes involving the Martian surface, as well as dust and ice aerosols, on the abundance and altitude distributions of HO_x species. The effects of these processes are compared to those of lowering the H_2O abundance, and the implications for CO_2 chemistry are discussed.

2.3. Model Description

The potential impact of HO_x adsorption was assessed by calculating HO_x altitude profiles in the presence of ice and/or dust using a one dimensional photochemical model, including transport. The Caltech/JPL generalized planetary atmosphere photochemistry code is described elsewhere (Allen *et al.*, 1981). The model used here is a modified version of the model of Yung *et al.* (1988). Details of this Mars model are described below.

2.3.1. *Heterogeneous Chemistry*

The rate of each HO_x adsorption reaction was set equal to the collision frequency of the reacting species with a surface, multiplied by a surface loss coefficient, γ , which represents the fraction of collisions which result in loss of the species from the gas phase ($0 < \gamma < 1$). Published measurements of γ for HO_x species are summarized in Table 2.1, and discussed further below. The collision frequency of a gas-phase species with an aerosol surface at a given altitude is a function of the mean thermal molecular speed (v; cm s^{-1}), and the surface area (S; cm^2 cm^{-3}) available at that altitude, following the equation:

$$\text{Rate } (cm^{-3}\ s^{-1}) = (1/4)\ \gamma\ S\ v\ N_i, \qquad (2.1)$$

where N_i (cm^{-3}) is the number density of the species being adsorbed (Michelangeli *et al.*, 1991). The temperatures used to calculate v are described below. The dust and ice surfaces available for reaction in the model are plotted in Fig. 2.1 as extinction coefficients. For spherical particles, surface area and extinction coefficient are approximately related by $S = 2$ x

(extinction coefficient), assuming that the optical cross section is equal to twice the geometrical cross section.

For dust, the available surface area was calculated from dust distributions and particle dimensions supplied by D. Michelangeli, based on the work of Michelangeli *et al.* (in press). An overall optical depth of approx. 0.2 was assumed; this represents a relatively clear Martian atmosphere, and does not simulate the much higher opacities observed during global dust storms. These data are similar to those obtained by *Phobos 2* (Blamont *et al.*, 1991). We note that the total surface area available for reaction on these particles is comparable to the area of the planet's surface.

Persistent, geographically extensive detached hazes of water ice are common in the Martian atmosphere (*e.g.,* Kahn, 1990). Two different ice distribution profiles were included in this study, because these hazes have been observed over a range of altitudes. The first profile, based on data supplied by D. Michelangeli, reaches a maximum ice abundance at ≈ 30 km. The second profile assumes the same distribution, but shifted 20 km higher to match observations by *Phobos 2* (Blamont *et al.*, 1991).

Once adsorbed, HO_x species are assumed to react with gas phase OH or H, resulting in conversion to H_2O or H_2, which are rapidly returned to the gas phase. This mechanism is necessary to preserve mass-balance and maintain the overall oxidation state of the atmosphere. For example, in the case of HO_2 adsorption (H and OH adsorption can be treated similarly), the surface chemistry is parameterized as:

(1) HO_2 + Surface ------> $(HO_2)_S$

(2) $(HO_2)_S$ + OH ------> H_2O + O_2

Net: HO_2 + OH ------> H_2O + O_2

where $(HO_2)_S$ denotes the adsorbed species. At steady-state, the rate of the net reaction must equal the rate of reaction (1). Thus, surface chemistry can be thought of as catalyzing the destruction of HO_x.

2.3.2. *Homogeneous Chemistry*

We have considered the gas phase chemistry of a CO_2 - H_2O atmosphere. The continuity equation, including transport, was solved for the species CO_2, CO, O_2, O, $O(^1D)$, O_3, H_2O, H_2O_2, OH, HO_2, H_2, and H. The gas-phase reactions incorporated in the model and their rate constants are listed in Table 2.2. Rate constants for three-body reactions were increased by a factor of two from the tabulated values to account for the efficiency of CO_2 as a third body (Yung and DeMore, 1982).

2.3.3. *Boundary Conditions*

In our model calculations, the number densities of O_2, CO and CO_2 at 0 km were fixed to observed values (2.34×10^{14} cm^{-3}, 1.26×10^{14} cm^{-3}, and 2.05×10^{17} cm^{-3}, respectively). The abundance of H_2O was also fixed at the ground. Two H_2O cases were modeled; one with an integrated column abundance of 16 prμm, and the other with 1.6 prμm. Following Shimazaki (1989), H_2O was modeled as well-mixed up to a "critical altitude," above which saturation was assumed. The height of the "critical altitude" is determined by the H_2O column abundance. In our 16 prμm and 1.6 prμm

models, the critical heights were ≈ 20 km and 35 km, respectively. The two H_2O profiles, shown in figure 2, are in agreement with those of Shimazaki (1989) below 50 km, but are somewhat larger at higher altitudes.

Following Yung *et al.* (1988), the escape velocities of H and H_2 were fixed to 6.76×10^3 cm s^{-1} and 1.70×10^2 cm s^{-1}. The O escape flux was set to 6×10^7 cm^{-2} s^{-1}, in agreement with McElroy (1972).

2.3.4. *Other Input Parameters*

The eddy diffusivity profile in the Martian atmosphere is uncertain, and has been the subject of some debate (*e.g.,* Kong and McElroy, 1977; Kahn, 1990; Atreya and Blamont, 1990). Our results should be insensitive to this profile, over the range of values that have been suggested. This is due to the exceedingly short lifetimes of the HO_x species relative to the transport timescale. At the ground, the lifetime of the HO_x family is on the order of $[HO_x]/k_{28}[OH][HO_2] \approx 10^4$ s, while the transport timescale can be approximated by H^2/K_z (H = atmospheric scale height; K_z = eddy diffusivity) ≈ $10^{12}/10^5 = 10^7$ s. Therefore, the HO_x family is in a state of photochemical equilibrium. The abundances of longer-lived species (*e.g.,* CO and O_2) which could be impacted by different eddy diffusivity profiles, and hence affect the partitioning of the HO_x species, have been fixed to observed values. Thus, the distribution of the HO_x species should be independent of the choice of the eddy diffusion profile. The eddy diffusion coefficients used in this model grade exponentially from 10^5 cm^2s^{-1} at the surface to 5×10^7 cm^2s^{-1} at 100 km, and remain constant at higher altitudes. This is similar to Shimazaki's profile *A* (1989).

The COSPAR temperature profile has been adopted below 100 km (Seiff, 1982), with an exospheric temperature of 365 K (Kong and McElroy, 1977). The temperature profile of the upper atmosphere was then found by fitting a spline curve to these data.

Solar flux values at 1 AU were obtained from Mount and Rottman (1983) and Torr and Torr (1985), and scaled to 1.52 AU. The cross sections used to calculate photodissociation rate constants are described in Anbar *et al.* (1992) and Nair *et al.* (in preparation). CO_2 cross sections were adopted from Lewis and Carver (1983), and the temperature dependence of CO_2 absorption was modeled following the procedure of Anbar *et al.* (1992). No adjustment was made for aerosol scattering or absorption in the results presented below. We find that incorporation of these effects into the model changes photolytic rate constants by a maximum amount of 10 - 20% at the ground. The magnitude of this effect decreases with increasing altitude. Since the bulk of HO_x formation occurs near 20 km, and since HO_x lifetimes are very short with respect to transport timescales, aerosol effects on the radiation field should not have much impact on our results. All computations employed a diurnally-averaged radiation field at equinox for $\approx 30°$ latitude.

2.4. Model Results

HO_x profiles were calculated for a number of different models (Table 2.3), and the results are summarized in Figs. 2.3 - 2.6. Models A and B (Fig. 2.3) invoke no heterogeneous chemistry, but assume water vapor abundances of 16 and 1.6 prμm, respectively. The results of model B are close to those of Shimazaki (1989), who also assumed $\approx$ 1 prμm H_2O. The depletions of HO_2, H and OH in model B relative to model A are largest in the lower atmosphere

(below 50 km), since the largest differences in water vapor abundances occur near the surface (Fig. 2.2), and the chemical loss timescales for these species dominate over transport timescales. The abundances of OH and HO_2 are most strongly affected; their column densities are depleted by ≈ 25% and ≈ 65%, respectively. Significantly, in both models, HO_2 is the dominant HO_x species between the ground and ≈ 35 km, which is where most of the dust surface area is available. This is also where most of the ice surface is available in the low-altitude ice haze case we have considered (Fig. 2.1). At higher altitudes, where the ice abundance may exceed that of dust (Fig. 2.1), H is the primary HO_x species. Thus, the influence of HO_x adsorption is determined by the rate of adsorption of HO_2 on dust and regolith, and on low-altitude ice, and of H on ice at higher altitudes; the rate of adsorption of OH on either surface is insignificant by comparison. Due to the reactions which relate the HO_x radicals to one another, heterogeneous loss of one of these radicals propagates through the entire HO_x family.

Heterogeneous chemistry was incorporated in models C1, C2, C3, D1, D2, E1, E2 and E3, all of which assumed 16 prμm of water vapor. Adsorption on dust and on the surface (C1, C2 and C3) was considered separately from adsorption on ice (D1, D2, E1, E2 and E3) to allow the effects of reactions on different surfaces to be distinguished. In models C1, C2, C3, D1 and D2, only HO_2 adsorption was considered. Models E1, E2 and E3 include only H adsorption. Since gas-phase HO_x-catalyzed CO oxidation is most rapid below 40 km (*e.g.,* Kong and McElroy, 1977; Shimazaki, 1989), the impact of heterogeneous HO_x depletion on CO chemistry can be assessed to first order by comparing the HO_x altitude distributions to this 40 km "threshold". The

abundance of OH is particularly critical, since the rate of CO oxidation is limited by the rate of R30 (CO + OH ---> CO_2 + H_2O).

Examination of the C models (Fig. 2.4) reveals that adsorption of HO_2 on dust can significantly deplete some HO_x species in the lower atmosphere, even for γ_{HO_2} = 0.001 (model C1). If γ_{HO_2} = 0.01, the total HO_x budget in model C2 approaches that of the 1.6 prμm water vapor case (model B). Although the abundance of OH is only reduced by ≈ 10% on a column-integrated basis (Table 2.3), the bulk of this reduction occurs below 20 km, where the rate of HO_x-catalyzed CO recombination is highest when heterogeneous chemistry is not included. Thus, the rate of CO recombination may be retarded substantially by adsorption of HO_2 on dust, with γ_{HO_2} = 0.01. If an even larger surface loss coefficient is considered (γ_{HO_2} = 0.1; model C3), then the total HO_x abundance is actually lowered below that of model B, and the OH abundance comes within 25% of model B. The plausibility of these values of γ is assessed below.

Adsorption of HO_2 on ice particles centered at 30 km was considered in model D1 and D2 (Fig. 2.5), while adsorption of H on a haze at 50 km was considered in models E1, E2 and E3 (Fig. 2.6). Adsorbed H was assumed to react with gas-phase H to produce H_2 gas, by analogy with the HO_2 surface chemistry described earlier. The influence of ice surfaces on HO_x abundances, as expected, is very sensitive to the altitude of the ice cloud. When the ice distribution is centered at 30 km and γ_{HO_2} = 0.01 (model D1), only a very small impact on HO_x is seen in the lower atmosphere. γ values on the order of 0.1 (model D2) are necessary to achieve an OH abundance comparable to that of model C2. Even higher values would be necessary to approach the depletions found in the case of low water abundance (model B). The inclusion

of H adsorption on ice in the lower atmosphere was found to have little effect on HO_x abundances.

If the ice distribution maximum is shifted to ≈ 50 km (models E1, E2 and E3), the predicted abundances of H and OH are substantially smaller than in the 30 km cases utilizing comparable values of γ (*e.g.*, compare models D1 and E2, or D2 and E3). Even if $\gamma_H = 0.001$ (model E1), OH is depleted by nearly 10% relative to model A. The sensitivity to the altitude distribution of the ice particles is due largely to the fact that, in the purely gas-phase case, the chemical loss timescale of OH (and, hence, its abundance) has a maximum near 50 km. Thus, the introduction of a heterogeneous loss process has its greatest effect on OH at this altitude.

Of all the heterogeneous cases studied, models E2 and E3 have the largest impact on the OH abundance, resulting in even lower abundances than in model B. However, due to the ice particle distribution, this depletion occurs primarily above 40 km (Fig. 2.5), where the rate of HO_x-catalyzed CO recombination is quite low (*e.g.*, Kong and McElroy, 1977; Shimazaki, 1989). Thus, heterogeneous processes on ice surfaces at these altitudes are likely to have a negligible effect on CO_2 stability.

2.5. Comparison to Laboratory Adsorption Data

The plausibility of the range of γ values described above can only be assessed by making comparisons to laboratory data. Unfortunately, the number of studies of HO_x adsorption is small, and most surfaces that have been studied are not directly relevant to the Martian surface or aerosols. They are, at best, crude analogs of the reactive surfaces available on Mars, which are likely to be composed of complex, iron-rich oxide and silicate

weathering products of basalts (*e.g.,* Bell *et al.,* 1990; Morris *et al.,* 1990; Pinet and Chevrel, 1990). Nonetheless, we believe the published data are useful to provide order-of-magnitude estimates of γ.

Table 2.1 summarizes the published values of HO_x surface loss coefficients on inorganic oxides. HO_x adsorption data on metal surfaces have not been included, although these tend to be substantially larger than the values on oxides (*e.g.,* Thrush, 1965). We have also omitted data from early studies which indicate relatively large values of γ_{HO_x} on oxide surfaces (*e.g.,* Smith, 1943); we are not confident of the reliability of these early measurements. Most data were collected at or near room temperature. At lower temperatures, it is expected that γ should increase. This can be understood if the data represent an equilibrium between an energetically-favorable adsorption reaction, and an endothermic desorption process. Such behavior has been observed for OH and HO_2 on H_3PO_4, where loss coefficients increase by an order of magnitude as temperature is lowered from 298 K to ≈ 220 K (Margitan, 1976; Howard, 1979). This observation is of special importance to the Martian atmosphere, where typical temperatures are < 220 K.

The HO_2 data demonstrate that a γ_{HO_2} value > 0.001 is entirely consistent with the few studies that have been done. A value of 0.01 on potential Martian surfaces is plausible if temperature effects are considered (see above). This conclusion is strengthened if the OH data are considered. Although adsorption of OH is probably not an important HO_x sink in the Martian atmosphere, we include these data because OH and HO_2 have similar affinities for many surfaces (Jech *et al.,* 1982); in Table 2.1, γ_{OH} and γ_{HO_2} are typically within an order of magnitude of each other for comparable

surfaces. Moreover, the OH data are the most comprehensive, since they cover a variety of complex oxides, including some containing iron. If the OH data are used to supplement the HO_2 data by inference, then $\gamma_{HO_2} \approx 0.01$ seems a reasonable estimate for adsorption on Martian dust and regolith, particularly at low temperatures. Higher values of γ are possible, but are not well supported by the laboratory data. The adsorption affinity of HO_2 for ice is unknown, but is likely to be ≥ 0.01 on the basis of comparison with data for adsorption on liquid water, as well as the OH data. A value as high as $\gamma_{HO_2} \approx 0.1$ is plausible.

The adsorption of H on ice is more problematic. The only laboratory study indicates $\gamma_H < 0.001$ (Gershenzon *et al.*, 1986), which is too small for an appreciable effect in the atmosphere. However, a theoretical study of adsorption on amorphous ice suggests $\gamma_H > 0.1$ at < 150 K (Buch and Zhang, 1991). The applicability of this result to Martian ice surfaces is doubtful, since typical Martian atmospheric temperatures are higher than those at which amorphous ice is stable. Thus, the adsorption of H is unlikely to be an important process.

2.6. Discussion and Conclusions

Our findings indicate that heterogeneous chemistry on aerosols is capable of lowering the abundance of HO_x species in the Martian atmosphere. Adsorption on either dust or ice surfaces below 40 km could have a non-trivial impact on the abundance of HO_x, and hence on the ratio of CO : CO_2; the predicted depletions of OH ($\approx$ 10% or more) approach those achieved by lowering the H_2O abundance from 16 prμm to 1.6 prμm ($\approx$ 25 %), which could significantly retard the rate of CO oxidation. The γ values required for such

an effect ($\gamma_{HO_2} \geq 0.01$ on dust; $\gamma_{HO_2} \geq 0.1$ on ice) are not unreasonable when compared to the few laboratory data available. However, there is a clear need for laboratory experiments on surfaces representative of Martian aerosols, and at temperatures approaching those of the lower Martian atmosphere.

Adsorption of H on ice near 50 km altitude can also result in substantial HO_x depletions, if $\gamma_H \geq 0.01$. However, these depletions are confined to altitudes at which the rate of HO_x-catalyzed CO oxidation is already low. Additionally, these values of γ_H are higher than observed in the only relevant laboratory study. Thus, little impact on the chemistry of CO is expected from H adsorption on ice.

While this study has demonstrated the *potential* influence of heterogeneous chemistry, a critical re-examination of Martian atmospheric chemistry is required to rigorously quantify the importance of such reactions. For example, the uncertainties associated with some of the rate constants used in this model are as large as ± 30% at room temperature, with somewhat higher uncertainties at Martian temperatures. Thus, it may be possible to reduce the abundance of HO_x radicals in the modeled atmosphere by manipulating key rate constants within the reported uncertainties. The abundance of HO_x is controlled by the rate of production, via H_2O photolysis with a contribution from $O(^1D) + H_2O$ -----> 2OH (R15) at the surface, and the rate of loss, dominated by the reaction $OH + HO_2$ -----> $H_2O + O_2$ (R28). Thus, the abundance of HO_x can be decreased by decreasing the production rate (R3a + k_{15} $[O(^1D)]$)$[H_2O]$, increasing the rate constant k_{28}, or a combination of these changes. The impact of reasonable "re-evaluations" of these gas-phase data must be quantified.

Additionally, reactions involving HO_x are considered critical to many processes in the Martian atmosphere (*e.g.,* the abundance of O_3, the escape rate of H, and the coupling of H escape to O escape). If HO_x abundances must be suppressed, we may need to revise our explanations of the chemistry governing such processes. For example, although it is generally assumed that O_3 loss is dominated by reaction with HO_x (*e.g.,* Lindner, 1988), catalytic NO_x chemistry may become important if HO_x levels are depressed. Hence, the photochemistry of nitrogen (Yung *et al.*, 1977) should be re-examined in light of this work.

It must be realized that the inclusion of heterogeneous HO_x chemistry introduces a complicated variable into Martian atmospheric modeling, since the altitude distributions of H, OH and HO_2 are sensitive to the altitude distribution of the aerosol surfaces (compare models C2, D1, and E2). Like the water vapor abundance, the altitude distribution of aerosol surfaces (especially ice surfaces) varies latitudinally, seasonally and diurnally. Thus, heterogeneous HO_x chemistry must be introduced with care, and should not be used to "solve" modeling difficulties until all the reasonable permutations of gas-phase chemistry have been explored. Despite this caveat, the importance of quantifying the role of heterogeneous chemistry in the atmosphere of Mars cannot be overlooked. In the comparative planetology of atmospheres, Mars is said to possess the "dustiest" atmosphere. The impact of aerosols on Martian atmospheric chemistry is largely unknown, despite some imaginative but unproved speculations (Huguenin, 1977; Atreya and Blamont, 1990). This study has combined laboratory data and photochemical modeling to demonstrate that heterogeneous chemistry could be important in regulating the abundance of HO_x. This opens the exciting possibility that the

Martian atmosphere may be a "natural laboratory" for the quantitative study of heterogeneous reactions, which are now considered important in the terrestrial atmosphere (Molina *et al.*, 1987; Tolbert *et al.*, 1987; Leu, 1988; Michelangeli *et al.*, 1991).

2.7. Acknowledgments

The authors thank D. Michelangeli for providing aerosol data in electronic format. The assistance of M. Allen was greatly appreciated. The comments of two anonymous reviewers were extremely helpful.

2.8. References

Allen, M., Y. L. Yung, and J. W. Waters, Vertical transport and photochemistry in the terrestrial mesosphere and lower thermosphere, *J. Geophys. Res.*, *86*, 3617-3627, 1981.

Anbar, A. D., M-T. Leu, and Y. L. Yung, The adsorption of HO_x on aerosol surfaces: implications for the stability of CO_2 in the atmosphere of Mars, *23rd Annual Mtg. AAS Div. Planet. Sci., Bull. Am. Astr. Soc., 23,* 1991.

Anbar, A. D., M-T. Leu, H. A. Nair, and Y. L. Yung, Adsorption of HO_x on aerosol surfaces: Implications for the atmosphere of Mars, *J. Geophys. Res., 98,* 10933-10940, 1993.

Anbar, A. D., M. Allen, and H. A. Nair, Photodissociation in the atmosphere of Mars: Impact of high resolution, temperature-dependent CO_2 cross section measurements, *J. Geophys. Res.,98,* 10925-10931, 1993.

Atreya, S. K., and J. E. Blamont, Stability of the Martian atmosphere: Possible role of heterogeneous chemistry, *Geophys. Res. Lett.*, *17*, 287-290, 1990.

Baulch, D. L., D. D. Drysdale, J. Duxbury, and S. J. Grant, *Evaluated Kinetic Data for High Temperature Reactions. Homogeneous Gas Phase Reactions of the O_2-O_3 System, the CO_2-O_2-H_2 System, and of Sulphur-Containing Species*, Butterworths, London/Boston, 1976.

Bell, J. F. III, T. B. McCord, and P. D. Owensby, Observational evidence of crystalline iron oxides on Mars, *J. Geophys. Res., 95,* 14447-14461, 1990.

Blamont, J. E., E. Chassefière, J. P. Goutail, B. Mege, M. Nunes-Pinharanda, G. Souchon, V. A. Krasnopolsky, A. A. Krysko, and V. I. Moroz, Vertical profiles of dust and ozone in the Martian atmosphere deduced from solar occultation measurements., *Planet. Space Sci.*, *39*, 175-187, 1991.

Buch, V., and Q. Zhang, Sticking probability of H and D atoms on amorphous ice: A computational study, *Astrophys. J., 379*, 647-652, 1991.

Clancy, R. T., A. W. Grossman, and D. O. Muhleman, Mapping Mars water vapor with the Very Large Array, *Icarus,* in press, 1992.

Clark, I. D., The chemical kinetics of CO_2 atmospheres, *J. Atmos. Sci., 28,* 847-858, 1971.

DeMore, W. B., and M. Patapoff, Temperature and pressure dependence of CO_2 extinction coefficients, *J. Geophys. Res., 77*, 6291-6293, 1972.

DeMore, W. B., S. P. Sander, D. M. Golden, M. J. Molina, R. F. Hampson, M. J. Kurylo, C. J. Howard, and A. R. Ravishankara, *Chemical Kinetics and Photochemical Data for Use in Stratospheric Modeling*, JPL Publication 90-1, 1990.

Gershenzon, Y. M., A. V. Ivanov, S. I. Kucheryavyi, and V. B. Rozenshtein, Annihilation of OH radicals on the surfaces of substances chemically similar to atmospheric aerosol particles, *Kinet. Katal., 27*, 1067-1074, 1986.

Gershenzon, Y. M., and A. P. Purmal, Heterogeneous processes in the Earth's atmosphere and their ecological consequences, *Russ. Chem. Rev., 59*, 1007-1023, 1990.

Hampson, R. F., Chemical Kinetics and Photochemical Data Sheets for Atmospheric Reactions, U.S. Dept. of Transportation, FAA Office of Environment and Energy, High Altitude Pollution Program, Washington, D. C., Report No. FAA-EE-80-17, 1980.

Hanson, D. R., J. B. Burkholder, C. J. Howard, and A. R. Ravishanhara, Measurement of OH and HO_2 radical uptake coefficients on water and sulfuric acid surfaces, *J. Phys. Chem., 96,* 4979-4985, 1992.

Howard, C. J., Kinetic measurements using flow tubes, *J. Phys. Chem., 83,* 3-9, 1979.

Huguenin, R. L., R. G. Prinn, and M. Maderazzo, Mars: Photodesorption from mineral surfaces and its effects on atmospheric stability, *Icarus*, *32*, 270-298, 1977.

Hunten, D. M., Aeronomy of the lower atmosphere of Mars, *Rev. Geophys. Space Phys., 12,* 529-535, 1974.

Jakosky, B. M., and C. B. Farmer, The seasonal and global behavior of water vapor in the Mars atmosphere: Complete global results of the Viking atmospheric water detector experiment, *J. Geophys. Res.*, *87*, 2999-3019, 1982.

Jech, D. D., P. G. Easley, and B. B. Krieger, Kinetics of reactions between free radicals and surfaces (aerosols) applicable to atmospheric chemistry, *Geophysical Monograph 26: Heterogeneous Atmospheric Chemistry,* D. R. Schryer, ed., 107 - 119, American Geophyscial Union, Washington D. C.,1982.

Kahn, R., Ice haze, snow, and the Mars water cycle, *J. Geophys. Res.*, *95*, 14677-14693, 1990.

Kong, T. Y., and M. B. McElroy, Photochemistry of the Martian atmosphere, *Icarus*, *32*, 168-189, 1977.

Krasnopolsky, V. A., Photochemistry of the Martian atmosphere (mean conditions), *23rd Annual Mtg. AAS Div. Planet. Sci., Bull. Am. Astr. Soc., 23,* 1991.

Leu, M-T. Laboratory studies of sticking coefficients and heterogeneous reactions important in the Antarctic stratosphere, *Geophys. Res. Lett., 15,* 17-20, 1988.

Leu, M.-T., J. E. Blamont, A. D. Anbar, L. F. Keyser, and S. P. Sander, Adsorption of CO on water-ice and oxide surfaces: Implications for the Martian Atmosphere, *J. Geophys. Res.*, *97*, 2621-2627, 1992.

Lewis, B. R., and J. H. Carver, Temperature dependence of the carbon dioxide photoabsorption cross section between 1200 and 1970 Å, *J. Quant. Spectrosc. Radiat. Transf.*, *30*, 297-309, 1983.

Lin, C. L., and M.-T. Leu, Temperature and third-body dependence of the rate constant for the reaction O + O_2 + M --> O_3 + M, *Int. J. Chem. Kinet.*, *14*, 417-434, 1982.

Lindner, B. L., Ozone on Mars: The effects of clouds and airborne dust, *Planet. Space Sci.*, *36*, 125-144, 1988.

Margitan, J. J., *Gas Phase Reactions of OH Radicals Studied by Molecular Resonance,* Ph.D. Thesis, University of Pittsburgh, 1976.

McElroy, M. B., and T. M. Donahue, Stability of the Martian atmosphere, *Science*, *177*, 986-988, 1972.

McElroy, M. B., Mars: An evolving atmosphere, *Science*, *175*, 443-445, 1972.

Michelangeli, D. V., M. Allen, and Y. L. Yung, Heterogeneous reactions with NaCl in the El Chichon volcanic aerosols, *Geophys. Res. Lett.*, *18*, 673-676, 1991.

Michelangeli, D. V., O. B. Toon, R. M. Haberle, and J. B. Pollack, Numerical simulations of the formation and evolution of water-ice clouds in the Martian atmosphere, *J. Geophys. Res.*, *in press*, 1992.

Molina, M. J., T. L. Tso, L. T. Molina, and F. C. Y. Wang, Antarctic stratospheric chemistry of chlorine nitrate, hydrogen chloride, and ice: Release of active chlorine, *Science*, *238*, 1253-1257, 1987.

Morris, R. V., J. L. Gooding, H. V. Lauer, Jr., and R. B. Singer, Origins of Marslike spectral and magnetic properties of a Hawaiian palagonitic soil, *J. Geophys. Res., 95,* 14427-14434, 1990.

Mount, G. H., and G. J. Rottman, The solar absolute spectral irradiance 1150-3173 Å: 17 May 1982, *J. Geophys. Res.*, *88*, 5403-5410, 1983.

Mozurkewich, M., P. H. McMurry, A. Gupta, and J. G. Calvert, Mass accommodation coefficient for HO_2 radicals on aqueous particles, *J. Geophys. Res.*, *92*, 4163-4170, 1987.

Nair, H. A., M. Allen, Y. L. Yung, Regulation of CO and O_2 abundance by the escape of oxygen and hydrogen in the atmosphere of Mars, *23rd Annual Mtg. AAS Div. Planet. Sci., Bull. Am. Astr. Soc., 23,* 1991.

Nair, H. A., M. Allen, Y. L. Yung, and R. T. Clancy, Martian atmospheric chemistry during the time of low water abundance, *MSATT Workshop on the Evolution of the Martian Atmosphere, LPI Contrib. No. 787.,* 1992.

Nair, H., M. Allen, A. D. Anbar, Y. L. Yung and R. T. Clancy. 1994. A photochemical model of the Martian atmosphere. Icarus 111:124-150.

Parisot, J.-P., and J.-M. Zucconi, Temperature effect on the photodissociation rates in the atmospheres of Mars and Venus, *Icarus*, *60*, 327-331, 1984.

Parkinson, T. M., and D. M. Hunten, Spectroscopy and aeronomy of O_2 on Mars, *J. Atmos. Sci.*, *29*, 1380-1390, 1972.

Pinet, P., and S. Chevral, Spectral identification of geological units on the surface of Mars related to the presence of silicates from Earth-based near-infrared telescopic charge-coupled device imaging, *J. Geophys. Res., 95,* 14435-14446, 1990.

Seiff, A., Post-Viking models for the structure of the summer atmosphere of Mars, *Adv. Space Sci.*, *2*, 3-17, 1982.

Shimazaki, T., Photochemical stability of CO_2 in the Martian atmosphere: Reevaluation of the eddy diffusion coefficient and the role of water vapor, *J. Geomag. Geoelectr.*, *41*, 273-301, 1989.

Smith, W. V., The surface recombination of H atoms and OH radicals, *J. Chem. Phys., 11,* 110, 1943.

Thrush, B. A., Reactions of hydrogen atoms in the gas phase, *Prog. React. Kinet.*, *3*, 63-95, 1965.

Tolbert, M. A., M. J. Rossi, and D. M. Golden, Antarctic ozone depletion chemistry: Reactions of N_2O_5 with H_2O and HCl on ice surfaces, *Science*, *240*, 1018-1021, 1988.

Torr, M. R., and D. G. Torr, Ionization frequencies for solar cycle 21: Revised, *J. Geophys. Res.*, *90*, 6675-6678, 1985.

Tsang, W., and R. F. Hampson, Chemical kinetic data base for combustion chemistry. Part 1. Methane and related compounds, *J. Phys. Chem. Ref. Data*, *15*, 1087-1279, 1986.

Wood, B. J., and H. Wise, The kinetics of hydrogen atom recombination on pyrex glass and fused quartz, *J. Phys. Chem.*, *66*, 1049-1053, 1962.

Yung, Y. L., and W. B. DeMore, Photochemistry of the stratosphere of Venus: Implications for atmospheric evolution, *Icarus*, *51*, 199-247, 1982.

Yung, Y. L., J. S. Wen, J. P. Pinto, M. Allen, K. K. Pierce, and S. Paulson, HDO in the Martian atmosphere: Implications for the abundance of crustal water, *Icarus*, *76*, 146-159, 1988.

Yung, Y. L., T. Y. Strobel, T. Y. Kong, and M. B. McElroy, Photochemistry of nitrogen in the Martian atmosphere, *Icarus*, *30*, 26-41, 1977.

Table 2.1. Surface Loss Coefficients on Inorganic Oxides.

Surface	γ	T(K)	Ref
	H Atom		
H_2O(*s*: amorphous)	>0.1	<150	1*
K_2CO_3	0.039	298	8
$NaNO_3$	0.013	298	8
Pyrex	6.0×10^{-3}	298	3
Quartz	2.8×10^{-3}	298	3
PbO	1.9×10^{-3}	298	2
ZnO	1.2×10^{-3}	298	2
H_2O(*s*)	1.6×10^{-4}	253	4
MgO	1×10^{-4}	298	2
H_2SO_4	$\leq 5 \times 10^{-5}$	298	4
	OH Radical		
H_2SO_4	1	298	4
H_2O(*s*)	≥0.4	250	4
$Fe(NO_3)_3$ - FeO_x	0.4	298	8
$Pb(NO_3)_2$	0.24	298	8
Al_2O_3 (on Al metal)	0.10	250	4
$FeSO_4 \bullet nH_2O$	0.12	298	8
H_2SO_4 (28 wt.%)	>0.08	249	5
$Zn(NO_3)_3$	0.045	298	8
FeO_x (on steel))	0.04	250	4
$NaNO_3$	0.036	298	8
Quartz	6.3×10^{-3}	250	4
H_2O(*l*)	$>3.5 \times 10^{-3}$	275	5
	HO_2 Radical		
H_2O(*l*)	0.2	298	7
H_2SO_4 (28 wt.%)	>0.05	249	5
H_2O(*l*)	>0.01	275	5
Stainless Steel	1.7×10^{-2}	320	6
Glass	8×10^{-3}	298	6
FeO_x (on steel)	3×10^{-3}	298	9
Quartz	4×10^{-3}	298	6

References: 1. Buch and Zhang (1991); 2. Thrush (1965); 3. Wood and Wise (1962); 4. Gershenzon *et al.* (1986); 5. Hanson *et al.* (1992); 6. Gershenzon and Purmal (1990); 7. Mozurkewich *et al.* (1987); 8. Jech *et al.* (1982); 9. Rozhenshtein *et al.* (1985)

*Theoretical value

Table 2.2. Gas-Phase Reactions in the Martian Atmosphere.

	Reaction			Rate Coefficient*	Reference
R1a	$O_2 + h\nu$	→	$2O$	1.1×10^{-7}	§
R1b		→	$O + O(^1D)$	6.8×10^{-7}	§
R2a	$O_3 + h\nu$	→	$O_2 + O$	3.3×10^{-4}	§
R2b		→	$O_2 + O(^1D)$	2.1×10^{-3}	§
R3a	$H_2O + h\nu$	→	$H + OH$	2.7×10^{-6}	§
R3b		→	$H_2 + O(^1D)$	1.7×10^{-7}	§
R3c		→	$2H+O$	2.0×10^{-7}	§
R4	$H_2O_2 + h\nu$	→	$2OH$	2.9×10^{-5}	§
R5a	$CO_2 + h\nu$	→	$CO + O$	3.7×10^{-7}	§
R5b		→	$CO + O(^1D)$	1.4×10^{-7}	§
R6	$2O + M$	→	$O_2 + M$	$4.3 \times 10^{-28} T^{-2.00}$	1
R7	$2O + O_2$	→	$O_3 + O$	$6.4 \times 10^{-35} e^{663/T}$	2
R8	$O + O_2 + CO_2$	→	$O_3 + CO_2$	$5.0 \times 10^{-35} e^{724/T}$	2
R9	$O + O_3$	→	$2O_2$	$8.0 \times 10^{-12} e^{-2060/T}$	3
R10	$O + CO + M$	→	$CO_2 + M$	$6.5 \times 10^{-33} e^{-2184/T}$	4
R11	$O(^1D) + O_2$	→	$O + O_2$	$3.2 \times 10^{-11} e^{70/T}$	3
R12a	$O(^1D) + O_3$	→	$2O_2$	1.2×10^{-10}	3
R12b		→	$O_2 + 2O$	1.2×10^{-10}	3
R13	$O(^1D) + H_2$	→	$H + OH$	1.0×10^{-10}	3
R14	$O(^1D) + CO_2$	→	$O + CO_2$	$7.4 \times 10^{-11} e^{120/T}$	3
R15	$O(^1D) + H_2O$	→	$2OH$	2.2×10^{-10}	3
R16	$2H + M$	→	$H_2 + M$	$1.5 \times 10^{-29} T^{-1.30}$	5
R17	$H + O_2 + M$	→	$HO_2 + M$	$k_o = 5.2 \times 10^{-28} T^{-1.60}$	3
				$k_\infty = 7.5 \times 10^{-11}$	
R18	$H + O_3$	→	$OH + O_2$	$1.4 \times 10^{-10} e^{-470/T}$	3
R19a	$H + HO_2$	→	$2OH$	6.8×10^{-11}	6
R19b		→	$H_2 + O_2$	2.9×10^{-12}	6
R19c		→	$H_2O + O$	1.4×10^{-12}	6
R20	$O + H_2$	→	$OH + H$	$1.6 \times 10^{-11} e^{-4570/T}$	1
R21	$O + OH$	→	$O_2 + H$	$2.2 \times 10^{-11} e^{120/T}$	3
R22	$O + HO_2$	→	$OH + O_2$	$3.0 \times 10^{-11} e^{200/T}$	3
R23	$O + H_2O_2$	→	$OH + HO_2$	$1.4 \times 10^{-12} e^{-2000/T}$	3
R24	$2OH$	→	$H_2O + O$	$4.2 \times 10^{-12} e^{-240/T}$	3
R25	$2OH + M$	→	$H_2O_2 + M$	$k_o = 6.6 \times 10^{-29} T^{-0.80}$	3
				$k_\infty = 1.5 \times 10^{-11}$	3
R26	$OH + O_3$	→	$HO_2 + O_2$	$1.6 \times 10^{-12} e^{-940/T}$	3
R27	$OH + H_2$	→	$H_2O + H$	$5.5 \times 10^{-12} e^{-2000/T}$	3
R28	$OH + HO_2$	→	$H_2O + O_2$	$4.8 \times 10^{-11} e^{230/T}$	3
R29	$OH + H_2O_2$	→	$H_2O + HO_2$,	$3.3 \times 10^{-12} e^{-200/T}$	3
R30	$OH + CO$	→	$CO_2 + H$	$1.5 \times 10^{-13} (1 + 0.6 P_{atm})$	3
R31	$HO_2 + O_3$	→	$OH + 2O_2$	$1.1 \times 10^{-14} e^{-500/T}$	3
R32	$2HO_2$	→	$H_2O_2 + O_2$	$2.3 \times 10^{-13} e^{600/T}$	3
R33	$2HO_2 + M$	→	$H_2O_2 + O_2 + M$	$1.7 \times 10^{-33} e^{1000/T}$	3

References: 1, *Hampson* [1980]; 2, *Lin and Leu* [1982]; 3, *Demore et al.* [1990]; 4, *Baulch et al.* [1976]; 5, *Tsang and Hampson* [1986]; 6, *Yung et al.* [1988].

§ Cross sections used to calculate photodissociation rate constants for CO_2, O_2 and H_2O are described in *Anbar et al.* [this issue]. Cross sections for O_3 and H_2O_2 photodissociation calculations are similar to those used in *Yung et al.* [1988].

*Units are s^{-1} for photolysis reactions, $cm^3\ s^{-1}$ for two-body reactions, and $cm^6\ s^{-1}$ for three-body reactions. Photolysis rate constants refer to the optically thin region. Reactions with CO_2 as a third body have had their rate constants increased by a factor of two from the values given here.

Table 2.3. Summary of Model Results: HO_x Column Abundances.

Model	H_2O prμm	Surfaces	γ	H x 10^{14}	OH x 10^{12}	HO_2 x 10^{14}	ΣHO_x x 10^{14}
A	16	--	--	2.58	1.20	5.05	7.64
B	1.6	--	--	2.51	0.88	1.74	4.25
C1	16	Dust & Regolith	$\gamma_{HO_2} = 0.001$	2.58	1.17	4.56	7.15
C2	16	Dust & Regolith	$\gamma_{HO_2} = 0.010$	2.52	1.10	3.20	5.75
C3	16	Dust & Regolith	$\gamma_{HO_2} = 0.100$	2.36	1.00	1.76	4.13
D1	16	Ice @ 30 km	$\gamma_{HO_2} = 0.010$	2.58	1.19	4.98	7.57
D2	16	Ice @ 30 km	$\gamma_{HO_2} = 0.100$	2.48	1.08	4.45	6.94
E1	16	Ice @ 50 km	$\gamma_H = 0.001$	2.30	1.11	5.06	7.37
E2	16	Ice @ 50 km	$\gamma_H = 0.010$	1.21	0.86	5.03	6.25
E3	16	Ice @ 50 km	$\gamma_H = 0.100$	0.71	0.74	5.01	5.72

Abundances of H, OH and ΣHO_x reported as cm^{-2}

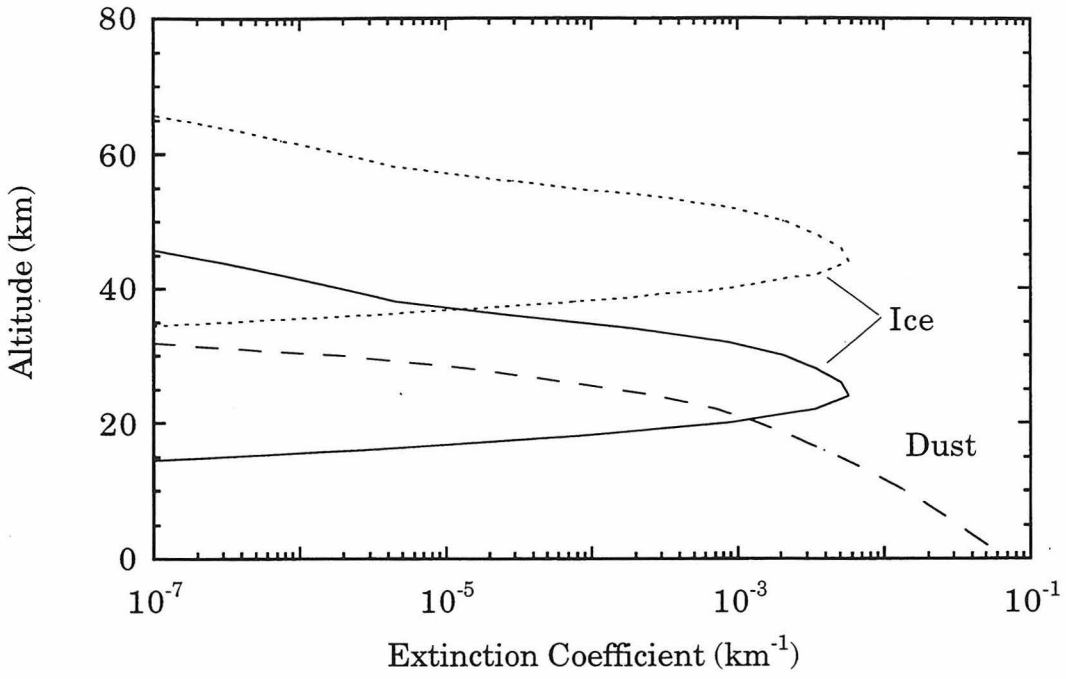

Fig. 2.1. Extinction coefficients of ice haze at 30 km (solid line), ice haze at 50 km (dotted line), and dust (dashed line). A total optical depth of ≈ 0.2 due to dust is assumed.

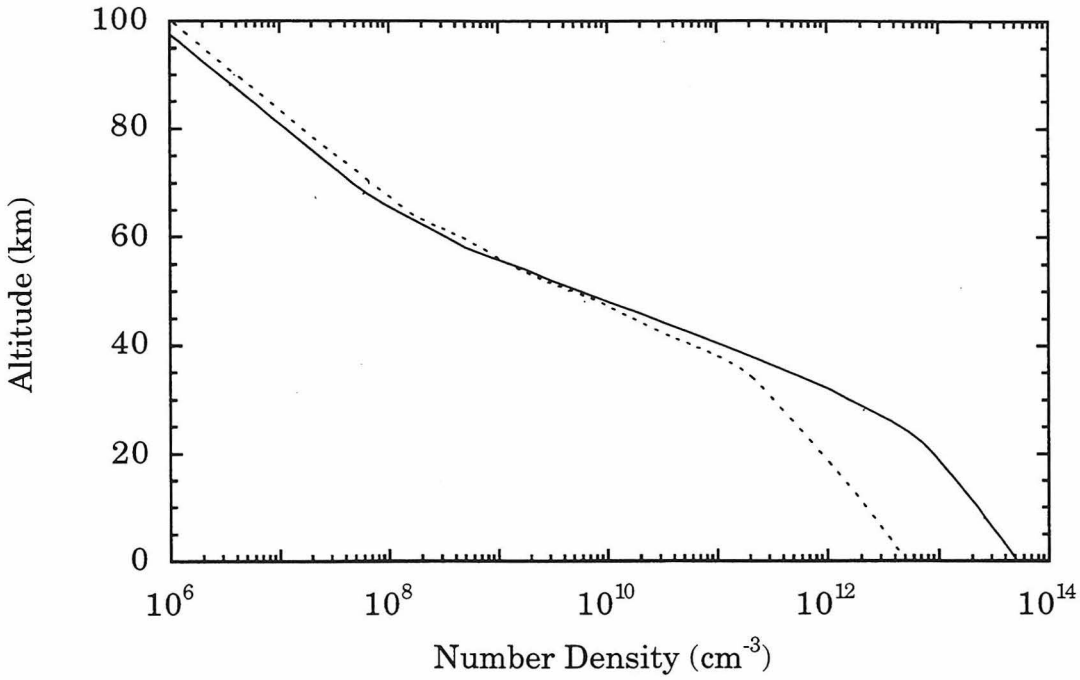

Fig. 2.2. H_2O profiles corresponding to globally averaged water vapor abundances of 16 prμm (solid line) and 1.6 prμm (dotted line).

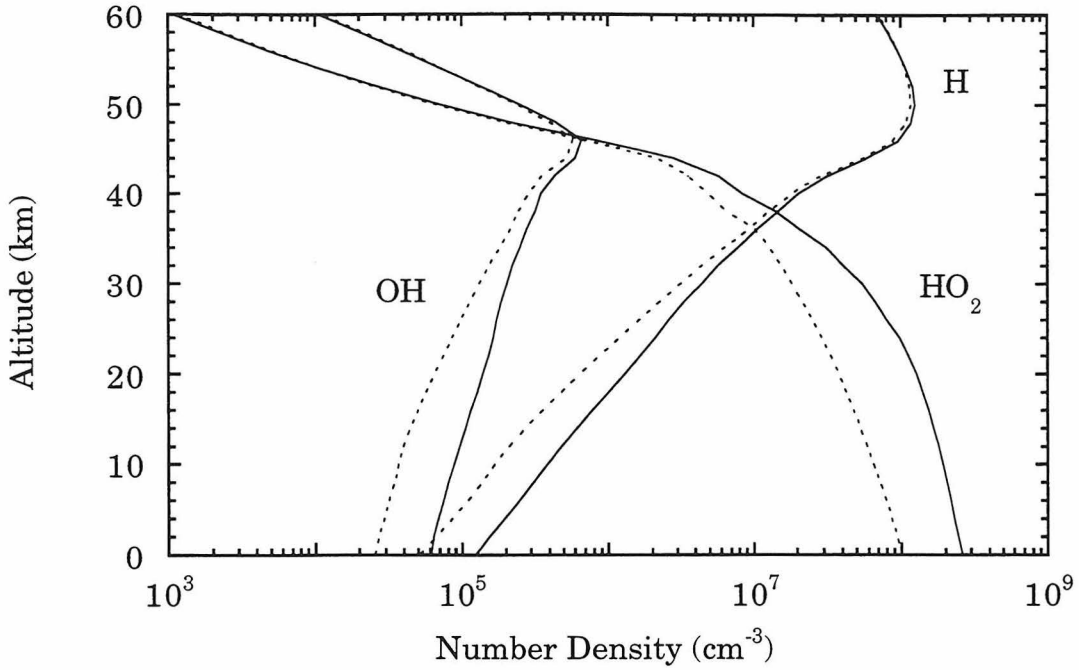

Fig. 2.3. Distribution of HO_x species calculated for model A (solid line) and model B (dotted line).

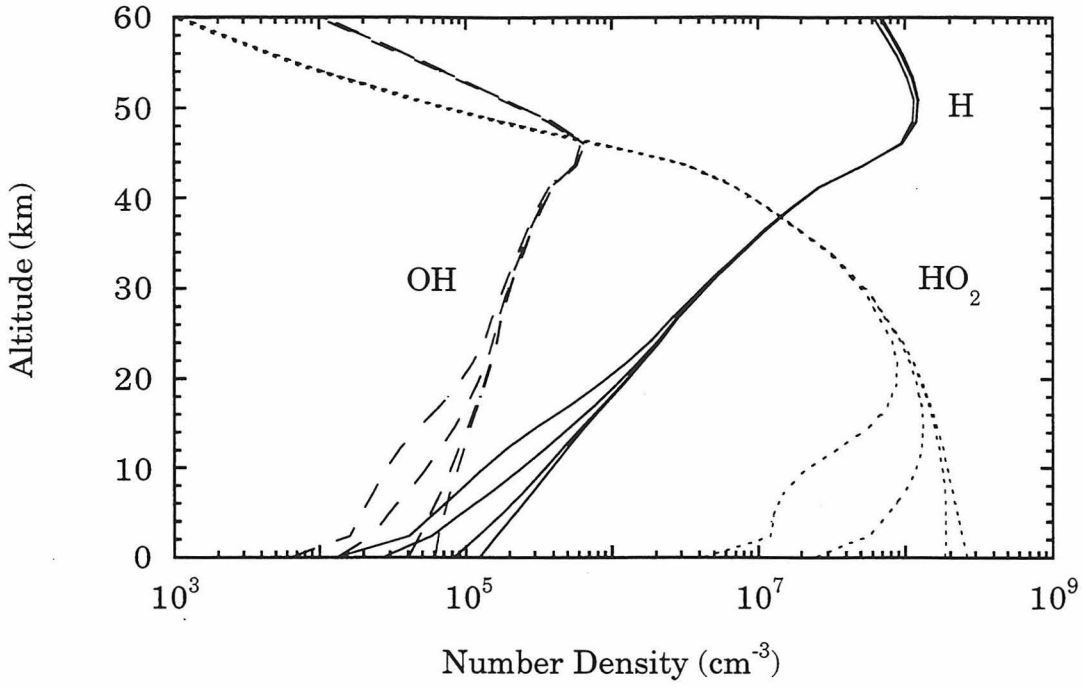

Fig. 2.4. Distribution of HO_2 (dotted line), H (solid line) and OH (dashed line) in models A, C1, C2 and C3. The highest abundances for all three species are those of model A. Abundances decrease as γ_{HO_2} increases from 0.001 (model C1) to 0.100 (model C3). A water vapor abundance of 16 prμm is assumed.

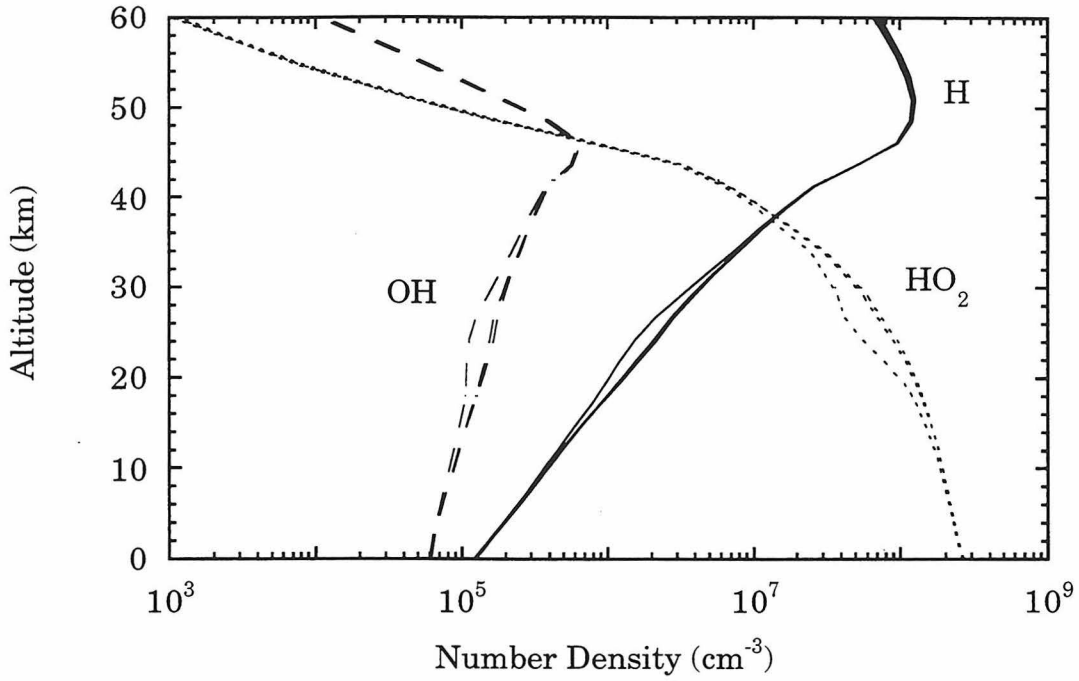

Fig. 2.5. Distribution of HO_2 (dotted line), H (solid line) and OH (dashed line) in models A, D1 and D2. The highest abundances for all three species are those of model A. Abundances decrease as γ_{HO_2} increases from 0.010 (model D1) to 0.100 (model D2). A water vapor abundance of 16 prμm is assumed.

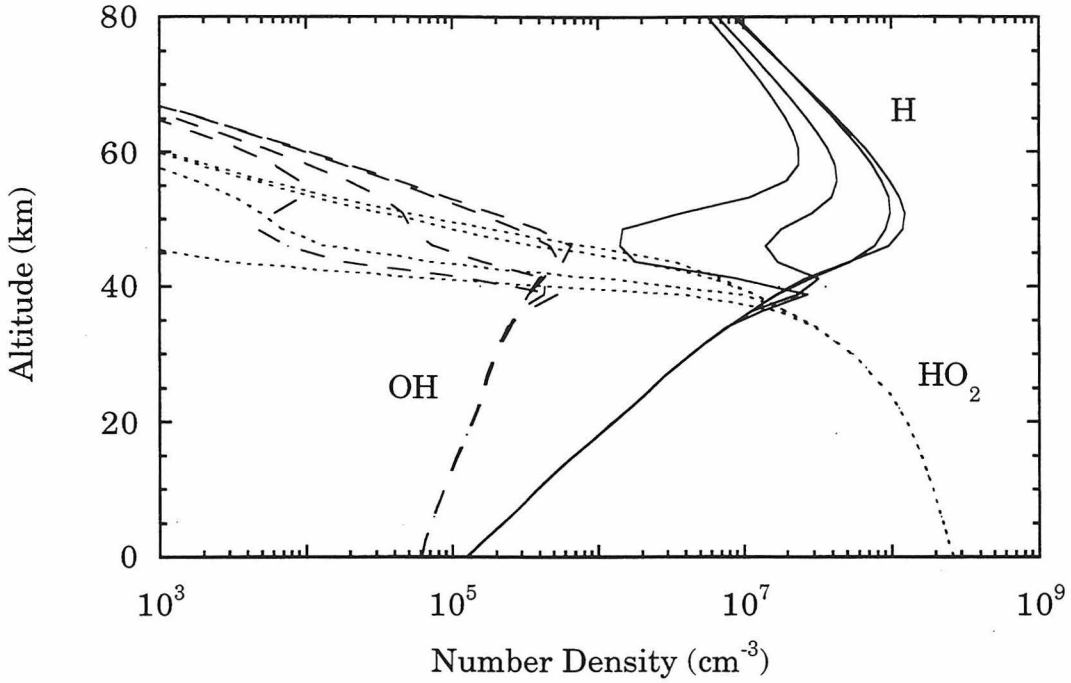

Fig. 2.6. Distribution of HO_2 (dotted line), H (solid line) and OH (dashed line) in models A, E1, E2 and E3. The highest abundances for all three species are those of model A. Abundances decrease as γ_H increases from 0.001 (model E1) to 0.100 (model E3). A water vapor abundance of 16 prμm is assumed.